ALLOSTERIC MODULATION OF G PROTEIN COUPLED RECEPTORS.

by

Naveena Yanamala

Bachelor of Computer Application, S. V. University, Tirupathi, India 2001
Master of Science (IT), Bioinformatics, International Institute for Informational Technology (IIIT), Hyderabad, India 2004

SUBMITTED TO THE GRADUATE FACULTY OF SCHOOL OF MEDICINE IN PARTIAL FULFILMENT OF THE REQUIREMENTS FOR THE DEGREE OF

DOCTOR OF PHILOSOPHY
AT THE
UNIVERSITY OF PITTSBURGH

APRIL 2009

This dissertation was presented by Naveena Yanamala.

It was defended on April 14th, 2009
and approved by

Professor Judith Klein-Seetharaman _____
(Dept. of Structural Biology) Thesis Advisor

Professor Susan G. Amara _____
(Detre Professor and Chair, Neurobiology)

Professor Donald B. DeFranco _____
(Professor and Vice Chair, Pharmacology & Chemical Biology)

Professor Thomas E. Smithgall _____
(Professor and Chair, Microbiology and Molecular Genetics)

Professor Pei Tang _____
(Department of Anesthesiology)

ALLOSTERIC MODULATION OF G PROTEIN COUPLED RECEPTORS.

Naveena Yanamala, M.S.

University of Pittsburgh, 2009

Structural coupling between the cytoplasmic (CP), transmembrane (TM) and extracellular (EC) domains of G protein coupled receptors (GPCRs) is crucial for their functioning in signal transfer from the extracellular to the intracellular side of the membrane. The focus of this thesis was to test the hypothesis that ligands can bind in each of the three domains. Depending on the location of the endogenous ligand binding site, the other two sites would become allosteric ligand binding sites. To test this hypothesis, we investigated the binding of accessory ligands to each of the three domains, CP, TM and EC. The major contributions of this thesis are as follows:

I. The anthocyanin Cyanidin-3-glucoside (C3G) and the chlorophyll-derivative chlorin e6 (Ce6), were shown to physically interact with rhodopsin. These studies demonstrated the presence of a novel CP allosteric ligand binding site in rhodopsin. Biophysical evidence indicated differential effects of binding of these ligands on rhodopsin function, structure and dynamics.

II. The allosteric TM ligand binding pocket in metabotropic glutamate receptors (mGluRs) was shown to be analogous in structure and function to the orthosteric TM retinal ligand binding pocket in rhodopsin. Docking of known allosteric modulators to structural models

of mGluRs based on rhodopsin conformations was used to predict allosteric modulatory effects. Structural comparison of the mGluR and rhodopsin binding pockets revealed high overlap and preliminary evidence was obtained showing that an mGluR ligand can bind to rhodopsin.

III. Evidence for the existence of an EC ligand binding domain was presented. Rhodopsin was shown to bind the extracellular chemokine ligand, CXCL11, an event which interfered with both rhodopsin and chemokine functions.

IV. As part of the above efforts, it became necessary to develop and improve NMR spectroscopic methodology to study ligand binding of membrane proteins such as GPCRs. Thus, ^{1}H and ^{19}F based NMR methods to screen for novel ligands that bind to GPCRs were developed and applied to rhodopsin.

Collectively, the studies presented in this thesis enhance the understanding of allosteric modulation of GPCRs in general, and of the molecular mechanism of rhodopsin and mGluR activation in the presence of allosteric ligands in particular. The results could help in the identification of new ligands to allosterically modulate receptor structures and in turn their functions at different binding pockets, thus paving new ways to selectively target this pharmacologically important class of receptors.

TABLE OF CONTENTS

ACKNOWLEDGEMENTS

I express my deepest gratitude to my advisor, Prof. Judith Klein-Seetharaman, for her constant support, and encouragement through out this process. I am also grateful to Prof. Judith for her willingness to train me, considering that I come from a computer background and giving me the opportunity to perform my dissertation research in the field of GPCRs. I feel fortunate to have had the chance to work with her, where I not only learnt that science is fascinating, but also dedication and hard work are key to success. I am also indebted to Prof. Raj Reddy, for giving me the opportunity to come to this country and pursue my doctoral studies. If it was not for this opportunity, I would have never envisioned myself in such a career path.

I would like to extend my thanks to Prof. Rieko Ishima (chapter 3, section 3.2.4 (b)), Dr. Inja Byeon from Dept. of Structural Biology for the help with NMR method development and Prof. Alexander Dömling from Dept. of Pharmaceutical Sciences for providing ^{19}F labeled ligands for the studies in chapter 6. During my thesis, I had the opportunity to work in collaboration with other members from Dr. Klein-Seetharaman's laboratory. I would like to acknowledge the collaborations with Eric Gardner(chapter 3 & 5, section 3.2 & 5.2), Fernanda Balem(chapter 3, section 3.2.4 (d)), Kalyan C. Tirupula(chapter 3, section 3.1.1 (a) and 3.2.3 (c)), and other former members of the lab, Harpreet Dhiman, Viji Manoharan, Yanjun Qi(chapter 5), Ivan Budyak, David Man, Neelima Mulpuri, and Jenny Wu.

Especially I would like to acknowledge the members of my dissertation committee, Prof. Susan Amara, Prof. Donald Defranco, Prof. Thomas Smithgall and Prof. Pei Tang for agreeing to serve on the committee and for their support throughout this process.

In particular, I would like to extend thanks to Prof. Abhijit Mitra and Prof. Sangal for the initial support and guidance during my masters at IIIT & CMU. Further, I would like to thank my best friends – Suresh, Bharathi, Jyothsna, Sapna and IIIT classmates; Friends from Klein lab - Madhavi, Oznur, Arpana, Andrew; Friends from CMU – Deepa, Ranjani, Vivian, Kishore, Lavanya, Vamshi, Hemanth, Pranjali, Helen, Ravi, Manjunath; Friends from pitt – Adelajda, Varsha, Lakshmi, Jonathan, Rakesh, Saketh, Prema, Prafulla, Sandeep, Reety, Melanie, Nagarjun; my classmates Kim, Eric, Xi and all my juniors for their kind cooperation in making this journey a pleasant experience.

Also, I thank Jennifer Walker, Janet Jambotti, Dean Duncan for their administrative support; Phil Greer, Doug Bevon for the technical support and Mike Delk for the support with NMR machines. I also thank Dept. of Pharmocology for supporting my studies with the one-year predoctoral fellowship during the period of 2007-2008.

I would like to thank Prabha Day, Santhosh Day, Durga Malepati, Vasu Malepati, Vijay Sai and Sai Lakshmi for their unconditional love and treating me as part of their family, with whom I always shared ups and downs, and happy moments of my life. Finally, I would like extend my gratitude to my family, my parents – Lakshmi and Ramprasad, for their inspiration and motivation in every aspect, in-laws – Lakshumamma, Siddhu, Pallavi, Surendra Babu and Sridevi, brothers – Harsha, Deepak, uncles – Prabhakar, Jayaram, Paramesh, and Sudhakar, aunts – Ramalakshumma, Parvathi, Jacintha, and cousins – Meenakshi, Bhavana and Teja, who were either involved directly or indirectly for making this happen and taking care of my son in india while I was here finishing my Ph.D. Last but not least, I whole heartedly thank my loving husband, Sivaram Prasad, for his constant love, support and always being there for me whenever I needed him.

Dedicated

To

My Parents: Lakshmi & Ramprasad,

My Son: Sairam

and

My Husband: Sivaram

JOURNAL PUBLICATIONS

Parts of this thesis have been published in the journal articles. The references to these are listed below in the order they appear in the different chapters.

Naveena Yanamala, Kalyan C. Tirupula, Fernanda Balem, Judith Klein-Seetharaman. (2009) pH-dependent Interaction of Rhodopsin with Cyanidin-3-glucoside. 1. Structural Aspects. *Photochemistry and Photobiology* **85:** 454-462

Kalyan C. Tirupula, Fernanda Balem, Naveena Yanamala, Judith Klein-Seetharaman. (2009) pH-dependent Interaction of Rhodopsin with Cyanidin-3-glucoside. 2. Functional Aspects. *Photochemistry and Photobiology* **85:** 463-470

Naveena Yanamala, Kalyan C. Tirupula, Judith Klein-Seetharaman. (2008) Preferential binding of allosteric modulators to active and inactive conformational states of metabotropic glutamate receptors. *BMC Bioinformatics* **9:** S16

In addition to the work reported above, I also participated in different projects during my dissertation. The references to these are listed below in the order they were published.

Fernanda Balem, Naveena Yanamala, Judith Klein-Seetharaman. (2009). "Additive Effects of Chlorin E6 and Metal Ion Binding on the Thermal Stability of Rhodopsin *In Vitro*" Photochemistry and Photobiology **85**(2): 471-478.

Ivan L. Budyak, Olga S. Mironova, Naveena Yanamala, Vijayalaxmi Manoharan, Georg Büldt, Ramona Schlesinger, and Judith Klein-Seetharaman. (2008). "Flexibility of the Cytoplasmic Domain of the Phototaxis Transducer II from Natronomonas pharaonis," Journal of Biophysics, Article ID 267912, 11 pages, doi:10.1155/2008/267912

Judith Klein-Seetharaman, Naveena V. K. Yanamala, Fathima Javeed, Philip J. Reeves, Elena V. Getmanova, Michele C. Loewen, Harald Schwalbe, and H. Gobind Khorana. (2004) " Differential dynamics in the G protein-coupled receptor rhodopsin revealed by solution NMR", Proceedings of the National Academy of Sciences, **101**: 3409-3413.

ABSTRACTS / PRESENTATIONS

Parts of this thesis have been either presented as a poster or as oral presentation at conferences. The list with references for these is listed below separated into two sections in the order they were presented.

Oral Presentations:

Naveena Yanamala, Kalyan C. Tirupula, Kasturi Nadella, Nagarajan Vaidehi, and Judith Klein-Seetharaman (2007) Modeling of Structure and Binding Site of Allosteric Modulators of Metabotropic Glutamate Receptors, 51st Annual Meeting of the Biophysical Society, Baltimore, Maryland, USA.

Naveena Yanamala, Kalyan C. Tirupula and Judith Klein-Seethraman (2007) Preferential Binding of Allosteric Modulators to Active and Inactive Conformational States of Metabotropic Glutamate Receptors, 6th International Conference on Bioinformatics, HKUST, HongKong.

E. E. Gardner, Y-J. Tung, Y. Qi, N. V. K. Yanamala, K. Tirupula, T. A. Reinhart, Z. Bar-Joseph, & J. Klein-Seetharaman (2007) Rhodopsin Interacts with Chemokines, 51st Annual Meeting of the Biophysical Society, Baltimore, Maryland, USA.

Ivan Budyak, Naveena V. K. Yanamala and Judith Klein-Seetharaman (2006) Conformational studies of the transmembrane-juxtamembrane region of the epidermal growth factor receptor, 50th Annual Meeting of the Biophysical Society, Salt Lake City, Utah, USA.

Harpreet Kaur Dhiman, Naveena V. K. Yanamala and Judith Klein-Seetharaman (2005) Development of New NMR Spectroscopic Methods for Determining Distance Constraints in

Membrane Proteins of Large Size in Detergent Micelles, 49th Annual Meeting of the Biophysical Society, Long Beach, USA.

Poster Presentations:

Kalyan C. Tirupula, Harpreet K. Dhiman, Naveena Yanamala, Judith Klein-Seetharaman (2009) Expression and functional characterization of Metabotropic Glutamate Receptor Type 6 (mGluR6) in detergent micelles, 53rd Annual Meeting of the Biophysical Society, Boston, Massachusetts, USA.

Naveena Yanamala, Kalyan C. Tirupula, Fernanda Balem, Judith Klein-Seetharaman (2009) pH Dependent Interaction of Rhodopsin with Anthocyanin Plant Pigments, 53rd Annual Meeting of the Biophysical Society, Boston, Massachusetts, USA.

Naveena Yanamala, Eric E. Gardner, Kalyan C. Tirupula, and Judith Klein-Seetharaman (2008) Binding of chlorophyll to the G protein coupled receptor Rhodopsin, 13th International Conference on Retinal Proteins, Barcelona, Spain.

Neelima Konuru, Naveena Yanamala, Kalyan C. Tirupula and Judith Klein-Seetharaman (2008) Preferential Binding of Ligands to Active and Inactive Conformational States of G Protein Coupled Receptors, 52nd Annual Meeting of the Biophysical Society, Long Beach, California, USA.

Naveena Yanamala, Qingguo Gong, Judith Klein-Seetharaman and Rieko Ishima (2007) ^{15}N and ^{19}F relaxation experiments at high field magnets, 48th ENC, Daytona Beach, Florida, USA.

E. E. Gardner, Y-J. Tung, S. K. Ravuri Y. Qi, N. V. K. Yanamala, P. Chelikani, K. C. Tirupula, T. A. Reinhart, H. G. Khorana, Z. Bar-Joseph, & J. Klein-Seetharaman (2007) Evidence for the interaction of the G protein-coupled receptor (GPCR) rhodopsin with chemokine CXCL11 (I-TAC), 21st Annual Symposium of the Protein Society, Boston, Massachusetts, USA

Jenny Hui Jue Wu, Naveena VK Yanamala, and Judith Klein-Seetharaman (2007) Determination of Stabilizing Residues in Dark State Mammalian Rhodopsin Using Fast Contact Analysis, 21st Annual Symposium of the Protein Society, Boston, Massachusetts, USA.

Eric E. Gardner, Yanjun Qi, Sudheer V. Ravuri, Naveena V. K. Yanamala, Prahsen Chelikani, Kalyan C. Tirupula, Todd A. Reinhart, H. Gobind Khorana, Ziv Bar-Joseph, and Judith Klein-Seetharaman (2007) Validation of Novel, Computationally-Predicated Protein-Protein Interactions with the G Protein-Coupled Receptor Rhodopsin. Joint Meeting of the 18th Annual Argonne Symposim for Undergraduates in Science, Engineering and Mathematics and the Central States Universities, Incorporated (CSUI) Research Conference. Argonne National Lab, Argonne, Illinois, USA.

Oznur Tastan, Arpana Dutta, Fernanda Balem, Jenny Hui Jue Wu, Naveena Yanamala and Judith Klein Seetharaman (2007) Comparison of simulated unfoldings of alpha-helical membrane proteins. 6th European Biophysics Congress, London, UK, 14-19 July.

E. E. Gardner, Qi, Y, Ravuri, S. K., Yanamala, N. V. K., Chelikani, P., Tirupula, K. C., Reinhart, T. A., Khorana, H. G., Z. Bar-Joseph and J. Klein-Seetharaman (2007) Validation of Computationally-Predicted Protein-Protein Interactions with the G Protein-Coupled Receptor (GPCR) Rhodopsin, Science 2007, University of Pittsburgh, Pittsburgh, Pennsylvania.

David Man, Kevin W.-H. Lo, Yanamala N, K. Kevin Pfister and J. Klein-Seetharaman, (2007) NMR Structural Investigation of a Region of the Cytoplasmic Dynein Intermediate Chain Important for Dimerization, Local Traffic Symposium 2007, University of Pittsburgh, Pittsburgh, PA, USA.

D. Man, K.T. Gallaher, N. Yanamala, Kalyan Tirupula, N. Waseem, B.J. Jennings, E. Reese, K. Gerwert, S.S. Bhattacharya, A. Iannaccone, J. Klein-Seetharaman (2007) Molecular Properties and Disease Phenotypes of Rhodopsin Mutants P23H and N15S Associated with Autosomal Dominant Retinitis Pigmentosa (ADRP), ARVO 2007 Annual Meeting, Fort Lauderdale, Florida, USA.

Naveena VK Yanamala, Kalyan C. Tirupula, Kasturi Nadella, Nagarajan Vaidehi, William A. Goddard III and Judith Klein-Seetharamanm (2006) Modeling of structure and binding site of allosteric modulators of metabotropic Glutamate receptors, Science 2006, University of Pittsburgh, PA, USA.

Naveena VK Yanamala, Nagarajan Vaidehi, William A. Goddard III and Judith Klein-Seetharaman (2005) Prediction of Metabotropic Glutamate Receptor Subtype 1 Structure and Ligand-Binding Properties, Science symposium 2005, University of Pittsburgh, Pittsburgh, PA, USA.

ABBREVIATIONS

GPCR	G-protein coupled receptor
TM	transmembrane
CP	cytoplasmic
EC	extracellular
PTH	parathyroid hormone
PTH_1R	parathyroid hormone receptor – 1
mGluR	metabotropic glutamate receotor
Ce6	chlorin e6
C3G	canidin-3-gucoside
DFB	di-fluoro-benzaldazine
Meta II	metarhodopsin II
G_t	G-protein transducin
GTP	guanosine 5'-triphosphate
GDP	guanosine 5'-diphosphate
PDE	phosphodiesterase
cGMP	cyclic GMP
UV/VIS	UV-visible
A_{500}	absorbance (λ500 nm)
$t_{1/2}$	half life
4-PDS	4,4'-dithiodipyridine
TET	trifluoroethylthio
NMR	nuclear magnetic resonance
^{19}F	fluorine-19
^{1}H	proton
^{15}N	nitrogen-15
T_1	longitudinal relaxation
T_2	transverse relaxation
R_1	longitudinal relaxation rate
R_2	transverse relaxation rate
WT	wild-type
DM	n-dodecyl-β-D-maltoside
OG	octyl-glucoside
FBS	fetal bovine serum
DMEM	Dulbecco's modified Eagle's medium high glucose
ROS	rod outer segment
TFA	trifluoroacetic acid

RT	room temperature
o/n	overnight
RP	retinitis pigmentosa

Residues at particular positions in rhodopsin are designated by using the three-letter code for the amino acid, followed by its sequence number.

LIST OF FIGURES

LIST OF TABLES

CHAPTER - 1
INTRODUCTION

TABLE OF CONTENTS

1.1. BACKGROUND

1.1.1. Introduction

The largest family of cell surface receptors responsible for transducing signals from the outside to the inside of the cell are G Protein Coupled Receptors (GPCRs) and the focus of this thesis is modulation of their structure and function through binding of allosteric ligands. In this section, a background is provided on GPCRs in general, their classification based on sequence and pharmacology, and specific details are provided for representative members from each major family. Principles for allosteric modulation of GPCRs and the advantages associated with using allosteric modulators as opposed to orthosteric ligands are also discussed.

1.1.2. G-Protein Coupled Receptors and Their Classification

GPCRs form the largest and most diverse family of cell surface receptors. The primary function of these membrane bound receptors is to mediate the communication between the cell and its environment by responding to signals via binding and activation of intracellular G proteins, in turn, initiating cellular responses (Figure 1.1). These receptors respond to a wide variety of signals including light, ions, peptides, hormones, odorants and neurotransmitters. GPCRs are structurally characterized by seven transmembrane (TM) helices, dividing each GPCR protein into extracellular (EC), cytoplasmic (CP), and transmembrane (TM) domains (Figure 1.1). For this reason, GPCRs are also known as 7TM proteins or serpentine receptors. The seven TM segments are interlinked with EC

loops (E1, E2, and E3) and CP loops (C1, C2, and C3), and the amino (N) and carboxy (C) termini of GPCRs are located at the EC and CP sides of the receptors, respectively.

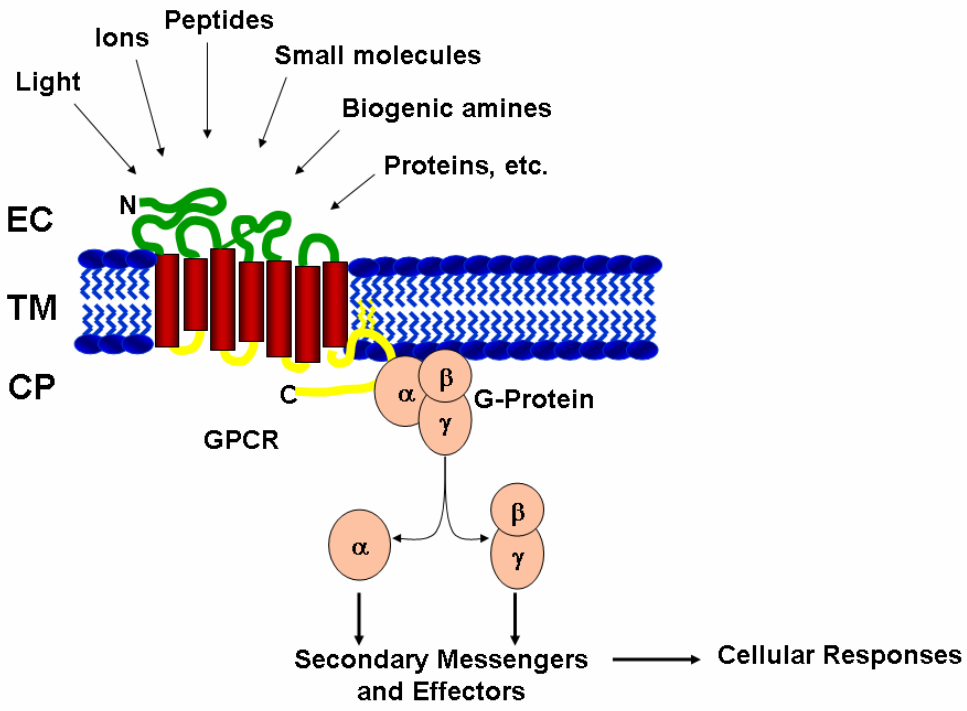

Figure 1.1: Schematic representation of the generic structure of GPCRs.

When specific ligands bind to GPCRs in the EC or TM regions, the event causes conformational changes in the receptors, which act like a switch transducing the ligand binding signal to the G proteins. The G protein then acts to either stimulate or inhibit the production of intracellular secondary messengers, which in turn trigger various signal transduction cascades. In general, the top one-third of the TM helices, along with the EC loops and N-terminus, play a major role in ligand binding. The rest of the TM helix region with CP domain (including loops and C-terminus) is very important for the interaction with downstream signaling proteins. With more than 1000 human sequences

deposited (Kolakowski 1994; Vassilatis, Hohmann et al. 2003), and more than 8000 sequences including other organisms (Finn, Tate et al. 2008), GPCRs are one of the most important family of receptors. They are associated with various disease conditions including diabetes (Winzell and Ahren 2007), cancer (Yowell and Daaka 2002; Li, Huang et al. 2005; Dorsam and Gutkind 2007), central nervous system disorders (Conn, Christopoulos et al. 2009), obesity (Yeo and Siddle 2003), inflammation (Lomas-Neira and Ayala 2005), cardiac diseases (Tang and Insel 2004) and others. Based on sequence homology and pharmacological considerations, the GPCR super-family is subdivided into six sub-families (Kolakowski 1994; Fredriksson, Lagerstrom et al. 2003). They are: Class A or the rhodopsin like or adrenergic receptor like family, Class B or the secretin receptor family, Class C or the metabotropic glutamate receptor like, Class D or the Fungal mating pheromone receptors, Class E or the cyclic AMP (cAMP) receptors, and Class F the frizzled or smoothened receptors. Very little sequence homology is observed between these different subfamilies; the greatest homology is observed within the TM regions. Major differences are observed in the lengths of their N-termini (Figure 1.2). Other differences pertain to the endogenous ligand binding sites between different members across the subfamilies and sometimes within a subfamily. The endogenous ligand typically binds at the TM domain near the EC domain in Class A GPCRs. In contrast, for Class B and C the ligand pocket is located in the EC domain. For some of the members of Class A GPCRs, the endogenous ligand binding site is also localized in the EC domain, but the majority of the members bind ligands in the TM domain. For example, chemokine receptors bind to their respective endogenous chemokine ligands at the EC domain similar to Class B and C receptors. The details of the structural features,

lengths of N-termini and the endogenous ligand binding sites for each of the major subfamilies, Class A, B and C, along with a representative member are discussed below.

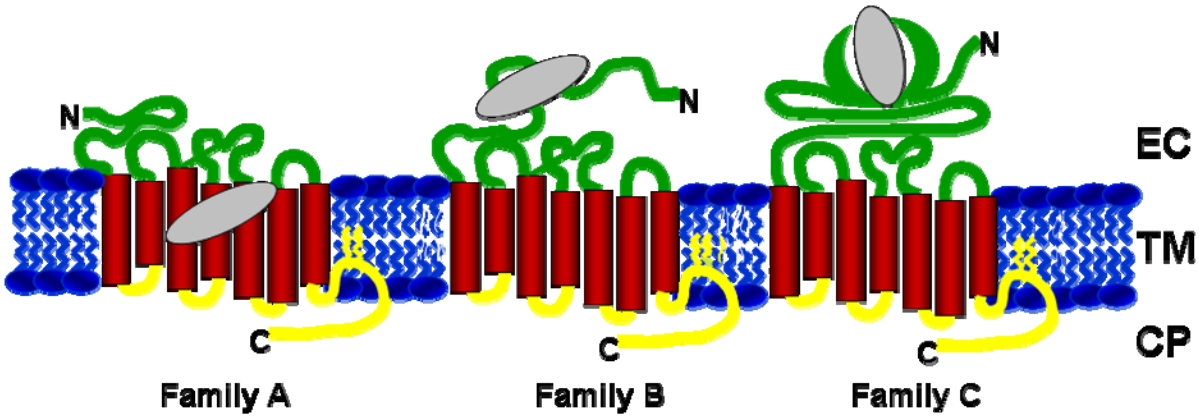

Figure 1.2: Schematic diagram of representative structural organizations of GPCRs highlighting the most common endogenous ligand binding site locations for each of the major GPCR family members. Extracellular and cytoplasmic loops are colored in green and yellow, respectively. Transmembrane helices are colored in red and represented as cylinders. The membrane bilayer is shown in blue color. The endogenous (orthosteric) ligand binding site in each family is represented by an ellipse colored in grey.

1.1.2. (a) Class A: Class A is the largest subfamily of GPCRs with 918 identified members in humans (Kolakowski 1994; Okuno, Tamon et al. 2008). Class A GPCR bind to ligands as diverse as amines, peptides, hormones, lipids, and viral proteins to name a few (Chalmers and Behan 2002). The members of this family are characterized by the presence of D/ERY and NPXXY motifs in the CP domain at the ends of helices 3 and 7,

respectively (Baldwin, Schertler et al. 1997). Residues Asp/Glu and Arg that are part of the D/ERY motif, are conserved across family A GPCRs, and are critical for receptor activation (Arnis, Fahmy et al. 1994; Acharya and Karnik 1996). Previous studies with mutants involving residue Asp/Glu often resulted in constitutively-active receptors of this family (Acharya and Karnik 1996; Kim, Altenbach et al. 1997; Morin, Cotte et al. 1998; Ballesteros, Jensen et al. 2001). The NPXXY signature motif is important for receptor internalization, activation, and also phosphorylation (Bouley, Sun et al. 2003; Fritze, Filipek et al. 2003; Kalatskaya, Schussler et al. 2004). In addition to these conserved motifs, a disulphide bond connecting EC loop 2 with the EC end of TM helix 3 is also highly conserved within the family (Findlay and Pappin 1986; Karnik, Sakmar et al. 1988; Karnik and Khorana 1990; Rader, Anderson et al. 2004). Disruption of this disulphide bond highly destabilizes the receptors (Davidson, Loewen et al. 1994) and, as described in more detail for rhodopsin below, is associated with receptor misfolding (Hwa, Reeves et al. 1999; Hwa, Klein-Seetharaman et al. 2001). Finally, the Class A family has the smallest N-terminus as compared to other subfamilies and the endogenous ligand binding domain in the majority of the receptors is situated in the TM domain, at the interface between TM and EC domains (Figure 1.2A). Rhodopsin is the representative member of this subfamily of receptors.

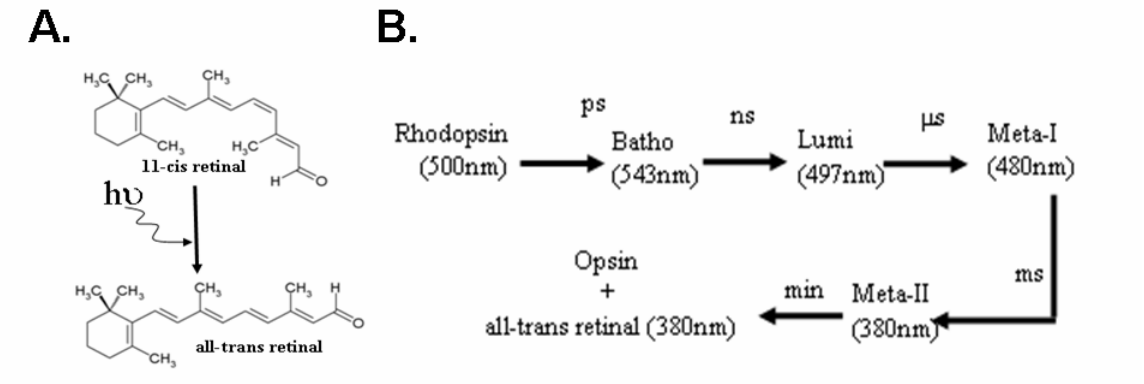

Figure 1.3: **Details of light-activation in rhodopsin.** (A) Isomerization of *11-cis* to *all-trans* retinal by light. (B) Intermediate states of rhodopsin upon light-activation.

Representative Class A Receptor Rhodopsin: Rhodopsin, the prototypical member of the GPCR Class A family, belongs to the opsin sub-family within Class A GPCRs. The opsins represent a subgroup of proteins that function as photoreceptors in different cell types and organisms. All opsins covalently bind to the chromophore retinal through a protonated Schiff base linkage to a lysine residue (Lys-296 in rhodopsin) found in the TM domain, close to the interface between the TM and EC domains. *11-cis* retinal plays a pivotal role in rhodopsin activation. Upon absorbing a photon, the chromophore isomerizes to *all-trans* retinal. This event triggers the rearrangement of the TM helices to give rise to the series of photo-intermediates shown in Figure 1.3. Each intermediate has a characteristic absorption in the visible range (Lewis and Kliger 2000; Sakmar, Menon et al. 2002; Schertler 2005). The Meta II state of rhodopsin is considered to be the active state of the protein and is an initiator of the visual signal transduction cascade. The Meta II state is characterized by conformational changes in the protein that initiate these

events. As a first step, Meta II binds to the G protein transducin (G_t). G_t then activates phosphodiesterase (PDE), which, in turn, hydrolyzes cyclic GMP (cGMP). Once hydrolyzed, cGMP initiates a cascade of events leading to the hyperpolarization of the cell through the closure of Na^+-Ca^{2+} channels. When the cell is hyperpolarized, the electrical potential inside the cell is negative. In contrast, in the dark state, cGMP keeps the channels in the photoreceptor membrane open, and Na^+-Ca^{2+} influx depolarizes the membrane potential.

There are two ways of shutting down the visual signal transduction cascade: through Meta II decay, a process of dissociation of protein and ligand to opsin and free *all-trans* retinal (Figure 1.3), or through binding of arrestin to the phosphorylated C-terminal end of rhodopsin (Chabre, Bigay et al. 1988). The phosphorylation can occur at any of seven threonine and serine sites in the C-terminus (Figure 1.4). The ligand free opsin formed when Meta II decays can readily uptake *11-cis*-retinal, a critical step required in the regeneration of the rhodopsin dark state which allows for the continuation of visual perception.

Mutations in the rhodopsin gene and dysfunctions lead to the diseases retinitis pigmentosa and congenital night blindness (Dryja, Berson et al. 1993; Dryja, Finn et al. 1995). Most of these mutations were found to be localized in the EC domain and TM domains. Previous studies from the Khorana lab (Kaushal and Khorana 1994; Ridge, Lu et al. 1995; Garriga, Liu et al. 1996; Liu, Garriga et al. 1996; Hwa, Garriga et al. 1997) provided conclusive evidence that most of these mutations lead to the formation of an incorrect disulphide bond between Cys185 – Cys-187, instead of the native Cys-110 – Cys187. The formation of this aberrant disulphide bond leads to the stabilization of

incorrectly folded protein that lacks the ability to bind *11-cis* retinal (Kaushal and Khorana 1994; Ridge, Lu et al. 1995; Liu, Garriga et al. 1996), suggesting a structural coupling between the EC and TM regions. The mutants G90D, T94I and A292E that cause congenital night blindness were shown to constitutively activate G_t, even in the absence of the *11-cis* retinal (Dryja, Berson et al. 1993; Rao, Cohen et al. 1994; Gross, Rao et al. 2003). Some of these mutants were found to disrupt the interaction between Glu-113 and Lys-296, important for locking the receptor in the ground, inactive state (Rao, Cohen et al. 1994).

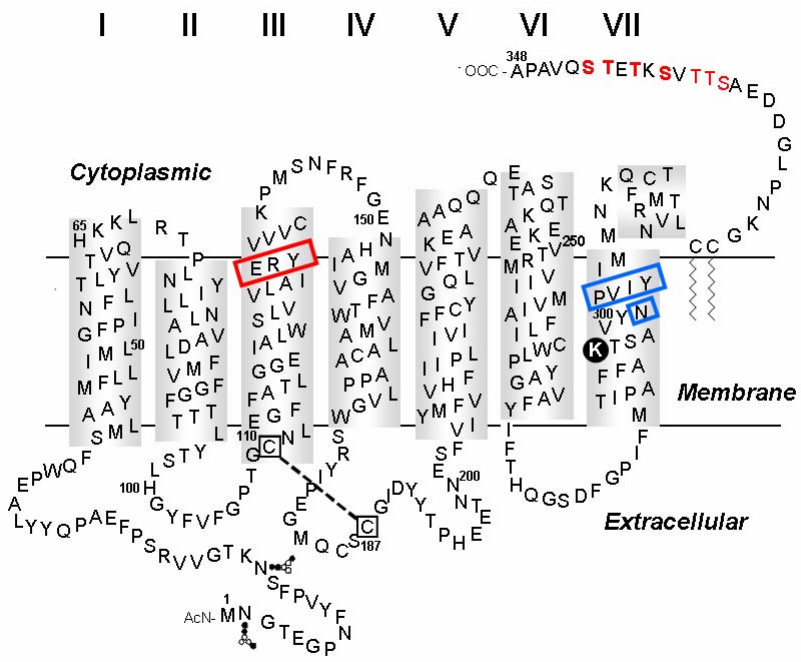

Figure 1.4: Secondary structure representation of rhodopsin. The disulphide bond between Cys-110 and Cys-187 is represented with a black dashed line. The conserved D/ERY and NPXXY motifs are indicated in red and blue rectangles, respectively. Phosphorylation sites located in the C-terminus are colored in red.

In this thesis we used bovine rhodopsin as a model system. Bovine rhodopsin is one of the most thoroughly studied receptors among GPCRs, and using it as a model system is beneficial for the following reasons: 1) rhodopsin can be purified easily and in large quantities from bovine retinae. 2) There is a large body of literature reporting biochemical and biophysical studies which can be used for reference (Klein-Seetharaman 2002). 3) Changes upon light activation in rhodopsin's structure have been investigated in great detail for bovine rhodopsin (Kusnetzow, Altenbach et al. 2006). Several groups have focused their efforts on studying rhopdopsin stability and function in the presence of different lipids and detergents (Williams, Baker et al. 1974; Pontus and Delmelle 1975; Stubbs, Smith et al. 1976; Plante, Maude et al. 1977; Davoust, Bienvenue et al. 1980; De Grip 1982; Margry, Jacobs et al. 1982; Sefcik, Schaefer et al. 1983; Yeagle, Selinsky et al. 1984; Motoyama, Hamanaka et al. 1985; Tiurin, Korol'kov et al. 1987; Renk, Crouch et al. 1988; Wiedmann, Pates et al. 1988; Boesze-Battaglia, Hennessey et al. 1989; Gibson and Brown 1991; Gibson and Brown 1991; Brown 1994; Albert, Boesze-Battaglia et al. 1996; Albert, Young et al. 1996; Bubis 1998; Jastrzebska, Maeda et al. 2004; Bennett and Mitchell 2008). Many biophysical studies such as high-resolution NMR spectroscopy depend on solubilization of rhodpsin in detergent micelles. Rhodopsin exhibits maximum stability in n-dodecyl-β-D-maltoside (DM) micelles (Cha, Reeves et al. 2000) and this detergent has therefore been the most widely employed. Recent EPR spectroscopic measurements have provided evidence that the conformational changes observed in DM closely resemble those observed in lipid environments (Kusnetzow, Altenbach et al. 2006), further supporting the validity of using DM.

Therefore, bovine rhodopsin, reconstituted in DM detergent micelles (unless otherwise mentioned) was used for the studies reported in this thesis.

1.1.2. (b) Class B: Class B is the second largest sub-family of GPCRs; 48 receptors have been identified in humans (Vassilatis, Hohmann et al. 2003; Finn, Tate et al. 2008; Okuno, Tamon et al. 2008). The N-terminus is with 60-80 amino acids generally larger as compared to Class A, but smaller than Class C (Soudijn, Van Wijngaarden et al. 2004). The members of this sub-family usually bind to peptide hormones such as secretin and glucagon (May, Leach et al. 2007). The ligand binding site for these endogenous ligand peptides is situated in the EC domain, typically involving the N-terminus as well as the EC loops in the interaction (Hoare 2005). This peptide ligand binding domain is composed of three or four cysteine residues and two tryptophan residues that are highly conserved across all members of the Class B GPCRs (Harmar 2001). In addition to this, the N-terminal domain contains a highly conserved signal peptide region that targets these receptors to the plasma membrane (Harmar 2001). The parathyroid hormone (PTH) receptor is the prototypical member of the hormone receptors in this family**.**

Representative Class B Receptor – Parathyroid Hormone (PTH) Receptor: The PTH receptor is member of sub-family B1 of Class B GPCR (Harmar 2001). There are two subtypes of this receptor, PTH_1 and PTH_2. The PTH_1 receptor is the best studied member of hormone receptors and plays a major role in regulating calcium levels and bone growth in humans, and as such, the PTH_1 receptor is expressed abundantly in bone and kidney cells (Lee, Deeds et al. 1994; Lee, Deeds et al. 1995; Lee, Brown et al. 1996). The PTH_1 receptor initiates signaling by binding to the endogenous hormone PTH

secreted by parathyroid glands. PTH is a 84 amino acid peptide and interacts at the N-terminal domain of the PTH_1 receptor. Upon binding to the hormone, the receptor undergoes conformational changes and initiates the binding of the G protein at its CP domain. Previous studies have identified that this receptor can couple to both G_s and G_q (Offermanns, Iida-Klein et al. 1996), thus activating protein kinase A and protein kinase C pathways (Muff, Born et al. 1994; Partridge, Bloch et al. 1994; Yang and Gerstenfeld 1996). Mutations that lead to constitutive activity in this receptor have been implicated in the genetic disease Jansen's metaphyseal chondrodysplasia (Schipani, Kruse et al. 1995). In contrast to this, mutations that result in inhibiting activity lead to a disease condition called Blomstrand's lethal chondrodysplasia (Jobert, Zhang et al. 1998; Karperien, van der Harten et al. 1999).

1.1.2. (c) Class C: A total of about 40 human receptors constitute the Class C GPCRs (Kolakowski 1994; Finn, Tate et al. 2008; Okuno, Tamon et al. 2008), with metabotropic glutamate, calcium sensing and γ-aminobutyric acid (GABA) receptors as the major receptor subtypes. The Class C GPCR sub-family in general, with the exception of GABA receptors, is structurally characterized by the presence of a large extracellular N-terminal domain comprising about 600 amino acids and a cysteine rich domain (CRD) connecting the TM with this EC domain. The only exception are GABA receptors. The endogenous ligand binding domain of Class C GPCRs is located in this long N-terminal EC domain, often referred to as a "Venus flytrap" (Acher and Bertrand 2005). This ligand binding pocket location is unusual when compared to other GPCR family members where the small molecule ligand binding domain is typically located in the TM

domain near its interface with the EC domain (Class A GPCRs) or in the EC loops and N-terminus close to the TM domain (Class B GPCRs). The representative members of Class C GPCRs are the metabotropic glutamate receptors.

Representative Class C Receptors – Metabotropic Glutamate Receptors: Glutamate is the most important excitatory neurotransmitter in the brain. Glutamatergic neurotransmission proceeds primarily via ion gated channels (ionotropic glutamate receptors). In addition, there are metabotropic glutamate receptors (mGluRs), which belong to the GPCR family. Both types of glutamate receptors share a common EC ligand binding architecture, albeit different topology and protein family membership. X-ray crystallographic structures are available for the soluble EC domains of mGluRs (Hampson, Huang et al. 1999; Kunishima, Shimada et al. 2000; Tsuchiya, Kunishima et al. 2002; Muto, Tsuchiya et al. 2007) and ionotropic glutamate receptors (Armstrong, Sun et al. 1998; Armstrong and Gouaux 2000; Mayer 2006). In humans, there are eight subtypes of mGluRs that are further divided into three groups based on their pharmacological and signaling properties. Group I mGluRs (subtypes 1 and 5) are primarily localized post-synaptically where they modulate ion channel activity and neuronal excitability. Groups II (subtypes 2 and 3) and III (subtypes 4, 6, 7, and 8) are primarily located pre-synaptically and regulate the release of neurotransmitters, including glutamate (Conn and Pin 1997).

mGluRs play modulatory roles in neuronal processes such as anxiety, learning, memory and perception of pain (Swanson, Bures et al. 2005). Because of these roles they are attractive drug targets for treatment of neuronal dysfunctions including seizures,

epilepsy, Parkinson's Disease and night blindness (Parmentier, Prezeau et al. 2002; Kew 2004; Dryja, McGee et al. 2005).

1.1.3. Allosteric Modulation in G Protein Coupled Receptors

With almost 50 - 60% of drugs in the market targeting GPCRs, they are one of the most important families of receptors in the drug discovery field. Most of the drugs developed in the past decade are agonists or antagonists that bind competitively to GPCRs, where "competitive" indicates the molecule binds at the same binding site as the endogenous ligand. Such drugs are often found to exert side effects. Recently, attention has been given to the development of drugs that do not target the orthosteric ligand binding site, but instead, bind to other sites on receptors and modulate receptor signaling. Such types of drugs are referred to as allosteric modulators. Binding of these modulators at the allosteric site is communicated to the endogenous or orthosteric ligand binding pocket via long-range conformational changes and these, in turn, affect receptor function. The modulation of receptor function is either positive or negative, stabilizing the active or inactive conformations of the receptors, respectively. Depending on whether the receptor function is enhanced or inhibited, the allosteric modulators are referred to as positive or negative allosteric modulators, respectively.

Developing allosteric modulators as opposed to orthosteric agonists and antagonists that directly target the endogenous or orthosteric ligand binding site is advantageous for several reasons. In the absence of the endogenous ligand most allosteric modulators do not exert any effect, thus preserving the physiological effects of the receptor (Christopoulos, May et al. 2004; May, Leach et al. 2007). As allosteric

modulators only act when the endogenous ligand is bound to the receptor, these ligands have the potential to exert fewer side effects, even when added in large excess, as compared to orthosteric ligands that directly affect signaling (Christopoulos, May et al. 2004). Further, as allosteric ligand binding sites are generally found to be located in non-conserved regions of receptors, as opposed to the highly conserved orthosteric ligand binding sites, it is possible to develop highly-selective ligands that can target subtypes of the receptors that are otherwise difficult to differentiate between (Christopoulos, May et al. 2004; Raddatz, Schaffhauser et al. 2007). In addition to this, allosteric modulators also provide a unique advantage in modulating the receptors that have peptides or small proteins as endogenous ligands. As these endogenous ligands are large and span an extensive area of interaction interface on the receptor, it is difficult to develop synthetic molecules that could directly target the orthosteric or endogenous ligand binding pocket (Jensen and Spalding 2004; Langmead and Christopoulos 2006; May, Leach et al. 2007).

Recent studies have reported allosteric modulators for almost all major subfamilies of GPCR (Table 1.1). For Class A receptors, allosteric modulators have been identified for many receptors and their subtypes including muscarinic, adenosine and adrenergic receptors. In particular, the muscarinic acetylcholine receptors are the best studied receptor type among the Class A receptors identified (Christopoulos, Lanzafame et al. 1998; Christopoulos and Kenakin 2002). As described above, in most members of Class A GPCRs, the endogenous ligand binding site is located in the TM domain near the EC side (Figure 1.2). Several structural studies have identified that the allosteric site comprises EC loops 2 and 3 and part of TM helix 7 (Krejci and Tucek 2001; Huang, Prilla et al. 2005; Prilla, Schrobang et al. 2006). In contrast, for the chemokine receptors

belonging to the same family where the endogenous ligand binding site is situated in the EC side, two allosteric binding sites have been proposed. One of them was located in TM helices 1, 3, 5 and 7 (Dragic, Trkola et al. 2000) and the other in the CP domain (Andrews, Jones et al. 2008).

Evidence presented in this thesis is mounting that there are also allosteric ligands for rhodopsin, the prototypic Class A GPCR (see above). This thesis work is the first indication of the presence of secondary ligands for rhodopsin, apart from the endogenous ligand *11-cis* retinal. This discovery was triggered by two recent studies. First, it was shown that the presence of the anthocyanin compound, cyanidin-3-glucoside (C3G) enhanced the rate of reaction of opsin with *11-cis* retinal, such that regeneration in rod outer segment preparations was increased (Matsumoto, Nakamura et al. 2003). Further, the chlorophyll derivative chlorin e6 (Ce6) enhances the sensitivity of deep-sea fish rhodopsin to light (Douglas, Partridge et al. 1999; Isayama, Alexeev et al. 2006). However, prior to the work reported in this thesis it was not known whether Ce6, C3G or any other secondary ligand apart from *11-cis* retinal physically binds to rhodopsin.

In the case of family B receptors, it was shown by mutagenesis studies that the allosteric small molecule ligand binding site is composed of TM helices 3, 5 for the corticotrophin releasing factor receptor (Liaw, Grigoriadis et al. 1997; Hoare, Sullivan et al. 2003) and helices 2, 3 for glucagon-like peptide receptor (Cascieri, Koch et al. 1999), towards the EC side of the receptors.

Finally, for family C GPCRs, in particular for mGluRs, it was shown by mutagenesis that allosteric modulators bind at the interface between the TM and EC domains similar to most of the endogenous ligand binding sites in class A GPCRs. The

allosteric ligand binding site was localized to TM helices 3, 5, 6 and 7 (Malherbe, Kratochwil et al. 2003; Malherbe, Kratochwil et al. 2003). It was also shown that allosteric mGluR ligands can either act as positive or negative modulators of mGluR activity in response to glutamate or glutamate analogs, enhancing or suppressing the responses, respectively (Goudet, Gaven et al. 2004). Small changes in the chemical structures of ligands were shown to switch their modulatory effects. For example, 4,4'-difluorobenzaldazine (DFB-4,4`) is a negative modulator for mGluR5, while 3,3'-difluorobenzaldazine (DFB-3,3`) is a positive modulator for the same receptor (O'Brien, Lemaire et al. 2003). For another member of this family, calcium sensing receptors, previous studies have shown that the allosteric ligand binding site is composed of the TM helices 2, 3, 6 and 7 (Hu, Mora et al. 2002; Petrel, Kessler et al. 2003; Miedlich, Gama et al. 2004).

1.1.4. G Protein Coupled Receptor Structures

Availability of three-dimensional structural information is central for structure based drug design studies. The first crystal structure of any GPCR was that of rhodopsin, a class A GPCR, published in 2000 (Palczewski, Kumasaka et al. 2000). Until 2007, rhodopsin, was the only GPCR with atomic level information available for the whole family of GPCRs. Recently, the atomic structures of 3 other class A GPCR members, A_{2A} adenosine receptor (Jaakola, Griffith et al. 2008), β_1 (Warne, Serrano-Vega et al. 2008) and β_2 (Rasmussen, Choi et al. 2007) adrenergic receptors has been published. In addition to these structures, the crystal structure of rhodopsin from an invertebrate organism, squid and other states of the vertebrate bovine rhodopsin, the activated Meta II (Salom,

Lodowski et al. 2006) and opsin (Park, Scheerer et al. 2008) state were also obtained. The overall structure of the transmembrane regions of the different crystal structures superimposed very well with the rhodopsin x-ray structure with the exception of squid rhodopsin. Squid rhodopsin did not align as well with either the dark state or opsin state structure of rhodopsin as compared to other crystal structures (Lodowski, Angel et al. 2009). TM helices 5 and 6 were extended and the CP loop 3 of squid rhodopsin had extra sequence in comparison to vertebrate rhodopsin. These differences were attributed to invertebrate specific signaling mechanisms (Mustafi and Palczewski 2009). The β_1 and β_2 adrenergic receptor (AR) was crystallized in complex with an antagonist, cyanopindolol and partial inverse-agonist, carazolol (Warne, Serrano-Vega et al. 2008). The major differences between the adrenergic receptor and the rhodopsin structures were mostly localized to CP loops, and were especially found in loops 2 and 3 and the EC loop 2. While the CP loop 2 of β_1 – AR adopts an alpha helical structure (Warne, Serrano-Vega et al. 2008), the same region in β_2- AR (Rasmussen, Choi et al. 2007) still remains in an extended conformation similar to rhodopsin CP loop 2 structure (Mustafi and Palczewski 2009). Furthermore, TM helix 1 of β_2- AR is straight and does not have a kink in the center of the helix as compared to rhodopsin. Remarkably, the EC loop 2 of both β_1 and β_2- AR forms an alpha helix towards the EC side in comparison to a beta sheet in rhodopsin. Furthermore, this loop is exposed to solvent in the adrenergic receptors but is highly buried in rhodopsin. In contrast to the rhodopsin and adrenergic receptor structures, the EC loop 2 of the A_{2A} adenosine receptor lacks secondary structure entirely (Jaakola, Griffith et al. 2008). Further, the ligand binding pocket of the adenosine receptor is located closer to helices 6 and 7, instead of helices 3, 5, and 6 in the case of

rhodopsin and adrenergic receptors. Apart from these differences the overall structural organization of the different receptors was similar to that of rhodopsin.

Table 1.1: Members of the major subfamilies of GPCRs exhibiting allosteric modulation. The data shown in the table is summarized from the work of other groups (May, Leach et al. 2007). The location of the orthosteric and allosteric ligand binding sites established for some of the receptors are mentioned respectively.

GPCR Family	Receptor Details	Endogenous Ligand Binding Site	Allosteric Ligand Binding Site
Family A	Adenosine A1, A2A, A3	TM helices 3,	EC
	Adrenoreceptors α–1, -2A, -2B, -2D		
	Chemokines CXCR1-4, CCR1,3,5	EC domain	TM and
	Dopamine D1, D2		
	Muscarinic M1-M5	TM helices 3,	EC and
	Serotonin		
Family B	Corticotropin Releasing Factor 1	EC domain	TM
	Glucagon	EC domain	
	Glucagon Like Peptide-1	EC domain	TM
Family C	Metabotropic Glutamate Receptors 1-5 and 7	EC domain	TM helices 3, 5, 6 and 7
	Calcium Sensing Receptor	EC domain	TM helices 3, 5, 6, and 7
	GABA-B	EC domain	

1.2. GOALS AND ACCOMPLISHMENTS

1.2.1. Open Questions

Previous studies have shown that the activity of many GPCRs is modulated by secondary ligands, which bind at a different site in comparison to the orthosteric ligand binding pocket. This may suggest that there are multiple ligand binding sites on GPCRs, conveying differential signaling effects. It is an important and unsolved general question to what extent the allosteric ligand binding pockets of different membrane receptors are conserved, as the homology between sequences is often very low, even when belonging to similar subtypes. In this thesis, I have focused on studying the binding and the effects of secondary or accessory ligands on the structure and dynamics of different GPCRs. Towards this end, I used a combination of computational and experimental biophysical and biochemical approaches. The questions addressed in this thesis are:

1. Where and how do allosteric ligands bind to GPCRs?
2. Is there a preferential binding of allosteric ligands to different structures/states of receptors?
3. How does ligand binding change receptor structure and dynamics?

We focused our efforts on studying the binding of the novel ligands, Ce6 and C3G to rhodopsin and the modulation of mGluRs by TM ligands. Addressing the above questions will help in understanding the mechanisms of conformational flexibility available in these receptors to accommodate different ligands. The long term goal is to

contribute to the mechanistic understanding of allosteric modulation in different types of GPCRs in general, with mGluRs and rhodopsin of particular interest.

1.2.2. Significance of the Study

The GPCR family is pharmacologically important as they allow targeting numerous biological functions through ligands that bind to them. Furthermore, dysfunctions and mutations of GPCRs are genetic causes for numerous diseases. They also play a role in cancer by cross-talking with epidermal growth factor receptors (Bhola and Grandis 2008) and are over-expressed in many tumor cells (Li, Huang et al. 2005). Despite being a major target in the drug discovery field, efforts focused on designing synthetic drugs that act as either agonists or antagonists for a specific subtype of receptor have failed to result in potential drugs. Previous efforts have mostly focused on drugs that bind in the same binding pocket as the natural ligand, which is highly conserved across different GPCRs and therefore difficult to target specifically. Recently, increased attention has been given to the understanding and development of drugs that bind at other sites, i.e. allosteric modulators. Studies on understanding the mechanisms of allosteric modulation may provide insights necessary for developing new therapeutic drugs that can selectively target subtype specific members of GPCRs.

The goal of this thesis was to enhance understanding of allosteric modulation of GPCRs in general, and of the molecular mechanism of rhodopsin activation in the presence of accessory ligands in particular. The results have significantly advanced the theory of conformational flexibility in different GPCR members to accommodate allosteric ligands in general. In this theory, we integrate the idea of structural coupling

between the three – EC, TM and CP – domains of GPCRs and allosteric modulation (Figure 1.5). While it is clear that every GPCR transmits the ligand binding signal occurring in the EC and/or TM domain to the CP domain via the TM domain, we propose the novel idea that it is possible to modulate this process at different points along this pathway using allosteric ligands. We propose that there are general ligand binding pockets that should in principal be available in all GPCRs (Figure 1.5). In some receptors, a particular pocket is orthosteric, while the same pocket becomes allosteric in others, depending on where the endogenous ligand binds. This implies a conservation of ligand binding pockets and the effects of ligand binding on conformational flexibility of the receptors. We have found evidence for this conservation in an in-depth study of the allosteric TM binding pocket of the Class C GPCR family mGluRs. We show that the allosteric ligand binding pocket is similar to the orthosteric TM binding pockets in Class A GPCRs. Furthermore, we provide evidence that active and inactive conformations are similarly stabilized in both cases. This finding has important implication for drug development in general, because we can potentially predict if a ligand would potentially inhibit or activate a particular GPCR, or serve as a negative or positive allosteric modulator, depending on the location of the orthosteric ligand binding pocket. Such ligands could be designed in a highly specific manner.

On the other hand, based on the structural coupling hypothesis above, we also proposed that there should be a allosteric ligand binding pocket in the CP domain (Figure 1.5), where normally the G protein binds. We provide experimental evidence that such a ligand binding pocket does exist in rhodopsin and can serve to allosterically modulate the receptor. Because all GPCRs bind the G protein in the CP domain, it is likely that this

binding pocket will be general for different GPCRs. Targeting this binding pocket could be developed into a novel way of activating or inhibiting this pharmacologically important class of receptors on a broad specificity basis. This may be useful for example in cancer drug development, where it could be useful to inhibit several GPCRs simultaneously to down regulate all pathways for crosstalk with the EGF receptor.

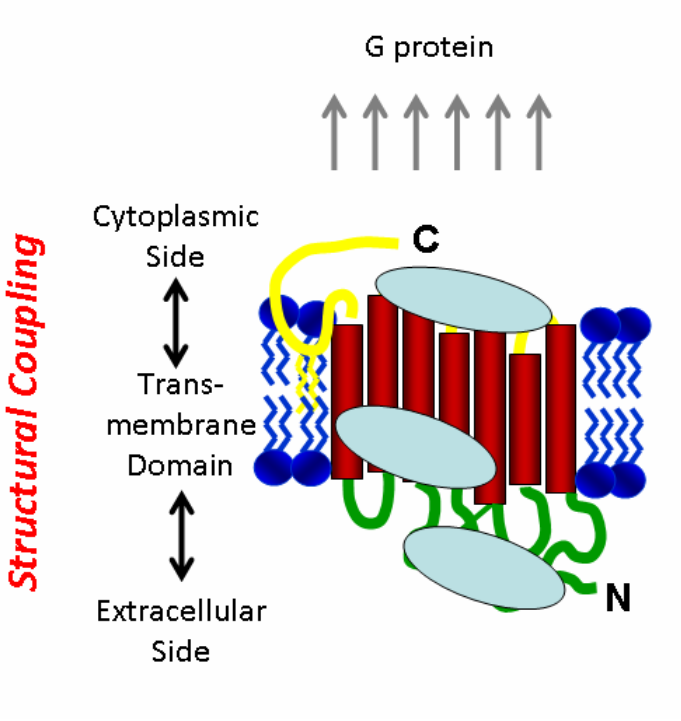

Figure 1.5: Schematic representation of structural coupling between EC, TM and CP domains in GPCRs. The different ligand binding sites are represented by blue filled ellipses.

1.2.3. Summary of Thesis Contributions

While allosteric modulators were known previously for all three major classes of GPCRs (Table 1.1), these were all ligands that bound mostly in the TM domain, at or near the

interface with the EC domain. Although the CP ligand binding allosteric site was predicted recently also by other groups for muscarinic receptors (Espinoza-Fonseca and Trujillo-Ferrara 2005), chemokine receptors (Andrews, Jones et al. 2008) and rhodopsin (Taylor, Barda et al. 2008), direct experimental evidence for binding has not yet been provided. Thus, further evidence for the existence of such allosteric sites in the CP domain is needed. The first major contribution of this thesis, contribution I, was to confirm the existence of a CP domain allosteric ligand binding pocket for rhodopsin. Furthermore, there was previously no framework to understand the relationship between orthosteric and allosteric binding pockets in GPCRs. In contribution II, I showed that the allosteric TM ligand binding pocket in mGluRs corresponds in structure and function to the orthosteric TM ligand binding pocket in rhodopsin. To further test the idea of the generality of ligand binding pockets across GPCR, in contribution III, I showed that rhodopsin whose orthosteric ligand binds in the TM domain binds chemokine, a ligand that binds in the EC domain. The approaches used for my studies were a combination of computational and experimental methods, but not all of the methodology was ready to be applied to the systems investigated. In contribution IV, I therefore combined different NMR spectroscopic approaches developed in other contexts to create a suite of NMR spectroscopic tools suitable to study ligand binding and conformational changes in membrane receptors.

Each contribution I-IV is summarized below, and is described in detail in subsequent chapters 2-5.

I. The existence of a cytoplasmic, allosteric ligand binding site in rhodopsin was demonstrated.

   a. Rhodopsin as a primary target of interaction for two ligands, C3G and Ce6, was demonstrated using fluorescence and selective excitation ^{1}H NMR spectroscopy. These studies showed differential interaction affinities of Ce6 and C3G for dark and light-activated states of rhodopsin.

   b. The location of interaction of these accessory chromophores was localized to the CP domain. Docking studies of these accessory ligands showed a strong preference for docking of ligands to the CP domain. This prediction is experimentally supported by evidence from 1D ^{1}H NMR of unlabeled rhodopsin and 2D ^{15}N-lysine labeled rhodopsin studies. These studies also suggest that binding modulates rhodopsin's structure and dynamics in both the dark and light-activated states. These studies in the case of Ce6, were further validated by labeling with ^{19}F at specific sites in the CP domain.

   c. An effect of C3G and Ce6 ligands on rhodopsin function was also established. C3G binding enhanced the regeneration rate of rhodopsin from opsin and *11-cis* retinal as monitored by absorbance spectroscopy. However, C3G binding exhibited little to no effect on G_t interaction with rhodopsin. In contrast, GTPγS filter binding and fluorescence studies showed that Ce6 binding greatly interferes with G_t binding to rhodopsin. Molecular modeling studies suggested that the predicted Ce6 ligand binding pocket highly overlaps with the G_t interaction site on rhodopsin, serving as evidence for the observed effects on G_t activation.

d. Stability and thermal denaturation studies suggest that C3G binding destabilizes the overall structure of rhodopsin. Further, these effects were attributed to be the underlying mechanism for the observed increased regeneration rates. In the case of Ce6, ^{19}F NMR studies monitoring time-dependent changes upon light-activation of two selectively-labeled sites in the CP domain showed modulation of conformational states of rhodopsin.

e. Application of ^{19}F NMR approaches to study dynamics of selectively labeled sites in rhodopsin was demonstrated for the first time. A significant change in the flexibility of one of the sites, at residue Cys-316 was demonstrated upon binding to Ce6. The ^{19}F NMR results together with the ^{1}H NMR studies (see b, above) collectively suggest that molecular mechanism by which Ce6 binding inhibits G_t activation may be due to the faster conversion of light-activated state to an opsin-like inactive state.

f. NMR data acquired using α-ε-^{15}N tryptophan labeled rhodopsin demonstrated that the structure of TM domain in rhodopsin is allosterically modulated upon binding to Ce6 and most likely induces conformation flexibility in this domain.

II. The structural and functional similarity between orthosteric and allosteric ligand binding pockets was demonstrated.

a. By docking allosteric modulators to active and inactive homology models of mGluRs, which are class C GPCRs, based on structures of rhodopsin, a class A GPCR, it was demonstrated that positive allosteric modulators (PAMs) and negative allosteric modulators (NAMs) of mGluRs

preferentially bind to class A-GPCR like active and inactive states of the receptor, respectively.

b. 3,3`-difluoro-benzaldazine (DFB-3,3`), a positive allosteric modulator of mGluR5, was shown to interact with rhodopsin. DFB-3,3` was predicted to bind at the same binding site as *11-cis* retinal using molecular modeling studies. The total amount of rhodopsin regenerated decreased after addition of DFB-3,3` in a concentration-dependent manner. This supports the idea that both *11-cis* retinal and DFB-3,3` may occupy the same binding pocket.

III. A chemokine ligand was found to bind to rhodopsin, indicating rhodopsin has a capacity for allosteric modulation in the extracellular domain.

a. An interaction between the chemokine ligand CXCL11 and rhodopsin was presented for the first time. The interaction was predicted using machine learning approaches, and experimentally validated using chemotaxis assays. Binding of chemokine to rhodopsin inhibited G_t activation.

b. From computational docking studies, we predicted CXCL11 to bind near the extracellular domain of rhodopsin. Further, comparisons of the interaction of chemokine ligand with chemokine receptor and rhodopsin showed similar interaction, involving extracellular loop 2. Previous studies on chemokine receptors indicated that the E2 loop by itself is capable of interacting with CXCL11 and inducing chemokine activity, confirming that molecular docking studies can be used to successfully predict ligand protein interaction sites in these receptors.

IV. We developed a suite of NMR spectroscopic tools applicable to membrane receptors in detergent micelles.

a. We extended the 1D proton based ligand screening method previously demonstrated for soluble proteins, to membrane proteins, by combining it with a selective excitation scheme to overcome the constraints posed by detergent micelles.

b. As the ^{1}H-based approach (a) may sometimes lead to overlapping signals between protein(s) and ligand(s), we also developed a ligand-based screening method for ligands labeled with ^{19}F. In this approach, the signal comes uniquely from the ligand as there is no ^{19}F background in proteins.

c. The above methods (a and b) were successfully applied to study the interactions of C3G and Ce6 with rhodopsin. We also showed that such approaches may be used as screening tools for receptor ligands. Both *in vivo* and *in vitro* based approaches were demonstrated as a proof of principle for a set of ligands labeled with ^{19}F.

CHAPTER - 2
EXPERIMENTAL PROCEDURES

TABLE OF CONTENTS

2.1. PREPARATION OF MATERIALS

All operations involving rhodopsin were carried out under dim-red light illumination unless otherwise stated. Buffer designations are listed in Table 2.1 at the end of this chapter (pg. 57).

2.1.1. Urea-washed ROS Membranes

ROS membranes were prepared from frozen bovine retinae, purchased from W. A. Lawson Co. (Lincoln, NE) as described (Papermaster 1982). The thawed retinae were homogenized in two batches with each 15 ml of buffer A containing 30% sucrose by vortexing for 1 min. Centrifugation (4500 rpm, 6 min, SA600 rotor) yielded a supernatant and a pellet, which was suspended by vortexing in 15 ml buffer A, 30% sucrose. After centrifugation as above the

combined supernatants were slowly mixed with one volume of buffer A. The crude ROS were pelleted (10000 rpm, 10 min, SA600 rotor) and then homogenized using a manual homogenizer in a total volume of 40 ml buffer A, containing 15% sucrose. Two 20 ml fractions of the homogenate were underlayed with 10 ml of 0.64 M sucrose in buffer A utilizing a long needle. After spinning the samples (10 min, 10000 rpm, SA600 rotor), the pellet was suspended in a total volume of 20 ml 0.64 sucrose in buffer A by manual homogenization with a pestle and by passage through a No. 23 gauge needle. 4 sucrose gradient tubes were prepared in Beckman ultra clear centrifuge tubes in the cold room, as follows. 9 ml of 0.78 M sucrose in buffer A was underlayed slowly at the base of the tubes with 1 M sucrose, buffer A, then with 1.2 M sucrose in buffer A. The crude ROS were carefully overlayed on top of each gradient, centrifuged (25000 rpm, 45 min, 4°C, SW28 rotor) and the 0.78M/1M interface was recovered by aspirating using a No. 18 needle. The ROS membranes were diluted to 50 ml with buffer A, pelleted (20000 rpm, 30 min, rotor Ti45) and suspended in buffer A using the pestle and the No 23 needle to refine the vesicles. The suspension was centrifuged (30000 rpm, 4°C, 20 min, Ti45 rotor). The pellet was washed again with buffer A before suspended in buffer B and the vesicles refined as above to give a final volume of 25 ml each tube. The suspension was end-over-end mixed at 4°C for 1 hour, followed by dilution with 2 volumes of buffer C and centrifugation (35000 rpm, 4°C, 45 min, Ti45 rotor). The pellet was washed 3 times with 70 ml of buffer C by manual suspension as described above followed by pelleting at 35000 rpm for 30min. After the final wash the ROS were suspended in 15 ml of buffer D. This ROS suspension was stored in aliquots of 250µl at -70°C after snap-freezing in liquid nitrogen.

2.1.2. Transducin

G_t was purified from bovine ROS as described (Baehr, Morita et al. 1982). All steps were carried out on ice in the light. Each vial of 50 retinae was divided into 2 x 50 ml Falcon tubes. Each fraction was homogenized in 15 ml of buffer A containing 30% sucrose by vortexing for 1 min. After spinning at 4500 rpm for 6 min using an SA600 rotor, the supernatant was kept separately and the pellet resuspended by vortexing in 15 ml of buffer A containing 30% sucrose. After spinning as above, all supernatants were combined and slowly mixed with one volume of buffer A. The crude ROS were pelleted (10000 rpm, 10 min, SA600 rotor). The pellet was homogenized using a manual homogenizer in a total volume of 40 ml of buffer A containing 15% sucrose. Two 20 ml fractions of the homogenate were underlayed with 10 ml of 0.64 M sucrose in buffer A utilizing a long needle. After spinning the samples (10 min, 10000 rpm, SA600 rotor), the pellet was resuspended in a total volume of 20 ml of buffer A containing 0.64 sucrose solution by manual homogenization with a pestle and by passage through a No. 23 gauge needle. 4 sucrose gradient tubes were prepared in Beckman ultra clear centrifuge tubes in the cold room as follows: 9 ml of 0.78 M sucrose in buffer A was under-laid with 1 M sucrose in buffer A, then with 1.2 M sucrose. About 5 ml of crude ROS were carefully overlaid on the top of each gradient. The balanced tubes were centrifuged (25000 rpm, 45 min, 4^{o}C, SW28 rotor). The 0.78M/1M interface was recovered by aspirating and diluted to 50 ml with buffer A. The ROS solution was centrifuged (20000 rpm, 30 min, rotor Ti45) and washed 4 times with buffer J, each resuspension followed by passage through a No. 23 needle. $G_{t(\alpha\beta\gamma)}$ was then extracted by

three further washes with buffer Fcontaining 100 μM GTP. This extract was applied to either a hexylagarose or a DE52 column.

A 6 ml (6 cm x 1.5 cm) hexyl agarose column (ICN) was equilibrated with buffer J. The GTP extractions were applied to this column at a flow rate of 0.3 ml/min. The column was then washed with buffer F containing 100 mM NaCl until reaching the pre-wash base-line of the equilibration (removal of GTP). At this point buffer F was supplemented with 300 mM NaCl and 1 ml-fractions were collected. Fractions containing the 280 nm peak were pooled and dialyzed o/n against 1 l of buffer K. The protein was stored in 200 μl aliquots at -20^{o}C.

As an alternative to purification on hexyl agarose, 50-100 ml of DE52 (a pre-swollen microgranular anion exchanger, Whatman) was end-over-end mixed o/n with 0.5 - 1 M of Tris pH 7.5 at 4^{o}C. After allowing the slurry to settle, the supernatant was decanted to remove any fines. The resin was then washed with water by vacuum filtration to lower the salt concentration. The ion exchanger was re-suspended in buffer F (1:1) and poured into a 3x23 cm column (50 ml bed volume). The column was pre-equilibrated with 5-10 volumes of buffer F prior to application of the GTP extractions. The flow rate was 0.6 ml/min. GTP was removed with buffer F containing 100 mM NaCl and the G-protein was eluted with buffer F containing 500 mM NaCl.

2.1.3. Expression of Rhodopsin in HEK293 Cells Grown in Suspension

Cells stored in liquid nitrogen were thawed as quickly as possible by placing vials in a 37^{o}C water bath after removal from liquid nitrogen. The cells were transferred to a 15 ml Falcon tube and slowly (over 2 min) 10 ml of buffer I medium was added to allow slow diffusion of the cryo-

preservative DMSO from the cell. Cells were pelleted at 1K for 10 min, the supernatant was aspirated and 10 ml of fresh buffer I medium was added. The cells were resuspended and transferred to a 10 cm tissue culture dish and incubated at 37^{o}C, 5% CO_2 (Forma model #3956) in buffer G medium, supplemented with L-glutamine/ Penicillin/Streptomycin (buffer H medium) and 10% fetal bovine serum (buffer I medium). Buffer G medium was purchased as a powder mixture (Irvine Scientific). After dissolving, it was supplemented with 3.7g $NaHCO_3$ per liter of media. Cells were maintained at about 90% confluence maximum to avoid damage to the cells by overgrowth. Cells were fed every three to four days, until ~80-90% confluence was reached. After approx. 3 days the confluent cells were split typically 1:5.

After removal of the medium, plates are washed with 8ml buffer F. 4.5ml buffer F, 0.5ml 10x trypsin (0.05%), 0.2% EDTA was sequentially added and the cells were left to detach from the plates. Cells were then transferred into the appropriate volume (20ml medium per plate) of buffer I media. The mixture was then added to new plates (20ml/plate). Cells were confluent after approx. 3 days for a 1:5 dilution.

Suspension cultures were set up using 2-liter spinner flasks containing 500 ml media as depending on whether isotope and non-isotope labeled material was to be prepared. For non-labeled material, cells were grown in buffer H medium, containing 10% fetal bovine serum. For isotope labeled material, media were in composition according to buffer G media formulation. However, since certain amino acids had to be omitted, the media were prepared from individual components. Thus, all solutions were prepared as 100x concentrated stock solutions, except glucose, NaCl, glutamine and the isotope labeled amino acid, which were added as solids. Deviations from the buffer G media formulation were as follows. 1. The glutamine concentration

was lowered by ½. The same amount was then added on day 5 or 6, together with the other additions described above. 2. The $CaCl_2$ concentration was lowered to 50 mg/l (Eilers, Reeves et al. 1999). Isotope labeling also required the serum to be dialyzed to remove any amino acids. Thus, e.g. 500 ml fetal bovine serum was dialyzed 3-times against 10 l buffer J at 4°C with a tubing cut off of 1 kDa as described (Eilers, Reeves et al. 1999). For both, labeled and unlabeled material, the media were supplemented with 0.1% Pluronic F-68, 50 μg/ml heparin. Spinner flasks were inoculated using three-four 15 cm tissue-culture dishes confluent with cells (6-9 x 10^7) per 500 ml of media and incubated at 37°C in a humidified incubator. After 5-6 days, when the media turned yellow, the culture medium was further supplemented with 6 ml of 20% (w/v) glucose and 4 ml of 8% (w/v) $NaHCO_3$, 5mM sodium butyrate. Cells were fed daily with glucose solution until the cells were harvested (usually on day 8). Cells were transferred to centrifuge vials equilibrated at 4°C and the spinner flask was rinsed with 2x50 ml of ice-cold buffer J and combined with the main culture. After centrifugation for 10 min at 4K, 4°C, in a Sorvall RC-3B centrifuge, the supernatant was immediately decanted and the cells kept on ice. 25 ml of ice-cold buffer J was added and the cells were resuspended. After transfer to a 50 ml Falcon tube, a further 25 ml was used to rinse the centrifuge pot and added to the Falcon tube. Cells were pelleted by centrifugation at 4°C. The wet-weight of the pellet was recorded and the cells resuspended in a final volume of 20 ml buffer J.

2.1.4. Preparation of *11-cis* Retinal

Opsin produced in HEK293 cells required reconstition with *11-cis* retinal. *11-cis*-Retinal was a gift from Dr. Rosalie Crouch (University of South Carolina and the National Eye Institute of the

National Institutes of Health, U. S. Public Health Services). It was also prepared from all-*trans* retinal following a published procedure (Knowles and Priestley 1978). Approx. 100 mg all-*trans* retinal was dissolved in 50 ml ethanol at approx. 5 mM concentration and cooled to 4^{o}C. This solution was irradiated with a 300 W >435nm light for 20-30 min. The resulting isomer mixture was dried under Argon in a water bath. The dry residue was dissolved in 10-20 ml hexane containing 6% ether. The solution was filtered through a 0.2 μm filter before injection in 4 ml batches into a Dynamax-60A (Si 83-121-C, 21.4mm x 300mm) silica column. Retinal isomers were separated in hexane containing 6% ether at a flow-rate of 8 ml/min. A separation profile is shown in Figure 2.1. The effluent was collected in the dark and evaporated to dryness under argon using a water bath. After dissolution of the residue in ethanol, the concentration of *11-cis* retinal was determined by absorbance spectroscopy (see below, pg. 42). The extinction coefficient used for *11-cis* retinal in ethanol at $A_{379.5}$ was 24,940$M^{-1}cm^{-1}$ and for all-*trans* retinal in ethanol at A_{383} 42,884$M^{-1}cm^{-1}$ (Knowles and Priestley 1978).

2.1.5. Reconstitution of the Opsin Expressed in HEK293 Cells with *11-cis* Retinal

Cell pellets from a 500 ml culture were resuspended in 20 ml of buffer J containing benzamidine (0.005%) and PMSF (0.7 mM). Cells harvested from plates were resuspended in 2ml buffer J per plate. *11-cis* Retinal was added to give 5 μM concentration and the suspension was incubated for at least 1.5 hours. The concentration of reconstituted mutant rhodopsin was estimated by UV/Vis absorbance difference spectrum analysis of an aliquot solubilized in buffer J containing 1% DM. Addition of *11-cis* retinal was repeated until no further increase at A_{500} was observed by difference spectroscopy.

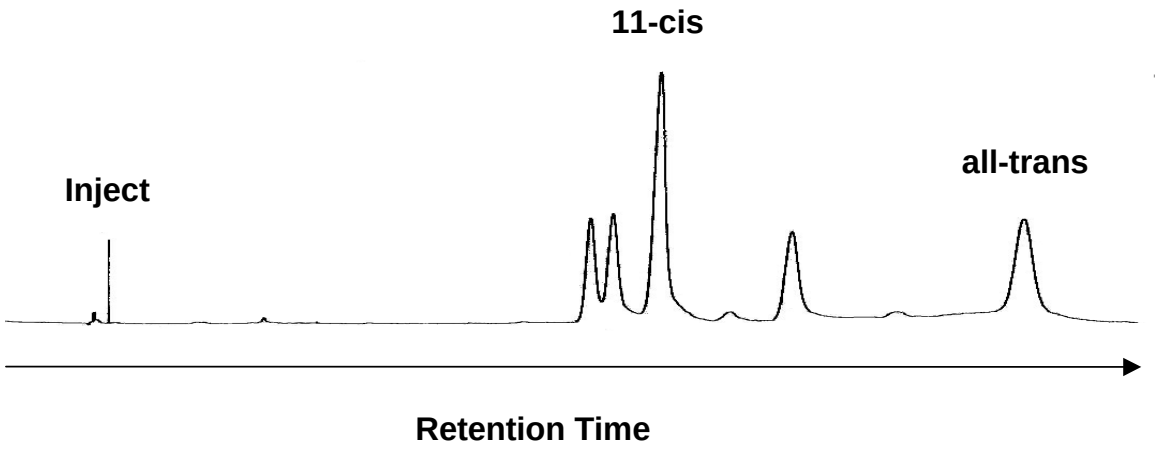

Figure 2.1. Preparation of *11-cis* retinal. Shown is an HPLC profile of the isomer mixture produced by irradiation with >435nm light. Peaks are labeled with their respective isomers.

2.1.6. Solubilization of Cell Pellets Containing Rhodopsin by Use of Detergents

For solubilization in DM, the rhodopsin containing cells or ROS membranes were end-over-end mixed for 1 hour in buffer J containing 1% DM. The volumes used for solubilization depended on the rhodopsin source. ROS membranes were solubilized at a final rhodopsin concentration of 1 mg/ml. HEK293 cells were solubilized at 10ml buffer/g wet pellet. Unsolubilized material was removed by centrifugation for 30 min at 4^{o}C, 35,000 rpm, rotor 60Ti or 45Ti, Beckmann Ultra Centrifuge, or for volumes <1ml 10 min at 35,000 rpm, rotor TLA100.3. The supernatant was added to 1D4-Sepharose beads as described below in Section 2.1.7.

For solubilization in OG, rhodopsin was solubilized in buffer J containing 4% OG as described above for solubilization using DM.

2.1.7. Affinity Chromatography of Rhodopsin Using 1D4-Sepharose

2.1.7. (a) Preparation of 1D4-Sepharose

CNBr-activated sepharose 4B was prepared from CNBr and sepharose 4B (Kumel, Daus et al. 1979), based on the rapid reaction of cyangen halides with the hydroxyl groups of carbohydrates at high pH to form cyanate esters (Figure 2.2). The monoclonal anti-rhodopsin antibody 1D4 (Oprian, Molday et al. 1987) was then coupled to CNBr-activated sepharose 4B via its amino groups (Oprian, Molday et al. 1987) with minor modifications.

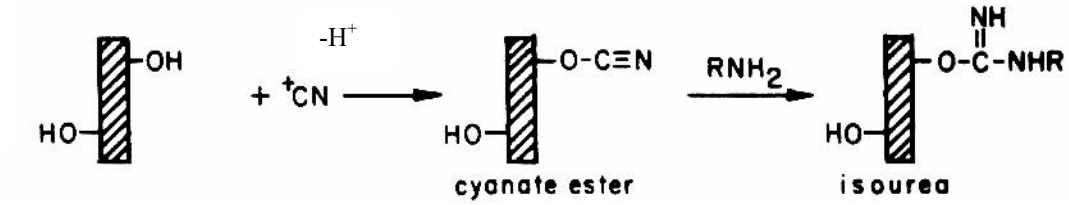

Figure 2.2: Activation of sepharose by CNBr and coupling of protein to the activated gel. This figure is taken from ref.(Kohn and Wilchek 1978).

Prior to coupling, 1D4 was purified from a myeloma cell line provided by R.S. Molday (University of British Columbia) as follows. 1500 mg 1D4 antibody (stored at -20°C) were

thawed. 300 ml of Protein A-sepharose 4B were packed and equilibrated with 5 times the bed volume of buffer K. All flow rates were between 0.5-1.5 ml/min, unless otherwise stated. The sample was diluted with 5 times its original volume of buffer K. The sample was loaded, followed by washing with buffer K until a straight baseline at A_{280} was reached. The sample was eluted with approximately 300 ml of buffer L. Fractions of 4ml each were collected while monitoring A_{280}. In order to store the column for future use, it was regenerated with 300ml buffer M at a flow rate of 0.5ml/min. The column was stored at 4°C after washing with 2-10 times the bed-volume of buffer N. Due to the poor stability of 1D4 at pH 3, the pH of the fractions was immediately after elution adjusted to pH 8.3 using 0.5 M $NaHCO_3$ pH 10. Fractions containing 1D4 sepharose were combined and used directly for coupling, as long as the concentration of 1D4 was above 3 mg/ml. If the concentration was lower, the solution was first concentrated to up to 10 mg/ml before coupling. The concentration of antibody was determined using A_{280} (A_{280} = 1.383 is equal to a concentration of 1mg/ml). Dialysis tubes (Spectrapor, 14 kD cut-off, but could be higher) were washed thoroughly with *aqua dest*. and filled with the 1D4 solutions. Dialysis was against 5-10 l of buffer O 4 hours to overnight. Dialysis buffer was subsequently changed at least 3 times. After dialysis, the concentration was determined using A_{280} as above.

The purified 1D4 antibody was coupled to CNBr sepharose as described below. First, 20 ml CNBr-Sepharose was prepared. 100-200 mg of 1D4 antibody can be bound to this amount of CNBr-Sepharose. If 100 mg of 1D4 was coupled the capacity of the final product was typically 1mg rhodopsin/ml of 1D4 sepharose. 500 µl acetonitrile was added per 1 g of BrCN (Sigma). The volume increased after dissolving the BrCN, so that the final concentration was 1g/ml. This stock solution could be stored at –20°C. 20 g of Sepharose 4B slurry (Sigma) was washed three

times with water in a filter funnel. 20 g of sepharose corresponds to 30 ml of slurry. Water was removed by vacuum and the sepharose was added to 30 ml of buffer P. While stirring vigorously with a regular stirring bar under the hood, 1 ml of BrCN-solution was added and stirred for exactly 2 min. The suspension was transferred quickly to the filter funnel that contained ice-cold water and was vacuum-filtered immediately. The beads were washed with 300 ml of ice-cold buffer Q followed by 500 ml 1 mM HCl. All the washes were carried out extremely rapidly, i.e. such that vacuum-filtering of 100 ml took less than 30 seconds. Thus prepared CNBr-sepharose could not be stored. Coupling to 1D4 had to follow immediately after preparation, ideally within 2 min. If CNBr-sepharose was purchased from Pharmacia, 1g of the dry powder CNBr-sepharose was equivalent to approx. 3.5ml gel slurry. The dry CNBr sepharose was washed on a sintered glass filter with 500 ml of 1mM HCl. All subsequent steps were the same for commercially available or self-made CNBr sepharose.

The coupling to 1D4 to CNBr sepharose was carried out at 3-10mg 1D4 per 1ml CNBr-sepharose 4B. 20 ml slurry was added to the concentrated sample of 1D4 containing 100 mg 1D4 in buffer O. Coupling was allowed to proceed by end-over-end mixing at until the supernatant after spinning down the beads for 5min contained less than 5% of the total protein (after 4-5 hours at RT). The supernatant was discarded. A volume equal to that of the original supernatant of blocking agent (1M ethanolamine pH 8) was added. Blocking was allowed to proceed for 2 h at RT or overnight at 4^{o}C. The beads were washed on a sintered glass filter 4 times with alternating solutions of buffer O and buffer R. Buffer J containing 0.05% NaN_3 was added in equal volume as the beads. The coupled 1D4-sepharose was stored at 4°C.

The capacity of 1D4-Sepharose was determined as follows. 500μg ROS membranes were solubilized using DM as described in Section 2.1.6 above (pg. 36) and the exact concentration was determined spectroscopically (as described below, pg. 42). 200μl of 1D4-sepharose were added and rhodopsin was purified as described in Section 2.1.7 and 2.1.9 below. The capacity was calculated using the ratio between the rhodopsin purified and the amount of rhodopsin originally solubilized. Typically the capacity was 1 mg rhodopsin per 1 mg 1D4-sepharose if 100 mg of 1D4 was coupled to 20 ml of CNBr-sepharose. A capacity of up to 1.7 mg/ml could be obtained if correspondingly larger amounts of 1D4 were used.

2.1.7. (b) Binding of Solubilized Rhodopsin to 1D4-Sepharose

After centrifugation of non-solubilized material (Section 2.1.6 above, pg. 36), the supernate was added to 1D4-Sepharose. The amount of beads necessary to bind quantitatively the rhodopsin present in the supernate could be calculated from the 1D4 sepharose binding capacity, usually 1 mg of rhodopsin per ml settled beads. About 10% excess of 1D4-Sepharose over rhodopsin content was used. After end-over-end mixing for at least 6 hours at $4^{o}C$, the suspension was packed into a column. For 10-15 mg of rhodopsin to be purified the dimensions of the column were 2.7 cm diameter x (2 to 3) cm. If smaller amounts were purified, i.e. 100-500 μg, Biorad disposable chromatographic columns were used. The packed beads were washed at RT with at least 50 column volumes of buffer J, containing 0.88% OG or 0.05% DM, for purification in OG or DM, respectively. This was followed by further washes with 10 bed volumes of buffer E, containing 0.88% OG or 0.05% DM, for purification in OG or DM, respectively. The flow rate was 0.5-1 ml/min.

2.1.8. ^{19}F Derivatization of Rhodopsin Bound to 1D4-Sepharose using TET

After the washing described in Section 2.1.7 (b) above, the total beads containing ~10 mg bound rhodopsin were resuspended in 40 ml of buffer E and 4-PDS was added from a 1 M stock solution in ethanol to give a final concentration of 1 mM. After end-over-end mixing for 5 min at RT, excess reagent was removed by multiple washing with 40 ml of buffer E under slight Argon pressure. A total of at least 35 times the column volume of buffer E was used. Complete removal of 4-PDS was tested spectrophotometrically, by monitoring the absorption at 323nm upon addition of 1mM DTT. After a flat baseline was observed at 323nm, the beads were then resuspended in 30 ml of buffer E and TET (3 μl of 11.2 M) was added to give a final concentration of approximately 1 mM. After end-over-end mixing for several hours at RT, excess reagent was removed as described above for 4-PDS removal.

2.1.9. Elution of Rhodopsin from 1D4-Sepharose

Unlabeled and TET labeled rhodopsin were eluted from 1D4-Sepharose using buffer E containing 70 μM epitope nonapeptide at a flow rate of 0.3-0.35 ml/min, the effluent being monitored by UV/Vis absorption spectroscopy. Complete elution of the rhodopsin mutants usually required ~5 column volumes of elution buffer. The elutions where A_{280}/A_{500} ratio's within the range 1.6 – 2.2 were considered for further studies, ensuring proper folding of rhodopsin.

2.1.10. Concentration and Buffer Exchange of Rhodopsin for Solution NMR Analysis

Fractions from 1D4-immunoaffinity chromatography containing >0.2 μM rhodopsin (A_{280}/A_{500}, 1.6-1.8) were pooled and concentrated using the membrane filter Ultracel-30 (Amicon). About 6-10 mg amounts of rhodopsin were concentrated to final volumes of 0.05-0.1 ml.

For analysis of rhodopsin by ^{19}F NMR spectroscopy, after concentrating as above, the solvent was exchanged to buffer S by the addition of 1 ml buffer S, followed by membrane filtration to a volume below 0.1 ml as above. This operation was repeated three times. The final volume was then adjusted to 0.3 ml with buffer S. TFA was added from a 50 mM stock solution (in D_2O) to give a final concentration of 0.2 mM.

For analysis of isotope labeled rhodopsin by heteronuclear and ^1H NMR spectroscopy, after concentrating as above, the solvent was exchanged to buffer S by membrane filtration as described above. The final volume was adjusted to 0.3 ml with buffer S.

2.2. SPECTROSCOPIC TECHNIQUES

2.2.1. Absorbance Spectroscopy

A Perkin–Elmer λ-25 spectrophotometer, equipped with a multiple water-jacketed cuvette holder was used to record absorption spectra. All spectra were measured at 20°C unless otherwise specified. All measurements were recorded in the 250nm to 650nm range, using a 10mm path length cell, bandwidth of 1nm, with a response time of 1s and scan speed of 960nm/min.

Rhodopsin concentrations were calculated using a molar extinction coefficient of the 500 nm chromophore absorption of 40,600 $M^{-1}cm^{-1}$ (Wald and Brown 1953). A_{500} was determined either directly from absorbance spectra of pure rhodopsin solutions, or for solutions with a high absorbance background, i.e. solubilized membranes, by absorbance difference spectroscopy. First, the dark spectrum was recorded. The rhodopsin solution was illuminated (see below) and the spectrum was again recorded. The difference between the two spectra allowed estimation of A_{500} and the concentration of rhodopsin was calculated as above.

For light-activating rhodopsin, the samples were illuminated with a 150-W fiber optic light (Fiber Lite A-200; Dolan-Jenner, Woburn, MA) equipped with a > 495 nm long-pass filter for 30 sec.

2.2.2. NMR Spectroscopy

All operations were carried out in the dark, unless otherwise stated. ^{19}F NMR spectra were recorded on a Bruker 600MHz spectrometer using a $^{19}F,^{1}H,^{15}N$ TXO 5mm triple gradient probe. Data acquisition and analysis was carried out using TopSpin Version 2.0 Software. The sample was locked on deuterium. The relaxation delay was 0.5 sec. Line broadening was 20 Hz. An internal standard, TFA was used as control or reference in each case. Acquisition time, number of scans averaged and specific parameters were as indicated in the text or legends.

For the ^{19}F dynamics study, longitudinal relaxation experiments were conducted using the Freeman-Hill method (Freeman and Hill 1971) with relaxation delays of 0.0, 0.05, 0.1, 0.15, 0.2, 0.25, 0.3, 0.4, 0.5, and 0.6 s. Transverse relaxation experiments were performed using a Carr-Purcell-Meiboom-Gill (CPMG) pulse sequence (Carr and Purcell 1954; Meiboom and Gill 1958)

with a half duration of CPMG pulses of 0.3 ms. Relaxation rates were determined by recording a series of spectra with the relaxation delays of 0.0, 1.2, 2.4, 3.6, and 4.8 ms (R_2). All experiments were conducted with ^{1}H decoupling during acquisition periods. Both longitudinal and transverse relaxation rate constants were determined at 10, 15, 20, 25, 30, and 35°C.

The 1D ^{1}H selective excitation NMR spectra were recorded at a spectrometer ^{1}H frequency of ~800 MHz at the Structural Biology Department, University of Pittsburgh using a Bruker spectrometer. The details of the acquisition of 1D selective excitation ^{1}H NMR spectra are as follows. As the samples contained detergent micelles, a selective excitation scheme with sculpting, using a double pulse field gradient spin echo sequence (DPFGSE) as described previously (Hwang and Shaka 1995; Stott 1995) was used. Each spectrum was obtained after applying two hyperbolic secant shaped pulses of length 2.8ms and 1.9ms, following a 90^o hard pulse of 9.9μs at 0.5db over a spectral width of 35ppm. A delay of 0.5sec between each scan was used. A total of 2048 scans were averaged to obtain the final spectrum except for pH titration experiments of C3G, where a total of 512 scans were recorded at each pH value. The total acquisition time was ~ 29min, 7min and 2.2min to acquire 2048, 512 and 160 scans, respectively. A line broadening of 0.3Hz or 1Hz was used to process the final spectra.

^{1}H-^{15}N HSQC NMR spectra of α-ε-^{15}N-tryptophan and α-^{15}N-lysine labeled rhodopsin were obtained at a spectrometer frequency of ~900 MHz and ~800MHz Bruker spectrometer mentioned as above, respectively. Data acquisition and analysis was then carried out using Topspin Version 2.0 Software. Different pulse sequences were used as indicated in the text.

The illumination of the NMR samples was carried out as explained above (refer to Section 2.2.1, pg. 43) by placing the light source ~1cm away from the NMR tube.

2.2.3. Fluorescence Spectroscopy

Tryptophan fluorescence of rhodopsin was recorded using a Varian Cary Eclipse instrument. In all experiments, the data acquisition parameters were similar to those described previously (Farrens and Khorana 1995): excitation and emission wavelengths were at 295nm and 330nm, with slit widths of 5nm and 10nm, respectively. Samples contained 0.25μM or 0.5μM (as indicated) of purified rhodopsin in 0.05% or 0.6% DM (as indicated) either in the absence or presence of additives and the fluorescence was measured in the dark and after illumination. The sample temperature was always kept at 20^{o}C unless otherwise specified.

For thermal denaturation experiments, the temperature was raised to 55^{o}C and changes in fluorescence were measured at this constant elevated temperature.

For highly absorbing species, fluorescence values were corrected for absorbance, as described in specific analytical procedures, Section 2.4.5, below.

2.3 MOLECULAR MODELING AND DOCKING STUDIES

2.3.1. Homology Modeling

All homology models were built using MODELLER software (Sali, Potterton et al. 1995; Fiser and Sali 2003). The generated models in each case were further evaluated using MOLPROBITY (Davis, Murray et al. 2004) for structural constraints.

The homology model of the chemokine receptor CXCR3 was generated based on the rhodopsin dark state crystal structure (PDB id: 1L9H) as a template.

A three-dimensional model of the G_t peptide (VLEDLKSCGLF) was built by homology modeling based on the NMR structure of the G_t C-terminal peptide IRENLKDSGLF (340-350) (PDB id: 1LVJ)(Koenig, Kontaxis et al. 2002) as the structural template.

2.3.2. Protein – Ligand Docking

2.3.2. (a) Docking with ArgusDock: All ligands were docked to inactive and active models of the respective receptors using ArgusLab software, version 4.0 (Thompson ArgusLab 4.0.1). Ligand pdb files were generated using JME Molecular Editor software (http://www.cambridgesoft.com/software/ChemDraw/). Hydrogen atoms were added to the ligand coordinate file prior to docking using ArgusLab. The docking between each receptor subtype and ligand was performed using the "Dock a ligand" option. All the residues of the receptor were defined to be part of the binding site i.e, cubic boxes measuring 151 × 123 × 145 points for the inactive model and 111 x 151 x 151 for the active model were built to include the entire protein in each case, allowing no bias towards the binding pocket. A spacing of 0.4 Å between the grid points was used. Docking simulations were performed by selecting "ArgusDock" as the docking engine. "Dock" was chosen as the calculation type, "flexible" for the ligand and the AScore was used as the scoring function. The AScore function, with the parameters read from the AScore.prm file was used to calculate the binding energies of the resulting docked structures. This file contains the coefficients for each term in the scoring function. Structures were visualized and the best docked structure was chosen based on lowest energy and minimal solvent accessibility of the ligand, as follows. First, the top 150 unique poses were retrieved. Typically, 20% of these conformations were ligands docked to the surface of the

protein, highly water accessible. These conformations were discarded manually. In at least ~2/3 of the remaining structures, the ligand was bound in a pocket analogous to the retinal binding pocket. Those ligands that were only partially buried in the protein interior, with parts of the ligand facing the outside of the helical bundle, were also discarded. Only ligands with maximal burial in the protein interior were retained. This typically included a list of 50 structures. These structures were rank-ordered by minimum energy and the structure with the lowest energy was chosen as the predicted receptor-bound conformation of the ligand.

2.3.2. (b) Docking with AutoDock: Ligands were docked to the receptors using the Lamarckian Genetic algorithm (LGA) provided by the AutoDock program, either version 3.0 or 4.0 (Goodsell, Morris et al. 1996). Solvation parameters were added to the protein coordinate file with the "Addsol" option in AutoDock, and the ligand torsions were defined using the "Ligand torsions" menu option of AutoDock. The grid maps representing the protein were calculated using the "AutoGrid" option. A cubic box was built around the protein with 126 × 126 × 126 points; a spacing of 0.403 Å between the grid points was used. The protein was centered on the geometric center prior to docking. Docking simulations were carried out with an initial population of 300 individuals, and a maximum number of 50,000,000 energy evaluations. Apart from this a maximum number of 27,000 generations, a translation step of 2 Å, a quarternion step of 50° and a torsion step of 50° were used as the docking parameters for obtaining the final docked structures. Resulting orientations that have less than or equal to 0.5 Å root mean square deviation were clustered. In addition to returning the docked structure, AutoDock also calculates an affinity constant for each ligand-receptor configuration. The best ligand-receptor structure

from the docked structures was chosen based on lowest energy and minimal solvent accessibility of the ligand, analogous to the procedure described above for ArgusLab, with the difference being that only the top 10 or 25 most favorably bound ligand structures were analyzed as mentioned in the text.

2.3.3. Protein – Protein or Protein – Peptide Docking

A three-dimensional model of the G_t peptide (VLEDLKSCGLF) and crystal structure of chemokine ligand CXCL11 (PBD id: 1RJT) were docked to the rhodopsin dark state crystal structure (PDB id: 1L9H:A)(Palczewski, Kumasaka et al. 2000) and/or the Meta II ANM model (Isin, Rader et al. 2006). The Docking was performed using the ClusPro docking software (Comeau, Gatchell et al. 2004). The ZDOCK algorithm along with the available default parameters were used in the docking procedure. From the set of returned favorable conformations, the top 2000 scoring structures were further filtered by analyzing the desolvation and electrostatic energies. The top 2 models were submitted to the FastContact analysis program (Camacho and Zhang 2005) to further analyze the binding energy of the conformations and to identify the residues which are at the interface between the two proteins in the docked complex that either stabilize/destabilize the complex.

2.4. ANALYTICAL PROCEDURES

2.4.1. Protein Quantification

Protein concentrations were determined using the Bradford assay. A calibration curve was obtained by mixing 0, 10, 20, 30, 40 and 50 µl of a 0.1 mg/ml bovine serum albumin stock solution with water such that the final volume was 100 µl. The sample solution was also adjusted to 100 µl at appropriate dilutions. The Bradford reagent (Biorad) was diluted 5 fold and 1 ml was added to each Eppendorf tube. After mixing and incubation for 5 min, the 595 nm absorbance was measured in a disposable plastic cuvette. The concentration was determined using the bovine serum albumin standard curve.

2.4.2. Meta II Decay

The rate of Meta II decay was measured, after illumination of the samples, by following the rate of fluorescence increase, which corresponds to the rate of retinal release (Farrens and Khorana 1995), using a solution of 2-4 µg of the protein in 200 µl of buffer E containing 0.05% DM. The samples were bleached at 20^{o}C for 30 sec and the fluorescence increase was measured. The excitation and emission wavelengths were 295 nm (slit width = 5 nm) and 330 nm (slit width = 10 nm), respectively.

2.4.3. Rhodopsin Regeneration

Regeneration studies (n=2) were performed with samples containing a rhodopsin concentration of 0.5µM and either a C3G concentration of 1mM or DFB-3,3` concentration of 0.5 or 2.5µM.

All the samples used in the regeneration experiments contained a final DM concentration of 0.6%. 11-*cis* retinal was added to rhodopsin from a 0.5mM stock in ethanol, prior to illumination, to obtain a final concentration of 0.5μM.

For C3G studies, the changes in the A_{500} absorption upon illumination were monitored as a function of time.

The increase in the A500 absorption upon addition of 11-cis retinal 1.5 hours after illumination was monitored to estimate the regeneration.

The total amount of increase at 500nm for the samples in the absence and presence of additives was normalized to 100%.

2.4.4. Transducin Activation

2.4.4. (a) By Fluorescence Spectroscopy: Activation of G_t by rhodopsin was monitored using fluorescence spectroscopy (PTI fluorimeter) at 20 °C as described with minor modifications (Phillips and Cerione 1988; Fahmy and Sakmar 1993; Yang, Farrens et al. 1996). The excitation wavelength was 295 nm with a 2 nm slit width, and the emission wavelength was 340 nm with a 12 nm slit width. G_t was added (final concentration of 250 nM) to buffer A containing 0.012% DM. The solution was stirred for 300 s to establish a baseline. Photobleached rhodopsin was then added to the mixture to a final concentration of 5 nM. Photobleaching was carried out using >495 nm light for 10 s. After an additional 600 s, GTPγS was added to the reaction mixture to a final concentration of 5 μM, and the increase in fluorescence was followed for an additional 2000 s. To calculate the activation rates, the slopes of the initial fluorescence increase after

GTPγS addition were determined by linear regression through the data points covering the first 60 s.

2.4.4. (b) By [^{35}S]GTPγS Filter Binding Assay: Binding of transducin to rhodopsin with and without chlorin e6 (Ce6) was monitored using a [^{35}S]GTPγS filter binding assay previously established (Wessling-Resnick and Johnson 1987), with several modifications described below. Transducin (G_t) and urea-washed ROS membranes were prepared as described above (refer Section 2.1.1, pg 30) from dark adapted bovine retinas (W.A. Lawson and Co.) and were stored at -80^{o}C prior to use. G_t activation studies were carried out in the absence and at varied concentrations of accessory ligands, stored as a 100mM stock solution in DMSO. Each reaction contained 1μM G_t, 50nM ROS or rhodopsin, 1nM [^{35}S]GTPγS (1250Ci/mmol; American Radiolabeled Chemicals, Inc.), 499nM cold GTPγS and 1μM GDP. Samples were illuminated with >495nm light for two minutes, then shaken at 250rpm until the reactions were stopped by filtering 25μl aliquots through nitrocellulose membranes using a Millipore vacuum manifold, washing 3 times with 5ml of ice-cold wash buffer (10mM Tris, pH 7.4, 100mM NaCl, 5mM $MgCl_2$, 2mM DTT). Washed membranes were dried on the manifold then placed in 5ml of 30% ScintiSafe LSC-cocktail (Fischer Scientific). Total [^{35}S]GTPγS bound was measured using a Beckman LSC 6500 counter. Reactions were performed in triplicates with control samples remaining in the dark.

To determine the relative IC_{50} values of Ce6 in ROS and rhodopsin in DM micelles, 5nM of either ROS or rhodopsin in DM micelles were incubated with various concentrations of Ce6 for 30min post-illumination (2min) then filtered as described above. Final DMSO

concentrations for each reaction were 1% and radioligand concentrations were identical to that described above. The IC_{50} values were estimated by fitting the data using the sigmoidal dose-response function of ligand binding provided by Sigmaplot.

2.4.5. Binding of Small Molecules Monitored by Fluorescence Spectroscopy

Binding of either C3G, Ce6 or as a control Chlorophyll-a (Chl-a) was quantified by measuring the fluorescence of 4μg of rhodopsin in 500μl of 2mM sodium phosphate pH 6, 0.05% β-dodecyl-D-maltoside (DM) as described (Farrens and Khorana 1995). C3G, Ce6 or Chl-a was added prior to illumination from a 100mM DMSO stock solution or its dilutions, at the final concentrations indicated. The different in total fluorescence between rhodopsin in the absence and presence of various concentrations of ligands was used to estimate the affinity of interaction. The binding affinities for the interaction were calculated with the one-site saturation ligand binding function using Sigmaplot 10.0 scientific graphing software.

For the studies with Ce6 and Chl-a, the fluorescence measured at each concentration was corrected for the resulting inner filter effect, where the excitation light is being absorbed by the added ligand at the excitation wavelength and the emitted fluorescence from intrinsic tryptophan residues is reabsorbed by the added ligand at the emission wavelength, as follows. We corrected for the inner filter effect using the Parker method (Parker 1968; Birdsall, King et al. 1983). The function used for correcting the data is

$F_{(real)} = (F_{(measured)}*2.303*A)/(1-10^{-A})$ where A is the absorbance of the sample at 295nm (excitation) or 330nm (emission). $F_{(real)}$ and $F_{(measured)}$ are the corrected and observed fluorescence

values at each concentration of Ce6 or Chl-a measured (Birdsall, King et al. 1983). The same correction was applied to dark and light samples, as the absorbance spectra at the excitation and emission wavelengths used did not change. We also determined an empirical correction function experimentally by checking the fluorescence intensity decrease of solutions containing 2.5μM and 25μM concentrations of tryptophan giving the same fluorescence counts as rhodopsin samples in the dark and in the light, respectively, as a function of increasing concentrations of Ce6, covering a similar range as used for rhodopsin. (Note that we experimentally verified the absorbance of each sample to obtain the exact Ce6 concentration in solution in all experiments reported here, to ensure accuracy.) The decrease in fluorescence was fit to a linear equation which was used to extrapolate to the exact concentrations of Ce6 in each sample. The ratio between the original fluorescence counts of tryptophan solutions in the absence of Ce6 and the actually observed fluorescence counts in the presence of Ce6 were used to scale the rhodopsin fluorescence counts accordingly.

2.4.6. Thermal Denaturation

Thermal stability experiments (n=2) were performed at 50^{o}C using 0.5μM of both rhodopsin and C3G. Samples were placed in the cuvette holder and the first spectrum was taken at 20^{o}C. Subsequently, the temperature was raised to 50^{o}C, and the corresponding spectra were recorded every 5 minutes. All experiments were carried out at the three different pH values of 4, 6 and 8. The data was analyzed by fitting the increase and decrease observed at 500 nm absorbance for regeneration studies and stability experiments, respectively, to a non-linear regression function using Sigmaplot 10.0 scientific graphing software.

2.4.7. Calculating Binding Affinities from NMR Data

All spectra were processed using Bruker using Bruker Topspin1.3 software and corrected for phase and baseline using identical parameters. The peaks in the spectra were manually selected by using the peak picking module in the Topspin software.

C3G binding affinities were calculated from ^{1}H NMR spectra essentially as described (Fielding, Rutherford et al. 2005) with the following modifications. The NMR spectra of 50μM rhodopsin in the absence and presence of 25, 50, 100 and 200 μM C3G were processed as described above. Changes in intensities of ligand peaks 2, 11 and 14 were quantified in comparison to the ligand alone peak. The peak intensity in each case was estimated using the most intense protein peak (number 13) as a reference, which was normalized to 1.0. We also analyzed chemical shift changes in protein signals, specifically in peaks numbered 3, 4, 7, 8, 9 and 10 in Figure 3.6A.

Ce6 binding affinities were estimated from the changes in ligand signal intensities upon addition of various concentrations of rhodopsin in comparison to free ligand control. We estimated the dissociation constants of interaction between the ligands and rhodopsin as described previously (Shortridge, Hage et al. 2008). The dissociation constant is given by:

$$K_D = \frac{[L_F][P_F]}{[C]}$$

L_F, P_F and C correspond to the concentration of free ligand, free protein and complex between protein-ligand, respectively. For estimating the fraction bound or the total concentration of complex formation, we assumed that the signal intensity observed after addition of rhodopsin was due to the free ligand species present in the solution. Therefore, the intensity of the bound

ligand (I_B) peak was determined by subtracting the intensity of the observed ligand peak (I_O) in the presence of rhodopsin from the intensity of the free ligand peak (I_F):

$$I_B = I_F - I_O$$

Binding constants were determined from the ratios of bound and free ligand concentrations quantified by integrating ^{1}H signals. While this is not as accurate a way of determining binding constants in comparison to T_2 relaxation based measurements which contain a weighted average of relaxation rates of the free and bound forms of a ligand at different concentrations, it is so far the only method that gives rise to signals in the ^{1}H NMR spectrum in the presence of detergents. Relaxation based ligand binding approaches cannot be applied to membrane proteins because of the dynamic range problem, i.e. the suppression of protein signals as a result of high intensity of signals from detergent micelles, and the unfavorable relaxation properties of membrane proteins in large detergent micelles, which decay very fast. In addition to this, the protein does not give rise to distinct and equally intense peaks even in selectively isotope labeled samples, as they experience selective conformational exchange broadening. Thus, the binding affinities cannot be estimated using relaxation based and line broadening methods.

The data obtained from the changes in ligand peak intensities were fitted using the non-linear regression function (one site specific binding) in Graphpad Prism5.0 to estimate the K_D. Errors were calculated from the fit for each peak analyzed.

Table 2.1: List of buffer compositions.

[A] 70mM K_2HPO_4/KH_2PO_4 (pH 6.8), 1mM MgOAc, 5 mM β-mercaptoethanol, 0.1mM PMSF
[B] in 50 mM Tris-HCl (pH 7.4), 5M urea, 5mM EDTA
[C] 50mM Tris-HCl (pH 7.4)
[D] 20mM Tris-HCl (pH 7.2), 2mM EDTA, 10% sucrose, 1mM β-mercaptoethanol, 0.1mM PMSF
[E] 2mM Na_2HPO_4/NaH_2PO_4 (pH 6)
[F] 5 mM Tris (pH 7.5), 5 mM MgOAc, 5 mM β-mercaptoethanol, 0.1 mM PMSF
[G] Amino Acid Composition of DMEM (Irvine Scientific):

Essential Amino Acid	mg/l	Non-essential Amino Acid	mg/l	Vitamins	mg/l	Inorganic Salts and other	mg/l
Arginine * HCl	84	Alanine	None	D-Ca pantothenate	4	$CaCl_2$	50
Histidine * HCl * H_2O	42	Asparagine	None	Choline Chloride	4	$Fe(NO_3)_3$ * 9 H2O	0.1
Isoleucine	105	Aspartate	None	Folic Acid	4	MgSO4	97.7
Leucine	105	Cystine* 2HCl	63	i-Inositol	7.2	KCl	400
Lysine * HCl	146	Glutamate	None	Niacinamide	4	NaCl	6400
Methionine	30	Glutamine	584	Pyridoxal*HCl	4	NaH_2PO_4 *H_2O	125
Phenylalanine	66	Glycine	30	Riboflavin	0.4		
Threonine	95	Proline	None	Thiamine*HCl	4		
Tryptophan	16	Serine	42			Phenol Red * Na^+	15
Valine	94	Tyrosine* 2 Na^+ * 2 H_2O	104			Glucose	4500

[H] buffer G plus 2 mM L-glutamine, 100 units/ml Penicillin, 100 units/ml streptomycin
[I] buffer H plus 10% FBS
[J] 137 mM NaCl, 2.7 mM KCl, 1.8 mM KH_2PO_4, 10 mM Na_2HPO_4 (pH 7.2)
[K] 1.5M glycine, 3M NaCl
[L] 0.1M citric acid, 0.15M NaCl (pH 3)
[M] 6M guanidinium-HCl
[N] 50mM Na_2HPO_4/NaH_2PO_4 (pH 7), 0.01% thimerosol
[O] 0.25M $NaHCO_3$, 0.5M NaCl (pH 8.3)
[P] 3.3 M K_3PO_4 (pH of 11.9 at 10-fold dilution)
[Q] 0.25 M NaH_2PO_4/Na_2HPO_4 (pH 6)
[R] 0.1 M NaOAc, 0.5 M NaCl (pH 4)
[S] 20 mM NaH_2PO_4/Na_2HPO_4, pH 6 in 10% D_2O (Cambridge Isotopes, Andover, MA).

CHAPTER – 3

CYTOPLASMIC ALLOSTERIC LIGANDS: BINDING OF CHLORIN E6 (CE6) AND CYANIDIN-3-GLUCOSIDE (C3G) TO RHODOPSIN.

TABLE OF CONTENTS

SUMMARY

Recent studies indicated that anthocyanin compounds, in particular cyanidin-3-glucoside (C3G) (Matsumoto, Nakamura et al. 2003) and the chlorophyll derivative chlorin e6 (Ce6) (Washington, Brooks et al. 2004; Isayama, Alexeev et al. 2006), modulate the function of the photoreceptor rhodopsin. Using fluorescence spectroscopy, here we show that Ce6 and C3G directly interact with rhodopsin. Further, the binding affinities of interactions were determined by a selective excitation ^{1}H NMR approach, overcoming some of the limitations posed by using fluorescence spectroscopy for these compounds. Molecular docking studies indicate that the binding pocket for both ligands is located in the CP domain. Further, ^{19}F and ^{1}H NMR experiments indicate that the binding of both, Ce6 and C3G, modulate the structure of the CP domain, which is a key functional region in rhodopsin,. GTPγS binding assays indicate that binding of these compounds to rhodopsin exert differential effects on G protein binding to rhodopsin at the CP domain.

Ce6 strongly inhibits activation of G_t, the associated G protein for rhodopsin, while C3G only modestly alters its activation. Thermal denaturation and stability studies using circular dichroism (CD), fluorescence and UV/Visible absorbance spectroscopy show that C3G exerts an overall destabilizing effect on rhodopsin structure. The results provide a molecular mechanism for the previous observation that C3G accelerates rhodopsin regeneration by 2 folds (Matsumoto, Nakamura et al. 2003): modulation of rhodopsin structure via long-range mediated structural effects enhances access to the retinal binding pocket. Ce6 binding to rhodopsin investigated by NMR spectroscopy of α-ε-^{15}N-tryptophan labeled samples show that ligand binding in the CP domain can allosterically modulate the TM domain.

SIGNIFICANCE

The studies presented here identify C3G and Ce6 as the first small organic molecules that bind to rhodopsin, other than *11-cis* retinal. The results obtained clearly demonstrate the presence of a novel ligand binding pocket in the CP domain of rhodopsin. The idea that binding of small molecules in this pocket may result in allosteric modulation of rhodopsin (either by accelerating regeneration or by inhibiting the G protein) is intriguing, since allosteric modulation is an emerging concept in the GPCR field. Previously, there were no known allosteric modulators for rhodopsin, and all known modulators for other GPCRs bind in either the TM or EC domains. Moreover, as the CP binding pocket identified is relatively conserved in class A GPCRs, it is possible that ligands binding in this pocket could be developed into universal modulators of GPCR activity. This could have potential for the medical and drug development communities

for developing therapeutics for such cancers where multiple GPCRs are involved in growth regulation (Gschwind, Prenzel et al. 2002; Lui, Thomas et al. 2003; Thomas, Bhola et al. 2006; Zhang, Bhola et al. 2007).

INTRODUCTION

Several lines of evidence suggest that rhodopsin in the presence of anthocyanins and porphyrin compounds show enhanced sensitivity to light of low intensities and of longer wavelengths (Matsumoto, Nakamura et al. 2003; Washington, Brooks et al. 2004). Rhodopsin, the prototypical class A GPCR, is a dim light photoreceptor in rod outer segments that has a covalently bound ligand, *11-cis* retinal (a vitamin A derivative). On light-activation, *11-cis* retinal isomerizes to *all-trans* retinal, resulting in a series of intermediate conformational states. Of these, the Meta II state of rhodopsin is considered to be the active state of the protein and is an initiator of the visual signal transduction cascade. Meta II activates two opposing signaling cascades, sensitization and desensitization. In sensitization, Meta II binds and activates the G protein transducin (G_t), ultimately resulting in hyperpolarization of the cell. Although it is often presented in the literature that G_t interacts with rhodopsin only upon activation, compelling evidence for a dark-state rhodopsin-G_t complex has also been proposed. Previous studies by Fung et al., have shown that G_t cannot bind to pure phospholipid vesicles but binds well to phospholipid vesicles containing either dark state or light activated Meta II state of rhodopsin (Fung 1983; Fung and Nash 1983). In addition to this, a rhodopsin antagonist that blocks G_t binding to purified Meta II state in the absence of phospholipids was also shown to dissociate G_t from the ROS membranes in the dark (Hamm, Deretic et al.

1987). However, the binding affinity of G_t is greater for Meta II than for dark state rhodopsin. In desensitization, the binding of the protein arrestin, following the phosphorylation of the C-terminus of rhodopsin by rhodopsin kinase, down-regulates the signal (Chabre, Bigay et al. 1988; Farrens, Altenbach et al. 1996; Sokal, Pulvermuller et al. 2002; Janz and Farrens 2004). Meta II gives rise to the opsin state (the apoprotein) through release of the *all-trans* retinal chromophore from the binding pocket, ultimately leading to the dissociation of protein and ligand to opsin and free retinal. All the proteins involved signaling interact at the CP domain of rhodopsin.

Evidence for anthocyanin interactions with rhodopsin: Anthocyanins, plant pigments belonging to the large group of phenolic compounds, the flavonoids, are abundant in a diet rich in fruits and vegetables. A large subset of anthocyanins are derivatives of the cyanidin backbone structure shown in Figure 3.1, where the 3,5,6,7,3',4' and 5' positions (Figure 3.1A) are substituted to give the vast array of anthocyanin structures observed in nature (Veitch and Grayer 2008). The variation in color is not only due to the different chemical substituents of the cyanidin backbone, but is also observed as a function of pH, solvent and co-pigments (Brouillard and Dubois 1977; Malien-Aubert, Dangles et al. 2001). The effect is based on the fact that anthocyanins interconvert between different species that exist in an equilibrium that is highly dependent on pH. The different species of the cyanidin backbone are shown in Figure 3.1A-D.

Anthocyanins exert potent antioxidant activity and are highly beneficial for human health, but like most nutrients, their target spectrum is broad (Lila 2004). However, one particularly consistent physiological function which eating fruits

containing high concentrations of anthocyanins is associated with, is vision. Enhancement of normal vision, protection from visual damage, and treatment of visual dysfunctions have all been investigated as potential application areas for anthocyanins (Muth, Laurent et al. 2000; Nakaishi, Matsumoto et al. 2000; Matsumoto, Inaba et al. 2001; Matsumoto, Nakamura et al. 2003; Lila 2004). British and French war pilots are said to have eaten berries before night flights for enhanced night vision, but this effect by anthocyanins as a general benefit is still a matter of debate as it appears to be strongly dependent on the individuals under study (Lee, Lee et al. 2005). The specific example shown in Figure 3.1A is for cyanidin-3-glucoside, found in black currant extracts (Koeppen and Herrmann 1977). Recently, it was observed that these compounds have functional effects on rhodopsin, the photoreceptor in rod cells; in rod outer segment preparations the rate of reaction of opsin with *11-cis* retinal (referred to as regeneration) was enhanced (Matsumoto, Nakamura et al. 2003). Because the retinal preparations contained many proteins of the visual signal transduction cascade, it was not known whether these effects on regeneration are mediated by direct binding of anthocyanins to rhodopsin.

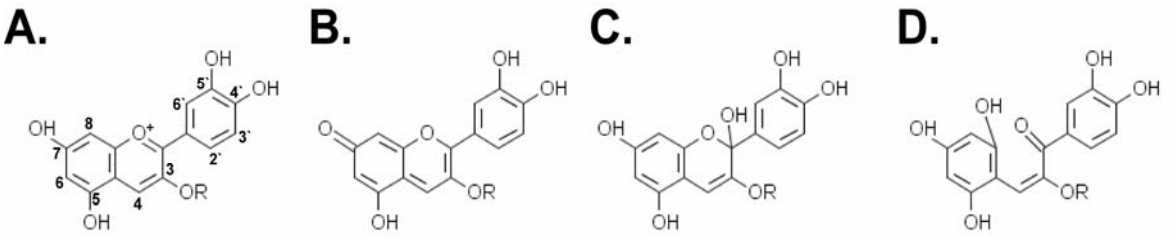

Figure 3.1: Chemical structures of pH dependent equilibrium species of the cyanidin-3-glucoside. (A) Flavylium cation. (B) Quinoidal base example. (C) Carbinol pseudobase. (D) Chalcone. 'R' in the chemical structures of C3G represents the glucoside sidechain. Numbering of C3G is indicated in 3.1A.

Evidence for Ce6 interaction with rhodopsin: The chlorophyll derivative Ce6 (Figure 3.2) is believed to enhance sensitivity of rhodopsin to red light in deep-sea fish rhodopsin (Douglas, Partridge et al. 1999; Isayama, Alexeev et al. 2006). Indeed, *in vivo* studies with salamander and mouse models have confirmed that Ce6 can effectively enhance vision in other animals as well (Washington 2007). A decrease in the 500nm peak of a UV-Vis spectrum of salamander rhodopsin was observed by illuminating the sample at 668nm, a wavelength at which Ce6 absorbs while rhodopsin essentially does not (Isayama, Alexeev et al. 2006). Additionally, mice administered with Ce6, showed an two fold increase in electroretinogram b-wave amplitudes (the electrical signaling to brain upon a flash) as a response to red and blue light (Washington 2007). It is so far not known whether Ce6 physically binds to rhodopsin, but it has been proposed that there may be an energy transfer between Ce6 and *11-cis*-retinal (Isayama, Alexeev et al. 2006).

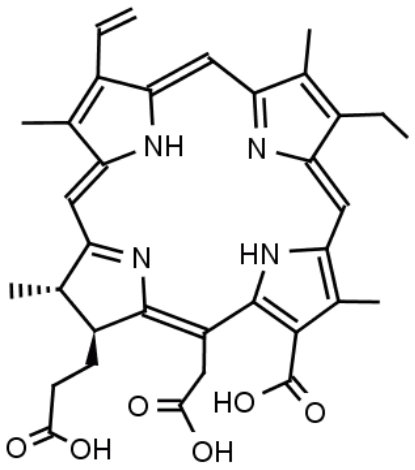

Figure 3.2: Chemical structure of Ce6.

Although the evidence presented above suggests that there is a direct interaction between rhodopsin and these compounds, prior to this thesis it was not known experimentally if and where these compounds bind to rhodopsin and what the molecular determinants and consequences of binding are. Here, we investigated these questions using bovine rhodopsin reconstituted in n-dodecyl-β-D-maltoside micelles as a model system. Bovine rhodopsin is the best studied membrane receptor to date, providing the most thorough baseline on structure, dynamics and function of the receptor in the absence of these chromophores. We used a combination of computational and experimental approaches to test the hypothesis that rhodopsin is a direct target. We further focused our efforts on C3G and Ce6 in particular, the ligands that showed the greatest effects in each case. Previous studies with rats and rabbits have shown that both anthocyanins and chlorin e6 localize to the retina and retinal pigment epithelium when administered either orally or intravenously (Haimovici, Ciulla et al. 2002; Matsumoto, Nakamura et al. 2006; Washington 2007).

3.1. CYANIDIN-3-GLUCOSIDE INTERACTION WITH RHODOPSIN

3.1.1. Ligand Binding and Affinity Estimation

As an initial step we tested the binding of C3G to rhodopsin using intrinsic rhodopsin tryptophan fluorescence. Tryptophan fluorescence of rhodopsin in the absence of additives is largely, but not fully, quenched in the dark due to bound retinal (Figure 3.3A, black trace). Upon light-activation, tryptophan fluorescence increases as a function of time, due to the retinal leaving the binding pocket (Farrens and Khorana 1995) (Figure 3.3A, see arrow for point of illumination). To quantify ligand binding, we first investigated C3G's ability to quench rhodopsin tryptophan fluorescence, but then moved to using ^{1}H NMR spectroscopy to obtain more detailed and quantitative data on ligand binding.

3.1.1. (a) Fluorescence Spectroscopy Studies of C3G Binding to Rhodopsin: As a first step, we investigated whether C3G binds and quenches rhodopsin fluorescence. Shown in Figure 3.3A are the fluorescence traces of rhodopsin in the absence and presence of varied concentrations of C3G. A concentration-dependent quenching of fluorescence of rhodopsin was observed both in the dark and upon light-activation. At 750-fold excess C3G over rhodopsin, the signal was similar to background fluorescence of C3G solutions alone. These studies suggest that C3G might bind to both dark and light-activated states of rhodopsin. The differences in fluorescence in the dark and in the light with and without addition of C3G were used to estimate the fractions of free and bound conformations of rhodopsin. This data was fitted using a non-linear regression

function to estimate binding affinity of interaction. The affinity of interaction of C3G with rhodopsin was calculated as 90μM for the Meta II state and 450μM for the dark state.

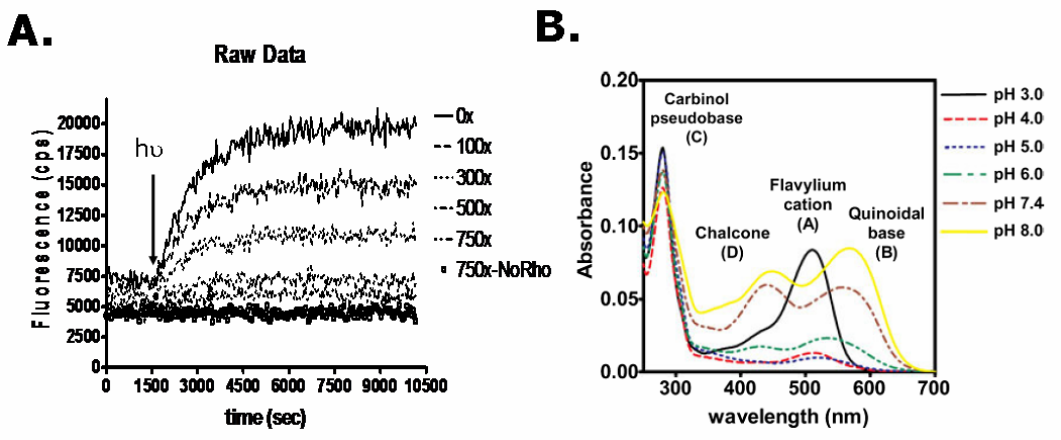

Figure 3.3: Binding of C3G to rhodopsin in the dark and in the light as monitored by fluorescence spectroscopy. *The image is a courtesy of Kalyan Tirupula and Judith Klein-Seetharaman.* (A) Fluorescence traces obtained at wavelengths for excitation of 280nm and for emission of 330nm in the presence of increasing amounts of C3G. (B) Absorption spectra of C3G alone at different pH conditions. The figure shows the absorption spectrum of 5μM C3G at different pH values. The predominant species of C3G observed at each pH is labeled in the spectrum (Levi, Scarminio et al. 2004).

Because of the known equilibrium dependence of C3G on factors such as pH, we also measured the absorbance spectra of detergent containing solutions of C3G under different pH conditions. The UV-Vis spectrum of C3G was measured at pH 3.0, 4.0, 5.0, 6.0, 7.4 and 8.0. Overall, the spectrum had four major absorption maxima (Figure 3.3B), corresponding to the different species of C3G (Figure 3.1). Further, the distributions of these species varied with pH. At least three different species are observed at pH 6.0, the

conditions at which the fluorescence spectra were obtained. Thus, although fluorescence spectroscopy indicates that C3G binds to both dark and light-activated states of rhodopsin, it cannot differentiate between the different C3G species that may be responsible for binding to rhodopsin to different extents. Thus, the fluorescence studies can only give a qualitative indication of C3G binding to rhodopsin. They demonstrate that overall C3G binds with higher affinity to illuminated rhodopsin (including Meta II and opsin species) than the dark state.

3.1.1. (b) Development of NMR Technique to Study Ligand Binding in Membrane Proteins using Selective Excitation ^{1}H NMR: As described in 3.1.1 (a), it is difficult to estimate binding affinities accurately based on fluorescence spectroscopy alone. As the results obtained using these methods often need to be adjusted for inner filter effects, for the case of Ce6 (refer to section 3.2.1. (a)) and in some cases cannot differentiate between the different species present at equilibrium (Figure 3.1), as confirmed by absorbance spectroscopy above for C3G, we wanted to establish a method that would be able to overcome these limitations. ^{1}H NMR spectroscopy may be the best suited method in this case because different structures will give rise to different chemical shifts, imparting specificity. However, ^{1}H NMR based methods to study ligand binding are constrained by the presence of background signals. In the case of rhodopsin being a membrane protein, the detergent micelles required to keep the protein in solution interfere with detection of protein signals. Moreover, as detergent concentrations are several orders of magnitude higher than the protein concentrations, the high signal intensity originating from the detergent leads to the suppression of signal intensities from the protein and also results in

overlapping of signals. To overcome these problems, we proposed a solution that has extended the applicability of ^{1}H NMR-based approaches to membrane proteins, described in more detail in Chapter 6. The principle of the approach is briefly outlined here. Because detergent signals are only observed upfield of the water signal and many protein resonances of interest appear downfield of the water signal, we can focus on the latter region of the spectrum. Using selective excitation sculpting (Hwang and Shaka 1995; Stott 1995) applied to full-length rhodopsin in detergent micelles using a hyperbolic secant shaped pulse centered around 10-12ppm, we have been able to observe the ^{1}H chemical shifts from both backbone and side chain regions of rhodopsin, removing contributions of the detergent signals altogether. Here, we extend this approach to study ligand binding to rhodopsin. Selective excitation ^{1}H spectra of C3G alone in 0.6% DM and Ce6 alone in 0.3% DM (Figure 3.4) show that many of the ligand resonances appear in the region downfield of the water signal and can therefore be observed simultaneously with protein resonances that typically show backbone and side chain NH resonances as well as aromatic side chain proton resonances in this region. This establishes the selective ^{1}H excitation approach as a suitable assay to study both C3G and Ce6 binding to rhodopsin.

3.1.1. (c). pH Dependence of C3G Selective Excitation ^{1}H NMR Spectra in Detergent Micelles: Because the equilibrium concentration between different C3G species is pH dependent we first recorded NMR spectra of C3G alone at different pH values (Figure 3.5). Using chemical shift values reported in the literature (Kucharska and Jan 2002; McGhie, Rowan et al. 2006; Yawadio, Tanimori et al. 2007), we partially

assigned some of the resonances observed. The most prominent resonances at pH 4 are the protons at positions 4, 6' and 2' of the cyanidin rings (Figure 3.5A). As the pH is raised, the 2' and 6' resonances show changes in chemical shift and their signal intensity increases significantly. At pH 6, the 2' resonance begins to show a shoulder, indicating formation of the quinoidal base with carbonyl formation probably at the neighbouring 5' position (Figure 3.5C). As the pH is raised further, the 2' resonance splits into 4 distinct, but overlapping peaks that, at pH 8, combine into one sharp and highly intense signal (Figure 3.5E). The increase in signal intensity is due to increased flexibility of the ring, first with disruption of the electron delocalization as the flavylium ion is lost, and ultimately, with chalcone formation in which the middle ring is replaced essentially by a flexible linker (Figure 3.1).

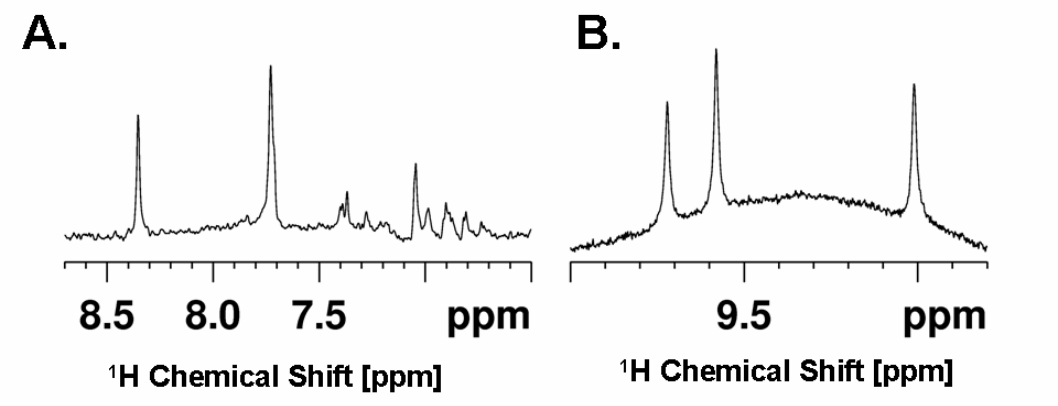

Figure 3.4: One dimensional ^{1}H NMR spectra of C3G (A) and Ce6 (B). The spectra were acquired using 50μM of each ligand at pH 6.0 with the selective excitation NMR approach.

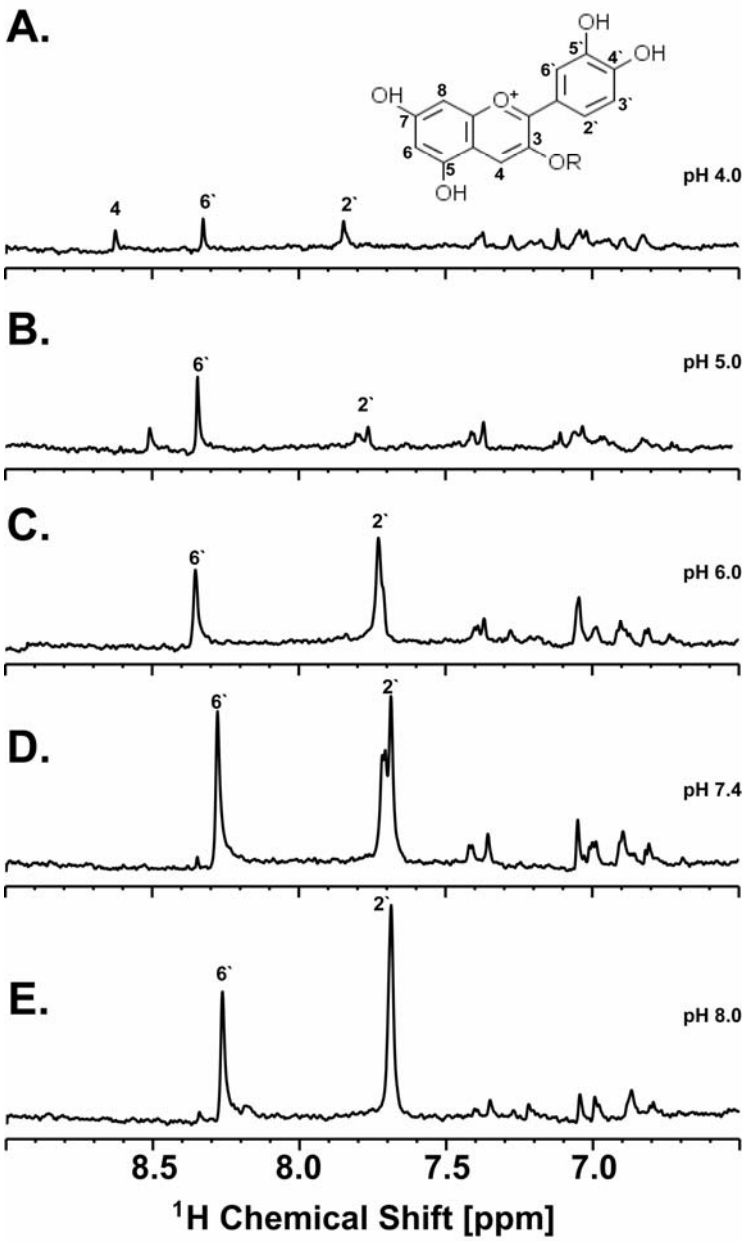

Figure 3.5: pH dependence of C3G monitored by selective excitation ^{1}H NMR Spectroscopy. One dimensional selective ^{1}H excitation NMR spectra of C3G in 0.6% DM at pH (A) 4.0, (B) 5.0, (C) 6.0, (D) 7.4 and (E) 8.0.

3.1.1. (d). Selective Excitation ^{1}H NMR Studies at pH 6 Confirm Binding of C3G to Rhodopsin: The selective excitation ^{1}H NMR spectra of C3G in the presence of rhodopsin at pH 6 are shown in Figures 3.6. We have chosen pH 6 because of rhodopsin's stability at this pH (Tirupula, Balem et al. 2009) and the presence of both quinoidal as well as chalcone forms (Figure 3.1, 3.3(B)). The ^{1}H NMR spectra of 50M dark-adapted rhodopsin in the presence of 50μM C3G in the chemical shift range 6.5ppm to 8.5ppm is shown in Figure 3.6A-C. We sequentially numbered the major peaks observed arbitrarily from 1-24. For reference, the C3G alone spectrum is shown in Figure 3.6D and the peak numbers are those corresponding to the respective peaks in the rhodopsin/C3G spectrum (Figure 3.6A,B).

The ^{1}H NMR spectrum of dark rhodopsin in the presence of C3G showed clear signals from ligand peaks at positions 2, 11, 14, 18 and 19 (Figure 3.6A, red dotted trace). However, the intensity of each signal was less as compared to that observed for 50μM C3G alone. Some of the peaks from the ligand disappeared, namely the two peaks labeled with an 'X' and peaks 22, 24 (Figure 3.6D). The decrease in signal intensity suggests binding of C3G to dark-state rhodopsin because the ligand experiences restriction in mobility. The changes in ligand peaks at varying concentrations of C3G were used to estimate the affinity of the C3G-rhodopsin interaction (refer to Chapter 2, pg. 55). The calculated K_D values were 51$\pm$12μM, 100$\pm$45μM and 45$\pm$6μM for peaks 2, 11 and 14, respectively.

Next, we analyzed light-activated rhodopsin in the presence of C3G (Figure 3.6B) and compared the light-activated spectra in the presence and absence of C3G (Figure 3.6C). The C3G ligand peaks showed differences when comparing the states bound to

dark and light-activated rhodopsin (Figure 3.6B). A decrease in intensity for the peaks at positions 2, 11, 18 and 22 was observed after activation (Figure 3.6B, red trace) as compared to dark state (Figure 3.6B, black trace). In contrast, ligand peaks 14, 23 exhibited no changes. The differences between ligand peaks bound to dark and light-activated rhodopsin can be seen when comparing Figure 3.6A and Figure 3.6C. In particular, ligand peak 11, arising mostly from chalcone and quinoidal base species of C3G showed differential effects as compared to dark-adapted rhodposin. In the dark , an overall decrease in signal intensity was observed in comparison to the ligand alone control. Upon light-activation, the signal corresponding to the quinoidal base (refer to Section 3.1.1. (c)), drastically decreased in intensity, indicating a preferential binding of this species to lightactivated rhodopsin. This finding suggests that the quinoidal base has a higher affinity of interaction for the light-activated state, further validating the results obtained from the docking studies (see above, Section 3.1.2. (a)).

In addition to the major peaks 2, 11, 14 and 18, there are significant changes in peaks 19, 22 and 24. For example, while peaks 22, 24 were absent in the dark-state spectrum, they are clearly visible in the light-activated spectrum. These results suggest that C3G binds not only to the rhodopsin dark state, but also its light-activated, Meta II, state. The binding of C3G to Meta II exerts different effects on ligand signals as compared to binding to the dark state. This indicates that different C3G species and/or the same species bind with different orientations to the rhodopsin dark and light-activated states.

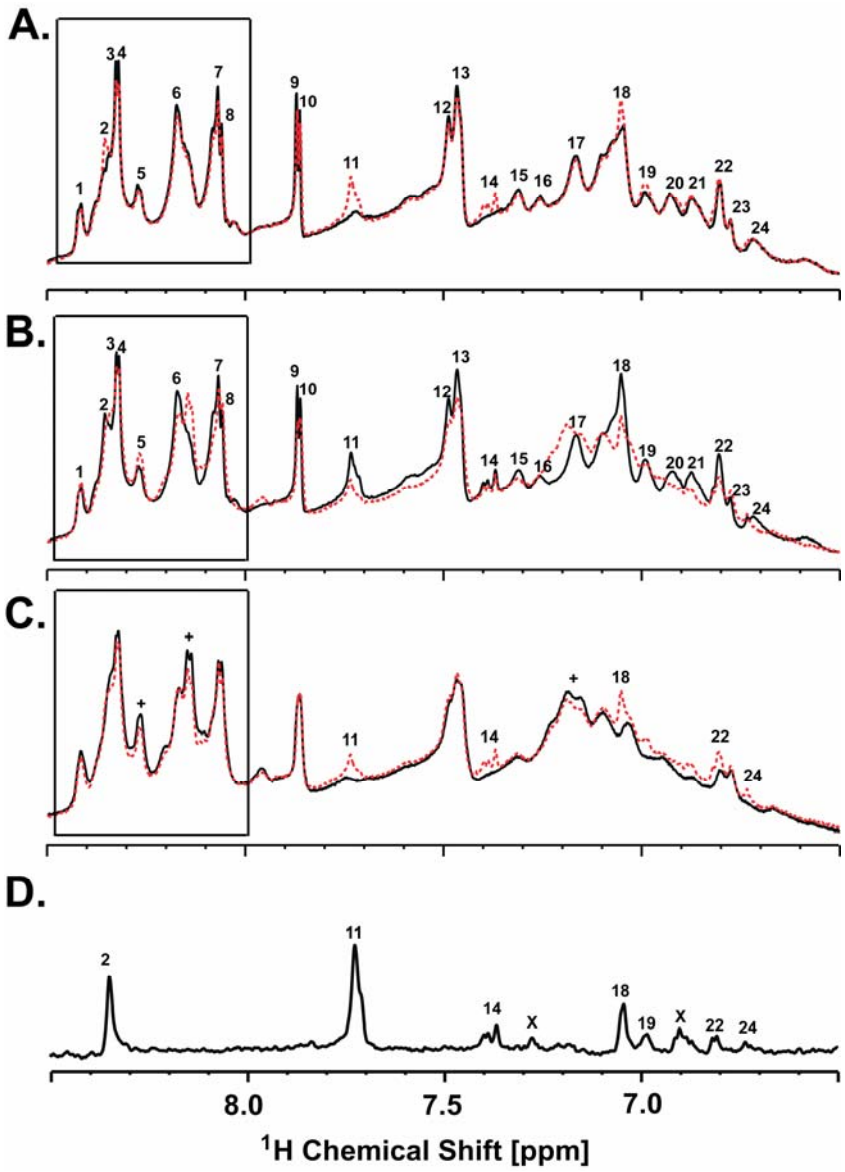

Figure 3.6: Monitoring binding of C3G to dark and light-activated rhodopsin with and without C3G. One dimensional selective excitation ^{1}H NMR spectra of (A) rhodopsin in the absence (black solid line) and presence of C3G (red dotted line). (B) Rhodopsin with C3G in the dark (black solid line) and upon light-activation (red dotted line). (C) Illuminated rhodopsin in the absence and presence of C3G (red dotted line). (D) C3G alone in phosphate buffer and 0.6% DM. NMR samples contained 50μM of rhodopsin in 20mM sodium phosphate buffer (pH 6.0), 0.6% DM and 10%D_2O. C3G was added from a stock solution of 10mM in DMSO, yielding a final DMSO concentration of 0.5% (v/v) in NMR samples containing C3G.

3.1.2. Location of C3G Binding on Rhodopsin

3.1.2. (a) Docking of Different Isoforms of C3G to Dark-state, Opsin and ANM Conformations of Rhodopsin: The absorbance and NMR spectroscopic results described above (section 3.1.1 (a), (b) and (d)) confirm that different species of C3G exist at equilibrium concentrations depending on the pH of the solvent used and indicate that these species bind differentially to dark- and light-activated states of rhodopsin. To better understand these effects and to see where and how the different cyanidin species bind to rhodopsin, we performed computational docking studies using Autodock 4.0 (Morris, Goodsell et al. 1998). First, the ligands shown in Figure 3.1 were docked to the dark-state rhodopsin crystal structure (Okada, Fujiyoshi et al. 2002). These ligands were found to dock mostly at the CP side of rhodopsin for all species (Figure 3.7), but the conformation, orientation, and predicted binding affinity differed for the various species. Out of the four cyanidin species docked, the chalcone structure exhibited 6 out of 25 conformations bound in the CP domain.

The top ranked structure had an energy of -8.44 kcal*mol^{-1}, the most favorable energy as compared to the other three species (Table 3.1). The quinoidal form was the next most favorable structure with a predicted binding energy of -7.69 kcal*mol^{-1}. 2 conformations were bound at the CP interface. The ligand binding site was essentially identical for the quinoidal and chalcone species (Figure 3.7 B and D) and similar binding energies were observed (Table 3.1). In all cases, the top ranked or most energetically favorable structure showed C3G bound at the CP surface.

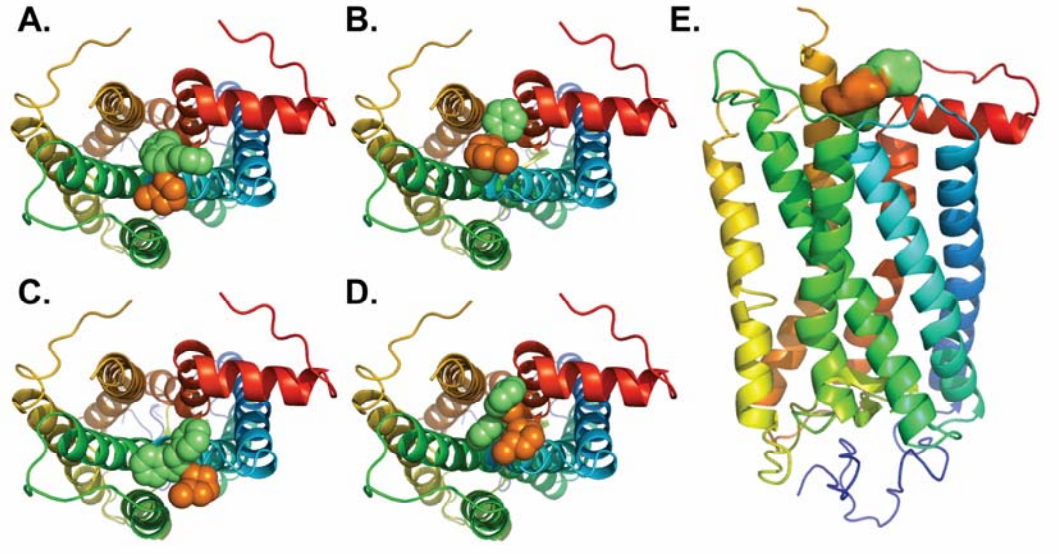

Figure 3.7: Docking of various isoforms of C3G to rhodopsin. Docking of C3G chemical structures: (A) Flavylium cation, (B) quinoidal base example, (C) carbinol pseudobase, (D) chalcone, and (E) cyanidin-3-glucoside (C3G) to dark state rhodopsin. The dark state of rhodopsin (pdb id 1l9h (Okada, Fujiyoshi et al. 2002)) is shown in cartoon representation. The helices in the rhodopsin structure are colored from blue to red, with helix 1 being blue and helix 7 being red. The ligand C3G in (A), (B), (C), and (D) is rendered as spheres and in (E) is a surface representation. The ligand is colored lime green for the cyanidin moiety and orange for the glucoside moiety.

To examine potential changes in binding to different conformations of rhodopsin, we docked all four ligand species also to the ANM generated active model with *all-trans* retinal (Isin, Rader et al. 2006) and to the opsin state crystal structure without any chromophore (Christopher J R Illingworth 2008). The binding energies are shown in Table 3.4. The quinoidal species was bound with the most favorable energy and highest number of conformations (4/25) followed by chalcone (3/25). These results are the reverse of the preferences observed for the dark state of rhodopsin described above. In

contrast, neither of these two species was favorably bound to the opsin state. Instead, the carbinol pseudobase (Figure 3.1 C) was bound to the opsin state with the highest energy, namely -8.38 kcal*mol^{-1}. Recall that the carbinol pseudobase is predicted to bind with least energy to the dark and Meta II states (Table 3.1). These results confirm theoretically the experimental observations from NMR spectroscopy that C3G exerts differential effects for different C3G species and for different conformations of rhodopsin. Because the equilibrium between the C3G species is pH dependent, this would suggest that the nature of C3G binding to rhodopsin is dependent on pH.

Overall the CP binding site was the most prominent binding site observed in the docked structures (Figure 3.7). Further analysis of predicted binding energies (Table 3.1) also provides an explanation for the differences in the ligand peaks observed in the dark and upon illumination. At pH 6.0, both chalcone and quinoidal forms are present in equilibrium as established by absorbance spectroscopy (see section 3.1.1 (a)). The chalcone form was found to bind with high energy to dark state rhodopsin. In contrast, the quinoidal species exhibited the highest binding energy when docked to the light-activated ANM model of rhodopsin, supporting the differential effects of binding of different C3G species to dark and light-activated rhodopsin measured by ^{1}H NMR (Figure 3.6). Because pH affects the equilibrium of the different species as mentioned above, these findings imply that binding is pH dependent.

3.1.2. (b) Changes in CP Domain upon C3G Binding Monitored by ^{1}H NMR Spectroscopy: To investigate the effect of C3G binding on the CP domain, one-dimensional selective excitation ^{1}H NMR spectra without and with C3G were recorded, as these spectra give rise to signals preferentially from flexible residues in proteins. In

rhodopsin, these would be the CP residues (refer to Chapter 6). As the C-terminus is the most flexible region in rhodopsin, we measured the NMR spectra of a peptide corresponding to the last nine amino acid residues corresponding to the C-terminus of rhodopsin (Figure 3.35D). The majority of the signals in the the ^{1}H NMR spectra recorded in the dark for 50μM rhodopsin in the absence of any additives were found at identical chemical shift values as those observed in the 9-mer peptide. In particular, the signals at positions 1, 3, 4, 7, 8, 12 and 13 are proposed to originate from the C-terminus residues of rhodopsin (compare Figure 3.6A and Figure 3.35). In the presence of 50μM C3G, the spectrum resulted in an upfield shift of the peaks at positions 3, 4, 7, 8, 9 and 10 (Figure 3.6A. red dotted trace). Especially, the signals at position 3, 4, 7 and 8 overlapped with C-terminus signals in the dark, validating the predicted CP binding domain. Upon illumination, in the presence of C3G no further shift in the peaks at positions 3, 4, 7, and 8 was observed. However, an overall decrease in the peak intensities arising from the flexible residues of rhodopsin, along with chemical shift changes at peak positions 6 and 17 was observed (for more detailed comparisons pls. refer to section 3.2.4 (a)). These results indicate that the binding of C3G to rhodopsin may be at the CP domain.

Table 3.1: Predicted binding energies for dark state (Okada, Fujiyoshi et al. 2002), ANM generated activated model (Isin, Rader et al. 2006), and opsin state (Christopher J R Illingworth 2008) of rhodopsin with different species of cyanidin-3-glucoside as shown in Figure 3.1. The top 25 most highly ranked structures were considered. For the proposed primary binding site in the center of the CP side of the helical bundle, we also provide its rankings amongst the top ranked structures. Note that for each of the four conformations of C3G, the structure with the lowest energy is found in the CP binding pocket, with the exception of the ANM computational model of the activated state, where it was the second highest rank (and also other highly ranked structures).

	Binding Energy (kcal*mol^{-1}) (Conformations docked)			
	Flavylium	**Quinoidal**	**Carbinol Pseudobase**	**Chalcone**
1L9H (Okada, Fujiyoshi et al. 2002)	-7.14 (2)	-7.69 (1,3)	-7.40 (1)	-8.44 (1,3,5,6,13,19)
ANM (Isin, Rader et al. 2006)	-5.34 (7,20)	-6.92 (2,5,12,19)	-5.03 (17)	-5.71 (4,5,8)
OPSIN (Christopher J R Illingworth 2008)	did not dock	-6.12 (11)	-8.38 (1)	-5.21 (14)

3.1.3. Effects of C3G Binding on Rhodopsin Function

3.1.3. (a) C3G Slightly Inhibits G Protein Activation: The proposed CP binding site is also the site of interaction of rhodopsin with its G protein transducin (G_t). We therefore investigated if C3G binding affects rhodopsin activity in terms of G_t activation. Upon light incidence rhodopsin catalyzes GDP to GTP exchange of G_t. The GTP-bound G_t is quantified in vitro by [^{35}S]GTPγS filter binding assays (refer to Chapter 2, pg. 52). The

activation of G_t by rhodopsin is measured as the increase in GTP-bound G_t. When tested at low concentrations of C3G, such as a 10-fold excess over rhodopsin concentration, the decrease in G_t activation was not significant and was within the error range observed in the absence and presence of C3G. We then tested G_t activation at the highest concentration possible, 1mM C3G, corresponding to a 200,000-fold excess over rhodopsin concentration. The ratio of radioactivity counts for light-activated over dark-adapted rhodopsin was 2.2+0.3 (n = 4) and 1.5+0.1 (n = 4) in the absence and presence of 1mM C3G, respectively. Thus, there is a 58% decrease in G_t activation in the presence of these high concentrations of C3G. Thus, it was not possible to completely inhibit G_t activation, even at such high concentrations.

3.1.3. (b) C3G Enhances Regeneration of Purified Rhodopsin in Detergent Micelles: Previous studies had shown that regeneration of rhodopsin in rod outer segment membranes was accelerated in the presence of cyanidin compounds from black currant such as C3G (Matsumoto, Nakamura et al. 2003). However, it was not clear whether C3G targets rhodopsin directly or acts in an indirect manner through other proteins present (Matsumoto, Nakamura et al. 2003). To investigate if C3G also enhances rhodopsin regeneration in the absence of any other proteins, the rates of regeneration were measured for purified rhodopsin reconstituted in detergent micelles. The increase in 500nm absorbance by addition of *11-cis* retinal after light-activation was followed by UV/Visible spectroscopy (Figure 3.8). The normalized change in absorbance at 500nm of 0.5μM rhodopsin at pH 6 in the presence of 0.5μM *11-cis* retinal after illumination in the absence (filled circles) and presence of C3G (open circles) is shown in Figure 3.19 A.

The corresponding regeneration rates for rhodopsin in the absence and presence of C3G at pH 6 are 0.072±0.009 min^{-1} and 0.119±0.008 min^{-1}, respectively. In the presence of two-fold excess (1μM) C3G over rhodopsin, the rate of regeneration was increased by 1.65-fold as compared to rhodopsin alone (Figure 3.8 A). Furthermore, the presence of C3G decreased the total amount of rhodopsin regenerated by 9±2% to a total of 81±1% efficiency as compared to rhodopsin alone at pH 6, which could be regenerated with 89±3% efficiency (Figure 3.8 C). Thus, we find that the effect of C3G on regeneration of rhodopsin in detergent micelles is two-fold – an increase in the rate, but a decrease in the extent of regeneration. The effects are observed at relatively low concentrations of C3G (1 μM), supporting the notion that the affinity of rhodopsin for C3G after light-activation is likely higher than that for the dark state, which is estimated at 50-100μM at pH 6 (refer section 3.1.1 (d)).

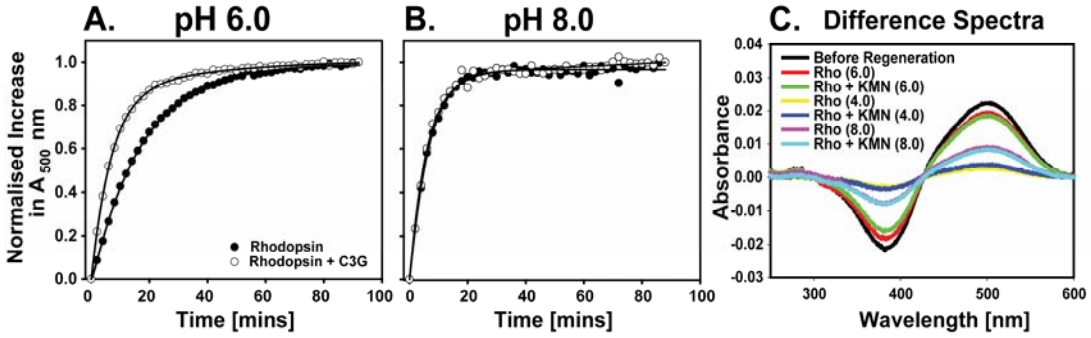

Figure 3.8: Regeneration studies of rhodopsin at different pH conditions. Regeneration of rhodopsin in the absence (filled circles) and presence (open circles) of C3G at (A) pH 6 and (B) pH 8. Shown in panel (C) are the difference spectra (regenerated rhodopsin dark minus light) of regenerated rhodopsin (0.5μM) in the presence and absence of C3G (1μM) at pH 4 (intermediate gray), 6 (black), and 8 (light gray). For the samples in A and B, the total amount of increase at 500nm at pH 6 and 8 both in the presence and absence of C3G was normalized to 100%. All samples contained a final DM concentration of 0.6%. The plots were generated using Sigmaplot 10.0 scientific graphing software.

3.1.4. Effects of C3G Binding on Rhodopsin Structure and Dynamics

3.1.4. (a) Changes in Rhodopsin Structure upon C3G Binding Monitored by ^{1}H NMR Spectroscopy: Having shown that rhodopsin binding alters C3G ligand resonances, we then studied if C3G binding affects rhodopsin structure and dynamics. To this effect, the one dimensional ^{1}H NMR spectra without and with C3G were analyzed from a protein peak perspective. The ^{1}H NMR spectra recorded in the dark for 50μM rhodopsin in the absence and presence of 50μM C3G (Figure 3.6 A), showed clear changes in protein peaks, in addition to the changes in ligand peaks described above:

Binding of C3G to rhodopsin resulted in the upfield shift of the peaks at positions 3, 4, 7, 8, 9 and 10 (Figure 3.6A). For clarity, an expanded region of the spectrum, indicated by the box in Figure 3.6A, is shown in Figure 3.9A. We used the upfield chemical shift changes in these protein signals upon titrating rhodopsin in the dark with varying concentrations of C3G to estimate the binding affinities. However, even though all peaks resulted in curves that reached saturation within the concentration range used, large variations in both K_D and B_{max} values prevented reliable estimates (data not shown).

Upon illumination, an overall decrease in peak intensities was observed as compared to rhodopsin with C3G in the dark (Figure 3.6B, 3.9B), indicating a restriction in mobility at these positions. Further, a shift in the peaks at positions 6 and 17 was observed, indicating a structural change upon illumination (Figure 3.6B and 3.9B, red dotted trace). Furthermore, we observed changes in protein signals upon illumination without and with C3G in the range 9.7ppm to 10.0ppm, which are shown in Figure 3.10. Two signals corresponding to aromatic residues at 9.96ppm and 9.90ppm were observed upon light-activation. None of these peaks were observed in the dark, both in the absence and presence of C3G.

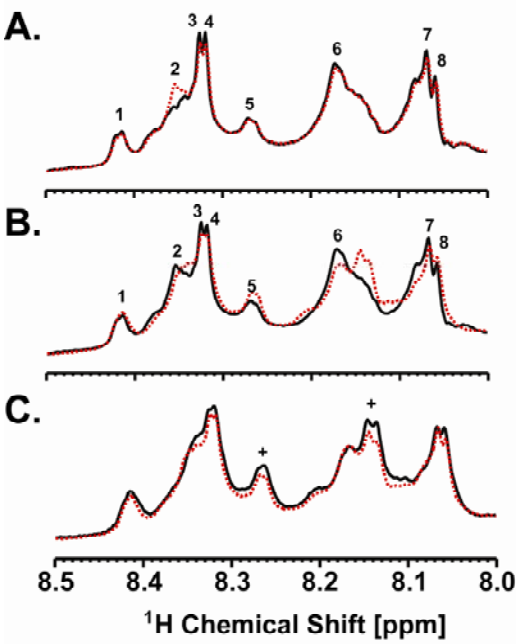

Figure 3.9: One dimensional selective excitation ^{1}H NMR spectra of the expanded regions represented in a box in 3.6A, B and C. For the legends of (A), (B) and (C), refer to Figure 3.6.

In addition to these signals, the NMR spectra in the presence of C3G gave rise to an additional peak at 9.8ppm (Figure 3.10, black trace). These signals were absent in the dark, both in the absence and presence of 50μM C3G. When we titrated different concentrations of C3G (25μM, 50μM, 100μM and 200μM, data not shown), we found that the signal at 9.8ppm only appears at higher concentrations of C3G, at 100μM C3G concentration and above. In addition to chemical shift changes, we also observed changes in the dynamics of protein peaks when comparing the binding of C3G to dark and light-activated rhodopsin. The overlay of the 1D ^{1}H NMR spectra of the illuminated samples of rhodopsin without (Figure 3.6C, black solid trace) and with C3G (Figure 3.6C, red dotted line), reveals that binding of C3G restricts the mobility of some of the

residues, as indicated by decrease in peak intensities at peak positions represented as '+' in Figure 3.6C. These results confirm binding of C3G to rhodopsin and suggest that binding modulates the structure and dynamics in both the dark and light-activated states of rhodopsin.

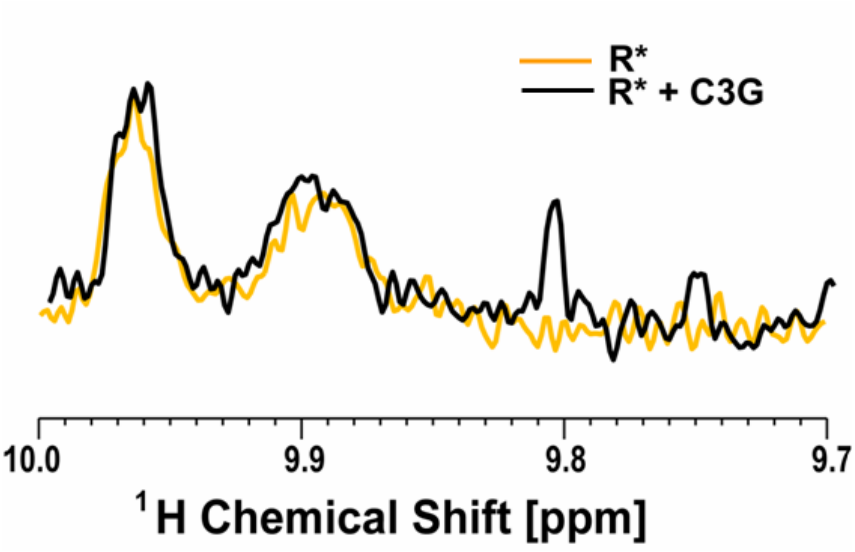

Figure 3.10: One dimensional selective excitation ^{1}H NMR spectra of the aromatic amino acid side chain region of rhodopsin. The spectra for rhodopsin in the presence and absence of C3G upon light-activation are colored in black and orange, respectively. The spectra for rhodopsin in the dark both without and with C3G displayed no peaks in this region and are therefore not shown in this figure.

3.1.4. (b): C3G Binding Destabilizes Secondary and Tertiary Structure of Rhodopsin: To corroborate the findings from NMR spectroscopy that C3G alters the structure of rhodopsin, we used fluorescence and UV Absorbance spectroscopy to monitor the effects of C3G on rhodopsin structure and stability. As a first step we monitored the thermal stability of rhodopsin at 55°C in the absence and presence of C3G

using fluorescence. Initially, the samples were kept at 20^{o}C for 5min, and then the temperature was raised to 55^{o}C. Following this an increase in fluorescence was observed as a function of time. This is due to the leaving of the *11-cis* retinal from the binding pocket as a result of disruption of the retinal-protein interactions at elevated temperatures. Shown in Figure 3.11A are the fluorescence traces of rhodopsin in the absence and presence of C3G at pH 6.0. The maximal fluorescence of rhodopsin in the presence of 10 fold excess C3G over rhodopsin was quenched, similar to observed before (Figure 3.3A). However, such a decrease in maximal fluorescence will not affect the thermal decay rates. The thermal decay rate of rhodopsin in the presence of C3G was accelerated ~ 2-fold as compared to rhodopsin alone with $t_{1/2}$ values 73±6 min and 111±11 min, respectively.

To further characterize the observed effects, we measured the stability of the retinal-protein interaction using UV/Vis spectroscopy. A decrease in 500nm peak with a concomitant increase in 380nm peak is followed over time as a result of thermal decay. These changes in 500nm peak at pH 6.0 in the absence and presence of 10 fold excess C3G are shown in Figure 3.11B. This data was fitted to an exponential decay function to estimate the decay rates. The decay rates for rhodopsin without and with C3G were 0.025min^{-1} and 0.066min^{-1}, with a $t_{1/2}$ of 27.77min and 10.54min, respectively. The rate of decay in the presence of C3G was accelerated approximately by 3 folds as compared to rhodopsin. Collectively the studies from fluorescence and UV/Vis spectroscopy stability studies indicate that C3G binding changes in the overall structure of rhodopsin.

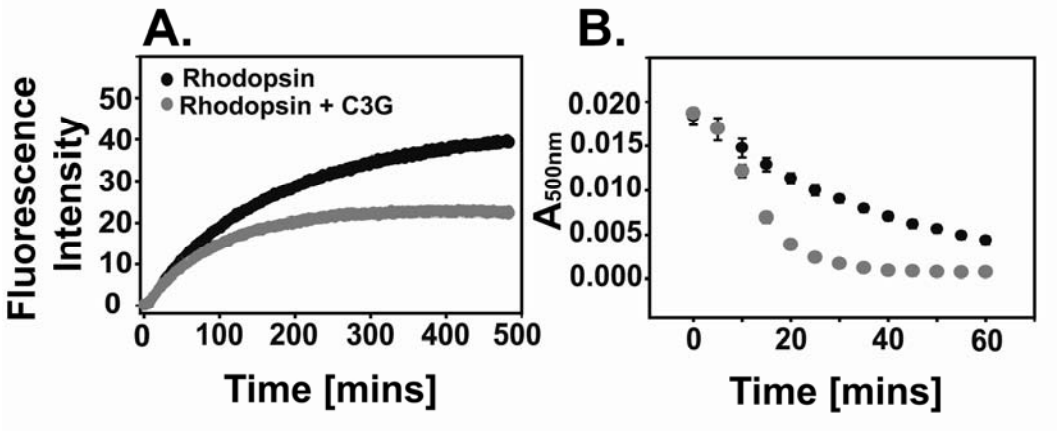

Figure 3.11: Changes in secondary and tertiary structure of rhodopsin in the absence (black) and presence of C3G (gray) probed by spectroscopy techniques. (A) Stability of rhodopsin at 55°C measured by fluorescence spectroscopy. (B) Retinal-protein interactions probed by UV spectroscopy at 50°C.

3.1.5. Discussion

Our goal of the studies described in this section was to investigate whether C3G interacts directly with rhodopsin, and if so, what the mechanisms are by which anthocyanins aid in regenerating rhodopsin as was first reported by Matsumoto et al. (Matsumoto, Nakamura et al. 2003) and confirmed here in a purified system in detergent micelles (Figure 3.8). First, we investigated the binding of C3G to rhodopsin using fluorescence spectroscopy. The results obtained indicated that C3G physically binds to rhodopsin both in the dark and after light-activation, but with higher affinity to the light-activated states. However, referring to C3G as a molecular entity is inaccurate because it consists of multiple species that are at equilibrium with each other (Figure 3.1). The relative distributions of the species depend on the pH. We confirmed the pH dependency of the equilibrium species of C3G using UV/Vis spectroscopy (Figure 3.3). Based on earlier studies (Levi,

Scarminio et al. 2004) we identified a predominant flavylium cation at lower pH (~3), chalcone and anhydrobase (quinoidal) conformations at slightly acidic and neutral pH (6 and 7.4) and an ionized anhydrobase at basic pH from our spectra. Thus, while the fluorescence studies reported here suggest that C3G physically binds to rhodopsin, it being a bulk biophysical technique cannot be expected to differentiate between the species. To investigate binding taking the pH depend species distribution into account, we next investigated binding using ^{1}H NMR spectroscopy. This was possible because the different species gave rise to differential ^{1}H NMR spectra. This laid the ground for investigation of C3G binding to rhodopsin. To do so, we developed an NMR based C3G binding assay using the selective excitation sculpting scheme (Hwang and Shaka 1995; Stott 1995). The ^{1}H NMR spectra of C3G at pH 4.0 – pH 8.0 (Figure 3.5), suggested that our approach is suitable. Detailed analysis of the ^{1}H NMR spectra recorded in the dark and in the light, with and without C3G clearly indicated that both the ligand and rhodopsin peaks are modulated in an activation-state dependent manner. These findings showed that studies of ligand binding to membrane proteins by ^{1}H NMR spectroscopy are possible for membrane proteins such as rhodopsin using selective excitation. The selective excitation scheme (Hwang and Shaka 1995; Stott 1995) we used to record these ^{1}H NMR spectra tends to highlight flexible regions in the protein because of the extended length of the experiment and the fast relaxation of immobilized rhodopsin resonances in the large detergent micelle environment. In particular, there is overlap between the peaks observed and those reported previously for the C-terminus of rhodopsin (Werner, Richter et al. 2008), implying that many of the resonances arise from flexible regions of the protein, such as the CP loops and the C-terminus. We find that both rhodopsin and C3G

ligand structure and dynamics are modulated in the C3G-rhodopsin complex, both in the dark and upon light-activation.

Although NMR spectroscopy is not the best method to quantify ligand binding affinities, as they can be associated with high error margins and uncertainties on the binding stoichiometry (Fielding, Rutherford et al. 2005), we estimated the affinity using intensity changes in the ligand peaks with increasing amounts of ligand added to constant rhodopsin concentrations as described (Shortridge, Hage et al. 2008). We obtained values on the order of 50-100μM indicating moderate to weak binding of C3G to dark-state rhodopsin at pH 6. The affinity is comparable to, for example, ANS binding to proteins (Latypov, Liu et al. 2008), a ligand that binds with relatively broad specificity to molten globule-like states of proteins. Thus, the anthocyanin ligand investigated here is certainly not a high-affinity ligand that can compare in affinity to retinal ligands.

It is also not likely that C3G will only bind to rhodopsin, given the broad spectrum of physiological effects that anthocyanins display (Lila 2004). However, all of our binding curves show saturation, indicating that binding to rhodopsin is to a specific site (or sites). C3G is also a specific ligand in terms of its structure, because a relatively small change in chemical structure at the 3' position (Figure 3.1A) from –H to –OH resulted in loss of the enhancement of rhodopsin regeneration (Matsumoto, Nakamura et al. 2003). Furthermore, the mode of binding is conformation-specific. Upon light-activation of rhodopsin, both protein peaks and ligand peaks exhibited changes. The binding of C3G to light-activated rhodopsin resulted in decreased chemical shift intensities of protein peaks as compared to rhodopsin alone (Figure 3.6C, labeled '+'), suggesting that the binding affinity might be higher as compared to dark state of

rhodopsin. The analysis of peak 11 indicates that only one of the populations of the ligand is affected after light-activation, suggesting a preference of this ligand conformation for light-activated rhodopsin. Thus, it appears that both structural changes in the protein upon light-activation and changes in the binding constant alter C3G binding to rhodopsin in the light.

To complement the NMR data, we performed computational docking studies of different species of C3G to different states of rhodopsin (rhodopsin, Meta-II and opsin) for predicting the binding sites and modes of binding. The CP binding site was the most prominent of the docked structures (Figure 3.7). This finding fits well with the NMR results, especially since most of the signal observed probably arises from the flexible regions of rhodopsin including the flexible CP domain. Analysis of predicted binding energies (Table 3.1) also provides an explanation for the differences in the ligand peaks observed in the dark and upon illumination. At pH 6.0, both chalcone and quinoidal forms are present in equilibrium as established by absorbance spectroscopy. The chalcone form was found to bind with high energy to dark state rhodopsin. In contrast, the quinoidal species exhibited the highest binding energy when docked to the light-activated ANM model of rhodopsin, supporting the differential effects of binding of different C3G species to dark and light-activated rhodopsin measured by ^{1}H NMR (Figure 3.6B). Because pH affects the equilibrium of the different species, these findings imply that binding is pH dependent.

Having shown that C3G physically interacts with rhodopsin, we repeated the regeneration assay with just rhodopsin in DM micelles and C3G to confirm that it is a direct rhodopsin binding effect and not mediated by other signaling proteins. We found

that regeneration is enhanced to similar degree as was found by Matsumoto et al. (Matsumoto, Nakamura et al. 2003), clarifying that these effects are not mediated by any other components than rhodopsin and C3G alone. As discussed above, C3G binds to dark-state rhodopsin with apparent K_D values ranging form 50 to 100 μM depending on which C3G peak in ^{1}H NMR spectra was chosen for analysis. It was also clear that C3G binds to the Meta II and opsin states based on changes in the ^{1}H NMR spectrum, probably with affinities higher than the dark-state. Due to the instability of the light-activated state, we have so far been unable to determine the actual K_D value upon illumination. Comparison of the ^{1}H NMR spectra of rhodopsin 0.5 and 1.5 hours post-illumination clearly indicated that C3G still remained associated with the opsin state as there is no change observed in the ligand peaks as compared to Meta II state. Further, some of the ^{1}H peaks in the presence of C3G also exhibited restriction in mobility both in the Meta II and opsin states. In light of these NMR results, the regeneration studies obtained prove that the effects of C3G on regeneration are a direct result of the binding of C3G and modulating the structure of rhodopsin upon illumination.

While previously only an effect on the rate of regeneration was reported (Matsumoto, Nakamura et al. 2003), we here find that the presence of C3G not only changes the rate, but also the extent of regeneration. C3G decreased the total amount of rhodopsin regenerated by ~10% as compared to rhodopsin alone at pH 6 (Figure 3.8C). This relatively small, but significant, difference was not noted earlier (Matsumoto, Nakamura et al. 2003) probably because the rhodopsin concentrations were not kept constant across different experiments as the samples were from opsin membranes. The data were thus normalized to 100% rhodopsin levels. Our system with pure components

of rhodopsin and anthocyanin allowed us to quantify more precisely the rhodopsin concentrations before and after regeneration from which the extent and rate of regeneration can be obtained with high accuracy.

As anthocyanins undergo reversible modifications at different pH, and binding to rhodopsin was observed to be pH dependent (see section 3.1.1), we also performed regeneration studies at pH 4.0 and 8.0. At both low and high pH values rhodopsin is destabilized and the extent of regeneration is dramatically decreased (~20% and ~30% of rhodopsin is regenerated at pH 4 and 8, as compared to ~90% at pH 6). C3G does not further decrease or increase the extent or rate of regeneration at these extreme pH values.

Next, we investigated whether C3G binding alters rhodopsin function at a further downstream level. After light-activation, rhodopsin binds and activates the G protein, transducin (G_t). We therefore performed functional assays with rhodopsin and G_t in the presence of 1mM concentrations of C3G. At this high of a concentration, which even for the low estimate of a K_D for the dark state (50μM) would amount for 95% receptor occupancy, 42% of G_t activity remains. This relatively modest decrease in G_t activation at such elevated concentrations of C3G argues that the C3G effects on G_t activation are comparatively small.

After having ruled out an effect of C3G on activity as the cause for the enhanced regeneration rates, we studied the stability of secondary and tertiary structures of rhodopsin at pH 6.0 to understand the mechanism underlying the regeneration effects. Thermal denaturation at constant elevated temperature (55^{o}C) showed that in the presence of C3G there is a faster thermal decay rate in fluorescence spectra. This indicates an overall destabilizing effect on rhodopsin structure. Further, we also

investigated the effects of C3G interaction on rhodopsin chromophore stability in the dark, by measuring the rate of retinal leaving from the rhodopsin binding pocket at 50^{o}C by UV/Visible spectroscopy at pH 6.0. The decay rate of rhodopsin in the presence of C3G was drastically accelerated. This clearly demonstrates that the retinal-protein interactions are destabilized by the presence of C3G.

Collectively, these studies suggest that C3G binds directly and enhances the regeneration of rhodopsin. Furthermore, loss of flexibility in residues giving rise to ^{1}H resonances in NMR spectra of illuminated rhodopsin in presence of C3G along with a shift in the C3G peaks as observed in NMR studies hint at a higher affinity of some species of C3G over others for binding to illuminated rhodopsin (Meta II and opsin states). Additionally, computational docking studies supplement the experimental observations and predict that C3G preferably binds in the CP side of rhodopsin. One explanation for the increased rates of regeneration could be that the binding of C3G in the CP side results in destabilization of the rhodopsin structure upon light-activation. Such destabilization in the overall structure of rhodopsin might lead to easier access to retinal binding site, thus allowing the *11-cis* retinal to interact faster with rhodopsin.

3.1.6. Conclusions

In summary, our results confirm that there is increase in the rate of regeneration of rhodopsin, while the G protein activation is only slightly affected if at all. Especially at the low concentrations used for the regeneration assay, we could not detect any changes in G_t activation. Thermal denaturation experiments suggest that there may be a structural effect of C3G binding on rhodopsin. Further, UV absorbance spectra also confirm that

the retinal-protein interactions are altered by C3G. This suggests that the mechanisms of C3G enhancement of rhodopsin regeneration may be based on changes in rhodopsin structure upon light-activation, enhancing access to the retinal binding pocket. The studies presented here aid in understanding the mechanism of action of anthocyanins on rhodopsin. The knowledge gained here could be useful in developing small molecule drugs that enhance or correct normal or weakened vision.

3.2. CHLORIN E6 INTERACTION WITH RHODOPSIN

3.2.1. Ligand Binding Studies

In analogy to the studies described above for C3G, we conducted fluorescence and NMR spectroscopic measurements to investigate if Ce6 also binds to rhodopsin. As a first step, we performed fluorescence assays based on intrinsic tryptophan fluorescence of rhodopsin. To obtain more quantitative and detailed information, we then measured ^{1}H NMR spectra using the methodology developed above for C3G.

3.2.1. (a) Fluorescence Spectroscopy Studies of Ce6 Binding to Rhodopsin: Selected tryptophan fluorescence traces in the dark and upon light-activation in the presence of increasing quantities of Ce6 are shown in Figure 3.12A, colored traces. The fluorescence is quenched in the dark, indicating binding of Ce6 to dark-state rhodopsin. At 25-fold excess Ce6 to rhodopsin, the signal is close to background fluorescence of Ce6 solutions alone. Upon light-activation, the maximal fluorescence signal obtained after Meta II decay is quenched, in a concentration-dependent fashion, showing that light-activated and subsequent opsin species also bind Ce6. The Meta II-decay half-lives are not changed (Table 3.2), indicating that the residual increase in fluorescence is due to Ce6-free rhodopsin. Thus, the differences in fluorescence in the dark and in the light can be used to calculate the fractions of free and bound conformations. This is shown in Figure 3.12B for light-activated rhodopsin (circles) before (black trace) and after (red trace) correction for Ce6 absorbance using the Parker equation (refer to Chapter 2, pg. 53). We also recorded identical buffer solutions containing free tryptophan as a control (Figure

3.12B, triangles, black trace) and corrected the results with the Parker method (Figure 3.12B, triangles, red trace). While the Parker correction was able to recover some of the original fluorescence counts, there was still a significant linear decrease in fluorescence with increasing Ce6 concentrations. It is likely that this is due to some unspecific interaction between tryptophan and Ce6 that probably would not occur with rhodopsin. Nonetheless, to err on the conservative side, we also corrected the rhodopsin fluorescence for the observed decrease in free tryptophan fluorescence. We calculate for the Parker corrected affinities: 0.82±0.06μM (light), 2.6±0.2 μM (dark); for the tryptophan corrected affinity in the light 0.79±0.03μM. The dark affinity could not be calculated for the tryptophan correction because the fluorescence counts were too low so that correction introduced a large variation in the counts. Because the light-affinity is almost identical between the Parker and tryptophan corrected affinities, we assume that the dark affinity would be similar for both types of corrections as well. It is important to note that due to the quenching of rhodopsin tryptophan fluorescence by Ce6, regardless of the presence of absence of retinal, we can no longer use fluorescence spectroscopy to assess the decay of Meta II to opsin and free retinal for the Ce6-bound rhodopsin.

To rule out the possibility that crowding of the relatively hydrophobic Ce6 into the DM micelle alone, rather than specific binding, would result in a similar degree of tryptophan fluorescence quenching, we used chlorophyll-a (Chl-a) as a control. Chl-a is identical in structure to Ce6 except for the presence of Mg^{2+} and a phytol chain, the highly hydrophobic tetramethylhexadecenol substitution at a carboxyl side chain. Ideally, we would have used pheophytin-a (Pheo-a) instead of Chl-a, as this would be lacking Mg^{2+} and more similar to Ce6; however, due to the chemical instability of Pheo-a

in solution we used Chl-a as a control, as the critical structural difference is the presence of the phytol chain, carried by both Chl-a and Pheo-a. The phytol substitution makes the molecule significantly more hydrophobic than Ce6, and crowding into the micelle would be expected to be enhanced. In titrations of fluorescence quenching with increasing amounts of Chl-a, identical to the experiments described above for Ce6, we find that there is no quenching of dark-state rhodopsin tryptophan fluorescence at any concentration tested (Figure 3.13).

Table 3.2: Meta II decay half-lives of rhodopsin in the absence and presence of additives (chlorophyll-a and Ce6) at various concentrations indicated. All samples contained a rhodopsin concentration of 0.5μM.

Chl-a Concentration	Half-life	Ce6 Concentration	Meta II decay Half-life
0μM	13.8833	0.0μM	13.51 ± 0.3
0.2μM	13.8	0.5μM	12.86 ± 0.76
0.4μM	13.16794	1.0μM	12.47 ± 0.75
1.77μM	10.42296	1.8μM	12.28 ± 0.78
3.19μM	8.734177	2.4μM	11.57 ± 2.81
7.08μM	6.818182	7.93μM	Cannot be estimated with accuracy

This indicates that Chl-a does not bind to dark-state rhodopsin at physiological concentrations and that partitioned Chl-a in the micelle is not able to quench tryptophan fluorescence of rhodopsin in the dark. In contrast, there is some quenching of tryptophan fluorescence of light-activated rhodopsin. The degree of quenching is low compared to Ce6, and we calculate an apparent binding affinity of 5.0±0.3μM. This result rules out the possibility that unspecific partitioning of Ce6 into the micelle results in the high

degree of rhodopsin tryptophan quenching observed with Ce6 and confirms the validity of the use of fluorescence spectroscopy as a Ce6 binding assay. Note, that Chl-a does slightly affect the Meta II half-live (Table 3.2) and at increasing Chl-a concentrations, Meta II is increasingly destabilized.

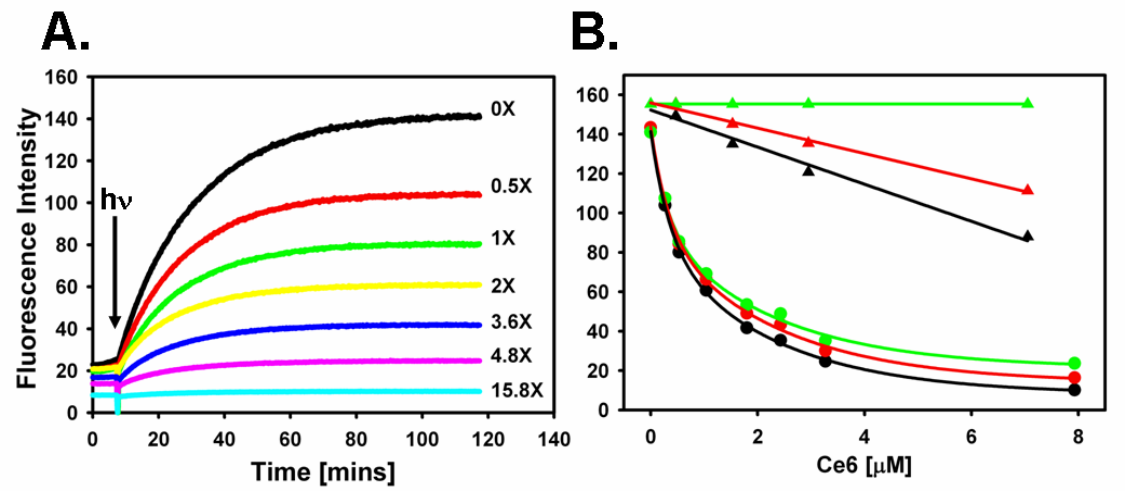

Figure 3.12: Binding of Ce6 to rhodopsin in the dark and in the light as determined by fluorescence spectroscopy. (A) Fluorescence traces obtained at wavelengths for excitation of 280nm and for emission of 330nm in the presence of increasing amounts of Ce6. (B) Decrease in the difference in fluorescence counts between rhodopsin kept in the dark and 1.5 hours after light-activation (circles) and free N-acetyl tryptophan (triangles) as a function of Ce6 concentration. The N-acetyl tryptophan concentration was 25μM and the rhodopsin concentration was 0.5μM. The uncorrected fluorescence counts are shown in each case in black, after Parker correction in red and after correcting for the linear decrease observed in the tryptophan fluorescence that could not be corrected for with the Parker equation in green. All plots were created using SigmaPlot scientific graphing software.

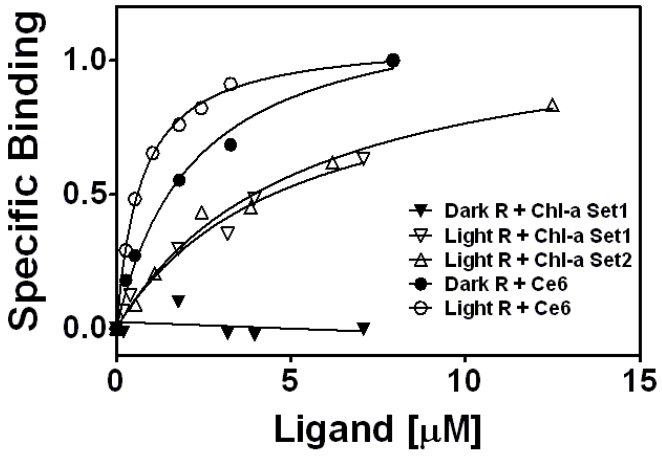

Figure 3.13: Plots of the relative populations of bound and free states in the dark (filled symbols) and in the light (open symbols) for chlorin e6 (circles) and chlorophyll-a (triangles). A rhodopsin concentration of 0.5μM was used to obtain each data point.

Finally, in order to also rule out the possibility that the oxygen species released as a result of illumination of Ce6 into the buffer is not the reason for the effects observed for rhodopsin in the presence of Ce6, we measured the Meta II decay using fluorescence spectroscopy by addition of dark and illuminated Ce6. The fluorescence traces of rhodopsin upon light-activation of rhodopsin in the presence of activated and dark Ce6 are shown in Figure 3.14. The results indicated no significant effects on Meta II decay rates and the quenching effects (Figure 3.14).

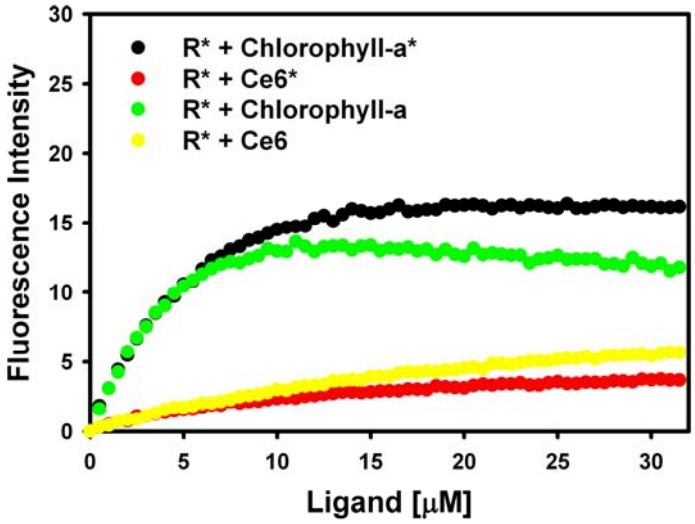

Figure 3.14: Effects of illuminated Ce6 on dark and light-activated rhodopsin. Fluorescence traces of rhodopsin in the presence of dark Chlorophyll-a (green circles), illuminated Chlorophyll-a (black circles), dark Ce6 (yellow circles) and illuminated Ce6 (red circles). A rhodopsin concentration of 0.5μM was used to record each fluorescence trace. A '*' represents that the sample is illuminated.

Overall, we find that rhodopsin tryptophan fluorescence is strongly quenched by Ce6, especially in the light. Control experiments with non-illuminated Ce6 and with separately illuminated Ce6 confirm that these effects do not require Ce6 excitation. Thus, it is unlikely that the Ce6 effects described in this paper are indirect effects, such as through reactive oxygen species formation mediated by the presence of Ce6, after excitation. Furthermore, we show that these effects are consequences of Ce6 binding to rhodopsin by comparing tryptophan fluorescence quenching by Ce6 with that by Chl-a, which is more hydrophobic than Ce6 and would result in stronger unspecific interactions with rhodopsin, being recruited into the detergent micelles. The results described above confirm that Ce6 binding is specific, as Chl-a results in a much lower degree of

fluorescence quenching, even lower than that observed for Ce6 binding to dark-adapted rhodopsin. Chl-a does have an effect on rhodopsin, namely on Meta II half-life (Table 3.2). This result is not unexpected, as the Meta II half-life is highly dependent on the relative lipid and detergent environment (Mitchell, Straume et al. 1992; Brown 1994; Szundi, Lewis et al. 2005).

3.2.1. (b) Application of Selective Excitation ^{1}H NMR for Studying Ce6 Binding to Rhodopsin: As described above (Section 3.1.1. (b)) and in more detail in Chapter 6, below, the selective excitation 1H NMR approach allows us to investigate the binding of Ce6 (analogous to C3G described above) to rhodopsin. The selective excitation ^{1}H NMR spectra of Ce6 in the absence and presence of various concentrations of rhodopsin in the chemical shift range 8.9ppm to 10ppm is shown in Figure 3.15. The ^{1}H NMR spectra of 50μM Ce6 in the absence of rhodopsin gave rise to three chemical shift signals at 9.72, 9.58 and 9.00ppm. For convenience, we will refer to these peaks as peak1 (9.72ppm), peak2 (9.58ppm) and peak3 (9.00ppm), respectively.

The ^{1}H NMR spectrum of Ce6 acquired in the dark in the presence of 10μM (Figure 3.15, red trace), 25μM (Figure 3.15, blue trace) and 50μM (Figure 3.15, magenta trace) showed clear signals from ligand peaks. The intensity of each signal was less as compared to that observed in the NMR spectrum of 50μM Ce6 alone (Figure 3.15, black trace), indicating restriction in mobility of the ligand resonances in a concentration dependent manner. This decrease in signal intensity suggests binding of Ce6 to dark-state rhodopsin. The change exhibited in the ligand peaks at varying concentrations of rhodopsin was used to estimate the affinity of the Ce6-rhodopsin interaction in the dark.

The binding curves for the dark state are shown in Figure 3.16 A. The K_D values were estimated based on ligand peaks 1, 2 and 3 were 16±7μM, 16±9μM and 25±3μM, respectively.

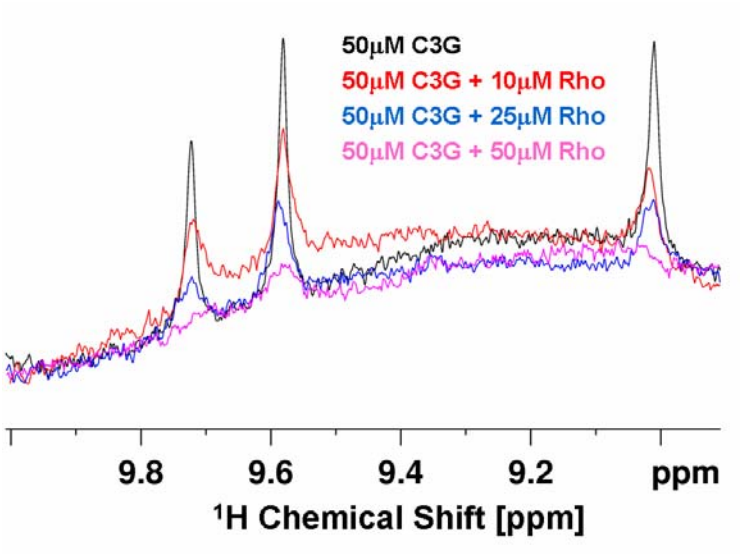

Figure 3.15: Overlay of the selective excitation ^{1}H NMR spectra of 50μM C3G in the absence and presence of 10μM, 25μM and 50μM rhodopsin in the dark.

We also acquired selective excitation ^{1}H NMR spectra immediately at t=0 and t=30 minutes after light-activation to monitor the binding of Ce6 to Meta II and Opsin states. We compared ^{1}H NMR spectra of Ce6 at various concentrations of rhodopsin acquired immediately after light-activation in the absence and presence of Ce6. A complete disappearance of the ligand peaks was observed. Even at the lowest concentration (10μM) of rhodopsin tested, Ce6 ligand peak signals were absent. This clearly suggests that the Ce6 binds to the Meta II state of rhodopsin with much higher affinity than what was observed for the dark state. However, at this time we have not yet

estimated the binding affinity of this interaction. In order to determine affinities in this case one has to acquire data points below the 5:1 ligand:protein ratios. To obtain this data, we will need to increase the concentration of ligand at least by 2-3 fold to get good signal to noise levels. Nonetheless, it is clear from the studies obtained above that Ce6 binds to Meta II and preferably with higher affinity than observed for dark state.

Finally, we also monitored the interaction of Ce6 with the opsin state. The comparison of the ^{1}H NMR spectra acquired in the absence and presence of rhodopsin 30 min after light-activation, gave rise to detectable ligand peak resonances. As explained for dark state rhodopsin above, a decrease in the intensity of peaks 1, 2 and 3 upon addition of rhodopsin protein as compared to free ligand peak intensities can be used to estimate binding affinities (Figure 3.16B). We estimated an affinity of 7.6 ± 2.4, 10.9 ± 2.3 and 5.6 ± 6.4 based on ligand peak 1, 2 and 3, respectively.

The data obtained suggests that Ce6 binds to dark, activated Meta II and also opsin states of rhodopsin, albeit with different affinities. Though it was not possible to obtain an estimation of the interaction between Ce6 and Meta II, it appears that the affinity of this interaction is higher than the dark and opsin states, consistent with our results obtained from fluorescence spectroscopy. However, the affinities obtained from NMR spectroscopy are lower for the dark state (16±8μM) as compared to fluorescence studies (2.6±0.2μM). This is likely due to an over-estimation of quenching that was not fully corrected for by the Parker method.

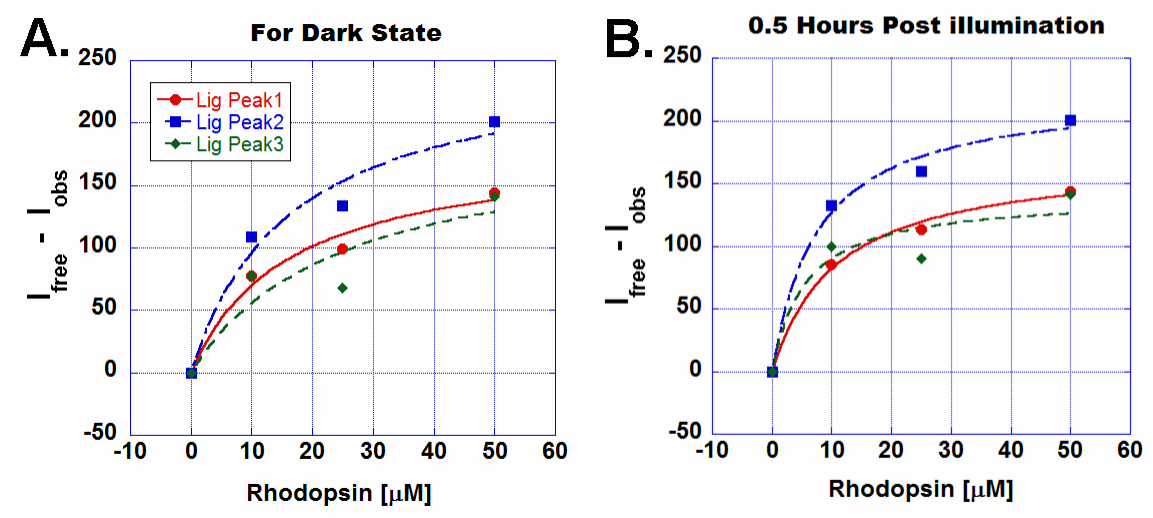

Figure 3.16: The binding curves for the ligands peaks in the (A) dark and (B) 1.5 hours post illumination. Peak 1, 2 and 3 are labeled using red circles, blue squares and green diamonds colors respectively.

3.2.2. Location of Ce6 Binding on Rhodopsin

3.2.2. (a) Ce6 is Predicted to Bind to Rhodopsin at the CP domain: To better understand the molecular details of Ce6 binding to rhodopsin, we conducted computational docking studies of Ce6 in comparison to two other putative ligands (methylene blue and tetra-porphobenzine) studied previously (Washington, Brooks et al. 2004) as well as Pheo-a as a control (see above section 3.2.1 (a)). All four ligands were docked to the dark-state bovine rhodopsin crystal structure (Palczewski, Kumasaka et al. 2000) using the Autodock software (Goodsell, Morris et al. 1996). In each case, the best scoring 10 conformations were considered for analysis, and for Ce6, methylene blue and tetra-porphobenzine more than 80% of these docked in near identical locations. In contrast, Pheo-a was observed in variable regions. Ce6 bound with the most favorable energy of the four ligands docked. Of these ligands, Ce6 also showed the most effective

response of bovine rhodopsin to red light excitation (Washington, Brooks et al. 2004). Thus, our ligand docking results are validated by the available experimental data. The location of Ce6 docking is in the center of the CP domain in all of the top ten most highly-ranked conformations of Ce6, methylene blue and tetra-porphobenzine (Figure 3.17A, Table 3.3). In contrast, Pheo-a is predicted to bind to the TM helices at sites facing the outside of the helical bundle, dominated by hydrophobic interactions (Figure 3.18). The lack of a single highly-ranked binding site also suggests that the affinity of Pheo-a would be low. This confirms the results obtained by fluorescence spectroscopy (Figure 3.13).

Ce6 and Pheo-a were also docked to our recently developed model of the Meta II state (Isin, Rader et al. 2006). Ce6 again docked only in the CP domain, but with differences in the details of the interactions and the orientation of Ce6 as compared to the dark-state (compare Figure 3.17 A,C with Figure 3.17 B,D). Pheo-a again docked only to the hydrophobic TM outside of the helical bundle, but also displayed some differences between dark and light-activated models (Figure 3.18). The analysis of the 5Å binding pocket residues of Ce6 (Figure 3.17 B,D, Table 3.3) revealed that most of the binding pocket residues in the dark and light-activated models overlapped, namely Lys-67, Arg-69, Thr-70, Pro-71, Glu-134, Arg-135, Val-138, Ala-246, Ala-247, Val-250, Asn-310, Gln-312, Ser-334, Thr-335, Thr-336, Gln-344, Val-345, Ala-346 and Pro-347. Some of these residues are known to be important for G_t binding and activation, and include the highly conserved Glu-134 and Arg-135 of the D/ERY motif, indicating an overlap in the binding interfaces (see below).

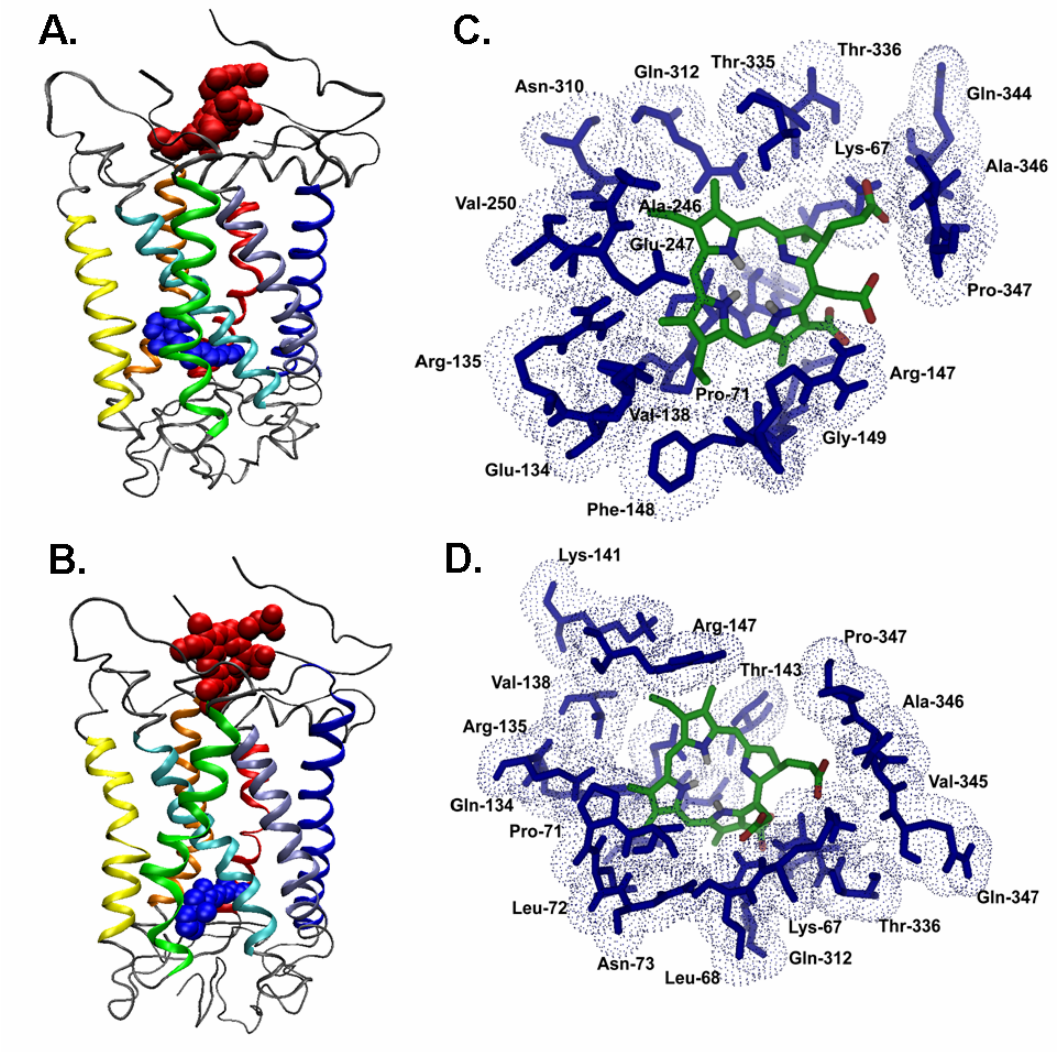

Figure 3.17: Docking studies of Ce6 to different states of rhodopsin. Docking of Ce6 to (A) dark state rhodopsin (PDB identification 1L9H) (Okada, Fujiyoshi et al. 2002) with *11-cis* retinal and (B) model of the Meta II state of rhodopsin with *all-trans* retinal (Isin, Rader et al. 2006). *11-cis* Retinal and *all-trans* retinal are colored blue and Ce6 is colored in red. All ligands are rendered space filling. The residues within 5Å of the docked Ce6 are shown for (C) dark state rhodopsin and (D) Meta II state rhodopsin. Images were generated using VMD (Humphrey, Dalke et al. 1996) and PyMol (http://www.pymol.org) software.

There are some residues that differentiate the dark and light-activated models: Phe-148, Gly-149 and Glu-150 were unique to the dark state (Table 3.3, labeled '•') and Leu-68, Leu-72, Asn-73, Lys-141, Thr-243 were unique to the light-activated model (Table 3.3, labeled '°'). The results obtained support the experimentally observed differences in affinity of Ce6 for dark and light-activated states of rhodopsin (Figure 3.13, filled and open circles) and suggest that binding of Ce6 may affect the structure and dynamics of the CP domain. Further, these predictions also suggest that Ce6 binding at the CP domain might impact G_t binding to rhodopsin.

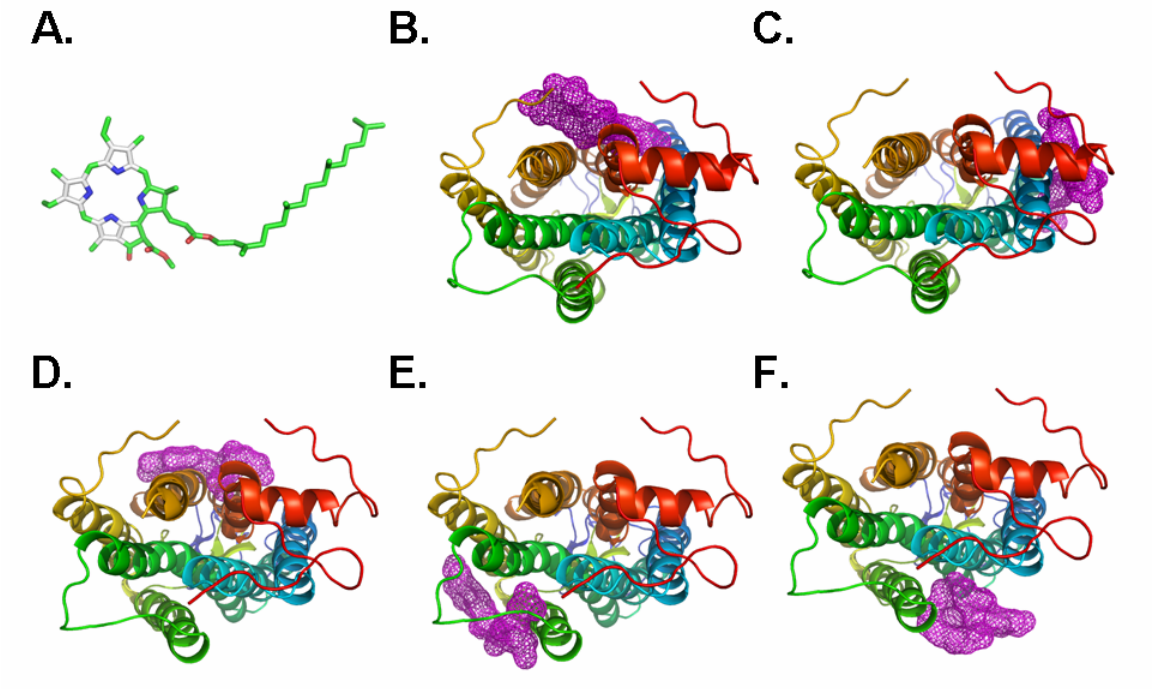

Figure 3.18: Pheophytin-a docking to dark, X-ray crystal structure (pdbid:1L9H (Palczewski, Kumasaka et al. 2000)) and ANM activated model (Isin, Rader et al. 2006) of rhodopsin. The chemical structure of pheophytin-a, demetallated chlorophyll-a derivative is shown in (A). The different positions at which the top 10 ligand conformations were found to dock are shown for dark (B), (C) and ANM activated model (D), (E), and (F). The binding energies and number of ligand conformations docked in B, C, D, E and F are -15.10 (6/10), -13.24 (4/10), -13.77 (6/10), -13.75 (3/10), and -9.51 (1/10) Kcal/mol, respectively.

Table 3.3. List of amino acids within 5Å of Ce6 in bovine rhodopsin and respective amino acids. For comparison, the amino acids within 5Å of the G_t C-terminal high affinity peptide docked to the rhodopsin crystal structure and the model of the Meta II state (Figure 3.8) are listed, as well as those amino acids within 5Å of the G_t C-terminal peptide bound in the opsin crystal structure (Scheerer, Park et al. 2008). Finally, we are also reporting the high connectivity residues in the CP domain (Christopher J R Illingworth 2008). These are residues that are likely to be involved in interactions with ligands. The cutoff range is represented in percentage, with higher percentages being more likely interacting residues. The labels, '•' and '°', indicate that these residues are part of the binding pocket in either only the dark (•) or only the light-activated Meta II model (°). The labels, '*' and '-', indicate if the amino acid is or is not part of the binding pocket, respectively.

Bovine	Gt-peptide Docking	Opsin+Gt-peptide X-ray Structure (3DQB) (Scheerer, Park et al. 2008)	High connectivity residues (Christopher J R Illingworth 2008)	Bovine	Gt-peptide Docking	Opsin+Gt-peptide X-ray Structure (3DQB) (Scheerer, Park et al. 2008)	High connectivity residues (Christopher J R Illingworth 2008)
Lys-67	*	-	-	Glu-150•	*	-	-
Lue-68°	*	-	80%	Thr-243°	*°	*	-
Arg-69	*	-	-	Ala-246	*	*	-
Thr-70	*	-	70%	Glu-247	*	-	-
Pro-71	*	-	70%	Val-250	*	*	-
Leu-72°	*	*	80%	Asn-310	-	*	70%
Asn-73°	*	*	70%	Gln-312	*	*	70%
Glu-134	*	-	70%	Ser-334	-	-	-
Arg-135	*•	*	70%	Thr-335	*	-	-
Val-138	*	*	-	Thr-336	*	-	-
Lys-141°	*	*	-	Gln-344	*°	-	-
Arg-147	*	-	-	Val-345	*°	-	-
Phe-148•	*	-	-	Ala-346	*	-	-
Gly-149•	*	-	-	Pro-347	*	-	-

3.2.2. (b) ^{19}F NMR Studies of Rhodopsin Labeled at Positions Cysteine 140 and 316 in the CP domain: To further corroborate the CP ligand binding site, we investigated rhodopsin labeled with NMR probes specifically introduced via cysteine chemistry into the CP domain. Rhodopsin has a total of ten cysteines, four of which are not reactive (Cys110 and Cys187 are engaged in a disulfide bond and Cys322 and Cys323 are palmitoylated). Two of the remaining cysteines are located in the EC domain, four in the TM and two in the CP domain (Figure 3.19). Out of all ten cysteines, only Cys-140 and Cys-316 are accessible in the dark or inactive form. Both of these cysteines are located in the CP domain (Figure 3.19). To enable ^{19}F NMR spectroscopy, we introduced, through a disulfide linkage, the trifluoroethylthio- CF_3-CH_2-S- (TET-) group to the cysteine residues (Cys-140 and Cys-316) of interest as previously reported (Klein-Seetharaman, Getmanova et al. 1999; Loewen, Klein-Seetharaman et al. 2001).

To study the effects of Ce6 binding on CP domain, we recorded dark and light ^{19}F NMR spectra of rhodopsin in the absence and presence of Ce6 (Figure 3.20). In the absence of Ce6, this gave rise to two distinct peaks at -65.0ppm and -65.4ppm (10.5ppm and 10.1ppm using TFE as internal reference) in the dark (Figure 3.20B and C, black solid trace), similar to those reported previously of 10.6ppm and 10.0ppm in reference to TFA (Klein-Seetharaman, Getmanova et al. 1999). Upon light-activation, these two peaks shifted to their Meta II positions (Figure 3.19C, red trace). Meta II peaks decayed to form opsin and gave rise to a broad peak with a maximum at -65.80ppm.

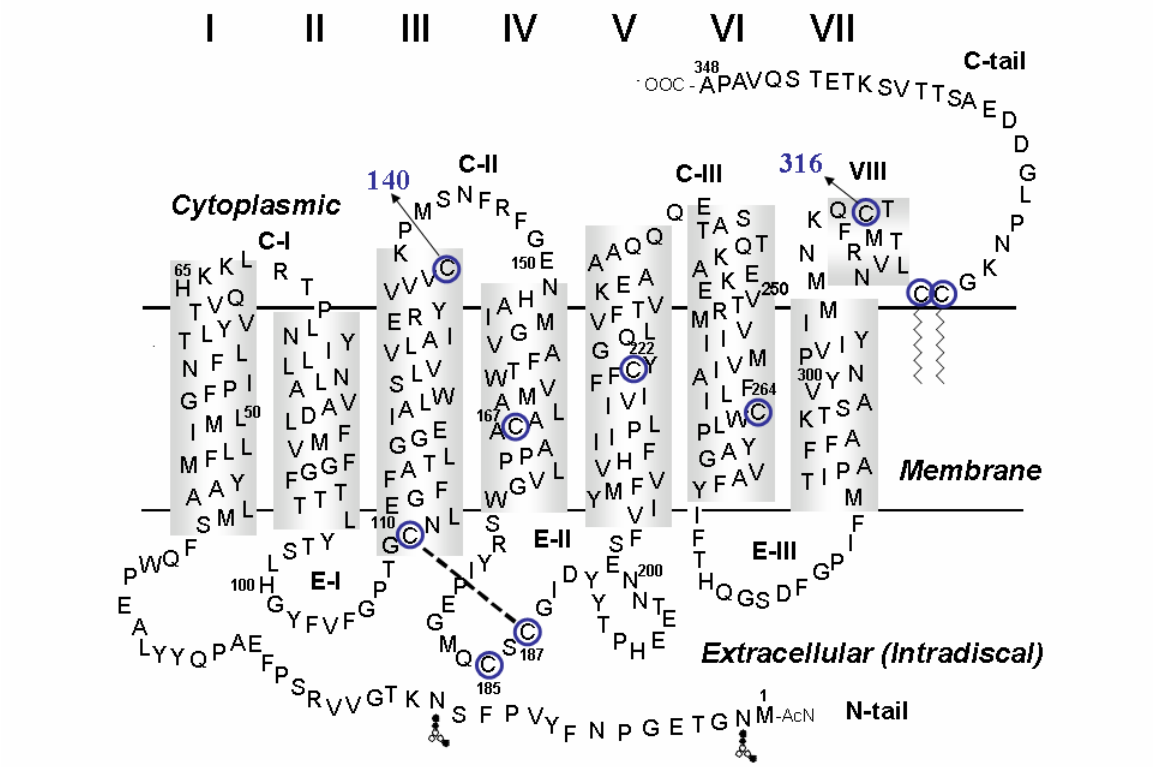

Figure 3.19: Secondary structure model of rhodopsin showing the positions of cysteines. All the cysteines in rhodopsin are enclosed in blue circles. The cysteines at positions 140 and 316 are indicated by an arrow and labeled in blue.

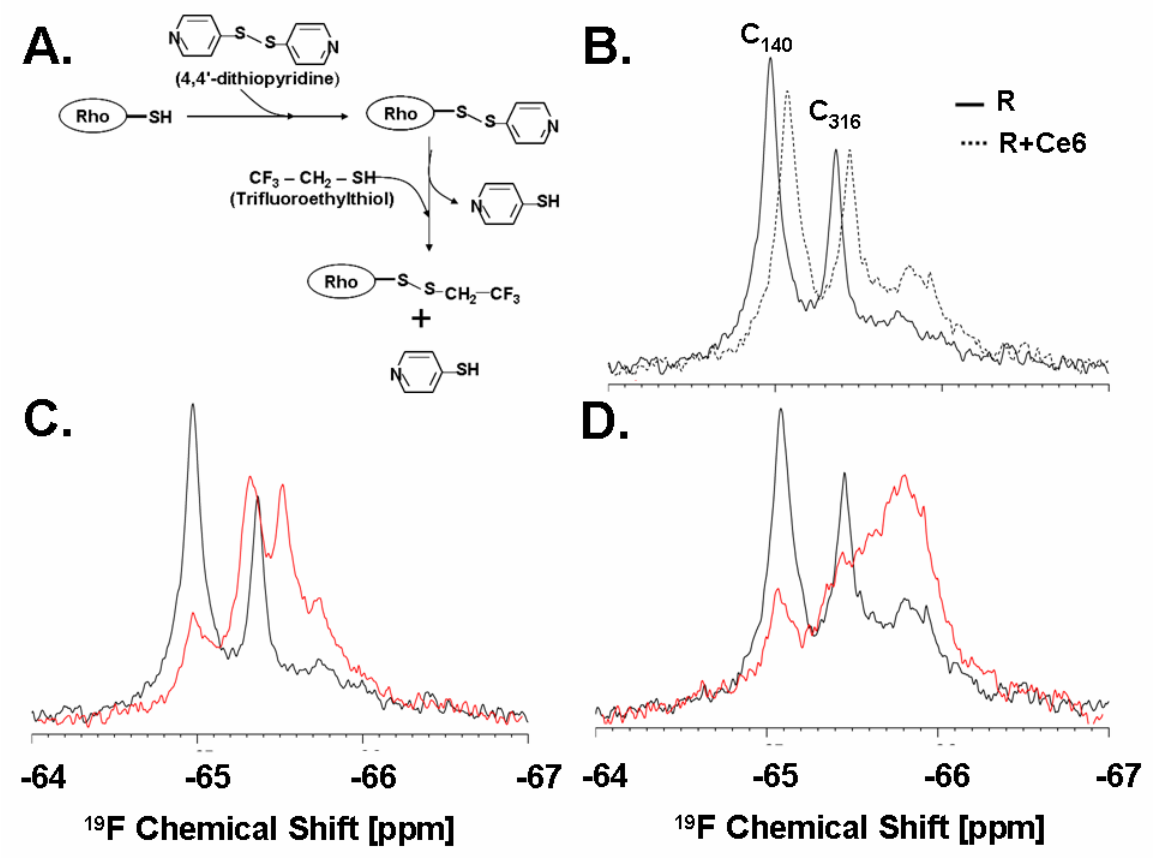

Figure 3.20: ^{19}F NMR spectra of Ce6 binding to the CP surface of dark and light state rhodopsin. (A) Scheme of attaching the ^{19}F label. Two samples of 7 mg of rhodopsin ^{19}F derivatized at positions Cys-140 and Cys-316 in a volume of 350µl DM micelles in NMR buffer (Methods) were investigated by NMR spectroscopy. The rhodopsin concentration was 0.5mM and the DM concentration was 7.4%. The two samples were identical and only differed in the presence or absence of Ce6. (B) Dark rhodopsin in the absence (solid trace) and presence (dotted trace) of Ce6. Overlay of rhodopsin in the dark and immediately after light-activation (with in 2 mins) in the absence (C) and presence (D) of 8.25 fold excess Ce6, at a final Ce6 concentration of 4.0mM. Each spectrum was acquired within 2 minutes on a 600MHz Bruker instrument, at 20^{o}C. Each Spectrum is an average of 105 scans. A line broadening of 10Hz was used.

In the presence of Ce6, small but significant shifts of 0.2ppm were observed in both Cys-140 and Cys-316 peaks in the dark (Figure 3.20B, dotted trace). Upon light-activation, the peaks did not shift to the positions of Meta II peaks observed in the absence of Ce6 (Figure 3.19D). Instead, the peaks shifted directly to a peak at -65.94ppm (identical for Cys-316 and Cys-140). This chemical shift is similar, but not identical to the one of the opsin peak in the absence of Ce6, which is observed at -65.80ppm. These ^{19}F NMR studies indicate that Ce6 binds in the CP face of rhodopsin.

3.2.3. Effects of Ce6 Binding on Rhodopsin Function

3.2.3. (a) Ce6 Interferes with G_t Binding to Rhodopsin: The functional role of Meta II rhodopsin is to activate G_t and initiate signaling. The observed differences in ^{19}F NMR spectra in the presence and absence of Ce6 as well as the docking results suggest that Ce6 may interfere with G_t activation. To test this hypothesis we measured the activation of G_t by light-activated rhodopsin using a [^{35}S]GTPγS filter binding assay in the absence and presence of Ce6. G_t activation was inhibited in a concentration-dependent manner (Figure 3.21). IC_{50} values of 65nM - 150nM were obtained for 5nM rhodopsin and 1μM G_t in DM micelles and ROS membranes (Figure 3.22A). A time course of light-dependent activation of G_t by rhodopsin in bovine ROS was measured in the presence and absence of a 25-fold excess Ce6 (Figure 3.22B). At 120 seconds post-illumination a sample free of Ce6 displayed near saturation in activation, whereas an identical sample containing 25-fold excess Ce6 displayed no activation as compared to dark controls (Figure 3.22B). These studies suggest that Ce6 interferes with G_t binding to rhodopsin and the effect is similar in ROS and rhodopsin in DM micelles.

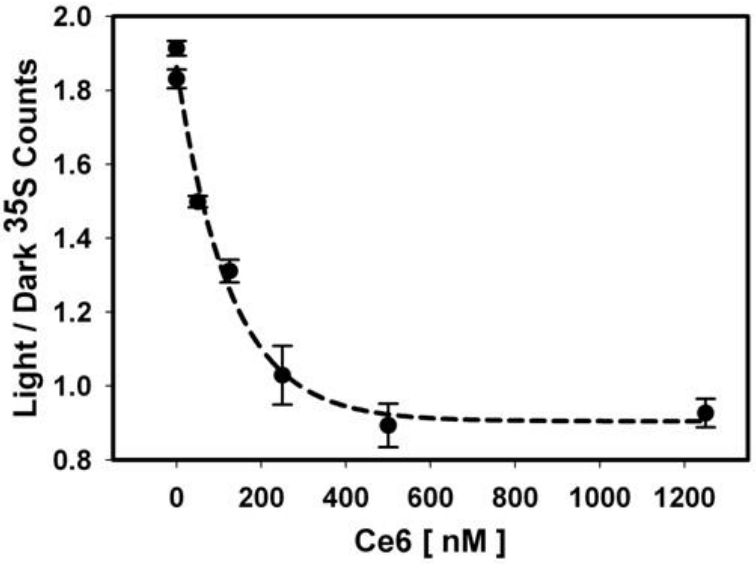

Figure 3.21: G_t activation in ROS by the [^{35}S]GTPγS filter binding assay. The relative ratio of light versus dark radioligand counts is plotted against the Ce6 concentration in nM. G_t activation is inhibited by the presence of Ce6. The rhodopsin concentration used was 0.25μM. Data was fitted with the exponential decay function.

3.2.3. (b) Modulation of G_t Peptide Binding to Rhodopsin in the Presence of Ce6: Further support for an interference of Ce6 with G_t binding came from studies with a high affinity analog of the G_t C-terminal peptide corresponding to the sequence VLEDLKSCGLF. This peptide quenches rhodopsin tryptophan fluorescence only upon light-activation, as described (Kisselev, Meyer et al. 1999; Arimoto, Kisselev et al. 2001). However, unlike Ce6, the G_t peptide is not able to quench fluorescence fully, and even at a 1500-fold excess of the peptide, 25% of the fluorescence remains (Figure 3.23). A similar level of quenched fluorescence is achieved with Ce6 with a 5-fold excess (Figure 3.12 and Figure 3.23). In the presence of both, a 5-fold excess Ce6 and 1500-fold excess G_t peptide fluorescence quenching is greater than in the presence of either compound

alone, consistent with the interpretation that Ce6 may largely displace the G_t peptide from rhodopsin, while the Ce6-free fraction is occupied by G_t.

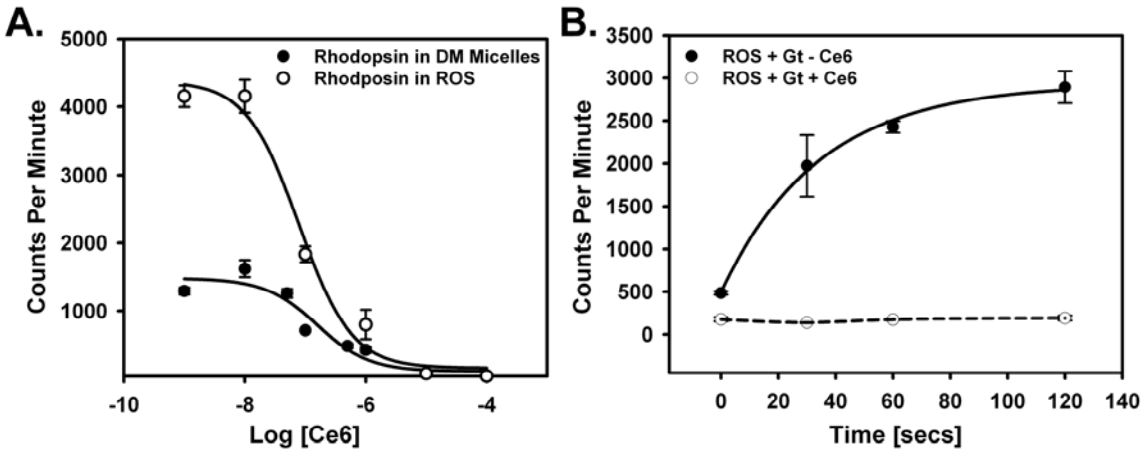

Figure 3.22: Concentration-dependent inhibition of G_t activation by Ce6. (A) Decrease in G_t activation monitored with 5nM ROS (open circles) and 5nM rhodopsin in DM micelles (closed circles). All reactions were incubated for 30 minutes following illumination (2 minutes) and stopped by filtering through nitrocellulose membranes as described in Supplementary Methods. (B) Time course of G_t activation with illuminated rhodopsin in the absence (filled circles) and presence of a 25-fold excess of Ce6 (open circles) over rhodopsin concentration. The rhodopsin concentration used was 0.25μM. The data in (A) was fitted with the sigmoidal dose-response non-linear regression function and using the exponential growth function for (B).

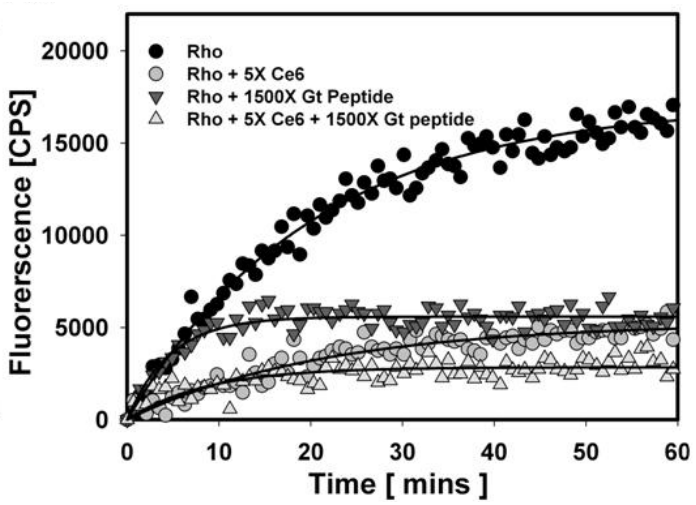

Figure 3.23: Modulation of G_t peptide binding to rhodopsin in the presence of Ce6. The effect of Ce6 on G_t peptide VLEDLKSCGLF binding to rhodopsin was determined by fluorescence spectroscopy. The rhodopsin concentration used was 0.25μM. Data was fitted using the exponential growth function.

3.2.3. (c) Docking Studies of C-terminal G_t Peptide to Rhodopsin: The most likely explanation for the effects of Ce6 on G_t peptide binding (Figure 3.23) is an overlap between the binding sites. To help understand these effects we docked the G_t peptide to both dark (PDBID: 1L9H:A) (Palczewski, Kumasaka et al. 2000) and light-activated rhodopsin (Isin, Rader et al. 2006) models using ClusPro software (Comeau, Gatchell et al. 2004). In each case, the top 10 best scoring conformations were considered for analysis, and 90% of the time they were docked in the CP domain of rhodopsin (Figure 3.24). The electrostatic and desolvation energies of both the dark and light-activated models of the peptide-rhodopsin complexes were estimated using FastContact analysis (Camacho and Zhang 2005). The electrostatic energy of peptide binding to the light-activated model was estimated at -14.1kcal/mol, as compared to -6.7kcal/mol for binding to dark-state rhodopsin. This result is validated by the experimentally known fact that the

peptide essentially does not bind to dark-state rhodopsin. The desolvation free energies calculated for the binding of peptide to dark and light state rhodopsin models was +1.1kcal/mol and -1.7kcal/mol, respectively, also supporting that the peptide binds better to the light-activated structure of rhodopsin. Shown in Table 3.3 are the amino acids predicted to be within 5Å of the peptide docked to dark and light-activated structures as compared to the respective binding pocket of Ce6. The predicted peptide binding pocket residues are in agreement with previously published data of the G_t C-terminal peptide (IRENLKDSGLF) (Filipek, Krzysko et al. 2004) and the recent crystal structure of opsin bound to the peptide (Scheerer, Park et al. 2008). We observe substantial overlap between the predicted Ce6 and Meta II binding pockets, and experimentally-observed peptide binding pockets in opsin (26 and 10 out of 28 residues, respectively).

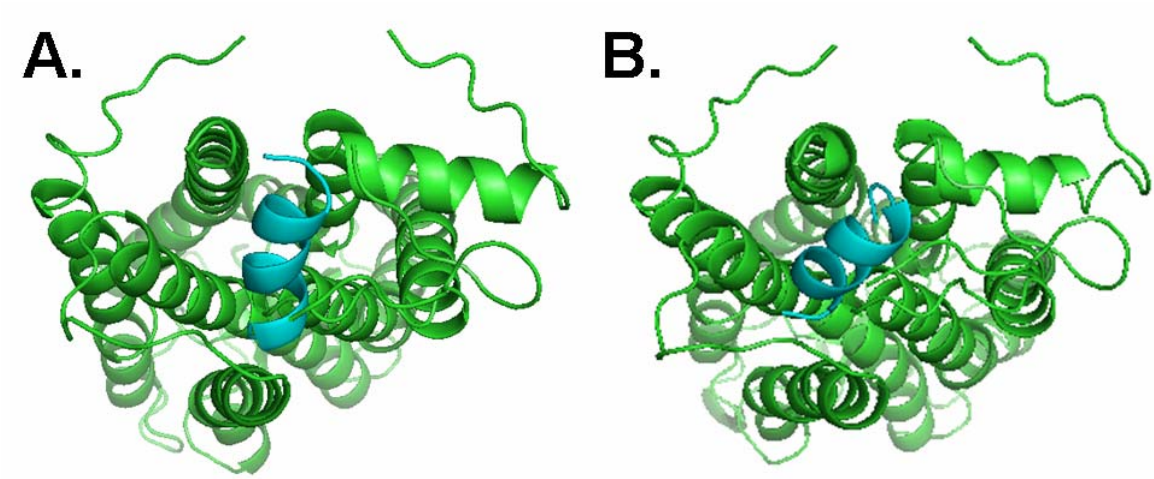

Figure 3.24: Docking of C-terminal peptide to rhodopsin. Docking of Gt C-terminal peptide IRENLKDSGLF to (A) Dark state and (B) ANM activated model of rhodopsin.

3.2.4. Effects of Ce6 Binding on Rhodopsin Structure and Dynamics

3.2.4. (a) Time Dependent Conformational Changes in the CP domain in the Dark and upon Light-activation using ^{19}F Labeled Rhodopsin at Cys-140 and Cys-316: To study the effects of Ce6 binding on rhodopsin structure and dynamics, we extended the ^{19}F NMR spectroscopy discussed in section 3.2.2. (b) to record time dependent changes of rhodopsin upon light-activation in the absence and presence of Ce6.

As described above (section 3.2.2. (b)), in the dark, the ^{19}F labels attached to sites Cys-140 and Cys-316 results in two peaks at -65.0ppm and -65.4ppm (Figure 3.25A). Upon illumination, these two peaks shifted to form light-activated rhodopsin, Meta II. The Meta II peaks decreased with concomitant increase of the opsin peak with an estimated half-life of 12.2 minutes for the Cys-140 and 15.7 minutes for the Cys-316 peak. These half-lives fit well with the Meta II decay of rhodopsin recorded in the presence of 10% DM using fluorescence spectroscopy (Figure 3.26).

In the presence of Ce6, in the dark we also saw two signals corresponding to Cys-140 and Cys-316 peaks (Figure 3.25B, black trace). However, upon light-activation, the peaks did not shift to the positions of Meta II peaks observed in the absence of Ce6 (Figure 3.25, red traces in A and B). Instead the peaks shifted directly to a peak at -65.94ppm (identical for Cys-316 and Cys-140). This chemical shift is similar, but not identical to the one of the opsin peak in the absence of Ce6, which is observed at -65.80ppm. Furthermore, the opsin peak is clearly visible only after 30 minutes in the absence of Ce6 (Figure 3.25A, orange trace), while it is instantly observed after illumination in the presence of Ce6 (Figure 3.25B, orange trace). This raises the question of whether the chemical shift difference of 0.14ppm represents an opsin-like structure or

corresponds to actually retinal-free opsin protein. The former would assume that Meta II is indeed formed in the presence of Ce6 but has a different conformation in the CP domain from Ce6-free Meta II. The latter would suggest that retinal leaves the binding pocket in less than 2min, the time it takes to record the first NMR spectrum after illumination. This question can be answered with absorbance spectroscopy. UV/Visible absorption spectra will show a 440nm peak after addition of 1% HCl (v/v) if the retinal is still bound to Lys296. Indeed, we find a 440nm peak even in the presence of Ce6 immediately after illumination, but not 1.5 hours after illumination, essentially identical to what is observed with rhodopsin in the absence of Ce6 (data not shown). This result suggests that the ^{19}F NMR peak at -65.94ppm observed immediately after illumination in the presence of Ce6 arises from an altered Meta II state, rather than opsin. The subsequent transition to opsin is essentially NMR-silent because the chemical shift values are very close and the peaks are very broad.

Interestingly, the gradual formation of the opsin state in the absence of Ce6 triggers the release of free ^{19}F label from the two cysteines, resulting in a decrease of the opsin peak and an increase in free label peak at -68.96ppm (Figure 3.27C). In the presence of Ce6, the decay of the opsin peak was slower (Figure 3.27A) and free label peak formation was minimal (Figure 3.27B), a very striking difference to what is observed in the absence of Ce6. We conclude from these ^{19}F NMR studies that Ce6 affects the local environment of both cysteines in the CP face of rhodopsin. Further, binding results in modulation of conformational states of rhodopsin upon light-activation.

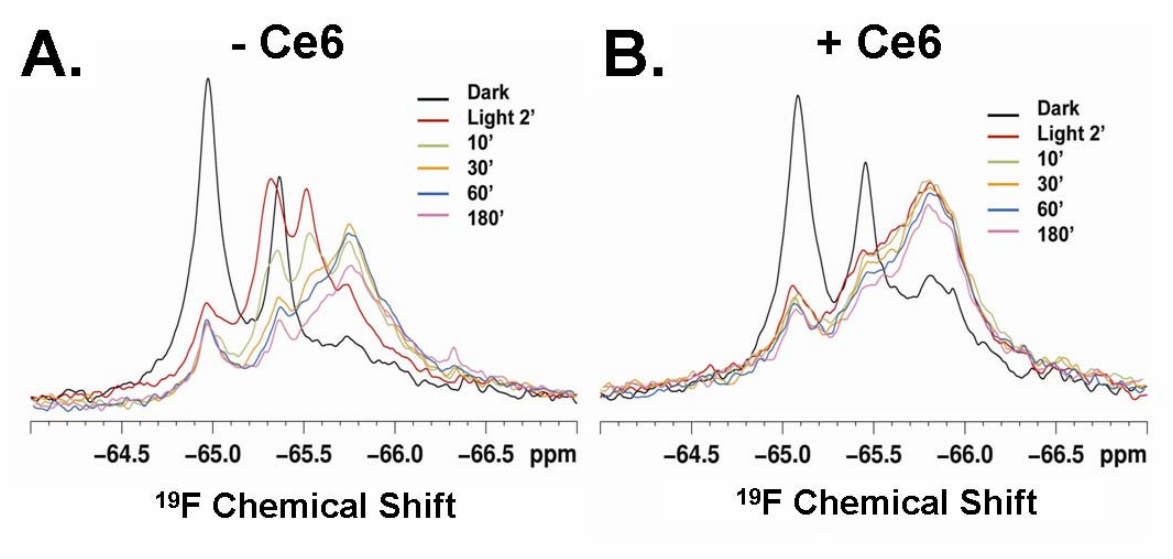

Figure 3.25: Time dependent changes in the CP domain of rhodopsin upon light-activation. Overlay of one dimensional ^{19}F NMR traces as a function of time in the dark and upon light-activation in the absence (A) and presence (B) of Ce6. Cysteine residues at positions 140 and 316 in rhodopsin were labeled by trifluoroethylthio (TET) groups as described previously (Klein-Seetharaman, Getmanova et al. 1999). A total of 7mg of rhodopsin in 20 mM sodium phosphate buffer with 9% n-dodecyl-β-D-maltoside (DM) and 10% D_2O at pH 6.0 was used for each sample.

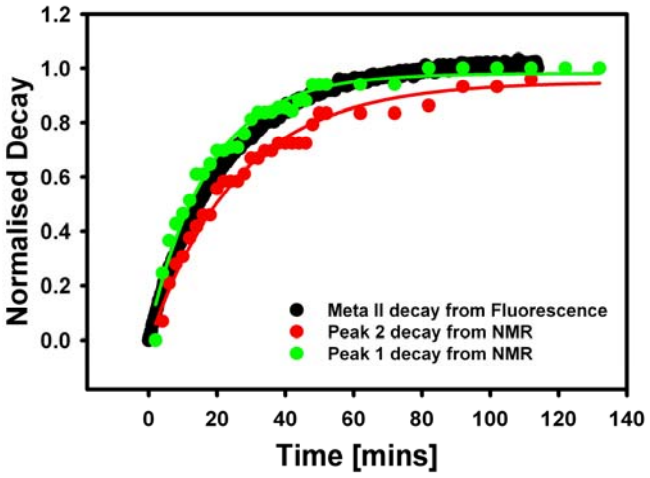

Figure 3.26: Comparison of the decay of Meta II peaks of Cys-140 and Cys-316 measured by NMR spectroscopy with Meta II decay kinetics obtained using fluorescence spectroscopy. The Meta II decay plot of rhodopsin at 10% DM obtained by fluorescence is shown as black circles and those from NMR spectroscopy as (red and green circles. Peak 1 and 2 correspond to the Meta II peaks of Cys-140 and Cys316 peaks after light-activation. The calculated decay rates for rhodopsin (fluorescence), peak 1 and peak 2 are 0.0454, 0.0566 and 0.0385 min^{-1}, respectively. A rhodopsin concentration of 0.5μM and 0.5mM was used to record fluorescence and NMR spectra, respectively. The results obtained from these two independent methods are in good agreement.

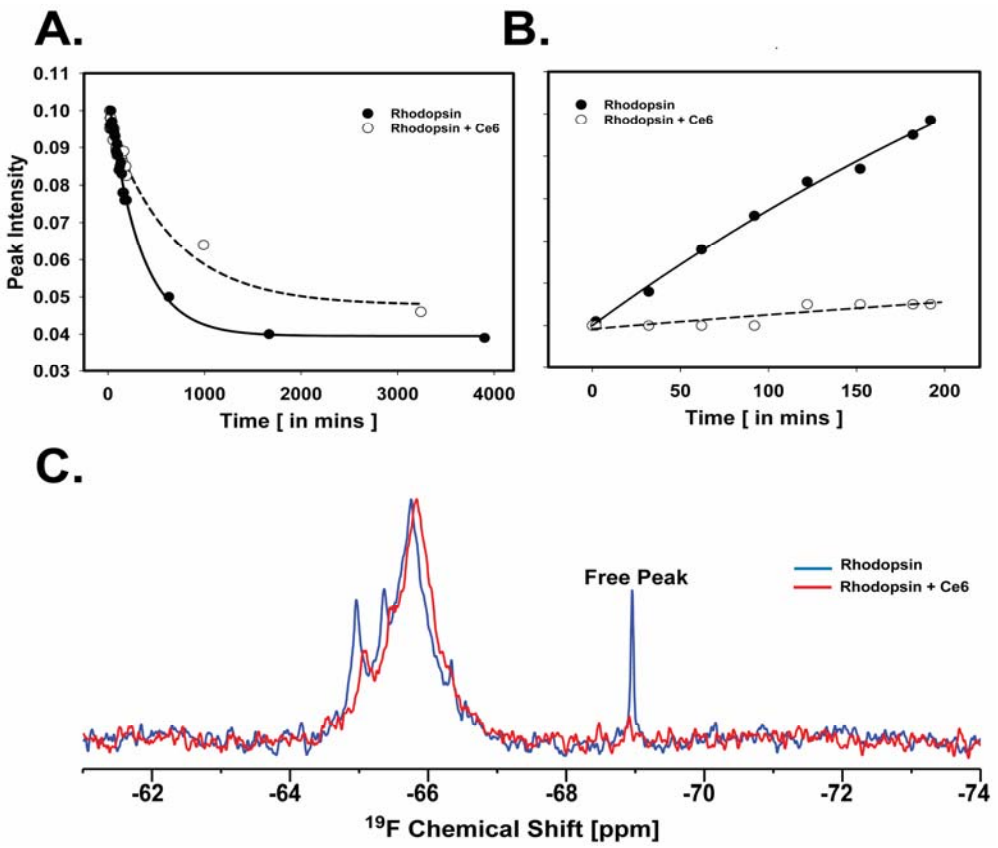

Figure 3.27: Decay of rhodopsin after light-activation and free label formation in the absence and presence of Ce6. (A) Decay of the broad peak around -66ppm (-65.80ppm and -65.94ppm for rhodopsin (blue line in (C)) and rhodopsin plus Ce6 (red line in (C), respectively) in the absence (filled circles) and presence (open circles) of 8.5 fold excess Ce6. The decay rate of opsin in the presence of Ce6 was decreased by a factor of 2. (B) Plot of the formation of the free label peak (its position in the spectrum is indicated in (C)) in the absence (filled circles) and presence (open circles) of Ce6. Less than 20% of the ^{19}F label appeared as free label after 16 hours. Data were fitted using the exponential decay function for (A) and linear function for (B). (C) Overlay of one-dimensional ^{19}F NMR spectra of rhodopsin 3 hours after illumination in the absence (blue line) and presence of Ce6 (red line).

3.2.4. (b) Development of NMR Methodology to Study Membrane Protein Dynamics by ^{19}F NMR Methyl Relaxation: The studies described in section 3.2.4 (a) strongly suggest the possibility of changed dynamics in the CP region upon binding to Ce6. Solution NMR relaxation techniques have been very useful to measure and characterize motions occurring in biological molecules on different time scales ranging from fast to slow internal motions. While this technique has proven successful for many soluble proteins, its application to membrane proteins is limited. This is due to constraints such as size of the molecule, detergent environment; and suppression of signal intensities due to large detergent peaks. ^{19}F NMR spectroscopy has been found especially useful for studying the conformational changes in rhodopsin (Klein-Seetharaman, Getmanova et al. 1999; Loewen, Klein-Seetharaman et al. 2001). As explained in section 3.2.2. (b), in the ^{19}F NNR strategy we follow conformational changes associated with residues specifically labeled at desired positions (Gerig 1989; Klein-Seetharaman, Getmanova et al. 1999; Loewen, Klein-Seetharaman et al. 2001; Klein-Seetharaman 2002). Furthermore, fluorine atoms are very sensitive to changes in the local environment and the overall mobility of molecule itself (Gerig 1989). Here, we developed a ^{19}F NMR spectroscopic approach to study the conformational dynamics in rhodopsin in the presence and absence of Ce6. This is the first application of quantification of ^{19}F-methyl dynamics to a membrane protein.

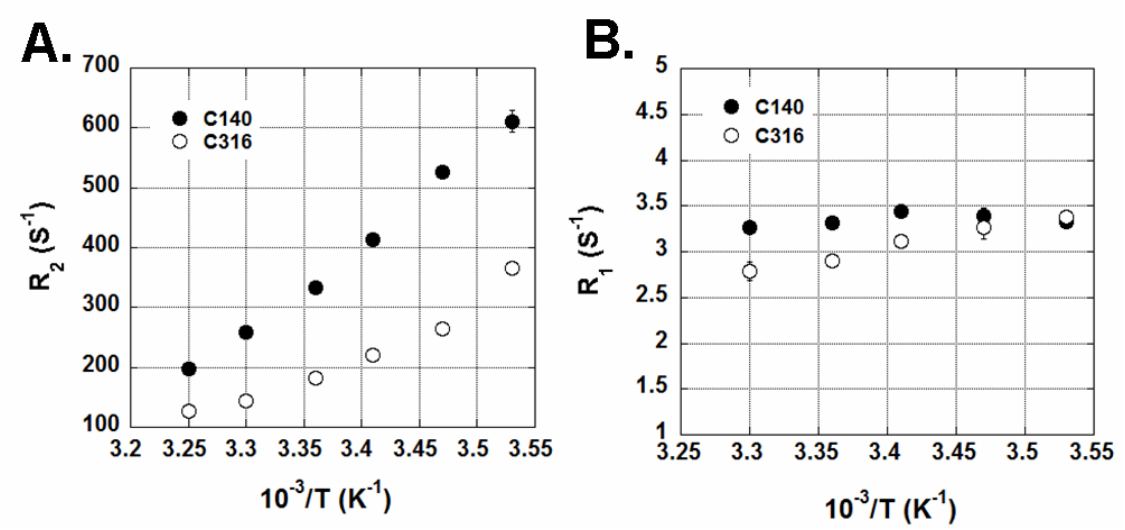

Figure 3.28: ^{19}F NMR relaxation rates of Cys-140 and Cys-316 in rhodopsin. (a) R_2 values and (b) R_1 values determined at various temperatures. The values are plotted for Cys-140 (filled circles) and Cys-316 (open cicles).

Longitudinal (R_2) and transverse (R_1) relaxation rates of ^{19}F methyl groups attached to two cysteine sites in the CP surface of rhodopsin, at positions Cys-140 and Cys-316, were recorded on a Bruker 600MHz instrument (Figure 3.28). For the details on labeling at these sites please refer to section 3.2.2 (b). The accessible cysteines in rhodopsin Cys-140 and Cys-316 contain the label –S-CH_2-CF_3. R_1 and R_2 rates were determined as a function of temperature in the range from 10 to 35°C, with an interval of 5°C. The R_2 values of both Cys-140 and Cys-316 exhibit almost linear Arrhenius plots (Figure 3.28A), indicating that they are predominantly determined by a single correlation time. Such linear dependence indicates that there are no conformational changes in the protein over the temperature range tested. Further comparison of the R_2 rates for Cys-140 and Cys-316 at different temperatures suggests that Cys-316 has shorter R_2 values compared to Cys-140. The calculated R_2 rates for Cys-140 and Cys-316 measured at

25°C are 334 ± 3 s^{-1}, and 183 ± 3 s^{-1}, respectively. This indicates that that Cys-140 might be less flexible compared to Cys-316 (Figure 3.28A). In contrast to the R_2 values, the R_1 values of both Cys-140 and Cys-316 display non-linear Arrhenius plots (Figure 3.28B). This suggests that R_1 values might be influenced by internal motions of the label, in addition to overall molecular rotation of the molecule. The studies presented here support that ^{19}F methyl relaxation, especially R_2 measurements, can be applied to study dynamics of large protein systems at high magnetic fields in detergent micelles.

Table 3.4: Fluoromethyl relaxation rates at 25°C in the absence and presence of Ce6.

rate	Without Ce6		With Ce6	
(s^{-1})	Cys-140	Cys-316	Cys-140	Cys-316
R_2	334 (2.5)	183 (3.3)	349 (2.1)	232 (6.3)
R_1	3.31 (0.03)	2.90 (0.04)	3.27 (0.06)	3.57 (0.03)

3.2.4. (c) Application of ^{19}F Dynamics Method to Rhodopsin-Ce6 Interaction: Shown in Figure 3.29 are the longitudinal and transverse relaxation values of ^{19}F labeled rhodopsin with and without Ce6. The dynamics of the CP domain upon Ce6 binding were monitored using the Cys-140 and Cys-316 positions in the CP domain as discussed above. The R_1 and R_2 measurements were recorded at 10, 15, 20, 25, and 30°C. In the presence of Ce6, the transverse (R_1) and longitudinal (R_2) relaxation values of Cys-316 were higher at the different temperatures tested. In contrast, the relaxation values of Cys-140 in the absence and presence of Ce6 exhibited similar values at the different

temperatures tested. The only exception was the longitudinal relaxation value acquired at 30°C, which was higher in the presence of Ce6. The comparison of the R_1 and R_2 values at 25°C for both the cysteines are listed in Table 3.4. Overall, these results suggest a significant change in the flexibility of the residue Cys-316 upon binding to Ce6. The observation that Cys-140 remains unchanged upon binding to Ce6, while more significant changes are observed in the flexibility of Cys-316 suggests that the CP binding site of Ce6 is closer to helix 8 than CP loop 2.

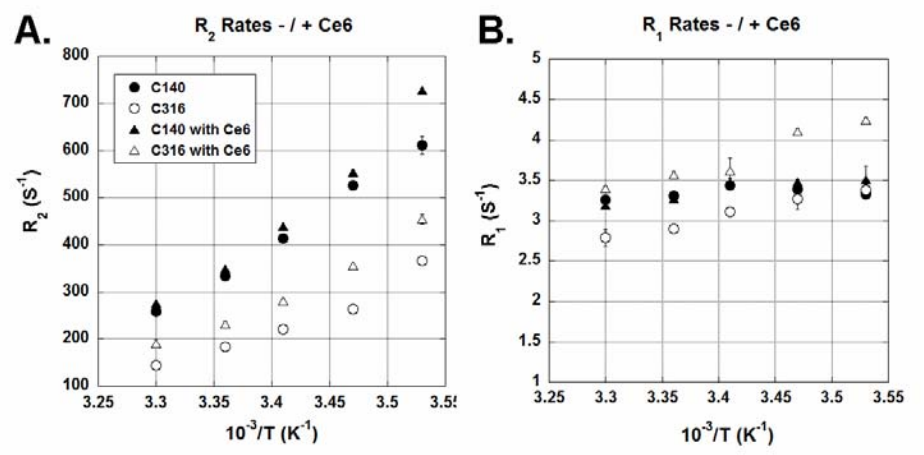

Figure 3.29: Comparison of ^{19}F NMR longitudinal and transverse relaxation rates of Cys-140 and Cys-316 in rhodopsin in the absence and presence of Ce6. The overlay of (A) R_2 and (B) R_1 values at various temperatures for Cys-140 (filled symbols) and Cys-316 (open symbols) without (circles) and with Ce6 (triangles).

3.2.4. (d) Conformational Changes in the EC and TM Domain induced by Ce6 Binding Probed by NMR Spectroscopy of α,ε-^{15}N- Tryptophan Labeled Rhodopsin: Structural communication between the TM and the CP domain is well established for GPCRs. Upon light-activation, the changes due to the dissociation of the retinal in the

TM are communicated to the CP domain where a hydrophobic interface becomes exposed that allows other signaling proteins to bind. In this case, a signal initiated at the interface between the TM domain and EC domain of rhodopsin is translated effectively to the CP domain. Here, we propose that the reverse could also be true - binding of a ligand at the CP site of rhodopsin may affect the conformation of the TM and perhaps the EC parts of the protein. To test whether the overall structures of the TM and EC domains of rhodopsin are changed upon Ce6 binding at the CP domain, we followed the behavior of tryptophan residues (Klein-Seetharaman, Yanamala et al. 2004; Werner, Lehner et al. 2007). There are several reasons behind selecting tryptophan residues for performing this experiment: (a) tryptophans are completely absent in the CP domain, (b) tryptophan residues are few in number (there are a total of five tryptophan residues in rhodopsin) and thus result in a less-crowded NMR spectrum, and (c) out of the five tryptophans present in rhodopsin, Trp-35 is in the EC domain, and the tryptophans in the TM domain are fairly distributed among different helices (Figure 3.30). As the $^{1}H,^{15}N$ resonances from all five backbone NH groups of tryptophans have been assigned recently (Werner, Lehner et al. 2007), we can identify which helices are predominantly affected by Ce6. Further, Trp-126, Trp-161 and Trp-265 were shown to play an important role in the activation of rhodopsin (Lin and Sakmar 1996; Borhan, Souto et al. 2000). In particular, Trp-265 is the highly conserved in GPCRs and participates in the ligand binding interactions.

To monitor if Ce6 binding at the CP domain exerts allosteric effects on EC and TM domains, we measured ^{1}H-^{15}N heteronuclear single quantum correlation (HSQC) NMR spectra of α-ε-^{15}N-labeled tryptophan rhodopsin at 37°C. In general, the ^{1}H-^{15}N HSQC spectrum contains chemical shifts originating from protons (H^{N}) that are directly

connected to nitrogen in the protein backbone or side chains. For example, the HSQC spectrum also contains peaks from NH_2 group protons of Lys, Asn, Gln, Trp and His. For the α-ε-^{15}N -Tryptophan labeled rhodopsin sample, this spectrum should result in five backbone and five side chain signals in the range 7.0 - 9.0ppm and 10.0 – 12.0ppm, respectively. An overlay of the conventional HSQC spectra of α-ε-^{15}N-tryptophan labeled rhodopsin in the absence and presence of 10-fold excess Ce6 is shown in Figure 3.31. In the absence of Ce6 (Figure 3.31, black trace), the HSQC spectrum gave rise to five distinct peaks in the range ~10.0 – 11.5ppm corresponding to the expected five indole side chain signals. The intensity of all the side chain signals was similar, except for the signal at ~10.6ppm. This peak was unambiguously assigned previously to Trp-175. Additionally, we observed approximately twelve peaks instead of five signals in the range of 6.5 - 9.0ppm corresponding to the backbone nitrogen atoms. A recent study combining both solid and solution state NMR, resulted in the assignment of signals in the backbone region corresponding to the five tryptophans (Werner, Lehner et al. 2007). Apart from these five assigned signals, all other signals have been attributed to be originating from the natural abundance of the amino groups from the flexible C-terminus residues (Werner, Lehner et al. 2007; Werner, Richter et al. 2008), while heterogeneity of tryptophan conformations has been proposed as an alternative explanation (Klein-Seetharaman, Yanamala et al. 2004). Based on Werner et al (Werner, Lehner et al. 2007), the signals observed at 7.2, 7.7, 8.2, 8.3, and 8.7ppm were assigned to Trp-161, Trp-35, Trp-265, Trp-175 and Trp-126, respectively (Figure 3.30 and 3.31).

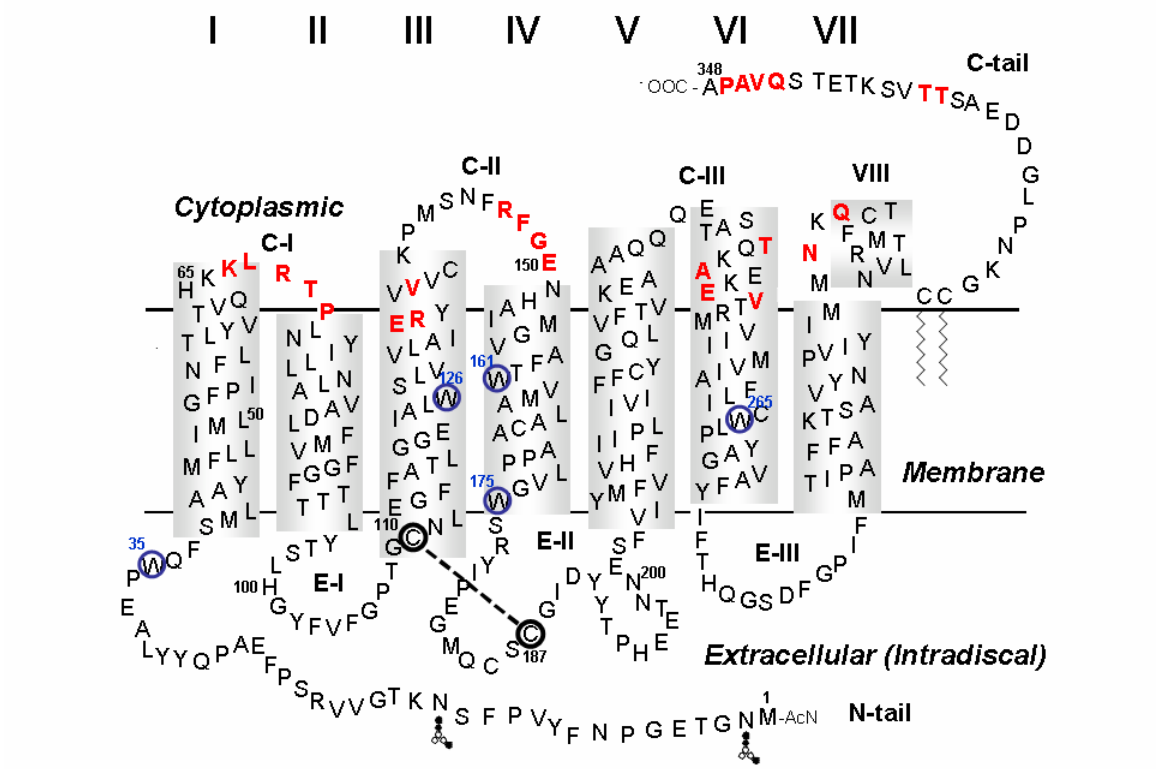

Figure 3.30: Secondary structure model of rhodopsin indicating all the tryptophan residues. The tryptophan residues in rhodopsin are labeled and circled in blue. The 5Å predicted Ce6 binding pocket residues in rhodopsin are highlighted in bold and colored in red. The disulphide bond between C_{110} and C_{187} is represented by a dotted line.

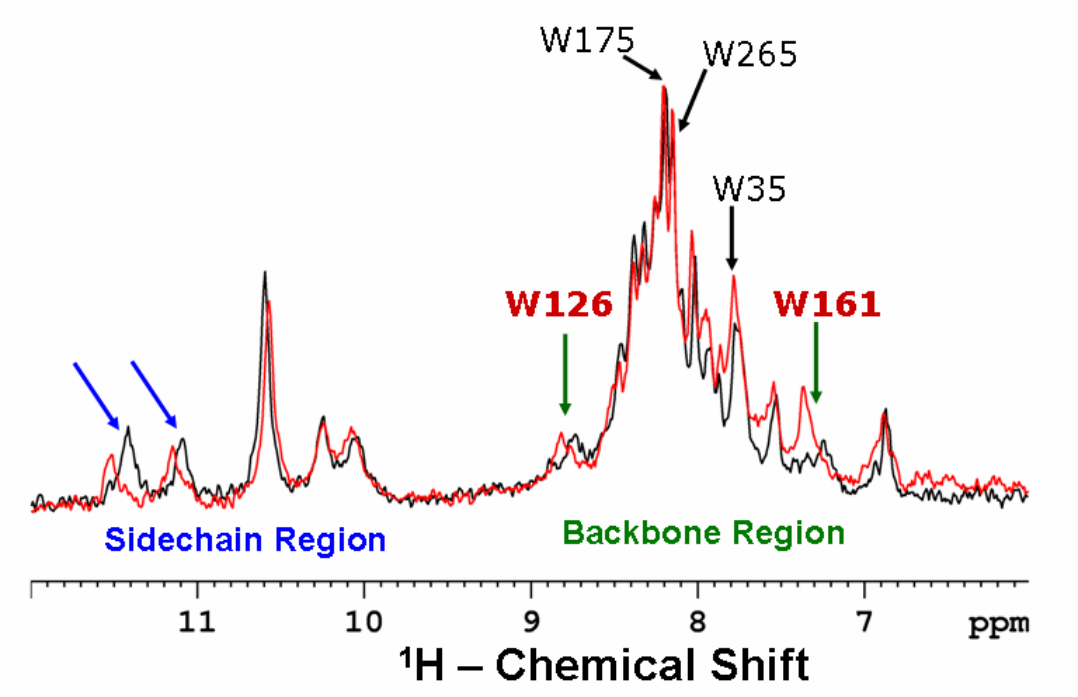

Figure 3.31: One dimensional NMR spectra of ^{15}N-α-ε-tryptophan labeled rhodopsin. The NMR spectra in the absence and presence of 10-fold excess Ce6 are colored in black and red traces respectively. The signals from the side chains and backbones are labeled clearly. The chemical shift changes in the backbone upon addition of Ce6 are indicated by green arrows and labeled in red and the blue arrows indicate the changes in the tryptophan side chains regions.

In the presence of Ce6, the overall spectrum looked similar to rhodopsin alone, except for the following changes. Two out of the five indole side chain signals were shifted in the presence of Ce6 as compared to rhodopsin alone (Figure 3.31, blue arrows). A shift of +0.11, +0.06 and +0.03ppm for the peaks at 11.4, 11.1 and 10.6ppm in the side chain regions were observed. So far, we cannot attribute these changes to specific tryptophans as there is no assignment yet for this region. Only two of the signals in the backbone region were found to be shifted in the presence of Ce6. The peaks corresponding to Trp-126 and Trp-161 were shifted by +0.07 and +0.11ppm. Further, an increase in the intensity of Trp-161 peak was observed in the backbone region, suggesting that Trp-161 might be experiencing increased flexibility in the presence of Ce6. These studies clearly suggest that binding of Ce6 at CP domain induces changes in the TM region, in particular Trp-126 on helix 3 and Trp-161 on helix 4 located near the *11-cis* retinal ligand binding pocket, but towards the CP domain. Further, these studies support the hypothesis that there may be an alteration in conformational flexibility in this region, which may be important for *11-cis* retinal binding and thus in relaying the TM/EC signal back to the CP domain after activation.

3.2.4 (e) NMR Analysis of α-^{15}N-lysine Labeled Rhodopsin in the Dark and upon Light-activation: To focus on amino acids mainly located at the CP side of the protein, we measured NMR spectroscopy of 50μM α-^{15}N-lysine labeled rhodopsin in the absence and presence of Ce6 (Klein-Seetharaman, Reeves et al. 2002). Rhodopsin contains a total of eleven lysine residues (Figure 3.32, circled in magenta). Almost all of these residues are located in the CP surface of rhodopsin, except for two lysines, Lys-296 in the

TM domain and Lys-16 in the EC domain. Lys-296 is an important lysine residue as it serves as the attachment site of *11-cis*-retinal. NMR studies suggest that each of the lysines in rhodopsin has a different mobility and experiences different chemical environments (Klein-Seetharaman, Reeves et al. 2002). To investigate if the mobility of these residues has been restricted upon binding of Ce6, we followed the changes in the chemical shifts that arise from ^{15}N-labeled lysine residues in the 2D-^{1}H-^{15}N-HSQC spectrum (Klein-Seetharaman, Reeves et al. 2002).

In the absence of Ce6, the 2D HSQC spectrum recorded at +25°C in the dark gave rise to three signals (Figure 3.33, black line). The intensity of the signals observed varied greatly with a sharp, highly intense peak at ~8.4ppm, a moderately intense peak at ~7.93ppm and another moderately to less intense peak at ~8.30ppm. Previous studies have shown that the signal at 8.4ppm corresponds to Lys-339, located in the flexible C-terminus region of rhodopsin (Figure 3.32) (Klein-Seetharaman, Reeves et al. 2002). After 1.5hours post light-activation, the 2D HSQC spectrum resulted in the disappearance of the peak at ~8.30ppm (Figure 3.33, indicated by a black arrow). However, no change in signals at ~8.4ppm and ~7.93ppm was observed. Further, the spectrum gave rise to three new less intense peaks at 8.53ppm, 8.1ppm and 8.06ppm (Figure 3.33, indicated by red arrows).

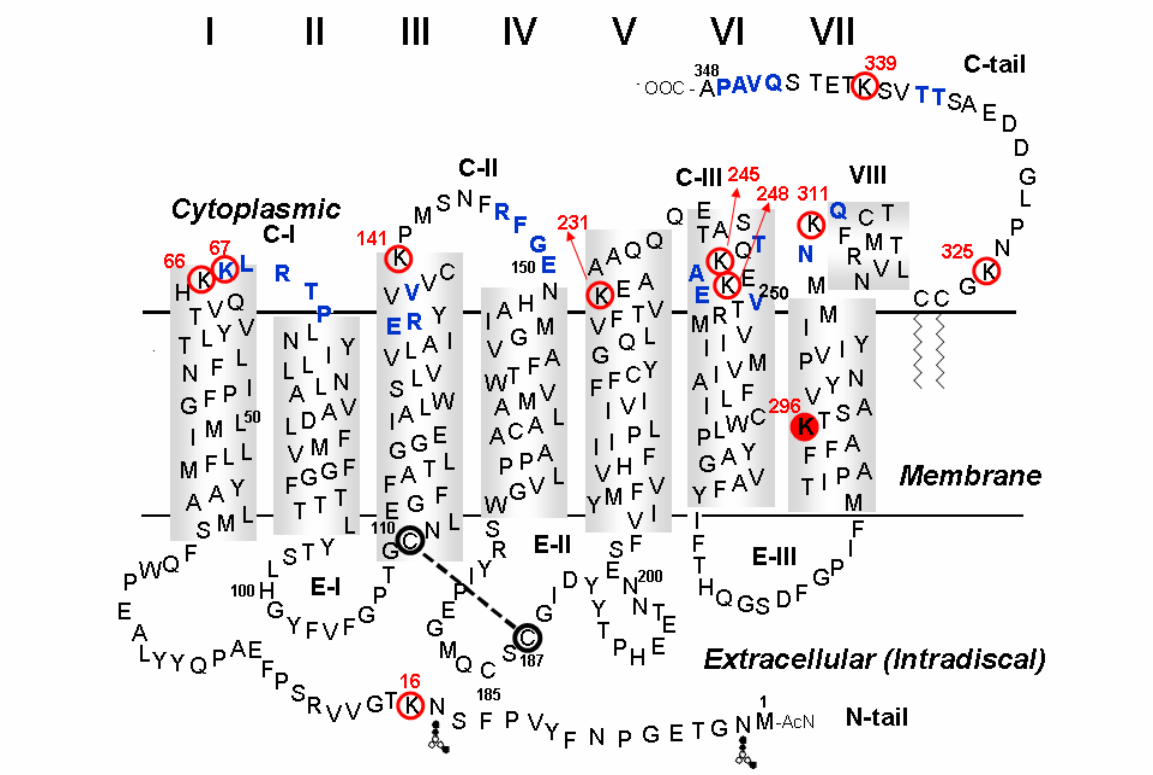

Figure 3.32: Secondary structure model of rhodopsin showing all the lysine residue positions. Lys-296 that participates as the direct attachment site for *11-cis* retinal is shown in filled red circle. All other lysine positions are labeled and colored in red circles. The predicted binding pocket residues are highlighted in bold and colored in blue.

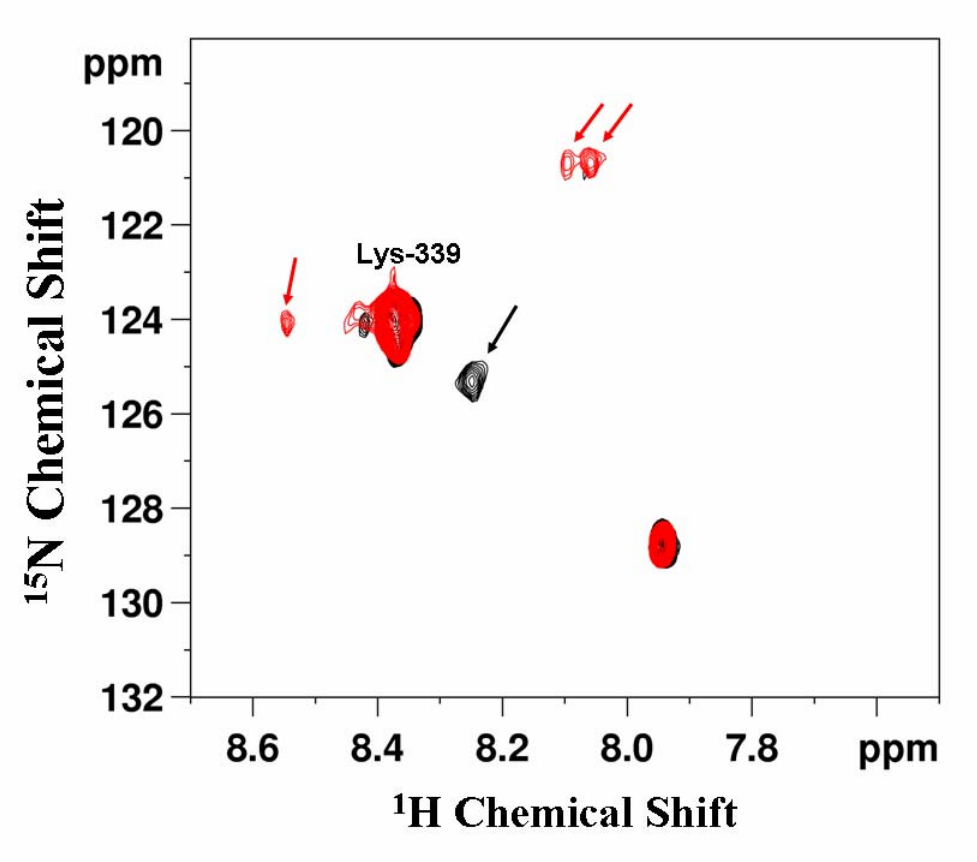

Figure 3.33: Two dimensional HSQC spectra of α-^{15}N-lysine labeled rhodopsin. HSQC spectra (A) in the dark (black traces) and (B) 1.5 hours after light-activation (red traces) recorded at +25°C on a 800MHz Bruker NMR spectrometer. A rhodopsin concentration of 50μM was used. The sample was illuminated with >495nm light for 30sec. The signals that either disappear or appear upon light-activation are indicated by black and red arrows, respectively. The signal corresponding to Lys-339 in the C-terminus is labeled.

Shown in Figure 3.34 is the comparison of the 2D HSQC spectra of 50μM α-^{15}N-lysine labeled rhodopsin in the presence of 50μM (1X) and 0.5mM (10X) Ce6 recorded in the dark and 1.5 hours post illumination. In the dark, addition of Ce6 resulted in the complete disappearance of the signal at ~8.3ppm (Figure 3.33, indicated by black arrow). In addition, in the presence of already a 1-fold excess of Ce6 over rhodopsin, a signal at ~8.53ppm started appearing. These changes occurring in the presence of Ce6 in the dark were only found after light-activation in the absence of Ce6 (compare Figure 3.33, red arrows and Figure 3.34A, black arrow). The overall spectrum showed a similar profile as compared to that of light-activated rhodopsin in the absence of Ce6 (Figure 3.33, red spectrum), with the exception of the peaks at 8.1ppm and 8.06ppm. However, in the presence of a 10-fold excess Ce6, the peak at 8.53ppm was absent and an overall decrease in the broadness of the spectrum was observed (compare Figure 3.34A and B, black spectra).

Upon light-activation, in the presence of 50μM Ce6 (Figure 3.34A, red spectrum), the overall spectrum in comparison to the rhodopsin alone sample was similar with the exception of the following changes. Instead of two distinct peaks at 8.1ppm and 8.06ppm, a broad peak around ~8.05ppm was observed (indicated by red arrow). Additionally the peak at ~8.53ppm decreased in intensity compared to dark state rhodopsin with Ce6 (Figure 3.34A, black trace) and in the absence of Ce6 upon light-activation (Figure 3.33, red trace). Also, the Lys-339 peak at ~8.4ppm became less broad. In the presence of a 10-fold excess of Ce6, the signal at 8.07ppm that was seen in both 0X and 1X Ce6 samples was no longer observed (compare 3.33, red trace and Figure 3.34A and B, red traces). Further, in comparison to the two distinct peaks in the

absence and one broad peak in the presence of 1X Ce6, a single distinct peak at ~8.07 was observed (compare Figure 3.33, 3.34A and B, red arrows). The results obtained clearly indicate that the mobility of some of the lysine residues is restricted in the presence of Ce6.

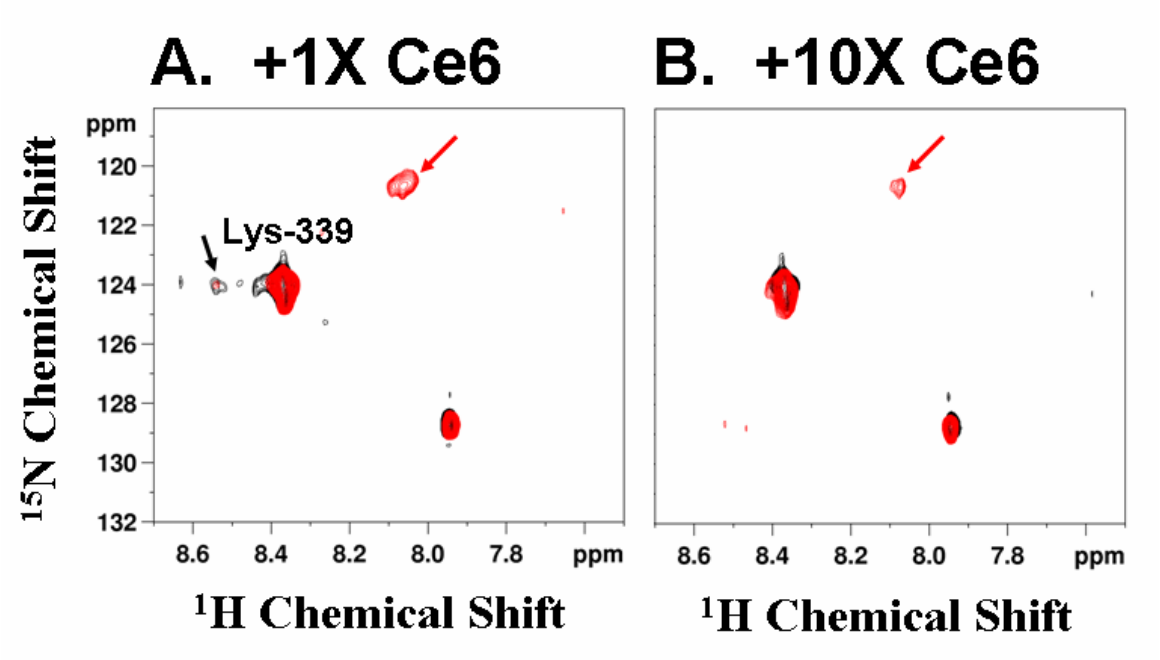

Figure 3.34: Comparison of conventional HSQC spectra of α-^{15}N-lysine labeled rhodopsin in the presence Ce6. HSQC spectra of 50μM α-^{15}N-lysine labeled rhodopsin with (A) 50μM Ce6 and (B) 0.5mM Ce6. The spectra were recorded in the dark (colored black) and after 1.5 hours light-activation (colored red) at +25°C on 800MHz Bruker Spectrophotometer. A rhodopsin concentration of 50μM was used in each experiment. The sample was illuminated with >495nm light for 30sec. The changes in the dark and upon light-activation as compared to rhodopsin alone are colored in black and red arrows, respectively.

3.2.4. (f) Monitoring Structural Changes in Rhodopsin upon Ce6 Binding using Selective Excitation ^{1}H NMR Spectroscopy: Further evidence for the changes in structure and dynamics in rhodopsin came from recording one dimensional ^{1}H NMR spectra of unlabeled rhodopsin without and with Ce6. Shown in Figure 3.35 is the selective exciation ^{1}H NMR spectra recorded in the range 7.3 – 8.7ppm for 50μM rhodopsin in the absence and presence of Ce6. The peaks observed were sequentially numbered from 1-10 for convenience in each case. Comparison of the spectra in the dark and upon light-activation in the absence of Ce6 showed an overall decrease in the peak intensities (Figure 3.35A). A signal at peak position 1 appears upon light-activation increases in intensity in a time dependent manner. The intensity of the peak at position 6 increases in a time dependent manner after light-activation (Figure 3.35A, black trace with others). Additionally the peak at position 9 decreases in intensity after 0.5 and 1 hours light-activated rhodopsin (Figure 3.35A, red and blue traces) and disappears completely in the 3 hour post illumination spectra (Figure 3.35A, magenta trace). These studies suggest that the time dependent changes observed at peak positions 6 and 9 correspond to the changes associated with structural transition from dark to opsin state. Further, the peaks at positions 2, 3, 7, 9, and 10 originated from the C-terminus residues of rhodopsin (Figure 3.35D, indicated as '*'). This supports the idea that the signals in selective excitation ^{1}H NMR spectra come from flexible residues in the proteins (refer to Section 6.1.1 for more details). These observations suggest that the majority of the signals observed in selective excitation spectra might be from the CP residues, as this domain is the most flexible as compared to all the other domains in rhodopsin.

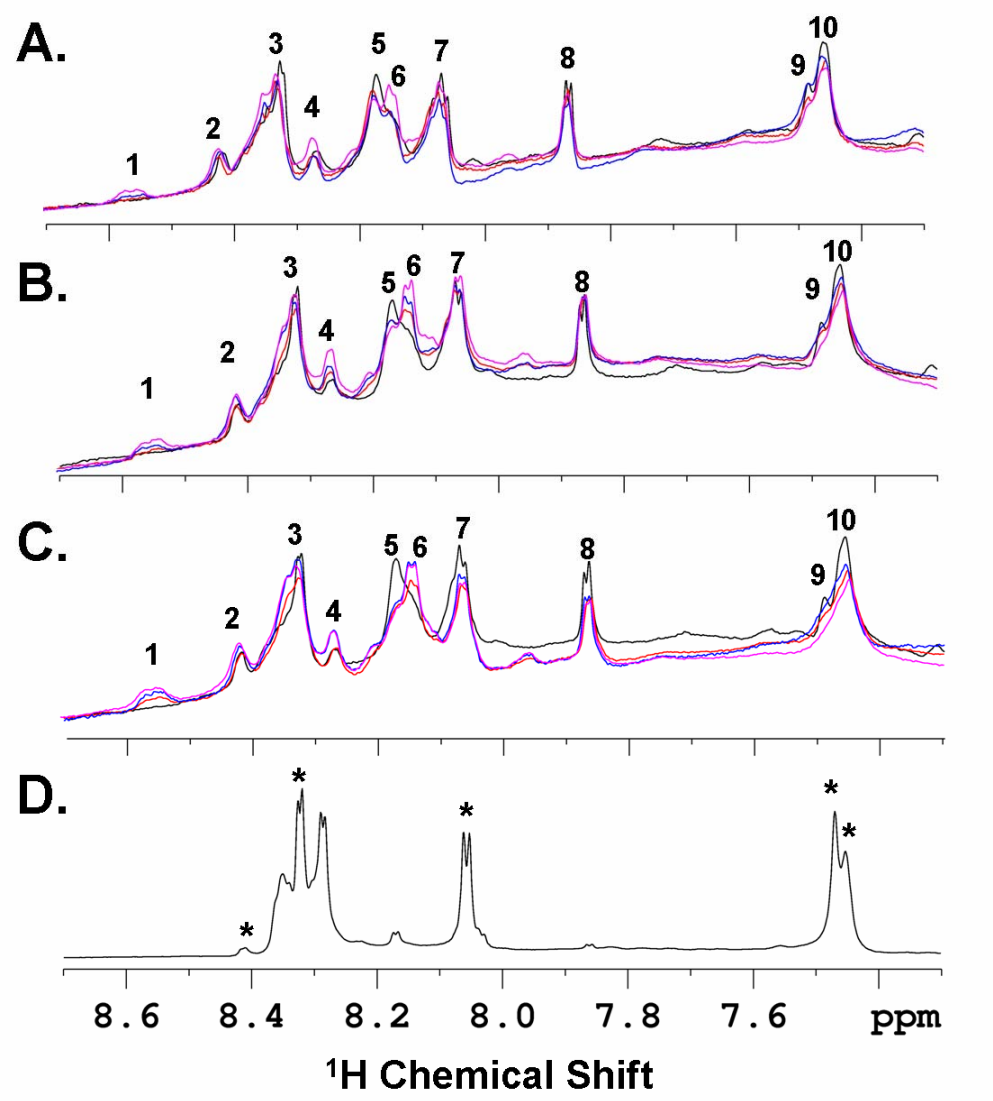

Figure 3.35: Monitoring binding of Ce6 to dark-adapted and light-activated rhodopsin. Overlay of one dimensional selective excitation ^{1}H NMR spectra in the dark and at different time points after light-activation of (A) rhodopsin (B) rhodopsin with 10μM Ce6 and (C) rhodopsin with 50μM Ce6. (D) 1mM C-terminal peptide corresponding to the last nine amino acids of rhodopsin in phosphate buffer and 0.3% DM. In A, B, and C the NMR traces corresponding to the dark, 0.5, 1 and 3 hours after light-activation are colored in black, red, blue and magenta, respectively. NMR samples contained 50μM of rhodopsin in 20mM sodium phosphate buffer (pH 6.0), 0.3% DM and 10% D_2O.

In the dark, titration of 10μM, 50μM, 400μM and 1mM concentration of Ce6 to 50μM rhodopsin resulted in changes at peak positions 9 and 10. Shown in Figure 3.36 is the overlay of the chemical shift region of rhodopsin for these two peaks in the absence and in the presence of various concentrations of Ce6. The peaks at position 9 and 10 gradually shifted upfield and downfield, respectively (Figure 3.36). Except for this change, we did not observe any changes in the other positions for dark state rhodopsin.

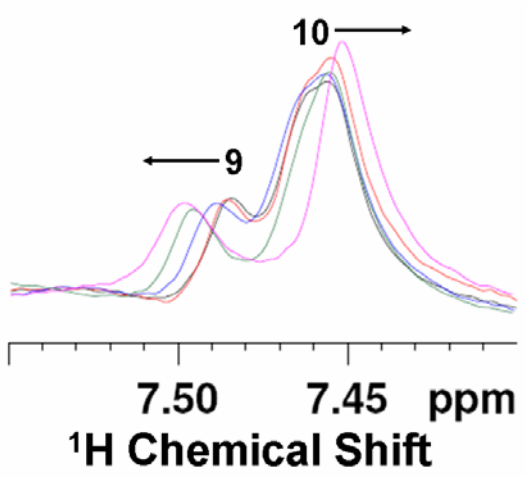

Figure 3.36: One dimensional selective excitation ^{1}H NMR spectra of dark rhodopsin without and at various concentrations of Ce6. The ^{1}H NMR spectra of dark state rhodopsin in the absence (black trace) and in the presence of 10μM (red trace), 50μM (blue trace), 400μM (green trace), 1mM Ce6 (magenta trace) in the chemical shift range 7.4ppm to 250μM 7.55ppm is shown. These peaks correspond to the positions 9 and 10 in Figure 3.35.

Shown in Figure 3.37 are the spectral changes of rhodopsin immediately recorded within 2mins after light-activation and after 1.5 hours post light-activation in the absence and presence of Ce6. Immediately upon illumination and after 1.5 hours light-activation

(representative of Meta II and opsin state, respectively), an increase in the peak at position 5 with a decrease at position 4 was observed in a concentration-dependent manner (Figure 3.37A, B). In the absence of Ce6, this was only observed after complete decay of Meta II to opsin state, which happens with a half-life on the order of ~10-13 minutes. Further, a decrease in the broadness of the peak at position 6 was also observed, indicating changes in the mobility of these residues upon illumination (Figure 3.37). These results suggest that addition of various concentrations of Ce6 modulates the structure of rhodopsin resulting in faster transition towards the opsin like state. Additionally, these studies also suggest that the Ce6 bound light-activated state might exhibit different conformational flexibility as compared to Meta II and opsin states.

Furthermore, we also observed changes in protein signals upon illumination without and with Ce6 in the range 9.8ppm to 10.1ppm, which are highlighted in Figure 3.38. Two signals corresponding to aromatic residues at 9.98ppm and 9.90ppm were observed upon light-activation. None of these peaks were observed in the dark both in the absence and presence of Ce6. Upon titrating Ce6, the signal at 9.90ppm disappeared completely, with the exception of the 10μM Ce6 sample. When we titrated different concentrations of Ce6 (10μM, 50μM, 100μM), we found that the signal at 9.98ppm shifted downfield in a concentration dependent manner. In contrast, this signal completely disappeared upon addition of 400μM and 1mM Ce6. These results clearly confirm binding of Ce6 to rhodopsin and suggest that binding modulates the structure and dynamics in both the dark and light-activated states of rhodopsin.

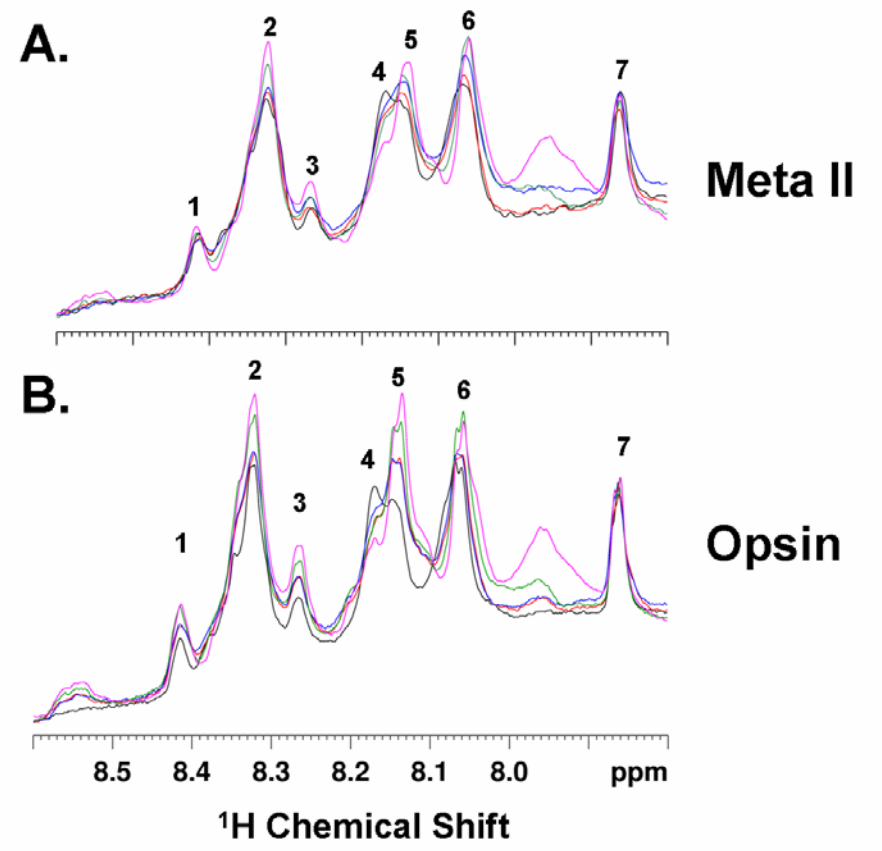

Figure 3.37: Change in the selective excitation ^{1}H NMR spectra of Meta II and Opsin state of rhodopsin in the absence and at various concentrations of Ce6. For the legends of (A), and (B), refer to Figure 3.36.

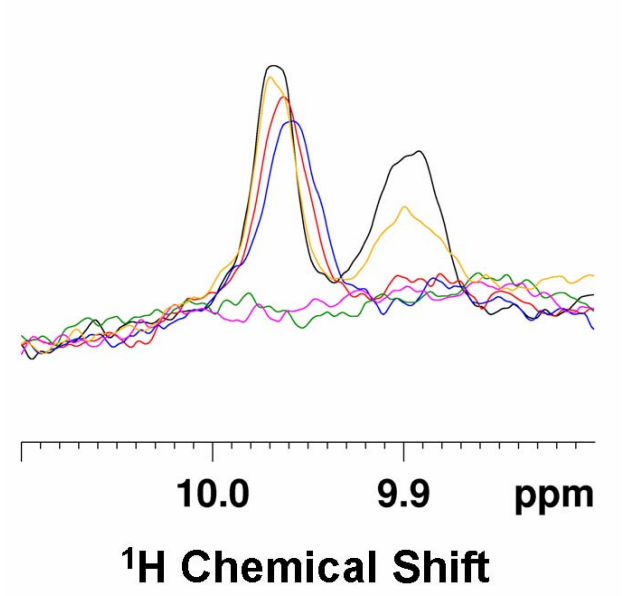

Figure 3.38: One dimensional selective excitation ^{1}H NMR spectra of the aromatic amino acid side chain region of rhodopsin with and without Ce6. The spectra for rhodopsin in the absence (black) and presence of 10μM (orange), 50μM (red), 100μM (blue), 400μM (green) and 1mM (magenta) Ce6 upon light-activation. The spectra for rhodopsin in the dark both without and with Ce6 displayed no peaks in this region and are therefore not shown in this figure.

3.2.5. Discussion

First, we developed a Ce6 binding assay based on fluorescence spectroscopy where we found that rhodopsin tryptophan fluorescence is strongly quenched by Ce6, especially in the light. Control experiments with non-illuminated Ce6 and with separately illuminated Ce6 confirm that these effects do not require Ce6 excitation (Figure 3.14). Thus, it is unlikely that the Ce6 effects described in this thesis are indirect effects, such as through reactive oxygen species formation mediated by the presence of Ce6. Consistent with this interpretation is also the fact that we observe similar fluorescence quenching in de-

oxygenated solutions (data not shown). Furthermore, we show that these effects are consequences of Ce6 binding to rhodopsin: Ce6 is essentially a degradation product of Chl-a, being demetallated and lacking the hydrophobic phytol chain. To assess the specificity of Ce6 binding to rhodopsin, we therefore compared tryptophan fluorescence quenching by Ce6 with that by Chl-a, which is more hydrophobic than Ce6 and would result in stronger unspecific interactions with rhodopsin, being recruited into the detergent micelles. The results confirm that Ce6 binding is specific, as Chl-a results in a much lower degree of fluorescence quenching, even lower than that observed for Ce6 binding to dark-adapted rhodopsin. Chl-a does have an effect on rhodopsin, namely on its Meta II half-lives (Table 3.2). This is not uncommon, for example the Meta II half-life is highly dependent on its lipid and detergent environment (Mitchell, Straume et al. 1992; Brown 1994; Szundi, Lewis et al. 2005).

Further, the ligand binding studies were also confirmed using the selective excitation ^{1}H NMR approach explained in section 3.1.1. (b). We estimated the affinity of Ce6 interaction based on intensity changes in the ligand peaks with increasing amounts of rhodopsin added to a constant ligand concentration. The lowest affinities values for the dark and opsin state of rhodopsin obtained are ~16$\pm$7μM and 8$\pm$3μM, respectively indicating moderate binding of Ce6. However, we were not able to estimate the affinity of interaction between light-activated Meta II state and Ce6, due to the instability of the activated state. The spectra obtained in the Meta II state qualitatively indicate a higher affinity of interaction for this state as compared to the other two states.

^{19}F NMR spectroscopy of rhodopsin carrying ^{19}F labels in the CP domain, at positions Cys-316 and Cys-140, confirms the binding of Ce6 to rhodopsin, as distinct

changes in the NMR spectra are observed for both dark and light-adapted rhodopsin samples in the presence and absence of Ce6. ^{19}F NMR further suggests that there are significant alterations in rhodopsin conformational preferences in the presence of Ce6, especially upon light-activation. Ce6 binding changes the conformation of Meta II in the CP domain quite drastically, as the two resolved peaks for Cys-316 and Cys-140 in the Meta II state are shifted to a single, broad peak. The chemical shift of this peak is similar, but not identical to that of a peak observed in the absence of Ce6, attributed to opsin. Absorbance spectroscopy suggests that retinal is still bound to this species. The peak does not decay to form free ^{19}F label when Ce6 is present, contrary to what is observed in the absence of Ce6. If we assume that the formation of free ^{19}F label is due to nucleophilic attack of the trifluoroethyl-cysteine disulfide bond by amino acids in the protein, this suggests that Ce6 binding stabilizes rhodopsin, presumably preventing the motions required for such an attack.

Computational modeling studies predict a binding pocket for Ce6 at the CP center of the helical bundle. We propose that this binding pocket overlaps to a great extent with that of the G protein, based on fluorescence spectroscopic and computational modeling studies of the binding of a peptide representing a high-affinity analogue of the C-terminus of G_t (Kisselev, Meyer et al. 1999; Arimoto, Kisselev et al. 2001). Analysis of the recent G_t peptide bound opsin crystal structure (Scheerer, Park et al. 2008) also overlaps between G_t and the predicted Ce6 binding pockets (Table 3.3). Consistent with the computational analysis, we find experimentally that Ce6 inhibits the activation of the heterotrimeric G protein in [^{35}S]GTPγS filter binding assays. The predicted CP binding site provides a plausible explanation for the observed effects of Ce6 binding on rhodopsin

conformation and G protein activation – it is located at the "heart of the action," where the largest conformational changes are observed after light-activation (Janz and Farrens 2004; Oldham and Hamm 2008), and where critical residues are exposed to interact with G_t (Janz and Farrens 2004; Oldham and Hamm 2008). In agreement with this key role, some of the residues in this pocket are highly conserved. For example, Glu-134 and Arg-135 are the residues of the D/ERY motif, which is conserved close to 100% in Class A GPCRs (Sakmar 2002).

The finding of a CP Ce6 binding pocket in rhodopsin fits well with recent independent predictions of small molecule binding pockets for rhodopsin based on analysis of high connectivity of residues in proteins (Christopher J R Illingworth 2008). Connectivity of a residue refers to the number of its neighboring contacts within a distance of 5.5Å where high connectivity residues were scored using the K-means algorithm (Christopher J R Illingworth 2008). In addition to the retinal binding pocket, this method identified a total of 34 residues in the CP domain as likely binding sites when searching for residues containing atoms with a local connectivity within 70% of the maximal energy value for the protein. Nine residues are part of both peptide and Ce6 5Å binding pockets (Table 3.3).

After, showing that Ce6 physically binds to rhodopsin and interferes with G_t activation, we then investigated if Ce6 binding alters rhodopsin structure and dynamics. Several lines of evidence (refer sections 3.2.2, 3.2.3), suggest Ce6 binds at the CP domain of rhodopsin. As traditional NMR relaxation measurements pose many constraints for membrane proteins (see section 3.1.1 (b)), a ^{19}F based relaxation technique was developed to measure transverse and longitudinal relaxation values. In the absence of

Ce6, the estimated R_2 values indicated that Cys-316 on perpendicular helix 8 is more flexible as compared to Cys-140 on helix 3. In the presence of Ce6, the conformational flexibility of Cys-316 was found to be decreased. In contrast to this, binding of Ce6 to rhodopsin did not affect Cys-140 relaxation values. They almost remained identical except at elevated temperatures. The fact that only one of the cysteines exhibits changes upon binding to Ce6 validates the existence of the CP binding domain.

In addition to monitoring the local effects induced by Ce6 binding we also investigated whether Ce6 binding at the CP domain has allosteric effects on the other domains of bovine rhodopsin. To do so, we recorded ^{1}H-^{15}N-HSQC spectra of α-ε-^{15}N-tryptophan labeled rhodopsin in the presence and absence of Ce6 in the dark. Comparison of the HSQC spectra indicated chemical shift changes both in the backbone and side chain signals. The backbone signals corresponding to Trp-126 and Trp-161 were found to be modulated in the presence of Ce6, already in the dark. Trp-126 and Trp-161 are located in the TM domain in helix 3 and helix 4, respectively. Though, they are in the middle of these helices, they are close to the CP side as compared to other three tryptophan residues in rhodopsin. Along with Trp-265, which participates in direct interaction with the retinal, Trp-126 and Trp-161 play a major role in rhodopsin activation (Lin and Sakmar 1996; Borhan, Souto et al. 2000). These results together with the changes in dynamics observed above, clearly indicate that Ce6 binding to rhodopsin alters the conformational flexibility of rhodopsin. This, in turn, could lead to altered signal transfer rates for interconversion between different conformational states. This conclusion may explain the results obtained from ^{19}F NMR (Figure 3.29) and G_t

activation studies (Figure 3.22B) where faster conversion to the opsin state provides a plausible interpretation of the results.

To better understand the effects of Ce6 binding on the mobility of the C-terminal residues and the CP domain in general, we analyzed 2D ^{1}H-^{15}N-HSQC spectra of α-^{15}N-lysine labeled rhodopsin in the presence and absence of Ce6 before and after light-activation. The spectrum recorded in the dark without Ce6 at 25°C gave rise to three peaks with varying intensities as opposed to eleven equally intense peaks. The variability in the intensity may be attributed to conformational exchange broadening where residues interchange between multiple conformations on the order of μs – ms timescales (Klein-Seetharaman, Getmanova et al. 1999; Klein-Seetharaman 2002; Klein-Seetharaman, Reeves et al. 2002; Klein-Seetharaman, Yanamala et al. 2004). Complete disappearance of one of the signals and appearance of three new signals upon light-activation, indicates changed mobility of these residues after *11-cis* retinal leaves the protein. No change in the two intense peaks at 8.4ppm and 7.93ppm was observed, suggesting that these residues still remain flexible upon light-activation. However, in the dark, upon addition of Ce6, the HSQC spectrum was similar in appearance to that obtained for light-activated rhodopsin. In the presence of Ce6, the signal at ~8.3ppm completely disappeared and a new peak at ~8.53ppm was observed, which was only seen after light-activation in the absence of Ce6. This suggests that Ce6 binding modulates the structure of dark state rhodopsin towards an opsin like state. Upon light-activation, formation of a broad peak around ~8.06ppm, instead of two distinct peaks at 8.1ppm and 8.05ppm in the absence of Ce6 was observed, suggesting that the opsin state structure and dynamics upon binding to Ce6 might not be identical to opsin state without Ce6. This observation was further

supported by the evidence from the studies in the presence of 10-fold excess Ce6 over rhodopsin. A distinct peak at ~8.08ppm was observed, as compared to a broad peak in the presence of 1X Ce6 and two distinct peaks without Ce6. Numerous lysine residues are in close proximity to the predicted Ce6 binding pocket residues. In particular, Lys-67 is predicted to participate directly in the binding of Ce6. Although we have not yet assigned the signals other than Lys-339, the results qualitatively indicate that the structure and dynamics of the CP domain is modulated in the presence of Ce6. Additionally, these results indicate that the overall structure of rhodopsin might be experiencing restriction in mobility upon binding to Ce6, as evidenced by the decrease in the broadness of the peaks. As the Lys-339 signal did not result in any changes upon either light-activation or addition of Ce6, this can be interpreted in two ways 1) it does not participate in binding as predicted, where as the dynamics of other residues in C-terminus are affected and 2) that C-terminus does not participate completely in Ce6 binding to rhodopsin.

Further evidence for the changes in the structure and dynamics of rhodopsin comes from the selective excitation ^{1}H NMR spectra. The ^{1}H NMR spectra recorded without and upon addition of Ce6 at various concentrations clearly indicated changes in peaks at positions 3, 5, 6, 7, 9 and 10. Specifically, the peaks at positions 3, 7, 9, and 10 directly originated from the C-terminus of rhodopsin (compare with Figure 3.35A, B, C with D). Comparison of the dark-adapted and light-activated states of rhodopsin in the absence of Ce6, clearly indicated these changes are time-dependent and arise as a result of transition from the Meta II state to opsin. Binding of Ce6 to rhodopsin was found to accelerate these changes, suggesting that Ce6 induces changes in the conformational

flexibility of rhodopsin. Such conformational flexibility can be further attributed to the accelerated signal transfer from *11-cis* binding site to the CP face. This might further serve as an explanation for the inhibition of G_t studies described above, as less time in the activated state would lead to decreased G_t activation. These studies along with the α-^{15}N-lysine labeled rhodopsin studies clearly indicate that the structure and dynamics of the rhodopsin in the CP face and also in the C-terminus are modulated.

3.2.6. Conclusions

Chlorophyll-derivatives have been proposed to act as photosensitizers in dragon-fish (Douglas, Partridge et al. 1999) and Ce6 was found to be an effective photosensitizer in retinas from model organisms salamander, cow and mouse (Washington, Brooks et al. 2004; Isayama, Alexeev et al. 2006; Washington 2007). Here, we show that these effects are mediated by direct interaction of Ce6 with rhodopsin. We identify a novel binding pocket in the CP domain and show that binding modulates rhodopsin structure, dynamics and function. This makes Ce6 the first allosteric small organic molecule modulator of rhodopsin. The interaction inhibits G_t activation of bovine rhodopsin, an effect that may prove general for other GPCRs because of the high conservation of predicted CP binding site residues for the GPCR family.

CHAPTER - 4
TRANSMEMBRANE (ALLOSTERIC) LIGANDS.

TABLE OF CONTENTS

SUMMARY

For metabotropic glutamate receptors (mGluRs), allosteric ligands are particularly promising drug targets because of their modulatory effects – enhancing or suppressing the response of mGluRs to glutamate (see section 1.1). While glutamate, the endogenous ligand for these receptors, binds in the EC domain, the allosteric ligand binding pocket is localized in the TM region. Many allosteric ligands have been identified for mGluRs including positive, negative and neutral modulators, but the mechanisms by which the modulations occur are not known. The binding of ligands for which allosteric effects on mGluRs are experimentally known was studied by docking to computationally generated models of different mGluR subtypes based on structures of rhodopsin. The results indicate that the allosteric ligand binding pockets of mGluRs are overlapping with the retinal binding pocket of rhodopsin, and that ligands have strong preferences for the active and inactive states depending on their modulatory nature. These findings strongly support the hypothesis that mGluR allosteric modulation occurs via stabilization of different conformations analogous to those identified in rhodopsin where they are induced by photochemical isomerization of the retinal ligand – despite the extensive differences in sequences between mGluRs and rhodopsin. To further test this hypothesis, we also investigated if rhodopsin can accommodate the allosteric mGluR ligand, 3,3`-difluorobenzaldazine, in its TM binding pocket normally occupied by *11-cis* or *all-trans*

retinal. We find that the regeneration of rhodopsin with *11-cis* retinal in the presence of 3,3`-difluorobenzaldazine is decreased, in a concentration-dependent manner. This suggests that binding of 3,3`-difluorobenzaldazine competes with *11-cis* retinal for binding, but with a lower affinity.

SIGNIFICANCE

We show in this chapter that positive and negative mGluR modulators can be distinguished by their higher affinities for the active and inactive conformations of the receptors, respectively. These conformations are based on rhodopsin structures. This versatility in accomodating allosteric and endogenous ligands for different members of the GPCR family is very intriguing and suggests that the structural determinants for active and inactive functional states may be conserved across the GPCR family. Thus, in future, we may be able to create a generic prediction algorithm. Being able to predict whether a given allosteric ligand will act as a negative, positive or neutral modulator would be highly beneficial in designing new drugs targeted at these receptors and GPCRs in general.

INTRODUCTION

In this chapter, we describe the binding of allosteric ligands to class C GPCRs, where the allosteric binding site is located in the TM domain, similar to most of the endogenous ligand binding sites in class A GPCRs. In particular, we investigated allosteric ligand binding to metabotropic glutamate receptors (mGluRs). mGluRs which are representative

members of class C GPCR. mGluRs bind to glutamate, an amino acid that functions as the major excitatory neurotransmitter in the brain. Thus, mGluRs perform numerous functions in the central and peripheral nervous systems and are involved in learning, memory, anxiety, and the perception of pain. Small changes in the chemical structures of allosteric ligands were shown to switch their modulatory effects. To understand the mechanism of action of allosteric modulators, we investigated their preferences for different receptor structures of mGluRs. Towards this goal, we generated computational models of the TM regions of different mGluR subtypes in two different conformations based on active and inactive models of rhodopsin. We then docked ligands with known allosteric effects to the modeled mGluR structures using ArgusLab (Thompson ArgusLab 4.0.1) and Autodock (Goodsell, Morris et al. 1996) softwares. To test, if the TM binding pocket of rhodopsin can accommodate allosteric ligands of other GPCR members, we tested for binding of the mGluR5 ligand 3,3`-difluorobenzaldazine to rhodopsin.

4.1. MODELING OF STRUCTURE AND BINDING SITE OF ALLOSTERIC MODULATORS OF METABOTROPIC GLUTAMATE RECEPTORS

4.1.1. Structure Prediction of mGluR Subtypes by Homology Modeling

As explained above (see chapter 1, pg. 11), in humans, there are a total of eight subtypes of mGluRs. These subtypes are divided into three groups based on their pharmacological and signaling properties. Because there is no structural information available for the TM regions of mGluRs, we generated homology models of mGluRs based on rhodopsin. As a first step, an alignment of the seven-TM helices of rat and human mGluR1, mGluR2,

mGluR4, mGluR5 and mGluR7 with respect to the TM helices of bovine rhodopsin (Protein Data Bank code 1f88 (Palczewski, Kumasaka et al. 2000)) was generated using ClustalW (Thompson, Higgins et al. 1994). The alignment was manually validated by comparison with the alignment proposed in previous molecular modeling studies of mGluRs (Malherbe, Kew et al. 2002; Malherbe, Kratochwil et al. 2003; Malherbe, Kratochwil et al. 2003). Sequences were obtained from SWISS-PROT: mGluR1 (P23385(rat), Q13255(human)), mGluR2 (Q14416), mGluR4 (Q14833), mGluR5 (P31424(rat), P41594(human)) and mGluR7 (Q14831). The sequence of bovine rhodopsin was read directly from the rhodopsin crystal structure (Palczewski, Kumasaka et al. 2000).

Using the generated sequence alignment, three-dimensional models of the different mGluR subtypes were built by homology modeling using the MODELLER software (Sali, Potterton et al. 1995; Marti-Renom, Stuart et al. 2000). The crystal structure of dark, inactive bovine rhodopsin with pdb id 1f88 (Palczewski, Kumasaka et al. 2000) and the ANM generated model of the activated state of rhodopsin (Isin, Rader et al. 2006) were used as the structural templates for generating the inactive and active models of mGluRs, respectively. All models were evaluated using PROCHECK (Laskowski, MacArthur et al. 1993), MOLPROBITY (Davis, Murray et al. 2004) and WHAT-IF (Vriend 1990).

4.1.2. List of Ligand Abbreviations used in this Study

CPCCOEt, cyclopropan[*b*]chromen-1*a*-carboxylate; **DFB**, difluorobenzaldazine; **fenobam**, *N*-(3-chlorophenyl)-*N*'-(4,5-dihydrol-1-methyl-4-oxo-1-*H*-imidazole-2-yl)-

urea; **MPEP**, 2-methyl-6-((3-methoxyphenyl)ethynyl)-pyridine; **R214127**, 1-(3,4-dihydro-2*H*-pyrano[2,3-*b*]quinolin-7-yl)-2-phenyl-1-ethanone; **Ro01-6128**, diphenylacetyl-carbamic acid ethyl ester; **Ro67-4853**, (9*H*-xanthene-9-carbonyl)-carbamic acid butyl ester; **Ro67-7476**, (*S*)-2-(4-fluoro-phenyl)-1-(toluene-4-sulphonyl)-pyrrolidine; **SIB1757**, 6-methyl-2-(phenylazo)-3-pyrindol; **SIB1893**, ([phenylazo]-3-pyrindole)-2-methyl-6-(2-phenylethenyl)pyridine; **MTEP**, 3-[(2-methyl-1,3-thiazol-4-yl)ethynyl]pyridine; **YM298198**, (6-([(2-methoxyethyl)amino]methyl)-*N*-methyl-*N*-neopentylthiaolo[3,2-a]benzoimidazole-2-carboxamide; **EM-TBPC** – 1-ethyl-2-methyl-6-oxo-4-(1,2,4,5-tetrahydro-benzo[d]azepin-3-yl)- 1,6-dihydro-pyrimidine-5-carbonitrile; **PTBE**, (1-(2-hydroxy-3-propyl-4,4-[4-(2*H*-tetrazol-5-yl)phenoxy]butoxyphenyl)ethanone); **NPS2390**, 2-quinoxaline-carboxamide-*N*-adamantan-1-yl; **CPPHA**, *N*-(4-chloro-2-[(1,3-dioxo-1,3-dihydro-2*H*-isoindol-2-yl)methyl]phenyl)-2-hydroxybenzamide; **5MPEP**, 5-methyl-6-(phenylethynyl)-pyridine; **MPEPy**, 3-Methoxy-5-pyridin-2-ylethynylpyridine; **PHCCC**, *N*-phenyl-7-(hydroxylimino)cyclopropa[*b*]chromen-1a-carboxamide; **AMN082**, N,N'-Dibenzhydrylethane-1,2-diamine dihydrochloride.

4.1.3. Identification and Analysis of the Ligand Binding Pocket

A total of 24 ligands were identified that bind to three mGluR subtypes, the Class I mGluRs mGluR1 and mGluR5, the Class II mGluR, mGluR2 and the Class III mGluRs, mGluR4 and mGluR7. The structures of the ligands are shown in Figure 4.1. Receptor modulation was reported in human and in rat receptors (for references, see Table 4.3) and docking was performed with homology models of the mGluR of the respective species.

We compared the results from two different docking programs, ArgusLab and AutoDock. Of the rank-ordered list of bound ligand conformations, we have chosen in each case the ligand conformation where the ligand was most buried and had minimum energy in comparison to all other conformations in the same binding pocket. In some cases, ligands were predicted not to bind, but this was only the case for one of the two programs. If a ligand did not dock in AutoDock, it did dock in ArgusLab, and *vice versa*, so that for all ligands binding could be examined. The unbiased searching of the whole receptor with each of the modulators studied revealed that all of the ligands preferentially bound in a region similar to that of retinal in rhodopsin (Figure 4.2), in the TM domain including helices 3, 5-7 near the interface with the EC domain, especially EC loop 2. The binding pocket was similar for all ligands docked to all receptors, and is exemplary described in more detail for mGluR5, below.

In order to compare the residues in contact with different ligands, we analyzed the residues predicted to be located within 5Å distance from the docked ligand. The results obtained with ArgusLab are listed in Table 4.1 and are shown in Figure 4.3 for mGluR5 in the active and inactive conformations. To demonstrate the similarities and differences between positive and negative modulators, we compared specifically the negative modulator MPEP with the positive modulator DFB-3,3`. Analysis of the binding pocket residues in the mGluR5 subtype revealed that Trp-784 was in closest proximity to both docked ligands and in both conformations, active and inactive. Trp-784 is highly conserved in all mGluRs and in class A GPCRs in general. This tryptophan corresponds to Trp-265 in rhodopsin. In addition to Trp-784, residues Arg-647, Tyr-658, Leu-743 and Phe-787 were found to be part of the binding pocket regardless of the type of modulator

and conformation of the receptor. In addition, Cys-732, Val-788, Met-801 and Ser-804 are found frequently in the binding pockets. In contrast, Ser-657, Leu-785, Cys-781 and Thr-734 were found to be unique for the positive modulator DFB-3,3` (Figure 4.3C,D; Table 4.1) and were not found in the binding pocket of the negative modulator MPEP. Conversely, Arg-726 and Val-805 were unique to the binding pocket of MPEP (Figure 4.3A,B; Table 4.1).

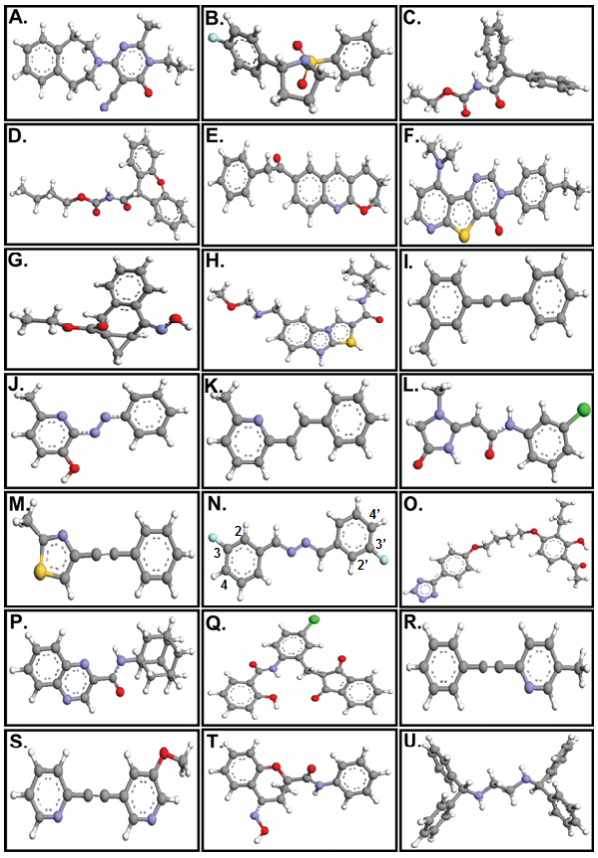

Figure 4.1: The structures of the ligands studied. (A) EM-TBPC (B) Ro67-7476 (C) Ro01-6128 (D) Ro67-4853 (E) R214127 (F) triazafluorenone (G) CPCCOEt (H) YM298198 (I) MPEP (J) SIB-1757 (K) SIB-1893 (L) Fenobam (M) MTEP (N) DFB-derivatives. The positions of the fluorine atoms are indicated for DFB-2,2' and DFB-4,4'. DFB-3,3' is shown. (O) PTEB (P) NPS2390 (Q) CPPHA (R) 5MPEP (S) MPEPy (T)

PHCCC (U) AMN082 . For definition of ligand names see abbreviations list above. Images were created using ArgusLab software (Thompson ArgusLab 4.0.1).

4.1.4. Validation of the Ligand Binding Pocket with Experimental Data

Site-directed mutagenesis to identify residues in mGluR5 that are critical for ligand binding have been reported in the literature (Malherbe, Kratochwil et al. 2003; Muhlemann, Ward et al. 2006). Table 4.1 summarizes the comparison between these experimentally identified ligand binding pocket residues and those predicted by our docking studies with ArgusLab. The results for AutoDock are not shown because the overlap between the predicted binding pockets and those experimentally determined was significantly less. The previous experimental studies with mGluR5 have shown that residues Pro-654, Tyr-658, Leu-743, Thr-780, Trp-784, Phe-787, Tyr-791 and Ala-809 are crucial for binding of the negative modulator MPEP (Malherbe, Kratochwil et al. 2003). Our prediction of MPEP binding to both active and inactive mGluR5 models predicted all of the above residues to be within 5Å of the ligand, except Ala-809, Thr-780 and Tyr-791 (colored in red in Table 4.1). Additionally there are several residues that are predicted to be important for MPEP binding but that have not yet been experimentally verified (colored green in Table 4.1). For the binding of the positive modulator DFB-3,3`, it was concluded from site-directed mutagenesis that Met-801, Ser-657 and Thr-780 are critical for binding and modulatory function (Muhlemann, Ward et al. 2006). There was also evidence that Pro-654, Ser-657, Leu-743 and Asn-733 may contribute more weakly to DFB-3,3` binding. All of these residues are predicted to be part of the DFB-3,3` binding pocket in the inactive model, but Ser-657 and Thr-780 are not present in the

active model. In addition, we predict several residues to be part of the binding pockets that have not been investigated previously (shown in green in Table 4.1). Thus, the comparison of the predicted ligand binding pockets in mGluR5 inactive and active models with the available experimental site directed mutagenesis data strongly validates our models. In addition, we generated testable hypotheses on important residues previously not investigated, and provide evidence that there may be differences in the roles of the amino acids in the binding pocket depending on the conformation of the receptor.

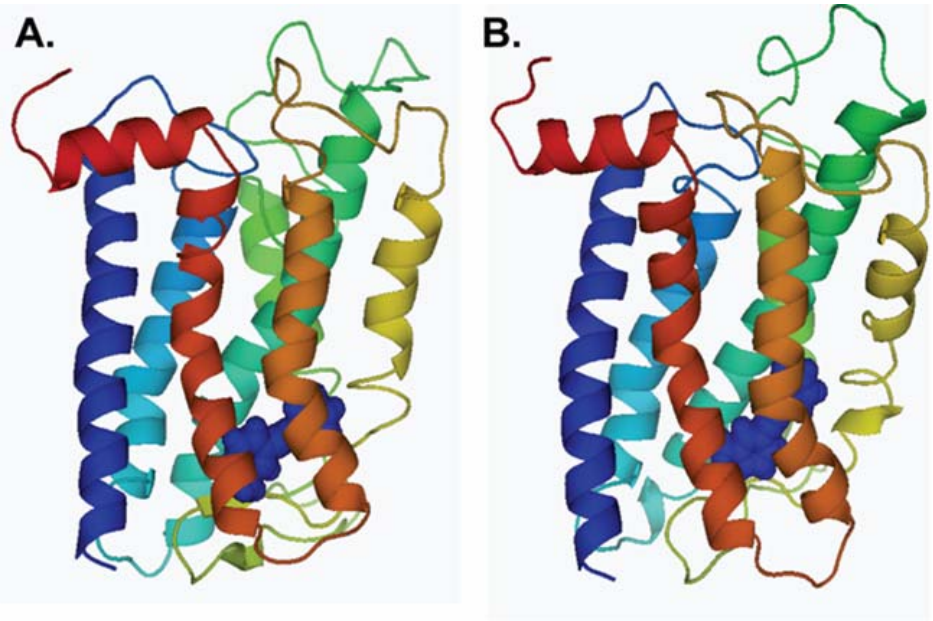

Figure 4.2: Cartoon representation of the mGluR5 receptor (A) active and (B) inactive models docked with negative modulator MPEP. MPEP is colored in dark blue and is rendered in spheres. MPEP refers to 2-methyl-6-(phenylethynyl)-pyridine. Images were created using Pymol Software (http://www.pymol.org).

Table 4.1: Residues within 5Å distance from the MPEP and DFB-3,3` ligands in active and inactive models of mGluR5 in comparison to the experimental results published. Residues colored in red – were not predicted in our docking, green- additional residues predicted and black – residues correctly predicted.

	MPEP Data (Malherbe, Kratochwil et al. 2003)	mGluR5/MPEP Active Model	mGluR5/MPEP Inactive Model	DFB-3,3` Data (Muhlemann, Ward et al. 2006)	mGluR5/DFB-3,3` Active Model	mGluR5/DFB-3,3` Inactive Model
TM3	Arg-647, Pro-654, Tyr-658	Arg-647, **Ile-650**, Tyr-658	Arg-647, **Ile-650**, Pro-654, Tyr-658	Arg-647, Pro-654, Ser-657, Tyr-658	Arg-647, Pro-654, Tyr-658	Arg-647, Pro-654, Ser-657, Tyr-658
EC2	Asn-733	**Arg-726, Glu-727, Ile-731, Cys-732,** Asn-733, **Asn-736**	**Ile-731, Cys-732,** Asn-733	Asn-733	**Arg-726, Ile-731, Cys-732,** Asn-733	**Cys-732**, Asn-733, **Thr-734, Asn-736**
TM5	Leu-743	**Leu-737**, Leu-743, **Pro-742**	**Pro-742**, Leu-743	Leu-743	**Leu-737, Gly-738,** Leu-743**, Gly-744, Pro-742**	Leu-743
TM6	**Thr-780**, Trp-784, Phe-787, Val-788, **Tyr-791**	Trp-784, Phe-787,Val-788	Trp-784, Phe-787	Thr-780, Trp-784, Phe-787, Val-788, Tyr-791	Trp-784, Phe-787, Val-788	Thr-780, Trp-784, Phe-787, **Cys-781, Leu-785,** Val-788, Tyr-791
TM7	Met-801, **Ala-809**	Met-801, **Cys-802, Ser-804, Val-805**	**Thr-800**, Met-801, **Cys-802, Ser-804, Val-805**	Met-801	**Thr-800**, Met-801, **Cys-802, Ser-804**	Met-801, **Ser-804**

4.1.5. Analysis of Binding Energies

The above in-depth analysis of the mGluR5 binding pocket suggests that there may be significant differences between the interactions made by negative and positive modulators with mGluRs depending on the conformation state of the receptor. To test if there is a general trend that distinguishes the action of positive and negative modulators on the receptors, we quantified the overall binding energies for the 24 different ligands with known modulatory nature (positive versus negative). Note that the absolute predicted binding energies from computational studies are not expected to be meaningful due to current limitations in docking methodology and are rarely consistent with experimentally determined affinities. In fact, the actual values are generally dependent on the docking program and scoring function used. We therefore only compared the relative difference between the binding energies of ligands docked to active vs inactive models. Table 4.3 shows the binding energies of the ligand-protein complexes calculated by ArgusLab and AutoDock and Figure 4.4 plots the difference between the respective energies for active and inactive conformations. Where the energies for the active and inactive conformations were very similar, the docking was repeated three times to estimate the error on the predictions (indicated in Table 4.3 and Figure 4.4). In general, the results obtained with ArgusLab were less variable between repeated runs than those obtained with AutoDock. A total of 9 ligands were experimentally shown to act as positive modulators of specific subtypes, 14 ligands were negative modulators and one ligand was neutral. In general, the positive modulators bound with more favorable energy to the model of the active mGluR conformation based on the rhodopsin ANM model (Isin, Rader et al. 2006), while the negative modulators bound with more favorable energy to the model of the inactive mGluR conformation based on the rhodopsin inactive, dark-state (Palczewski, Kumasaka et al. 2000). The neutral ligand,

5MPEP, showed relatively little differences between the energies of the inactive and the active models, but was consistently better docked to the active model using both programs. ArgusLab predicted 12 of the 14 (86%) negative modulators to bind with more favorable energy to the inactive model and 8/9 (89%) positive modulators to the active model, while the numbers for AutoDock were less correlated: 10/14 (71%) and 7/9 (78%). There were also more incidences in which AutoDock was not able to predict binding for the ligands. Five of the predictions for negative modulators and one positive modulator obtained with AutoDock were near or beyond the accuracy limit of AutoDock as judged by the error obtained when multiple independent docking experiments were carried out. In contrast, in the case of ArgusLab only one difference between docking to active and inactive models was within the noise level. We conclude that the relative difference between the binding energies of the docked ligands for the active and inactive models is highly predictive of the nature of the modulator, positive or negative. Positive modulators in most cases appear to prefer the active conformation over the inactive conformation and negative modulators *vice versa*.

4.1.6. Specificity of Ligands to Different mGluR Subtypes

The studies described above suggested that the relative difference between the active and inactive protein – ligand complexes is highly predictive of the modulatory nature of allosteric ligands. Next, we tested if the docking is able to predict the specificity of binding of allosteric modulators to different mGluR subtypes. We docked the allosteric negative modulators EMTBPC, MPEP, DFB-4,4` to mGluR subtypes 1 – 8 using AutoDock 3.0 docking software (Morris, Goddsell et al. 1998). Table 4.2 shows the predicted binding energies of interaction of

the selected ligands with both active and inactive models of the different mGluR models. Those ligands that were not predicted to bind to a particular mGluR subtype are represented with a '-' in the table. The comparison of the docking of EM-TBPC to different mGluR subtypes showed high specificity to mGluR1 in congruence with experimental data (Malherbe, Kratochwil et al. 2003). It also is predicted to interact with mGluR subtype 5, albeit with less energy. Apart from these two subtypes, EM-TBPC did not bind to other mGluR subtypes. Similarly, MPEP and DFB-4,4`, experimentally confirmed mGluR5-specific negative modulators (Malherbe, Kratochwil et al. 2003; O'Brien, Lemaire et al. 2003), were predicted to bind to mGluR5 with the highest energy as compared to other receptors. These studies clearly indicate that the interaction of the different allosteric modulators to mGluRs is subtype specific.

Table 4.2: Comparison of subtype specificity of different allosteric ligands to mGluRs. (I) indicates inactive model. (A) indicates active model.A dash (–) indicates that there was no binding of the ligand to the corresponding receptor model.

mGluR Subtype	EM-TBPC (-ve)	MPEP (-ve)	DFB-4,4` (-ve)
mGluR1 (I)	-8.08	-7.31	-7.54
mGluR1 (A)	-8.83	-7.56	-8.29
mGluR2 (I)	-	-	-
mGluR2 (A)	-	-7.57	-7.6
mGluR3 (I)	-	-8.33	-
mGluR3 (A)	-	-8.21	-
mGluR4 (I)	-	-	-
mGluR4 (A)	-	-	-8.08
mGluR5 (I)	-6.69	-8.98	-8.39
mGluR5 (A)	-	-8.83	-8.81
mGluR6 (I)	-	-6.63	-7.86
mGluR6 (A)	-6.87	-7.94	-5.3
mGluR7 (I)	-	-7.4	-6.78
mGluR7 (A)	-	-8.58	-8.12
mGluR8 (I)	-	-8.09	-5.42
mGluR8 (A)	-	-8.27	-7.44

Table 4.3: List of predicted binding energies for mGluR subtypes 1, 2, 4, 5 and 7 with different positive and negative modulators shown in Figure 4.1.

Class	Receptor	Modulation	Ligand	Species	Binding energies ArgusLab		Binding energies AutoDock	
					Active model [kcal/mol]	Inactive model [kcal/mol]	Active model [kcal/mol]	Inactive model [kcal/mol]
I	**mGluR1**	**Positive**	**Ro67-7476** (Knoflach, Mutel et al. 2001)	Rat	-10.02	-9.18	-8.56	-6.88
			Ro01-6128 (Knoflach, Mutel et al. 2001)	Rat	-12.54	-11.06	-7.06	Did not dock
			Ro67-4853 (Knoflach, Mutel et al. 2001)	Rat	-11.16	-10.73	-7.53	Did not dock
		Negative	**R214127** (Lavreysen, Janssen et al. 2003)	Human	-11.53	-12.09	Did not dock	-7.34
			R214127 (Lavreysen, Janssen et al. 2003)	Rat	-11.09	-11.97	-9.24	-10.11
			Triaza-fluorenone (Zheng, Bhatia et al. 2005)	Human	Did not dock	-7.81	Did not dock	-6.08 ± 0.15
			CPCCOEt (Lavreysen, Janssen et al. 2003)	Rat	-8.60	-9.37	-6.8	-7.46
			YM298198 (Kohara, Toya et al. 2005)	Rat	-7.98 ± 0.09	-8.04 ± 0.02	-6.41 ± 0.25	-5.8 ± 0.08
			NPS2390 (Zheng, Bhatia et al. 2005)	Rat	-9.43 ± 0.01	-10.46 ± 0.17	-8.41 ± 0.00	-8.72 ± 0.03
			EM-TBPC (Malherbe, Kratochwil et al. 2003; Malherbe, Kratochwil et al. 2003)	Rat	-8.51	Did not dock	-6.68 ± 0.09	-6.82 ± 0.11

Table 4.3 (Continued)

	mGluR5	**Negative**	**MPEP** (Gasparini, Andres et al. 2002)	Human	-12.83	-13.14	-6.73	-7.77
			DFB-4,4` (O'Brien, Lemaire et al. 2003; O'Brien, Lemaire et al. 2004)	Human	-10.47	-11.28	-6.83 ± 0.03	-6.86 ± 0.03
			SIB-1757 (Gasparini, Andres et al. 2002)	Human	-9.41	-9.74	-6.44	-6.94
			SIB-1893 (Gasparini, Andres et al. 2002)	Human	-11.71 ± 0.03	-11.82 ± 0.00	-5.83 ± 0.32	-6.63 ± 0.04
			MPEPy (O'Brien, Lemaire et al. 2003)	Human	-7.94 ± 0.00	-7.68 ± 0.11	-6.15 ± 0.03	-6.1 ± 0.02
			Fenobam (Porter, Jaeschke et al. 2005)	Human	-7.64	-9.20		
			MTEP (Anderson, Rao et al. 2002)	Rat	-9.03	-9.40	-6.2 ± 0.07	-6.21 ± 0.01
		Neutral	**5MPEP** (Rodriguez, Nong et al. 2005)	Rat	-9.52 ± 0.00	-9.41 ± 0.04	-7.04 ± 0.06	-6.66 ± 0.00
		Positive	**DFB-3,3`** (O'Brien, Lemaire et al. 2003; O'Brien, Lemaire et al. 2004)	Human	-11.05	-10.06	-7.06	-6.43
			DFB-2,2` (O'Brien, Lemaire et al. 2003; O'Brien, Lemaire et al. 2004)	Human	-10.70	-10.02	-6.87 ± 0.04	-6.81 ± 0.01
			CPPHA (O'Brien, Lemaire et al. 2004)	Human	-11.38	-9.96	-6.78 ± 0.41	-7.32 ± 0.37
II	**mGluR2**	**Positive**	**PTEB** (Pinkerton, Vernier et al. 2004)	Human	-13.94	-12.16	-5.83	-5.1
III	**mGluR4**	**Positive**	**PHCCC** (Maj, Bruno et al. 2003)	Human	-9.37 ± 0	-9.31 ± 0.003	-8.07 ± 0.08	-6.16 ± 0.09
	mGluR7	**Positive**	**AMN082** (Mitsukawa, Yamamoto et al. 2005)	Human	-11.27	-13.11	Did not dock	-7.56

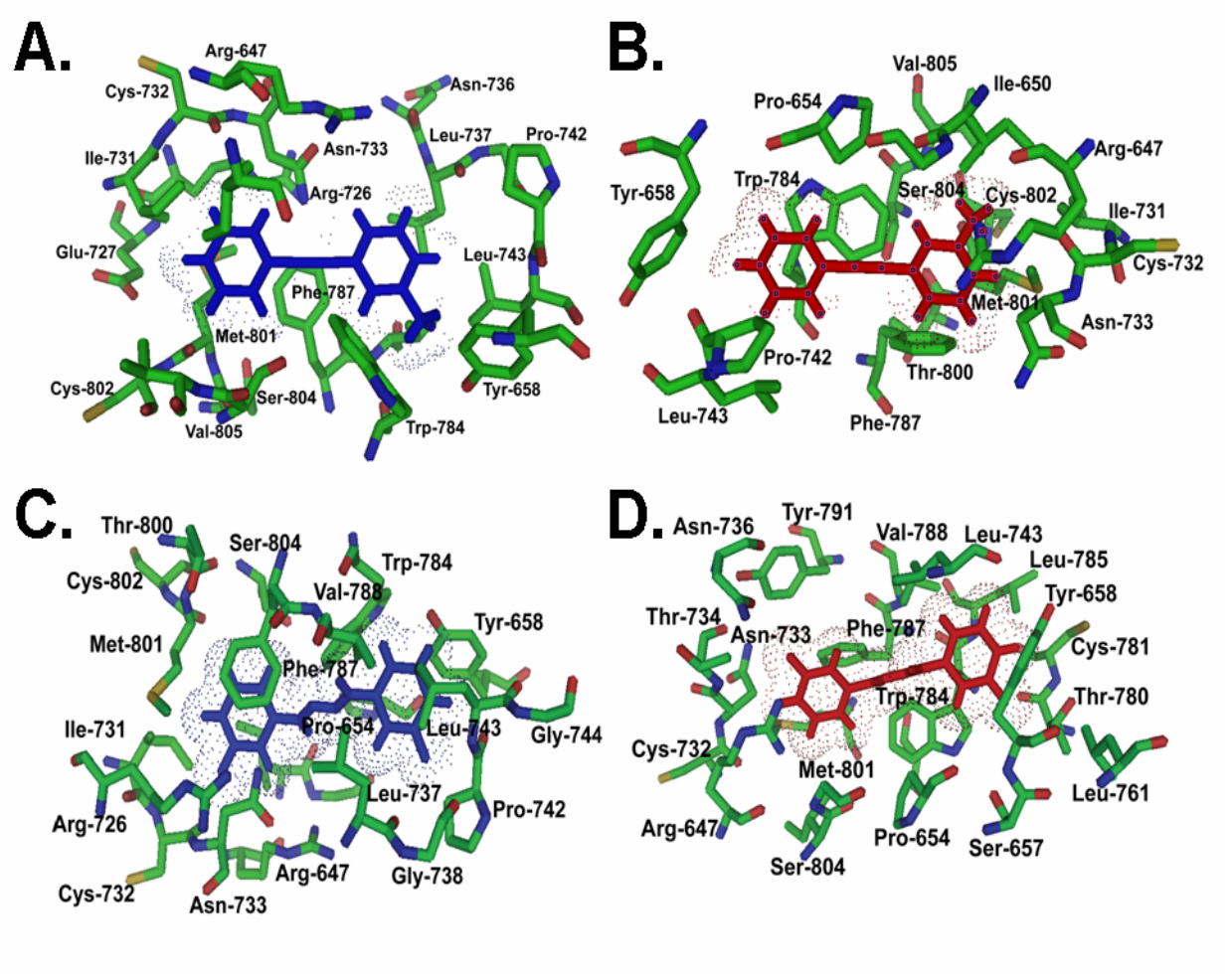

**Figure 4.3: Amino acid residues within 5Å of the docked ligands MPEP and DFB-3,3` in mGluR5.** The active receptor conformation is shown in A,C and the inactive receptor conformation is shown in B,D. Models were docked with negative modulator MPEP (A,B) and positive modulator DFB-3,3` (C,D). The ligands are colored in blue for the active models and in red for the inactive models. Images were created using Pymol Software (http://www.pymol.org).

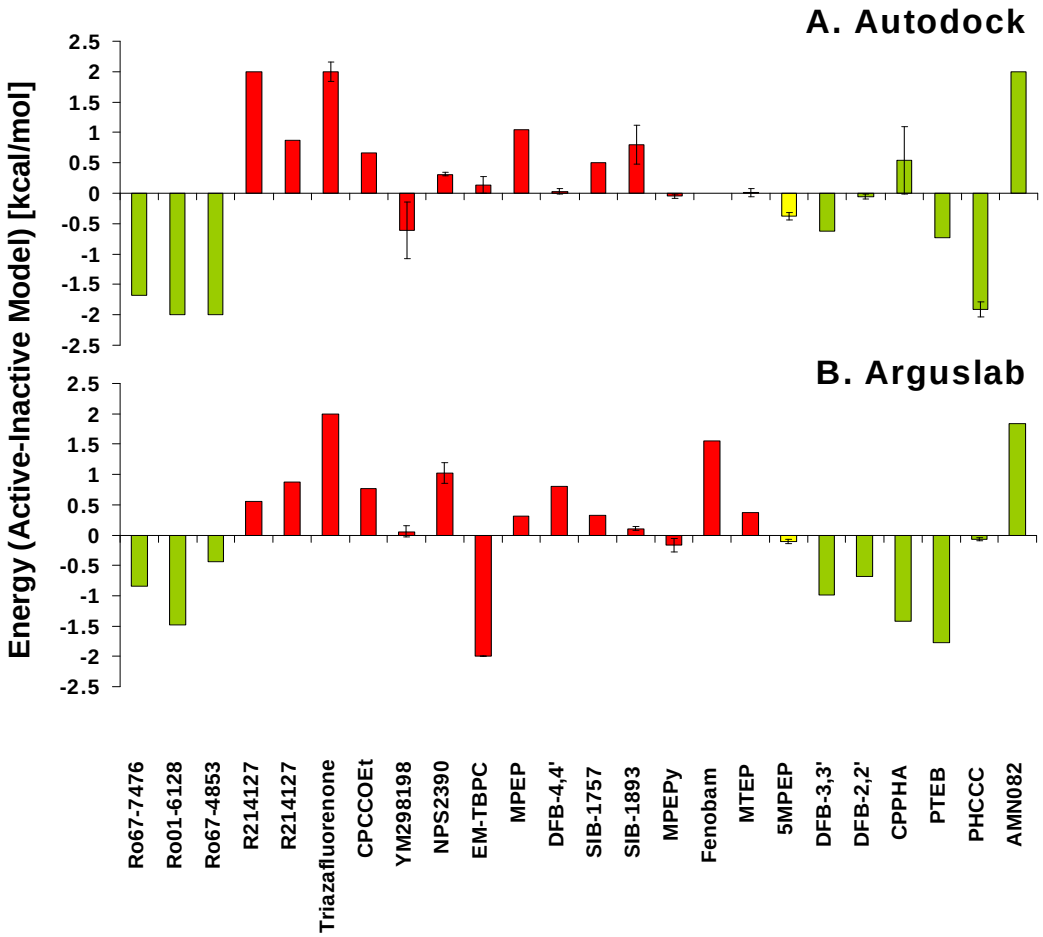

Figure 4.4: Differences in energy between active (ANM based) and inactive (rhodopsin crystal-structure based) models of mGluRs. The docked ligands are shown in Figure 1 and energies are listed in Table 2. Green bars indicate positive modulators, red bars negative modulators and the yellow bar represents a neutral ligand. Where values of 2 are shown, the ligand did not dock to the active model, where values of -2 are shown, the ligand did not dock to the inactive model. Error bars indicate standard deviation in three docking experiments each for the respective active and inactive models. If an error bar is placed at a -2 or 2 bar, the error represents the standard deviation of the ligand and model combination where docking was observed. A. Results from docking with Autodock software. B. Results from docking with ArgusLab software.

4.1.7. Discussion

At the time when this work was undertaken, the only available three-dimensional structure of any GPCR was that of rhodopsin (Palczewski, Kumasaka et al. 2000). Previous approaches to docking of ligands to GPCRs have therefore used mostly receptor models based on the rhodopsin structure (Kassack, Hogger et al. 2000; Greasley, Fanelli et al. 2001; Lopez-Rodriguez, Murcia et al. 2001; Nikiforovich and Marshall 2001; Chambers and Nichols 2002; Deraet, Rihakova et al. 2002; Gao, Chen et al. 2002; Johren and Holtje 2002; Mehler, Periole et al. 2002; Stenkamp, Filipek et al. 2002; Anzini, Canullo et al. 2003; Becker, Shacham et al. 2003; Berkhout, Blaney et al. 2003; Bhave, Nadin et al. 2003; Hulme, Lu et al. 2003; Kim, Gao et al. 2003; Malherbe, Kratochwil et al. 2003; Petrel, Kessler et al. 2003; Ruan, Wu et al. 2003; Schulz and Schoneberg 2003; Shim, Welsh et al. 2003; Trent, Wang et al. 2003; Man, Gilad et al. 2004; Miedlich, Gama et al. 2004). The advantages and disadvantages of this approach have been discussed (Archer, Maigret et al. 2003; Filipek, Teller et al. 2003) and it was shown that in some cases alternative approaches such as the Membstruk modeling approach provides more useful models than those based directly on homology to rhodopsin (Vaidehi, Floriano et al. 2002; Floriano, Vaidehi et al. 2004; Freddolino, Kalani et al. 2004; Hall, Floriano et al. 2004; Trabanino, Hall et al. 2004; Hummel, Vaidehi et al. 2005; Floriano, Hall et al. 2006; Peng, Vaidehi et al. 2006; Spijker, Vaidehi et al. 2006; Vaidehi, Schlyer et al. 2006). In particular, it was observed recently that there is a difference in the structures obtained after short molecular dynamics simulations depending on whether receptor agonists or antagonists were docked (Kinsella, Rozas et al. 2005; Kinsella, Rozas et al. 2006). These observations indicate that the conformation of the receptor will be important for the stability and nature of a receptor-ligand complex. To our knowledge however there has been no previous attempt to predicting different conformations of the

receptors first, and then docking ligands to these conformations. We describe here the docking of ligands to two different conformations of mGluR receptors, active and inactive, using two docking programs, ArgusLab and AutoDock.

AutoDock is a stochastic Grid-based approach that uses the genetic algorithm to sample different populations of ligand conformations in their binding to the receptor. Each bound conformation is energetically evaluated by a series of energy minimization steps, in which unsuccessful docking results are discarded. While the genetic algorithm is a widely used and reliable algorithm, it has known limitations (Morris, Goddsell et al. 1998), among the most significant is the possibility of the optimization of the ligand conformations getting trapped in local minima (Park, Lee et al. 2006). This is also confirmed by our observation that individual runs may give different results (Figure 4.4 and Table 4.3). ArgusLab therefore provides both algorithms, the stochastic search, analogous to the genetic algorithm provided by AutoDock, as well as an exhaustive search method based on identification of complementary shapes of the ligand and the receptor, referred to as "ShapeDock" or "ArgusDock". When using ArgusLab with the ArgusDock algorithm, 12 of the 14 (86%) negative modulators were predicted to bind with more favorable energy to the inactive model. Due to the high reproducibility between different runs, the error margins are small and in all cases but one the errors were significantly smaller than the differences observed between docking to active and inactive models. Similarly, 8/9 (89%) positive modulators bound significantly more favorably to the active model with ArgusLab. The results obtained for AutoDock were less correlated, as expected: 10/14 (71%) and 7/9 (78%) bound the predicted conformation more favorably. We consider the AutoDock results less reliable than those obtained with ArgusLab for several reasons. In six of the predictions, where the differences between docking to active and inactive models were small,

docking energy differences were close to or smaller than the noise level. There were also more incidences in which AutoDock was not able to predict binding for the ligands at all. Finally, the ligand binding pockets predicted by AutoDock showed less agreement with the experiments than ArgusLab. However, one should keep in mind that some ligand/binding site types are problematic because the shape does not match if the starting ligand conformation is not correct and/or if the scoring function is not appropriate. This could be the case in the prediction of AMN082, where both algorithms incorrectly predicted this ligand to be a negative modulator, because the ligand did not dock at all to the inactive conformation. Such difficulties may also give rise to larger errors when docking one ligand as compared to another. For example, the docking energies of ligand YM298198 were associated with a larger error when using both algorithms. If we were to equally weigh predictions made by ArgusLab and AutoDock, we would still have agreement between the two methods and strong preferences (i.e. strong differences in both AutoDock and ArgusLab) in 8 out of 14 cases (57%), where the negative modulators bound the inactive conformations with significant preference using both docking programs, and 6 out of 9 cases (67%), supporting the hypothesis.

In addition to comparing predicted ligand binding energies, we also investigated the details of the interactions between the ligand binding pockets and the ligands for mGluR5. Of the experimentally known ligand binding residues of MPEP, our prediction identified all residues, except Ala-809, Thr-780 and Tyr-791 (colored in red in Table 4.1). These three residues are more than 6.2 Å away from any atom within the ligand, and are not simply missed due to a too short cut-off distance in the definition of ligand binding residues. Furthermore, Ala-809 and Thr-780 are facing the outside of the helical bundle, and it is possible that the experimental effects reported might have been secondary effects. In the case of DFB-3,3` all known ligand binding

residues are also predicted. For both ligands on the other hand, we predict a number of residues to be important for ligand binding that have not been tested experimentally. Finally, we show that while there are several residues in the ligand binding pocket that are shared between active and inactive conformations, there are also residues that bind ligand only in one conformation, and that are specific for positive versus negative modulators. Thus, our models provide useful, experimentally testable hypotheses.

The dependence of the properties of ligand binding on receptor conformation has important functional implications. Recently, it was shown for rhodopsin that the dark-state inactive structure already contains the information needed to form the light-activated structure (Isin, Rader et al. 2006). This supports the notion that *all-trans* retinal in rhodopsin stabilizes a conformation that is already partially accessible to the *11-cis* retinal bound dark, inactive state of the receptor. Translated to other GPCRs, this suggests that receptors may partially form activated conformations and that agonists could stabilize such conformations, while inverse agonists would destabilize such conformations. In mGluRs, the situation is slightly different from other GPCRs because their ligand binding domain is located in an EC domain added to the conserved GPCR seven-TM helical scaffold. In this case, ligands also bind to the TM/EC domain interface but here they act as modulators for ligand binding in the EC domain. However, it was shown that in the absence of the EC domain, positive and negative modulators act as agonists and inverse agonists, respectively. Thus, the findings reported here for mGluRs are likely to have functional implications of the GPCR family in general, implying that agonists and antagonists are likely to prefer the active and inactive conformation of GPCRs, respectively.

4.1.8. Conclusions

Here we proposed the idea that allosteric ligands can be docked to inactive and active conformational models of mGluRs based on rhodopsin structural models of inactive and active conformations, respectively. We found that the relative difference in binding energy between the two conformations is highly predictive of whether the ligand is a positive or a negative modulator. A positive modulator will bind more favorably to the active conformation, while the negative modulator will bind more favorably to the inactive conformation. Furthermore, we identified similarities and differences in the interactions made between ligand and receptor depending on the nature of the modulator and the conformation of the receptor. The findings are likely to have general utility in predicting functional classification of ligands, such as classification as agonists or antagonists.

4.2. IDENTIFICATION OF LIGAND(S) THAT BIND(S) TO RHODOPSIN IN THE TM DOMAIN, APART FROM RETINAL

4.2.1. Evidence for 3,3`-Difluorobenzaldazine Interaction with Rhodopsin

The high similarity between the mGluR allosteric ligand binding pocket and the retinal binding pocket in rhodopsin prompted us to investigate if rhodopsin may be able to bind mGluR ligands. We tested 3,3`-Difluorobenzaldazine (DFB-3,3`), a positive modulator of mGluR5. Because of the presence of fluorine atoms in this ligand, we used ^{19}F NMR spectroscopy for this purpose. One-dimensional ^{19}F NMR spectra recorded in the absence and presence of DFB-3,3` is shown in Figure 4.5. (In this experiment, ten other in-house synthesized fluorinated ligands were also tested alongside for putative binding).

We investigated light-activated rhodopsin based on the assumption that the retinal would have to leave the binding pocket before DFB-3,3` could bind. Addition of 50μM DFB-3,3` to 5mg of activated rhodopsin sample gave rise to a broad peak at -109.8 ppm (Figure 4.5A red trace) as compared to a sharp peak at -112.5 ppm in the absence of rhodopsin (Figure 4.5B red trace). Further, DFB-3,3` peak in the presence of rhodopsin (Figure 4.5A red trace) is downfield shifted by Δ+2.7 ppm and the signal is decreased in intensity. There was no indication for the presence of a free peak for DFB-3,3` in the presence of rhodopsin. These results suggest the presence of an interaction between DFB-3,3` and rhodopsin supporting the idea that the TM binding pocket might be in part structurally conserved across such diverse GPCRs as rhodopsin and mGluR5.

4.2.2. Docking Studies of 3,3`-Difluorobenzaldazine to Rhodopsin

To investigate if DFB-3,3` would preferentially bind to the TM domain of rhodopsin, rather than the CP domain as was the case for Ce6 and C3G described in Chapter3, we docked DFB-3,3` to the inactive dark-state crystal structure (PDB id: 1F88 (Palczewski, Kumasaka et al. 2000)) and ANM generated activated model of rhodopsin (Isin, Rader et al. 2006). The top-scored conformations in both cases docked in a similar position (Figure 4.6), between helices III, V-VII in the TM domain. No pose in the CP domain was observed. Shown in Table 4.3 are the residues in mGluR5 that are critical for DFB-3,3` ligand binding identified with site-directed mutagenesis (Muhlemann, Ward et al. 2006) along with the predicted ligand pocket residues that are within 5Å from DFB-3,3` in rhodopsin. For the binding of DFB-3,3` to mGluR5 site-directed mutagenesis indicates that Met-801, Ser-657 and Thr-780 are critical for binding and modulatory function (Muhlemann, Ward et al. 2006). There was also evidence that Pro-654, Ser-657, Leu-743 and Asn-733 may contribute to DFB-3,3` binding, albeit with less preference as compared to the residues described above. All the corresponding residues are predicted to be part of the analogous DFB-3,3` binding pocket in the dark state of rhodopsin, except for Ser-657 and Leu-743. In the case of the ANM generated active state, the corresponding residues for Pro-654, Ser-657, Leu-743, and Thr-780 are not predicted. Apart from this, several residues are predicted to be part of the binding pockets rhodopsin (Table 4.4, uncolored residues). In particular, Lys-296, an important residue involved in interacting through a Schiff base with *11-cis* retinal is also predicted to be in the DFB binding pocket residues of both, the dark and activated models of rhodopsin. An aromatic cluster of residues on TM6 helix was shown to play an important role in the binding of ligands to mGluRs (Malherbe, Knoflach et al. 2001; Malherbe, Kratochwil et al. 2003; Malherbe, Kratochwil et al. 2003). Such a cluster is also observed in the dark state

rhodopsin binding pocket. Phe-261, Trp-265, and Tyr-268 constitute the cluster in rhodopsin. Thus, the comparison of the predicted ligand binding pockets in the rhodopsin dark state crystal structure (Palczewski, Kumasaka et al. 2000) and ANM active models (Isin, Rader et al. 2006) with the available experimental site directed mutagenesis data carried out for mGluR5 (Muhlemann, Ward et al. 2006) provide preliminary evidence that rhodopsin can accommodate the mGluR5 ligand, DFB-3,3`, in its retinal binding pocket. The predicted binding energies of interaction of DFB-3,3` to the rhodopsin dark-state and the Meta II activated ANM model without their retinal ligands present were almost identical with -6.81 and -6.88 kcal/mol, respectively

Next, we investigated the overlap between the *11-cis* and *all-trans* binding pockets with the DFB-3,3` binding pockets of rhodopsin dark (Palczewski, Kumasaka et al. 2000) and ANM (Isin, Rader et al. 2006) generated active states, respectively (Table 4.5). Except for 4 out of 23 residues (colored in green; Table 4.5), all those residues that were part of the *11-cis* binding pocket (within 5Å) of rhodopsin dark state were predicted for DFB-3,3` binding to dark state rhodopsin (Palczewski, Kumasaka et al. 2000). However, 8 out of 29 residues were not predicted to be part of the DFB-3,3` binding pocket of rhodopsin in comparison to the 5Å residues from *all-trans* retinal in the ANM generated Meta II state. In summary, the docking results strongly suggests that rhodopsin, a class A GPCR can accommodate DFB-3,3`, a positive modulator of mGluR, a class C GPCR member in its endogenous retinal binding pocket.

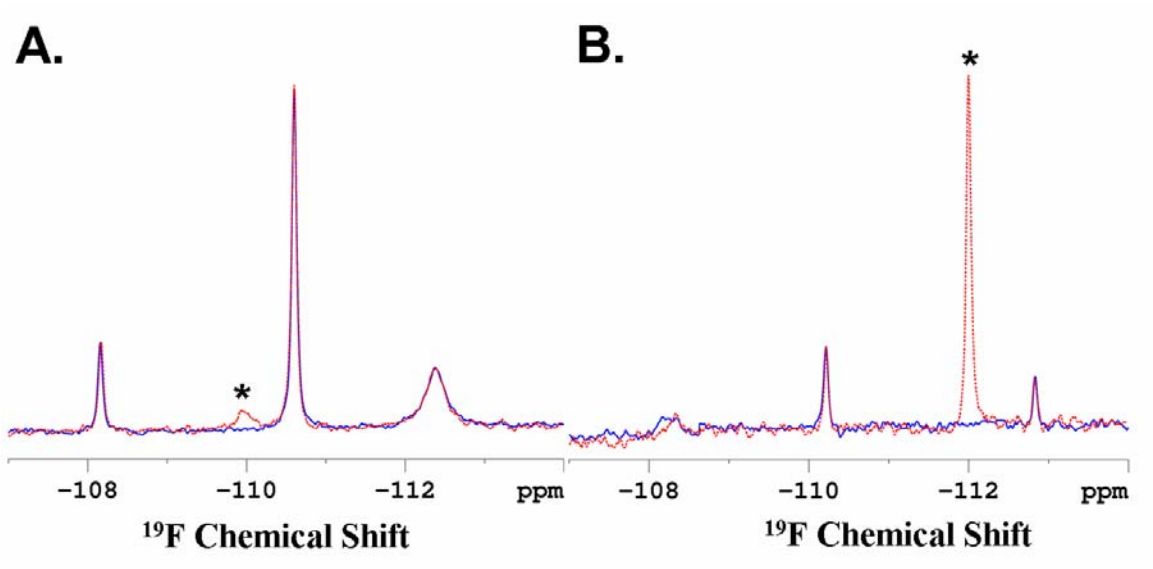

**Figure 4.5: ^{19}F NMR spectra of 3,3`-difluorobenzaldazine.** (A) Overlay of the rhodopsin ligand screening sample with and without DFB-3,3`. (B) Overlay of the ligand screening mixture in 20mM sodium phosphate buffer, 5%DM and 10%D_2O in the presence and absence of 50μM DFB-3,3`. The DFB-3,3` peak position is marked as '*'.

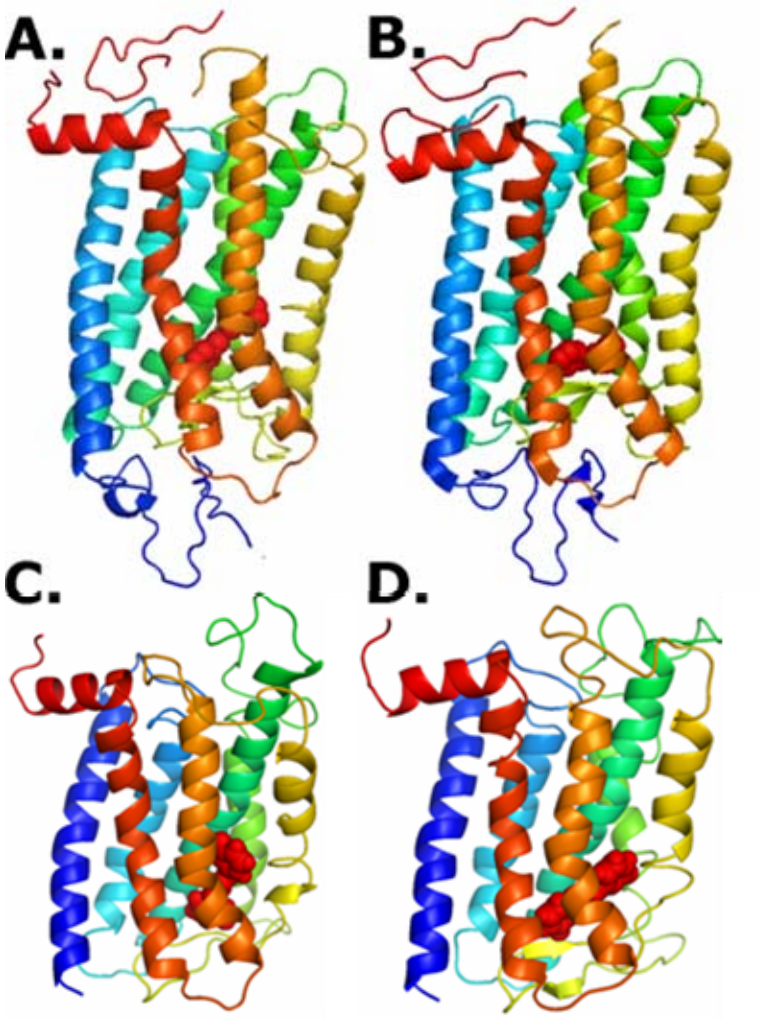

Figure 4.6: Location of 3,3`-difluorobenzaldazine binding to rhodopsin and mGluR5. Cartoon representation of the rhodopsin (A) dark state crystal structure (Palczewski, Kumasaka et al. 2000), (B) ANM model of the activated state of rhodopsin (Isin, Rader et al. 2006), (C) mGluR6 inactive and (D) mGluR6 active models docked with a positive modulator DFB-3,3`. Ligand docked is colored in red and is rendered in spheres. DFB-3,3` refers to 3,3`- Di-Fluoro-Benzaldazine. Images were created using Pymol Software (http://www.pymol.org)

Table 4.4: Residues within 5Å distance from the 3,3`-difluorobenzaldazine ligand in the rhodopsin dark-state crystal and the ANM structures. Residues that overlap between the mGluR5 experimental mutational data and the rhodopsin ANM activated and dark state structures are highlighted in bold and colored in red. Residues colored in blue and highlighted in bold represent the corresponding positions in rhodopsin for the red highlighted residues in mGluR5.

	DFB-3,3` Data (Muhlemann, Ward et al. 2006)	**Rhodopsin ANM activated Model (Isin, Rader et al. 2006)**	**Rhodopsin Dark state Crystal structure (Palczewski, Kumasaka et al. 2000)**
TM3	**Arg-647, Pro-654,** Ser-657, **Tyr-658**	Glu-113, **Gly-114,** Ala-117, Thr-118	Glu-113, **Gly-114**, Ala-117, Thr-118, **Gly-121,** Glu-122, **Leu-125**
EC2	**Asn-733**	Pro-171, Lue-172, Arg-177, Tyr-178, Glu-181, Ser-186, Cys-187, **Gly-188,** Ile-189, Tyr-191	Tyr-178, Glu-181, Ser-186, Cys-187, **Gly-188,** Ile-189
TM5	Leu-743	Phe-203, Met-207	His-211, Phe-212
TM6	**Thr-780, Trp-784, Phe-787,** Val-788, Tyr-791	**Trp-265, Tyr-268**	**Phe-261, Trp-265, Tyr-268**
TM7	**Met-801**	**Ala-292,** Ala-295, Lys-296	**Ala-292**, Lys-296

**Table 4.5: Comparison of 3,3`-difluorobenzaldazine with retinal binding pockets in rhodopsin.** Residues that overlap with the *11-cis* and *all-trans* binding pocket are highlighted in bold and colored in green and blue, respectively. The residues that are unique to DFB-3,3` are colored in red and highlighted in bold.

	Rhodopsin dark state crystal structure (Palczewski, Kumasaka et al. 2000)		**Rhodopsin ANM activated model (Isin, Rader et al. 2006)**	
	DFB pocket	***11-cis* retinal pocket**	**DFB pocket**	**All-trans pocket**
TM3	Glu-113, Gly-114, Ala-117, Thr-118, Gly-121, Glu-122, Leu-125	Glu-113, Gly-114, Ala-117, Thr-118, Gly-121, Glu-122, Leu-125	Glu-113, Gly-114, Ala-117, Thr-118	Glu-113, Gly-114, **Phe-115**, Ala-117, Thr-118, **Leu-119**, **Glu-122**
EC2	**Tyr-178**, Glu-181, Ser-186, Cys-187, Gly-188, Ile-189	Glu-181, Ser-186, Cys-187, Gly-188, Ile-189	Pro-171, Lue-172, Arg-177, Tyr-178, Glu-181, Ser-186, Cys-187, Gly-188, Ile-189, Tyr-191	Pro-171, Lue-172, **Val-173, Ser-176,** Arg-177, Tyr-178, **Ile-179**, Glu-181, Ser-186, Cys-187, Gly-188, Ile-189, **Asp-190,**Tyr-191
TM5	His-211, Phe-212	**Met-207, Phe-208,** His-211, Phe-212	Phe-203, Met-207	Phe-203, Met-207
TM6	Phe-261, Trp-265, Tyr-268	Phe-261, Trp-265, Tyr-268, **Ala-269**	Trp-265, Tyr-268	Trp-265, Tyr-268
TM7	Ala-292, Lys-296	Ala-292, **Phe-293**,Lys-296	Ala-292, Ala-295, Lys-296	Ala-292, **Phe293,** Ala-295, Lys-296

4.2.3. Effects of DFB-3,3` Binding on Rhodopsin Regeneration

The molecular modeling studies described above indicated that the DFB-3,3` binding pocket highly overlaps with that of the *11-cis* and *all-trans* binding pockets in rhodopsin. This suggests the possibility that DFB-3,3` and *11-cis* retinal might compete for the same binding pocket in rhodopsin. To test this, we investigated the total amount of rhodopsin that can be regenerated in the absence and presence of DFB-3,3`. The increase in 500nm absorbance by addition of *11-cis* retinal 1.5 hours after light activation was followed using UV/Visible spectroscopy (Figure 4.7). The change in absorbance at 500nm of 0.5μM rhodopsin upon addition of 0.5μM *11-cis* retinal 1.5 hours after illumination (a state equivalent to opsin, ligand free rhodopsin) in the absence (black trace) and presence of 0.5μM (red trace) and 2.5μM DFB-3,3` (blue trace) is shown in Figure 4.7B. Shown in Table 4.5 is the total amount of rhodopsin regenerated in the absence and presence of various concentration of DFB-3,3`. The total amount of rhodopsin regenerated after 1.5 hours of illumination was compared to the initial amount added (Table 4.6). In the absence of DFB-3,3`, a total of ~59% of rhodopsin could be regenerated. However, in the presence of 0.5μM DFB-3,3` corresponding to a 1:1 ratio of DFB-3,3` to rhodopsin, the total amount of rhodopsin regenerated was decreased by 15.3% to a total of 43.5% efficiency as compared to rhodopsin alone (Figure 4.7B). Additionally, in the presence of a five-fold excess over rhodopsin, a decrease of 31.3% to a total of 27.5% regenerated material was observed. Thus, we find that the addition of DFB-3,3` decreases the extent of rhodopsin regeneration in a concentration dependent manner.

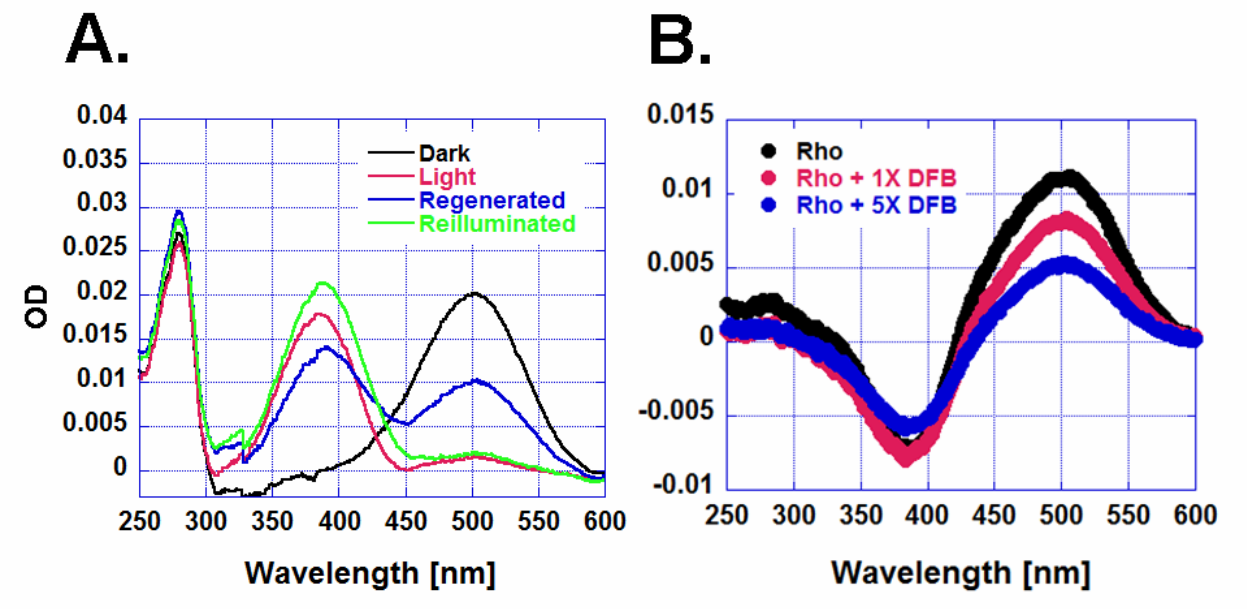

Figure 4.7: Comparison of rhodopsin regeneration in the absence and presence of various concentration of DFB-3,3`. (A). UV absorbance spectra of 0.5μM rhodopsin in the dark (black), immediately after light activation (red), after *11-cis* regeneration (blue) and after reilluminating the regenerated rhodopsin (green). (B) the difference spectra of regenerated minus reilluminated rhodopsin, in the absence (black), and in the presence of 0.5μM (red) and 2.5μM (blue) DFB-3,3`.

4.2.4. Discussion and Conclusions

The studies described in this chapter indicate that the GPCR TM binding pocket may be structurally conserved across GPCRs. Specifically for the comparison between mGluRs and rhodopsin, these findings indicate that what is an orthosteric binding pocket in one GPCR can become an allosteric ligand binding pocket in another GPCR. While the TM ligand binding pocket in mGluRs is the site for allosteric ligands, most other members of the GPCR family are shown to bind to endogenous ligands in this pocket. One such example is rhodopsin, a class A

GPCR. Rhodopsin binds to *11-cis* retinal, the endogenous ligand in the TM domain. Prior to this thesis, there were no known ligands apart from different retinal isomers that can bind to rhodopsin. The studies presented in Chapter 3 of this thesis (Ce6 and C3G) and this Chapter, DFB-3,3`, provide the first evidence for other ligands having affinity for rhodopsin. The evidence for DFB-3,3` binding is as follows. The ^{19}F chemical shift of DFB-3,3` was shifted by 2.7ppm and a decrease in intensity of the peak was observed upon addition of DFB-3,3` to light-activated rhodopsin, suggesting that DFB-3,3` indeed binds to rhodopsin. While the novel ligands identified in Chapter 3 were found to bind in the cytoplasmic domain, we propose that DFB-3,3` binds to the TM domain. Docking studies indicated that DFB-3,3` binds in the TM region and occupies the *11-cis* binding pocket. The comparison 5Å residues indicated that the DFB-3,3` binding pocket highly overlaps with that of *11-cis* and *all-trans* binding pockets. A total of 19/23 were similar between DFB-3,3` and *11-cis* retinal binding pocket in the dark state rhodopsin. Further, a total of 21/29 residues were predicted to be part of DFB-3,3` as compared to *all-trans* retinal pocket. Such a high overlap between retinal and DFB-3,3` binding pockets prompts for an competition between these ligands for the same binding pocket.

To test if DFB-3,3` is able to compete with *11-cis* retinal, we measured regeneration of rhodopsin with and without DFB-3,3` by monitoring the changes in 500nm peak using UV/Vis absorbance spectroscopy. These studies showed that the total amount of rhodopsin that can be regenerated 1.5 hours post illumination is decreased upon addition of DFB-3,3` in a concentration dependent manner. While the interaction affinity of DFB-3,3` to rhodopsin remains to be determined, these studies provide the first evidence for the novel observation that rhodopsin binds to DFB-3,3`, a positive modulator of mGluR5 in competition to *11-cis* retinal. These studies support the idea that the TM ligand binding pocket in GPCRs might be structurally

conserved. The affinities of interaction are expected to be specific for receptor type. Thus, even though rhodopsin can accommodate DFB-3,3` in its retinal binding pocket, it has a higher affinity for *11-cis* retinal. Thus, while GPCRs may have diverged evolutionarily to bind to specific endogenous ligand with higher affinity, at least some GPCRs appear to have retained the conformational flexibility to accommodate other GPCR ligands, which bind other receptors with higher affinity.

Table 4.6: Effects of DFB-3,3` on regeneration of rhodopsin. The total amount of rhodopsin regenerated after 1.5 hours of illumination was compared to the initial amount added.

DFB	Rho Conc	*11-cis*	Regneration in (%) after 1.5 hours	Normalized (in %)	decrease in regeneration (in %)
0	0.5µM	0.5µM	58.8	100	0
0.5µM	0.5µM	0.5µM	43.5	73.9	26.02
2.5µM	0.5µM	0.5µM	27.5	46.7	53.23

CHAPTER - 5
EXTRACELLULAR (ALLOSTERIC) LIGANDS

TABLE OF CONTENTS

SUMMARY

The results described in Chapters 3 and 4 suggest that rhodopsin has the conformational flexibility to accommodate accessory ligands at the CP domain as well as ligands from other GPCR members in the TM domain, respectively. Because the endogenous ligand

binding domains in some class A GPCRs are the EC domains, we suspected that rhodopsin may also bind to ligands in the EC domain. One such class of receptors are the chemokine receptors. While we do not expect chemokines to bind to rhodopsin with as high an affinity as they would bind to their cognate chemokine receptors, evidence for weak binding would still provide a proof-of-principle for a partially conserved binding pocket. A recently developed computational approach to predict protein-protein interactions (Qi, Bar-Joseph et al. 2006) was applied to predict human membrane receptor-protein interactions for rhodopsin. Amongst the potential binding partners were several members of the chemokine family, which are all protein ligands that interact with chemokine receptors at EC sites of the respective receptors. Analysis of the docking of rhodopsin with CXCL11 indicated an interaction at the EC domain, similar to the chemokine-chemokine receptor model of ligand binding.

The following experimental studies confirm the presence of an interaction between rhodopsin and CXCL11. First, the migration of B-cells in response to chemokine gradients showed that rhodopsin inhibits CXCL11-mediated chemotaxis. Furthermore, activation of G_t by rhodopsin was inhibited in the presence of CXCL11, indicating an antagonist-like effect. These findings provide a proof-of-principle that rhodopsin has an intrinsic ability to interact with chemokines, presumably in direct analogy to the interaction between chemokines and their cognate receptors. Further studies are needed to confirm the binding site and determine the affinity for the CXCL11-rhodopsin complex.

SIGNIFICANCE

The studies presented in this chapter provide preliminary evidence for an EC allosteric ligand binding pocket in rhodopsin. The results obtained suggest that rhodopsin has the conformational flexibility to accommodate ligands at the EC domain similar to other class A GPCRs. The fact that the EC domain in class A GPCRs can switch roles between a endogenous and allosteric binding pocket between different class A GPCR members is intriguing and suggests that the overall structure and the conformational sub-states available for different GPCRs may be conserved even at the EC domain. Moreover, as the EC domain is structurally coupled to the TM domain in rhodopsin, and mutations or alterations in this region often lead to malfunctions in rhodopsin, the allosteric modulators that bind specifically at the EC domain could be beneficial to rescue disease states that involve the EC domain.

INTRODUCTION

In our framework that integrates structural coupling between the three domains, the CP, TM, and EC domains, and allosteric or orthosteric ligand binding (see Chapter 1), we proposed that in principle any GPCR can bind ligands in any of these three domains. Prior to this thesis, no CP ligands were known for any GPCR. We showed for rhodopsin that there are such ligands. Thus, we now know that rhodopsin can accommodate ligands in its TM domain (its orthosteric ligand pocket) and in the CP domain, which is therefore an allosteric ligand binding pocket. In other GPCRs, it is known that endogenous ligands bind in the EC domain. Furthermore, the analysis of high connectivity residues

(Christopher J R Illingworth 2008) described in Chapter 3, pg. 143, suggested that in rhodopsin in addition to the CP domain, there may also be potential interaction sites in the EC domain of rhodopsin. Finally, a recently developed computational approach to predict protein-protein interactions using the random forest classifier integrating diverse biological features (Qi, Bar-Joseph et al. 2006) was applied to predict human membrane receptor-protein interactions. Amongst the potential binding partners for the dim-light photoreceptor rhodopsin, the prototypic member of the GPCR family, were several members of the chemokine family of ligands. All these independent lines of circumstantial evidences suggest that EC ligands such as chemokines may bind rhodopsin. This Chapter describes our preliminary results in supporting this hypothesis.

Chemokines, by definition, are chemotactic cytokines. These proteins exert their function by interacting with membrane proteins that belong to class A GPCRs – the chemokine receptors. Chemokines have shown to play a major role in guiding migration of cells, immune system responses, and HIV infection (Rottman 1999; Scotton, Wilson et al. 2001; Le, Cui et al. 2003; Manzo, Caporali et al. 2003; Us 2003; Cartier, Hartley et al. 2005; Yoshie 2005; Suresh and Wanchu 2006; Prado, Suetomi et al. 2007). However, an interaction with rhodopsin has not been anticipated or observed previously. Since the results presented in this thesis (Chapters 3 & 4) imply that GPCRs including rhodopsin may have the conformational flexibility to accommodate ligands other than their endogenous ligands, here *11-cis* retinal, we tested if chemokines can bind rhodopsin. We experimentally provide evidence for a physical interaction between the chemokine CXCL11 and rhodopsin. For this we investigated whether the respective functions of rhodopsin and chemokine receptors can be altered in the presence of the predicted

binding partner. In addition to this, we also performed docking studies to predict the site of interaction on rhodopsin.

5.1. RHODOPSIN – CHEMOKINE LIGAND INTERACTION

5.1.1. Effect of Rhodopsin Interaction with CXCL11 on Chemotaxis Assay in B-Cells

To validate the predicted interaction between rhodopsin and CXCL11, as a first step we measured binding of CXCL11 to rhodopsin indirectly through a chemotaxis assay commonly used to validate chemokine and chemokine receptor function. The assay is such that B-cells expressing chemokine receptors specific to certain chemokines are used as migratory markers in response to certain chemokine. In this assay, B-cells and chemokine are initially present in two individual chambers separated by a semi-permeable membrane. The B-cells are attracted to the chemokine gradient and move towards it by squeezing through the membrane into the chamber with chemokine. Using a hemacytometer, cells present in the chemokine-containing chamber are counted and are presumed to migrate in response to the chemokine where chambers containing a negative control are used to correct for random or nonspecific migration. The results for the chemokine ligands CXCL11 and CCL22 are shown in Figure 5.1. In the absence of rhodopsin, B-cells expressing CXCR3, the receptor for CXCL11, migrated toward CXCL11 (final concentration of 100nM) as hypothesized. But, in the presence of 75 μg of rhodopsin in asolectin lipid vesicles, corresponding to a molar ratio of 30:1 rhodopsin:chemokine, a drastic decrease in the number of cells that migrated was observed in the rhodopsin containing chambers as compared to those without rhodopsin.

Some inhibition, but significantly less than in the presence of rhodopsin, was observed when asolectin lipid vesicles without rhodopsin were used as a control (Figure 5.1 B). Less inhibition of chemotaxis of CCR4-expressing cells was observed with CCL22 in identical experimental conditions. These results suggest that the depletion of the chemoattractant CXCL11 by interaction with rhodopsin leads to the abolition of chemotaxis of the CXCR3 expressing B-cells.

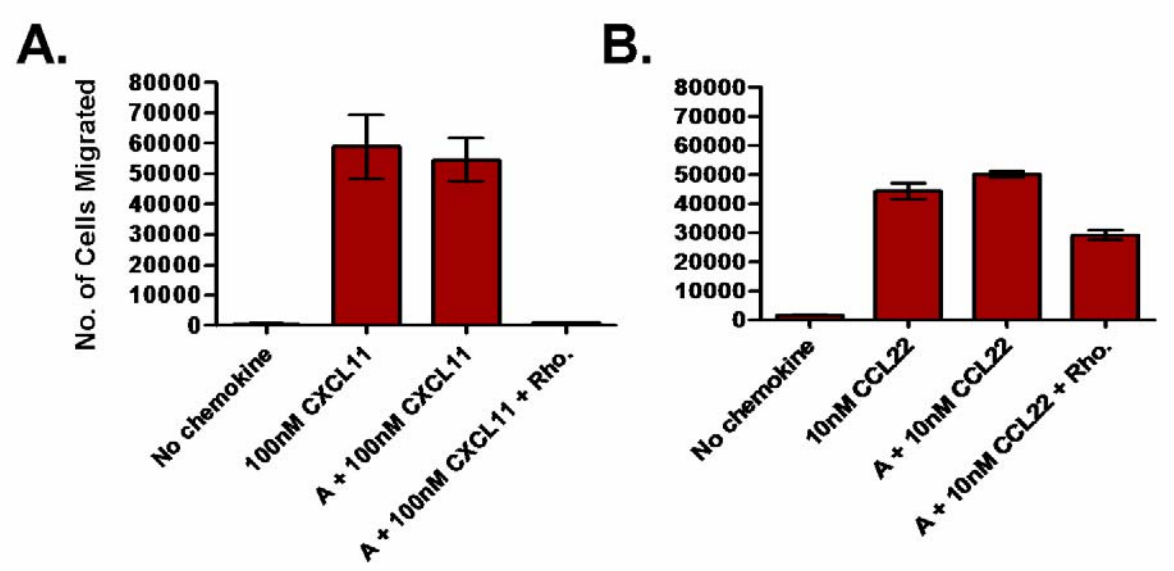

Figure 5.1: Rhodopsin interaction with chemokines CXCL11 and CCL22. Chemotaxis of B-cells expressing CXCR3 (A) or CCR4 (B) towards chemokines CXCL11 (A) or CCL22 (B). 75 µg of rhodopsin was reconstituted in asolectin vesicles and kept in the dark prior to the assay. Illuminated samples were used as a control and showed no difference as compared to the dark samples (data not shown). A = asolectin; n = 3.

5.1.2. Effect of CXCL11 Interaction with Rhodopsin on G Protein, G_t Activation

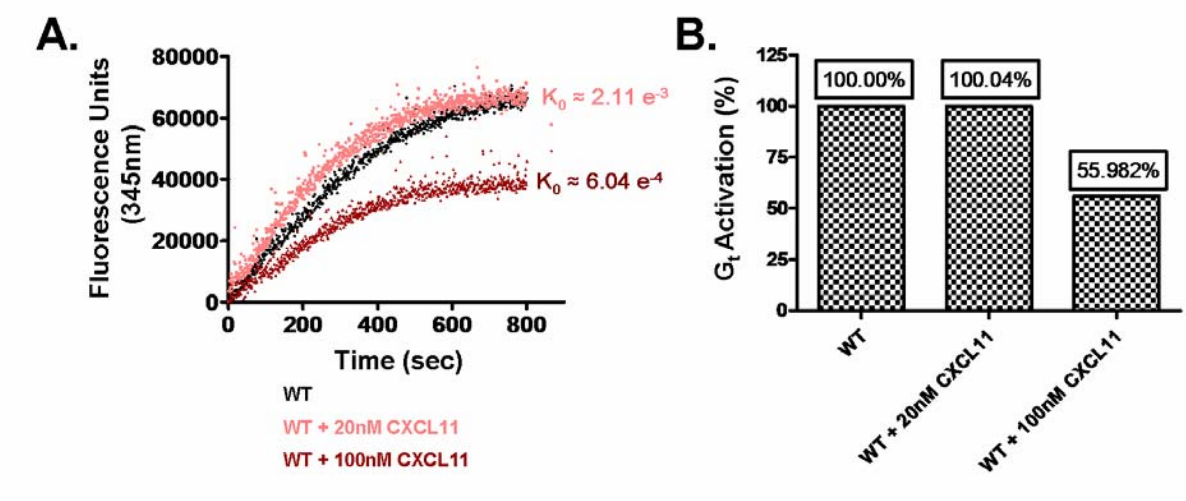

Figure 5.2: Effect of CXCL11 in G protein activation by rhodopsin. (A). G protein activation was measured by fluorescence spectroscopy as described (Jastrzebska, Fotiadis et al. 2006). (B) Normalized percentage of Gt activation in the absence and presence of CXCL11.

As a next step we also monitored the effects of CXCL11 interaction with rhodopsin on rhodopsin function. For this, we measured G_t activation by rhodopsin using fluorescence spectroscopy (Jastrzebska, Fotiadis et al. 2006). Shown in Figure 5.2A are the fluorescence traces of G_t activation upon addition of light activated rhodopsin in the absence and presence of 20nM and 100nM CXCL11. The initial activation rate of G_t in the absence of CXCL11 was $1.6e^{-3}$ seconds. In contrast, in the presence of 100nM CXCL11, the initial rate of activation of G_t was much slower as compared to rhodopsin alone. A decrease of ~3.5 folds in the initial activation rate was observed. In addition to

this, a greater than 40% decrease in total G_t activation was observed with 100-fold molar excess of CXCL11 over rhodopsin (Figure 5.2B).

5.1.3. Protein-Protein Docking of Rhodopsin and Chemokine Ligand, CXCL11

To determine whether the chemokine ligand binding site in rhodopsin resembles that of chemokine receptors, we used the ClusPro docking software (Comeau, Gatchell et al. 2004) for rigid docking of the NMR structures of CXCL11 (Booth, Clark-Lewis et al. 2004) with the X-ray crystal structure of rhodopsin (Okada, Fujiyoshi et al. 2002) and a CXCR3 homology model based on the dark state of rhodopsin using Modeller software (Sali, Potterton et al. 1995). Docking of rhodopsin (pdb id: 1L9H:A) and chemokine receptor CXCR3 with chemokine ligand – CXCL11 (PDB id: 1RJT) was performed using the DOT algorithm supplied by ClusPro docking software (Comeau, Gatchell et al. 2004; Camacho and Zhang 2005). In the case of CXCR3, CXCL11 was found to interact at the EC domain, as expected (Campanella, Lee et al. 2003; Colvin, Campanella et al. 2006). The position of the top scoring interaction along with the orientation is shown in Figure 5.3. Further, this docked conformation was submitted to FastContact analysis (Camacho and Zhang 2005) in order to determine the residues which are located at the interface formed by the two proteins in the docked complex. The stabilizing interactions between the CXCR3 and CXCL11 that contribute to the electrostatic and free energy interactions are listed in Table 5.1. Many of these residues were found to overlap with the experimentally determined interface residues (Campanella, Lee et al. 2003; Colvin, Campanella et al. 2006), further validating the obtained docked conformation. Specifically, residues Arg-8, Lys-46 and Lys-47 of CXCL11were shown to play a major

role in the interaction with CXCR3, where all of these residues are predicted to be part of the binding site (Table 5.1, colored red). In addition to this, residues Tyr-27, Tyr-29, Asp-112, Arg-212, Asp278 and Glu-293 along with the N-terminal residues 1 - 18 in CXCR3 were shown to interact with CXCL11 (Table 5.1, colored blue). These results strongly suggest that the predicted interface highly is consistent with the experimental results.

In the case of rhodopsin, all the top related orientations of CXCL11 were observed at the EC domain of rhodopsin, covering the top of helices 4 and 5 (Figure 5.4). The FastContact analysis (Camacho and Zhang 2005) of this conformation has shown a similar kind of interaction on CXCL11, with residues Arg-8, Lys-46 and Glu-47 (see above). The comparison of the stabilizing residues on rhodopsin with that of CXCR3 showed high overlap. Like in CXCR3, the contribution from N-terminal residues of CXCL11 was also observed to be important in the interaction with rhodopsin. In addition to this, in the case of CXCR3, residues from EC loop 1 and 2 were also shown to contribute to the interaction. In striking similarity to CXCR3, the analysis of the contributing residues from rhodopsin clearly showed strong involvement of EC loop 2; two residues were found in the case of CXCR3 and the rhodopsin interaction with CXCL11 showed 5 residues from EC loop 2. These studies support the hypothesis that the proposed interaction of rhodopsin with CXCL11 would be structurally similar to that of CXCR3. EC loop 2 in rhodopsin is shown to play a major role in locking the receptor in an inactive state. The CXCL11 interaction with rhodopsin is postulated to involve most of the accessible residues on EC loop 2, this may provide further evidence as to why the inhibition of G_t activation was observed.

Table 5.1: Residues in CXCR3 and CXCL11 contributing for the stabilizing electrostatic and free energy contacts. The residues at the interface of CXCR3 and CXCL11 were previously determined by mutagenesis studies (Campanella, Lee et al. 2003; Colvin, Campanella et al. 2006) are colored in blue for CXCR3 and in red for CXCL11.

Electrostatic Contacts		Free Energy Contacts		Electrostatic Contacts		Free Energy Contacts	
CXCR3	**CXCL11**	**CXCR3**	**CXCL11**	**Rhodopsin**	**CXCL11**	**Rhodopsin**	**CXCL11**
ASP – 28	LYS - 5	ASP - 28	LYS - 5	GLU – 5	**LYS - 46**	GLU - 5	**LYS – 46**
GLU – 33	**ARG - 8**	PRO - 42	PHE - 1	GLU – 201	LYS – 5	GLU - 196	CYS – 11
PRO – 42	PHE - 1	GLU - 33	**ARG - 8**	GLU – 196	GLY - 13	GLU - 201	LYS – 5
GLU – 15	LYS - 46	**GLU - 15**	**LYS - 46**	GLU – 196	ARG - 52	GLU - 196	GLY – 13
GLN - 209	GLU - 47	**VAL – 5**	ILE - 29	GLU – 196	ILE – 12	GLU - 196	ARG – 52
ASP – 35	**ARG - 8**	ASP - 46	PHE - 1	GLU – 197	SER - 33	GLU - 196	ILE – 12
GLN – 9	SER - 33	ASP - 28	LYS - 38	GLU – 196	CYS - 11	GLU - 197	**ARG – 8**
GLU – 31	GLN - 51	**TYR - 29**	PRO - 14	GLU – 197	**ARG – 8**	GLU - 197	SER – 33
GLN - 116	PHE - 1	**GLN – 9**	SER – 33	MET – 1	**GLU - 47**	MET - 1	**GLU – 47**
ASP – 46	PHE - 1	**VAL – 5**	ILE – 42	THR – 4	**GLU - 47**	PRO - 194	PRO – 14
ASP – 28	LYS – 38	CYS - 43	MET – 3	GLU – 196	LYS – 5	GLU - 196	LYS – 5
ASP – 28	**ARG – 8**	ASP - 28	ARG – 8	GLU – 5	ARG - 52	THR - 4	**GLU – 47**
ASP – 28	LYS – 57	GLN - 116	PHE – 1	THR – 198	GLN - 51	GLU - 5	ARG – 52
ASP – 7	**ARG – 8**	GLU - 31	GLN – 51	GLU – 196	LYS – 38	GLU - 196	LYS – 38
ARG - 212	**GLU – 47**	**TYR - 29**	CYS – 11	GLU – 197	LYS – 38	GLU - 196	CYS – 53
GLU – 31	**ARG - 8**	ASP - 28	LYS – 57	GLU – 196	CYS - 53	GLU - 197	LYS – 38
GLU - 293	PHE - 1	**ASP – 7**	**ARG – 8**	ASP – 190	**LYS - 46**	ASP - 190	**LYS – 46**
GLU - 31	**LYS - 46**	**ARG - 212**	**GLU – 47**	GLU – 196	LYS – 57	GLU - 196	LYS – 57
TYR - 27	**ARG - 8**	GLN - 209	**GLU – 47**	GLU – 196	**ARG – 8**	HIS - 195	PRO – 14
ASP - 28	ARG - 6	ASP - 35	**ARG - 8**	GLY – 6	**LYS - 46**	GLU - 196	**ARG - 8**

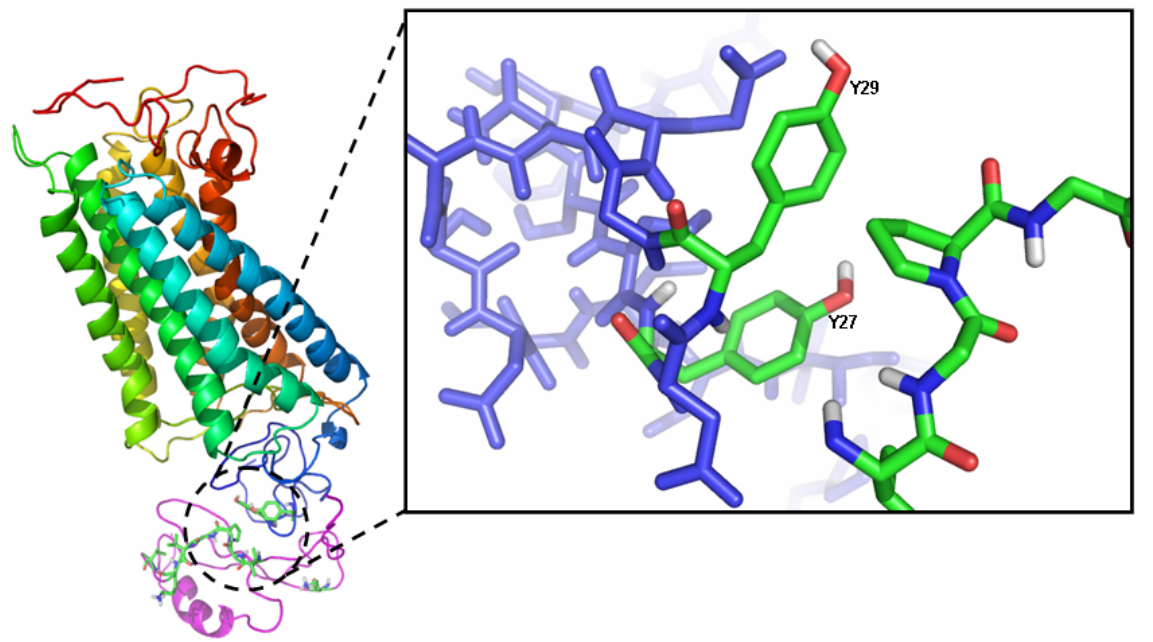

Figure 5.3: Docking of chemokine receptor CXCR3 with CXCL11 NMR structures. CXCL11 NMR structures, pdb id code 1RJT: model 1 (Booth, Clark-Lewis et al. 2004) were docked to the CXCR3 homology model based on the dark-state rhodopsin crystal structure, pdb id code 1l9h (Okada, Fujiyoshi et al. 2002) using the ClusPro software (Comeau, Gatchell et al. 2004). The interaction site is expanded to show tyrosine residues 27 and 29 of CXCR3 that were shown to be critical for the interaction of CXCL11 with CXCR3, where signalling may be sulfonation-dependent (Campanella, Lee et al. 2003; Colvin, Campanella et al. 2006).

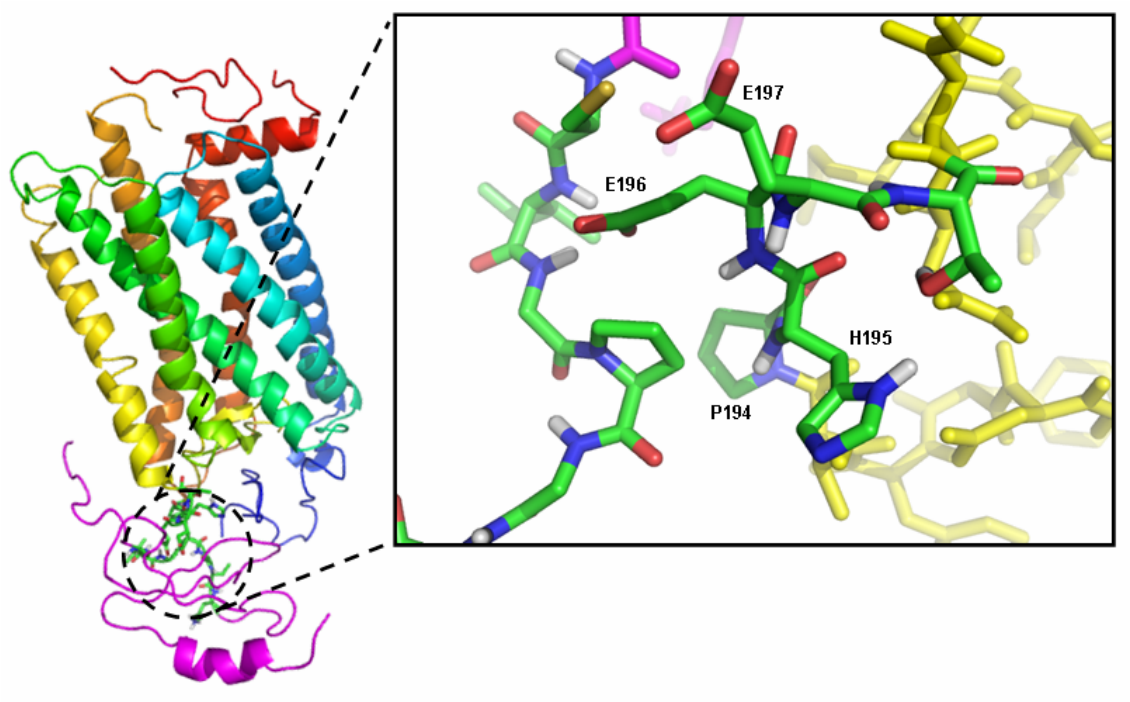

Figure 5.4: Interaction of rhodopsin with CXCL11 NMR structure. CXCL11 NMR structures, pdb id code 1RJT: model 1 (Booth, Clark-Lewis et al. 2004) were docked to the dark-state rhodopsin crystal structure, pdb id code 1l9h (Okada, Fujiyoshi et al. 2002) using the ClusPro software (Comeau, Gatchell et al. 2004). The interaction site is expanded to emphasize the EC loop 2 in rhodopsin with that of CXCL11. Residues 194-197 of rhodopsin are labelled.

5.1.4. Discussion and Conclusions

Evidence described in Chapters 3 and 4 suggests that rhodopsin has the conformational flexibility to accommodate ligands at different domains. The evidence described in this Chapter further support this notion. Functional studies have shown that the interaction between rhodopsin and chemokines inhibits both chemokine and rhodopsin functions suggesting that in addition to its established function as the visual photoreceptor, rhodopsin may modulate other signaling pathways. The interaction site of rhodopsin with CXCL11 was similar to that observed between CXCR3 and CXCL11. In particular, the contribution of the N-terminus and EC loop 2 was essential for the interaction with CXCL11 in both receptor models. These studies suggest that class A GPCRs may have conserved substates between different members of common or divergent origin to accommodate different ligands, given the possibility that the receptors have access to them. Thus, while we propose that an interaction between rhodopsin and CXCL11 occurs *in vitro*, such an interaction may be rare or non-existent *in vivo*. Although sharing similar structure and sequence, GPCRs have evolved to be specific to both tissues and ligands, suggesting specific functions. Given this, the probability that chemokines may interact with other GPCRs non-specifically, rhodopsin included, is small. Additionally, such an interaction may be difficult to observe and identify in real-time in a biological system, unless the system is reconstituted, as above. However, growing evidence shows that various chemokines are expressed during retinal inflammation (McMenamin, Forrester et al. 1992; Crane, McKillop-Smith et al. 2001), and more recently, it was also shown that CXCL11 can pass the blood – retina barrier (Crane and Liversidge 2008), thus the interaction is possible from an accessibility point of view. While further studies

would be needed to demonstrate the functional relevance of this observation *in vivo*, this was not the goal of this thesis. Here, we only aimed at obtaining a proof-of-principle that there may be a potential for an allosteric ligand binding site in rhodopsin involving the EC domain. While further work is needed to confirm the location and affinity of binding, the fact that chemokines are small proteins eliminates the possibility of a TM binding domain. A CP domain, while unlikely, still remains to be excluded experimentally.

In conclusion, the studies performed in this chapter suggest that rhodopsin can bind to ligands, either small molecules or proteins, from other members of GPCRs. This, along with the studies from earlier chapters indicates that the overall structure and the conformational sub-states available for different GPCRs may be conserved, despite the sequence diversity observed in these receptors. In addition to this, one may speculate that the diversity in sequences could have lead to subtype specificity in these receptors for the available endogenous ligands presented to them in the cells.

CHAPTER - 6
IDENTIFICATION OF NOVEL MEMBRANE RECEPTOR LIGANDS

TABLE OF CONTENTS

SUMMARY

Membrane proteins in general, and G protein coupled receptors are no exception, pose problems for application of NMR-based ligand binding studies due to the need to maintain the proteins in a membrane mimetic environment such as detergent micelles.

The high intensity of detergent signals suppresses the signals from the protein. Here, we proposed to study ligand binding by two alternative approaches: ^{19}F NMR spectroscopy and selective excitation using ^{1}H NMR spectroscopy. Selective excitation of the ^{1}H spectral region downfield of the water signal can reveal ligand-backbone and ligand-tryptophan interactions. The use of this method to identify ligands that bind to rhodopsin was demonstrated in chapter 3 (refer section 3.1.1 and 3.2.2). The ^{19}F nucleus provides an ideal NMR probe because of its high sensitivity and the lack of natural ^{19}F background in biological systems. One dimensional ^{19}F NMR spectra acquired on a set of ligands labeled with ^{19}F, to show as a proof of principle that this probe can be used to screen ligands with similar chemical groups either *in vitro* or *in vivo*.

SIGNIFICANCE

Membrane proteins are encoded by up to 30% of typical genomes and constitute the most important class of drug targets: more than 60% of current drugs are targeting membrane receptors, channels or transporters. Amongst these, the G protein coupled receptors are the largest group of drug targets because of their important role in mediating communication between the inside and outside of the cell in response to an enormous variety of different ligands, ranging from small proteins and peptides to small organic molecules, ions and even light. These ligands can be hormones, odorants, neurotransmitters, or other functional classes of biologically active compounds. Despite the importance of membrane proteins as drug targets, they have not yet been amenable to the structure-based drug design. This is due to constraints such as the size of the molecule and the need for the detergent environment. Thus, the NMR spectroscopy methods for

example, employing selective excitation ^{1}H and ^{19}F based approaches, overcoming many of the challenges associated in applying conventional NMR spectroscopy methods to membrane proteins will be highly beneficial in identifying new drugs targets for these receptors.

INTRODUCTION

Although NMR based screening is only one of many screening tools in drug discovery, its simplicity and wide range of application (including protein-protein and protein-nucleic acid interactions) has attracted much attention. NMR allows measurement of multiple parameters at different levels of complexity and information content. Thus, NMR based methods differ significantly from one another as a result of the particular approach used. NMR techniques for drug discovery are high content methods: they potentially provide binding information, the location of the binding site and the conformation of the bound ligand. NMR can also supply structural information that enables docking of the ligand to the protein's binding pocket. In addition, NMR provides very valuable information about the general behavior of the ligands that other high throughput methods do not reveal, including solubility, binding behavior (promiscuous ligands), precipitation potential and aggregation. Because NMR based screening is biased toward finding medium to low affinity ligands, the approach can also serve as an effective prescreening tool for subsequent assay-based high throughput screening. Thus, NMR based screening for small molecular weight drugs are now well established in industry and can be used complementary to high throughput screening methods and computational screening methods. The major limitation of current high information content NMR based screening

methods is the applicability to small and well behaved proteins with limited background from solvent, thus essentially excluding membrane proteins and proteins in complex environments such as the cell. Here, we discuss these limitations in details and propose approaches to overcome them.

6.1. LIMITATIONS IN APPLICABILITY OF NMR SPECTROSCOPY TO MEMBRANE PROTEINS

While ^{1}H NMR based methods to study ligand binding can be carried out with unlabeled protein, more sophisticated applications of NMR spectroscopic techniques such as SAR by NMR require labeling, typically the biosynthetic introduction of ^{13}C and ^{15}N nuclei. However, many proteins cannot be successfully expressed in *E. coli* or *P. pastoris* that make uniform ^{13}C,^{15}N labeling affordable. When proteins need to be expressed in mammalian or insect cell lines in order to obtain them in functional form, uniform labeling becomes prohibitively expensive when the protein expression levels are not unusually high. In such cases, specific ^{15}N and / or ^{13}C labeled amino acids are introduced (Klein-Seetharaman, Reeves et al. 2002; Klein-Seetharaman, Yanamala et al. 2004). Such proteins are not amenable to structure determination by NMR spectroscopy. Mammalian membrane proteins often belong to this group e.g. when they are glycosylated or otherwise posttranslationally modified in their native form, and require the mammalian or insect cell machinery for proper folding.

Another constraint on the applicability of NMR spectroscopy can be the presence of background signals. In the case of membrane proteins, a membrane mimetic is required, provided by detergent micelles when they are studied with solution NMR

methods. The detergent concentrations are typically 100 times higher than the protein concentrations to ensure that only one functional protein or protein complex is present per micelle for uniformity purposes. The high signal intensity originating from the detergent leads to the suppression of signal intensities from the protein (dynamic range problem) and also results in overlapping with that of protein peaks. An example is shown for a 0.7mM solution of the mammalian membrane protein and G protein coupled receptor rhodopsin in 1% octyl glucoside (Figure 6.1). A value of 1% is in fact relatively low; in many cases much higher detergent concentrations are used, making the dynamic range problem even more severe.

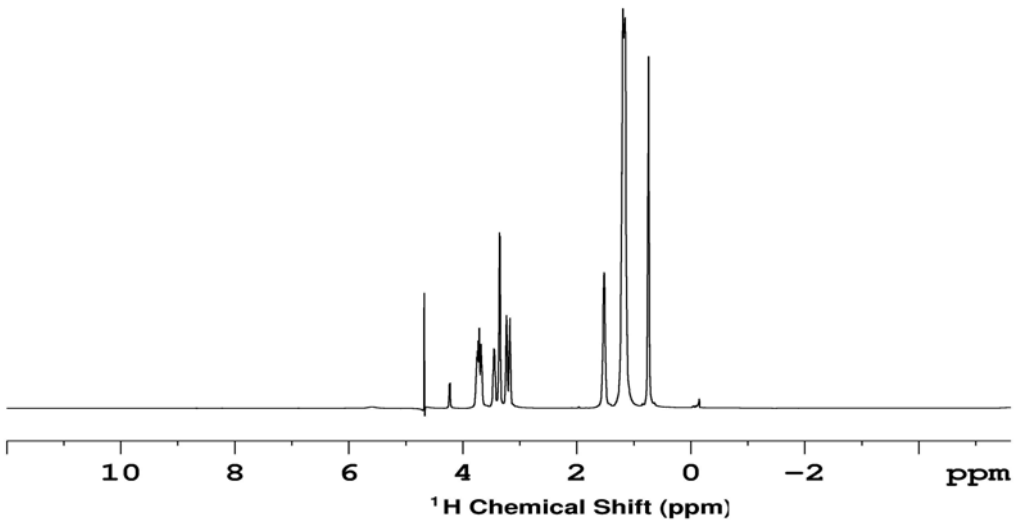

Figure 6.1: One dimensional ^{1}H NMR spectrum of rhodopsin in 1% octyl glucoside.

6.2. SELECTIVE EXCITATION ^{1}H NMR SPECTROSCOPY

Membrane proteins are generally excluded from ^{1}H NMR-based ligand screening approaches because of the high background signals from detergents (see Section 6.1, above; Figure 6.1). Here, we propose a solution to extend the applicability of ^{1}H NMR-based approaches to membrane proteins. NMR approaches involving ways to selectively excite the protein signals while suppressing the detergent peaks can be applied to such systems. Here, we show selective excitation sculpting studies using full-length rhodopsin in octyl glucoside micelles as a model system. Rhodopsin is the most extensively studied G-protein-coupled receptor, and knowledge about its structure serves as a template for other related receptors.

One dimensional ^{1}H NMR spectra recorded by selectively exciting the protein NH region by applying a 90° pulse centered around 10-12 ppm shows ^{1}H chemical shifts from both backbone and side chain regions of rhodopsin in octyl glucoside micelles (Figure 6.2A). Further, excitation of the same region using the hyperbolic secant shaped pulse to remove detergent and water signals significantly increased the intensities of the NH peaks in the range from 6.0 - 8.5 ppm (Figure 6.2B) (Hwang and Shaka 1995; Stott 1995). Note, however, that the number of peaks observed in the 1D ^{1}H NMR spectrum is significantly reduced. We tentatively propose that the observed signals arise mostly from the backbone C-terminus residues and other flexible loop regions (refer to Section 3.2.4 (f), pg. 135). This hypothesis is based on the previous observation (Klein-Seetharaman, Reeves et al. 2002) that sharp, highly intense and thus slowly relaxing signals are found only for Lys339 in a uniformly ^{15}N-lysine labelled rhodopsin sample. Furthermore, comparison between the observed signals and those obtained with a peptide

corresponding to the sequence of the C-terminal residues reveals extensive similarities between the rhodopsin C-terminus and the free peptide in solution (Werner, Lehner et al. 2007).

One-dimensional ^{1}H NMR spectra of rhodopsin recorded at different concentrations of octyl glucoside indicated chemical shift dependence of the C-terminus backbone peaks (data not shown), highlighting the need to control the detergent environment quantitatively to obtain reproducible NMR results. To investigate possible detergent-protein interactions, we recorded one- and two-dimensional ^{1}H-^{1}H selective excitation NOE spectra. We observed differential interactions of the rhodopsin backbone signals with those of the detergent micelles (Figure 6.3) (Stott 1995). We did not observe intramolecular protein NOE peaks. A potential solution that may allow future measurement of such NOEs could be provided by detergent deuteration. However, the high cost of isotope labelled detergent will prohibit extension to high-throughput studies.

The selective excitation approach described here can be used to investigate both NH backbone and tryptophan side chains and thus, in principle, the same innovative approaches developed for one-dimensional ligand screening using ^{1}H NMR of soluble proteins can be extended to membrane proteins when combined with the selective excitation schemes proposed here. We have successfully identified novel ligands binding to rhodopsin and interacting with C-terminal residues by measuring signal intensity, chemical shift and line-broadening effects in selectively excited ^{1}H spectra as a function of added ligand or protein (see Section 3.1.1 and 3.2.1).

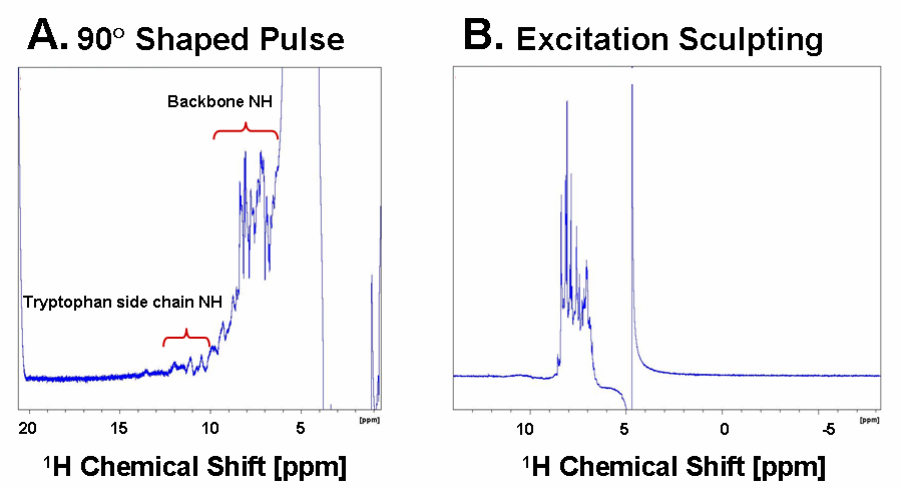

Figure 6.2: One dimensional NMR spectra of unlabelled rhodopsin in octyl glucoside micelles. (A) Selective excitation of the NH region using 90 degree pulse. (B) Selective excitation of the NH proton peaks with sculpting using hyperbolic secant shaped pulse (Hwang and Shaka 1995; Stott 1995).

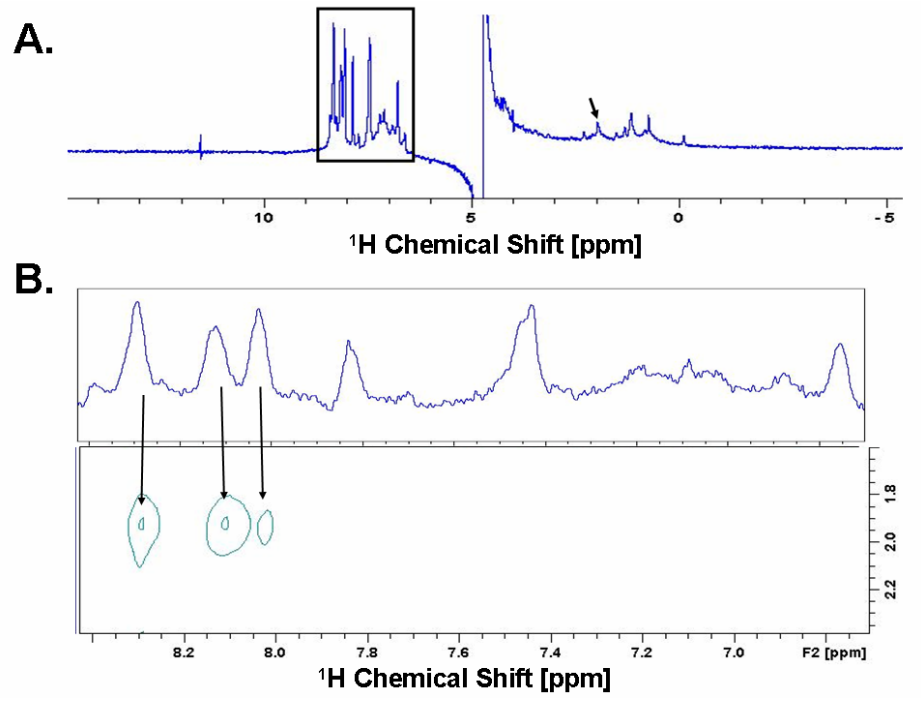

Figure 6.3: One- and two-dimensional ^{1}H-^{1}H selective excitation NOE spectra of rhodopsin. (A)**.** One dimensional solution selective NOE ^{1}H NMR spectrum of rhodopsin in 0.146% OG recorded at 600MHz, 25^{o}C. (B**).** Two dimensional solution ^{1}H - ^{1}H NOE spectrum of rhodopsin in 1% OG. The NOE's from the detergent peak (marked with an arrow in Figure 6.3A) to the ^{1}H peaks from Rhodopsin (represented in box in Figure 6.3A) are shown.

6.3. APPLICATION OF ^{19}F NMR SPECTROSCOPY TO SCREEN LIGANDS

As selective excitation overcomes the dynamic range problems posed by the detergent background, the following considerations still makes it difficult to use ^{1}H NMR based approaches for ligand screening. Often, It is not possible to clearly differentitiate the

multiple site binding modes of a ligand to a protein, i.e., if a ligand binds at more than one site on a protein with different affinities. In particular in the case of ligand-observe based screening, the ligands that have overlapping signals with protein peaks as well as that give rise signals upfield of water signal, the selective excitation approach cannot be successfully applied. ^{19}F NMR spectroscopy can be a viable alternative for one-dimensional NMR spectroscopic measurements, providing complementary results. Because there is no background from ^{19}F nuclei in either biomolecules such as neither proteins nor detergents used to dissolve membrane proteins, the applicability range of ^{19}F NMR to study ligand binding in soluble and in membrane proteins is identical.

^{19}F NMR studies of protein structure, dynamics and ligand binding offers several advantages over other NMR-spectroscopic approaches as a result of the unique chemistry of the ^{19}F atom. ^{19}F has 100% natural abundance and its sensitivity to NMR detection is 83% that of ^{1}H. The presence of nine electrons surrounding the ^{19}F nucleus makes it very sensitive to minor changes in its environment, including both Van-der-Waals and electrostatic interactions, which is reflected in its wide range of chemical shifts. This characteristic increases the probability of obtaining well-resolved peaks of fluorine atoms in different environments. Another major advantage of ^{19}F NMR over other conventional NMR techniques is the appearance of its NMR signals in the absence of any background signals, including membrane mimetic environments and even entire cells. These unique properties of the ^{19}F nucleus suggest that ^{19}F NMR spectroscopy could provide a highly-desirable alternative to high-throughput screening by conventional NMR spectroscopic techniques, in cases where the latter methods are not applicable, such as for membrane proteins or for in-cell studies. Both, approaches involving changes in line shape and/or

chemical shift of a free fluorinated ligand on binding to a protein (ligand observed method) or that of a fluorinated residue in a protein on ligand binding (protein observed method) can be employed in the context of high throughput screening. Here we investigated the application of ^{19}F NMR spectroscopy to screen for fluorine labeled ligands both *in vivo* and *in vitro.*

6.3.1. Screening for ^{19}F labeled Ligands for Membrane Proteins *in vitro*

The fluorine atom of a free ligand on binding to a protein is expected to show restricted motion compared to its free state and hence give a broader line shape. The chemical shift change may be either upfield or downfield depending on the nature of the change of interactions of the fluorine atom with its environment. A downfield shift indicates a more hydrophobic environment or a greater extent of Van-der-Waals interaction of the fluorine atom. Changes in electrostatic interactions of the fluorine atom with its environment, such as a ring current effect, can influence either a downfield or an upfield shift (Gerig 1989).

The ease of obtaining information from ligand binding studies by ^{19}F NMR has extended its applicability to high-throughput screening (HTS) of chemical libraries that is a routine procedure in the field of drug discovery. The broad chemical shift dispersion of the fluorine nucleus allows for identifying 'hits' in a screen with less chances of encountering the problem of spectral overlap from different chemical compounds. The simplicity of the ^{19}F spectra, unlike ^{1}H spectra, decreases the time for deconvoluting the spectra when a large mixture of chemicals is being screened. Changes in chemical shift values and/or line widths of the free fluorinated ligand upon addition of a protein will

indicate whether a compound is binding to the protein or not. Thus monitoring free ligand peaks allows the use of very low protein concentrations, in the tens of μM range. Information on binding constants and stoichiometry of binding from ligand titration experiments can be further used to rank order ligands in a screen. Such information was obtained while screening a library of compounds for chaperones PapD and FimC, involved in the assembly of pili on *E. coli*, and are essential targets for the development of antibacterial agents (Tengel, Fex et al. 2004). ^{19}F NMR studies can also be used to provide further information on binding sites to optimize the lead compound by characterizing the structural changes induced by their binding. This is done by using proteins substituted at different positions by fluorinated amino acids and monitoring their chemical shift changes on ligand binding. This is much less expensive and easier compared to ^{1}H NMR where the spectra are complicated and further deconvolution requires expensive isotope labeled samples of high concentration.

As a proof-of-concept for extending these approaches to membrane proteins, we screened binding of ^{19}F-labeled small molecules to rhodopsin by mixing the ligands with the receptor. Ligands were in a mixture of 10 compounds at 50μM concentration each. The receptor concentration was 0.2mM in detergent solution (5-fold excess). For a ligand with micromolar affinity, these conditions ensure that the majority of the ligand will be bound and therefore a maximal peak shift is expected for a hit. Excellent signal to noise ratio can be achieved with 7 min acquisition time (Figure 6.4). One-dimensional ^{19}F NMR spectra were recorded in the absence (Figure 6.4, blue trace) and presence of rhodopsin (Figure 6.4, red trace) in the dark. Due to the large chemical dispersion of 19F nuclei, even the ligands with minor modifications gave rise to distinct peaks (compare

compounds at positions 3, 4, and 8). The comparison of chemical shifts upon addition of protein indicated changes for a subset of ligands. In particular, an upfield shift in the signals for ligands corresponding to positions 1, 3, 5, and 8 were observed. The strongest effect was observed for signal at position 8. These subsets of ligands from the first screen can be further analyzed at different concentrations to understand the kinetics and strength of ligand binding effects.

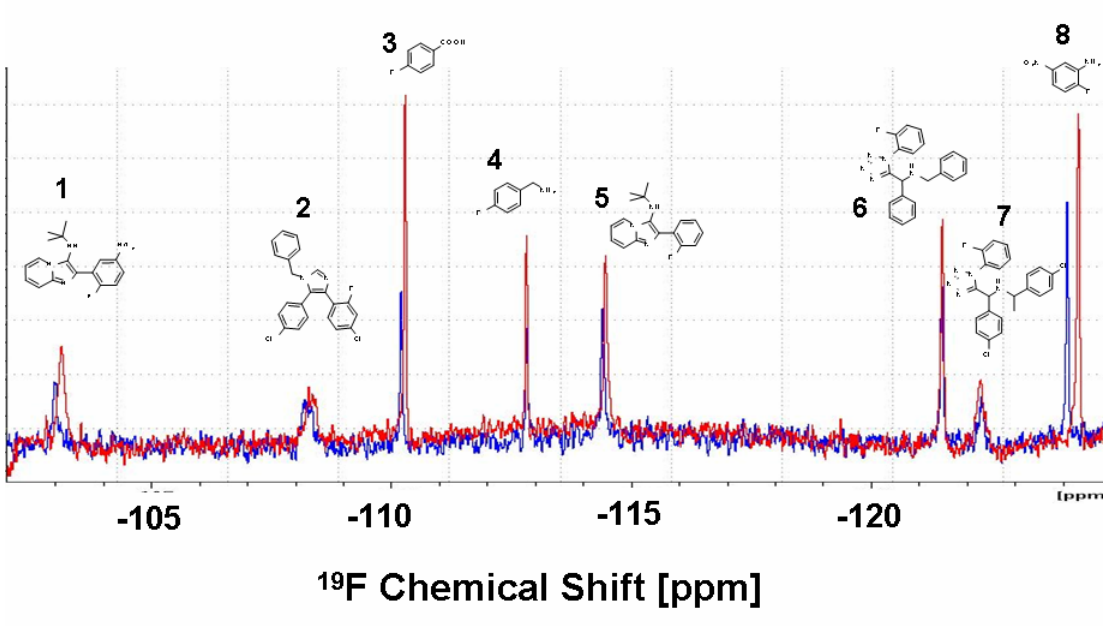

Figure 6.4: Example for a screening of a ^{19}F-labeled compound library against rhodopsin. NMR signals from eight compounds are visible in the particular range shown.

6.3.2. Screening for ^{19}F labeled Ligands for Proteins Expressed in Cells

NMR techniques developed to date for understanding ligand binding interactions, including the ^{19}F-NMR based approach described above, involve looking at purified

proteins in solution. When studying ligand-binding interactions with the goal of developing new drugs one has to consider that ligand binding *in vivo* is also influenced by drug uptake and crowdedness in the cells. One often reported observation in cancer drug discovery is that the measured cell based activities differ from the protein based screening activity. A potential explanation can be that a particular compound is a substrate for an efflux pump which are very active in cancer cells. Another reason could be that a particular compound cannot pass the cell membrane efficiently. In this section, we extended the studies described for purified proteins to proteins inside cells. As a proof of principle, we studied a soluble protein pair, Hdm2-p53. This interaction is important for cancer progression and its inhibition is desirable. A library containing fluorine labels to disrupt this interaction were given to us by collaborator Dr. Alex Doemling. To test for the uptake/efflux of representative fluorine labeled compounds targeting the Hdm2-p53 interface, we studied HCT-116 cells expressing $p53^{+/+}$. The representative compounds investigated are shown in Figure 6.5. Studies by the group of Dr. Alex Doemling identified that BEB-124 exhibits 40 folder affinity in comparison to BEB-125 towards Hdm2 isolated and purified from cells. However, the cell based activity assay for BEB-124 was found to be inefficient in inducing apoptosis. To investigate if the two compounds were able to enter the cells, the uptake of these compounds by HCT-116 cell expressing p53+/+ and Hdm2 was measured by one dimensional ^{19}F NMR spectroscopy. The two compounds BEB-124 and BEB-125 were titrated into HCT-116 cancer cells suspended in DMEM media in the NMR tube. One dimensional ^{19}F NMR spectra recorded of the compounds alone in the absence of cells gave rise to single sharp peaks with chemical shifts at –114.9, and –110.0 ppm (in reference to TFE at -75.6 ppm) for

BEB-124 and BEB-125 respectively. To understand if these compounds can enter the HCT-116 cancer cells expressing Hdm2, we did a series of titrations of BEB-124 and BEB-125 ranging from 0.1 - 2.8mM. Addition of 100μM BEB-124 into the HCT-116 cells gave rise to a single peak at -114.9 ppm, indicating no changes as compared to the control. The titration of BEB-124 (0.1, 0.2, 0.3, 0.4 and 1mM) compound indicated no changes in the spectrum except for an increase in the peak at -114.9 ppm. However, upon addition of 100μM BEB-125 we were not able to observe any signal in the NMR spectrum except for the TFE peak. Further titration of 0.2mM BEB-125 gave rise to a chemical signal at –108.2 ppm, downfiled shifted by 1.8 ppm as compared to free ligand peak at -110.0 ppm. This peak was broader as compared to free peak indicating that it might be experiencing a different chemical environment and viscosity as compared to free form. An overlay of NMR spectra of 0.1, 0.3, 0.7, 1.6 and 2.8mM BEB-125 into the HCT-116 cells is shown in Figure 6.6C. Initial titrations (until 300μM) of the BEB-125 showed an increase in the peak at -108.2 ppm and the peak shifted downfield by 0.1 ppm. At higher concentrations of BEB-125, a peak at –110.0 ppm started appearing corresponding to the free peak. Comparison of the various titrations did not show any changes in chemical shift corresponding to the free peak but a total shift of 0.6 ppm was observed for the peak at -108.2 (Figure 6.6B). These results suggest that BEB-125 is taken up very rapidly into the cell up to very high concentrations. BEB-124 despite its higher affinity for Hdm2 does not reach a high intracellular concentration and cannot effectively induce apoptosis and cell death in these cells.

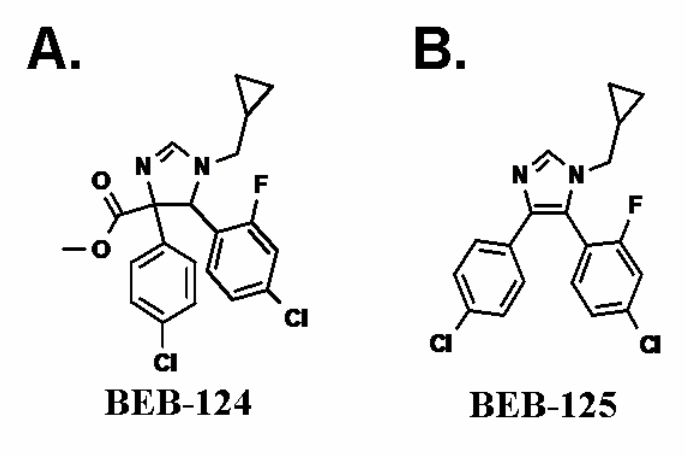

Figure 6.5: Chemical structures of the ^{19}F labeled compounds designed to target Hdm2.

To test if the binding of BEB-125 is specific to HCT-cells and to verify that the peak observed at -108.2 ppm is not due to unspecific binding of the compound to the cell membrane, we measured the interaction of these compounds with *E. coli* cells as a control. Shown in Figure 6.6B and 6.6D are the 1D NMR spectra representing the titration of BEB-124 (0.1, 0.3 and 1mM) and BEB-125 (0.1, 0.3 0.6 and 1.5mM) added to *E. coli* cells suspended in LB media. Addition of 0.1mM BEB-124 and BEB-125 immediately gave rise to peaks at -114.7 and -110.0 ppm (in reference to TFE at -75.6 ppm). The peak at -114.7 ppm corresponding to BEB-124 was shifted by 0.1 ppm as compared to ligand alone in LB at -114.8 ppm. Further, no change in peak corresponding to BEB-125 was observed. The BEB-124 interaction with HCT-116 and *E. coli* cells was similar (Figure 6.6A and 6.6B). In contrast, the results of the BEB-125 titration to *E. coli* cells were different as compared to HCT-116 cells and showed no differences compared

to ligand alone controls. These results indicate that BEB-125 specifically interacts with HCT-116 cells expressing Hdm2 and p53.

Table 6.1: Comparison of the activity of compounds *in vivo* and *in vitro*

Compound Name	Activity *invitro*	Active in cells
BEB-124	1μM	No
BEB-125	60μM	Yes

To investigate a possible mechanism for the results obtained, and further test if the broad peak observed around -108.1 to -108.7 ppm is due to the presence of ligand inside or outside of the cellular compartment, we measured the interaction of BEB-125 with HCT-116 cells in the absence and presence of 0.1mM verapamil, an efflux inhibitor. An overlay of addition of the compound BEB-124 to HCT-116 cells is shown in Figure 6.7A. Comparison of 1mM BEB-124 added to HCT-116 treated with (Figure 6.7A, red trace) and without (Figure 6.7A, black trace) verapamil showed no changes. In contrast, upon addition of 2.8mM BEB-125 to cancer cells treated with verapamil we observed an increase in the intensity of bound peak and a decrease in the free peak intensity as compared to untreated cells (Figure 6.7B). Additionally, the bound peak was shifted upfield by 0.1 ppm as compared to untreated cells. Addition of 100μM verapamil to a control of ligand alone did not have any effects on the spectrum nor on the peaks. These results suggests that by blocking the efflux receptors of cancer cells using verapamil, the

ligand that is present inside the cells is not shuttled out as in untreated cells. Note, however, that the free peak was only decreased in intensity and did not disappear completely. This might be because not all efflux receptors are completely blocked at the concentration of 100μM verapamil used in this experiment. These results indicate that *in vivo* ^{19}F NMR studies can be used to study complex interactions of ligands with their target cells in a realistic environment.

6.4. CONCLUSION

The prospects of NMR based screening of small molecule ligands binding to membrane proteins are very good: selective excitation ^{1}H and ^{19}F NMR spectroscopy can overcome many of the challenges associated with solution NMR studies of membrane proteins in detergent micelles. Fluorine is an extremely versatile element with many advantages in the drug discovery pipeline. At the screening stage, the ^{19}F nucleus provides a sensitive ligand binding as well as conformational probe without background signals. At the more biological level, the cellular uptake and fate of ^{19}F tagged compounds can be detected in a time- and space-resolved as well as otherwise label-free manner. In conclusion, it was shown that screening of ^{19}F libraries could be fast and cost-efficient and the discovery of novel small molecular weight ligands by NMR may become possible even for difficult membrane bound targets such as GPCRs and ion channels.

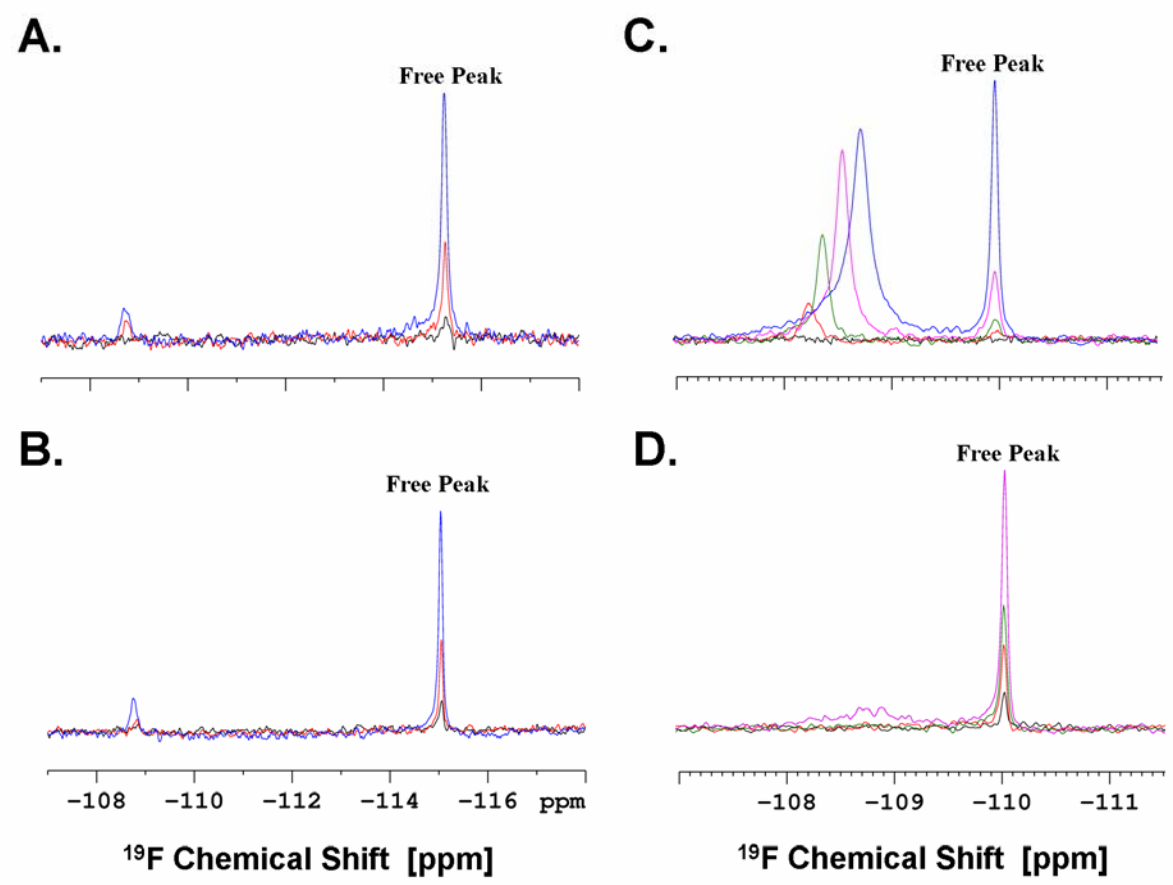

Figure 6.6: Screening for ^{19}F labelled ligands in *E. coli* and HCT-116 cancer cells. An overlay of one dimensional ^{19}F NMR spectra of 100µM (black), 300µM (red) and 1mM (blue) BEB-124 in (A) HCT-116 (B) *E. coli* cells and 100µM (black), 300µM (red), 900µM (green), 1.5mM (magenta) and 2.8mM (blue) BEB-125 in (C) HCT-116 cells and (D) *E. coli* cells.

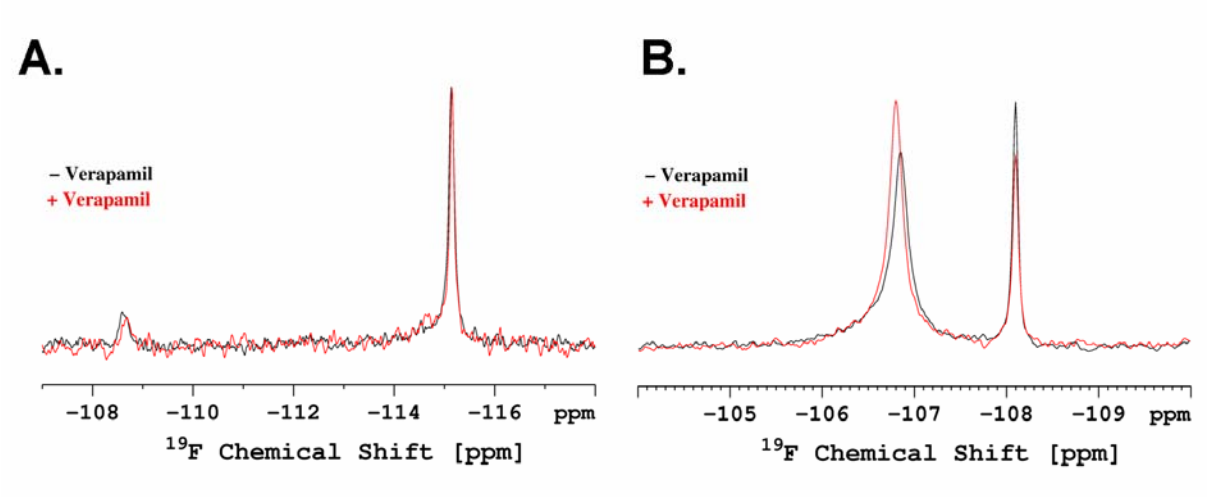

Figure 6.7: Monitoring the localisation of the ^{19}F labelled ligands inside vs outside the cells using NMR. One dimensional ^{19}F NMR spectra of (A) 1mM BEB-124 and (B) 2.8mM BEB-125 added to the cells treated without (black) and with (red) 100µM verapamil.

SUMMARY

This thesis investigated allosteric modulation of GPCRs. The emphasis was on allosteric modulation of the prototypic class A GPCR, rhodopsin. Using our understanding of structure and dynamics in rhodopsin, we were also able to explain allosteric modulation in other GPCRs. We developed a general framework in which we propose that GPCRs contain three potential binding sites, at the CP, TM and EC domains, and that depending on which of the ligand binding sites are occupied by the endogenous ligand, the other two sites can serve as allosteric sites.

Analysis of the interaction of C3G and Ce6 ligands with rhodopsin described in Chapter 3 demonstrated the existence of a novel CP ligand binding domain in rhodopsin. The interaction of these accessory ligands at the CP region exerted differential effects on rhodopsin structure and dynamics. While one ligand (Ce6) strongly inhibited G protein activation; the other (C3G) only slightly did so. While the binding of C3G resulted in the destabilization of retinal protein interactions explaining its functional effect of enhancing rhodopsin regeneration rates, the other (Ce6) stabilized rhodopsin secondary structure. Both ligands have in common that they prove the existence of a structural coupling between the CP domain and the EC and TM domains, allosterically modulating rhodopsin. Thus, information transfer not only occurs from the EC or TM domain to the CP domain, but also from the CP to the TM and EC domains, indicating bi-directional information flow in GPCRs. During the writing of this thesis, it was discovered that other

independent lines of evidences also support the presence of CP allosteric ligand binding pockets in muscarinic receptors (Espinoza-Fonseca and Trujillo-Ferrara 2005), chemokine receptors (Andrews, Jones et al. 2008) and rhodopsin (Taylor, Barda et al. 2008).

GPCR conformations differentiating active from inactive states are best understood for rhodopsin. We used this knowledge to explain allosteric modulation of mGluRs. Studies presented in Chapter 4 showed a preferential binding of positive and negative allosteric modulators to active and inactive states of receptors based on rhodopsin structures, respectively. This demonstrates the generality of the mechanisms of conformational flexibility for different GPCRs. Furthermore, while the endogenous ligand binding site in mGluRs is located in the EC domain, the allosteric ligand binding site in mGluRs was found to highly overlap with that of *11-cis* retinal pocket in rhodopsin, suggesting for the structural conservation of the ligand binding pocket in the TM domain across diverse GPCRs.

Finally, we also obtained preliminary evidence that rhodopsin contains an EC allosteric ligand binding pocket, supporting the idea that orthosteric ligand binding pockets in some GPCR can be allosteric binding pockets in others. Thus, rhodopsin would be a candidate receptor that shows the presence of all three pockets, in the CP, TM and EC domains. The effects of binding of chemokines, typical EC domain ligands endogenous for chemokine receptors, to rhodopsin are described in Chapter 5. In particular, chemokine ligand CXCL11 is predicted to bind at the EC domain involving similar sites on rhodopsin as compared to chemokine receptor, and binding modulates the ability of rhodopsin to activate the G protein. While chemokines activate chemokine

receptors, in the case of rhodopsin, the modulation is a negative one, and binding results in negative allosteric modulation, inhibiting G protein activation by rhodopsin.

Collectively, the studies presented in this dissertation demonstrate that rhodopsin, and GPCRs in general, can accommodate accessory ligands at any of the domains, TM domain near at the interface with EC side, EC domain and CP domains. However, different GPCR members will likely show a preference for one of the sites to accommodate the endogenous ligand. The studies performed clearly suggested that the TM domain plays a major in communicating the signals from one side to the other and thus might be conserved across different GPCRs. While a direct coupling between the TM and CP domain or the EC and CP domain mediated through TM domain was shown previously, the studies presented in this thesis consolidate the reciprocal nature of this structural coupling.

FUTURE RESEARCH DIRECTIONS

The evidence presented in this thesis for the existence of the novel cytoplasmic ligand binding domain in rhodopsin prompts for the immediate need to obtain crystal structures for the complexes between rhodopsin and Ce6 and C3G to confirm the location and mode of binding. This should include different activation states of the receptor, which is now feasible, given that several crystal structure representing such states have been successfully described in the literature. In addition to the structural details, other important questions that still remain to be investigated relate to the functional consequences of binding. The studies presented here only focused on the sensitization pathway (activation of the G protein), the effect of binding of Ce6 and other ligands in the CP domain on other signaling proteins involved in desensitization pathways will aid in better understanding the modulatory effects of these ligands on different pathways in visual signal transduction. Although our studies performed with Ce6 have shown that it has an inhibitory effect on signal sensitization in bovine rhodopsin, previous studies (Washington, Zhou et al. 2007) have proposed a signal enhancement mechanism in the presence of Ce6. The conclusions were derived at with very different approaches, and resolving this discrepancy is important for understanding the physiological relevance of this interaction, which has been proposed to enhance vision in deep-sea ocean fish. Thus, it is important to investigate if Ce6 has similar or different effects on G_t activation in deep-sea ocean fish-derived rhodopsin or rhodopsin from other related species. For

example, the recent dark state crystal structure of squid rhodopsin (Murakami and Kouyama 2008) resembles the G_t bound state, indicating that bovine signal transduction mechanisms could be different from more primitive rhodopsins. Since the signal transduction pathways in deep-sea ocean fish are not known and specimens are difficult to obtain, studies of squid rhodopsin are more feasible.

The observation that G_t activation by rhodopsin is inhibited in the presence of Ce6 may have practical significance. Many residues in the proposed Ce6 binding site are highly conserved in class A GPCRs. Thus, Ce6 may be a G protein inhibitor for other GPCRs also. As described in Chapter 1, a broad GPCR activity inhibitor could be useful in diseases where several GPCRs are involved in parallel pathways, such as cancer. Further experiments using other GPCR members, at least other class A GPCRs, are needed to demonstrate if Ce6 can be developed into a ligand that can target multiple GPCRs simultaneously. This would also be a useful tool to study generality of the principles discovered in this thesis for the GPCR family in general.

Also related to generality of the findings presented in this thesis for other GPCRs is the possibility to extend the studies presented in Chapter 4 on using rhodopsin conformations as templates to predicting positive versus negative allosteric modulation of mGluRs, to predict such functional outcomes for other GPCRs. Being able to predict *in silico* the nature of a given ligand, i.e. whether it will have an enhancing or suppressing effect on the receptor activation would be highly beneficial in designing new drugs targeted at GPCRs. Until recently, the only three dimensional information for any GPCR was that of rhodopsin, but over the past one and half year, the X-ray crystal structures of three other members of class A GPCRs along with the ligand free state of rhodopsin,

opsin, were published (Cherezov, Rosenbaum et al. 2007; Rasmussen, Choi et al. 2007; Jaakola, Griffith et al. 2008; Park, Scheerer et al. 2008; Scheerer, Park et al. 2008; Warne, Serrano-Vega et al. 2008). Although these receptors exhibit very similar overall structural architecture, the EC and CP loops exhibited striking changes in structure. In particular, EC loop 2 was found to be in the A_2A, β_1 and β_2 Adrenergic receptors (Cherezov, Rosenbaum et al. 2007; Rasmussen, Choi et al. 2007; Jaakola, Griffith et al. 2008; Warne, Serrano-Vega et al. 2008) in a different secondary structure conformation as opposed to rhodopsin. Generating homology models of GPCR members based on these new receptor structures will aid in generating models that may be more diverse as opposed to rhodopsin alone, a receptor that follows a two state model and binds to a ligand covalently. Since we showed in chapter 4 a preferential binding of ligands to the active and inactive conformations of mGluRs, similar studies of receptors with the different homology models may lead to more accuracy in the predictions. Thus, we propose that the studies presented in chapter 4 can be extended to other members of GPCRs and may lead to the development of a ligand classifier.

In addition to binary classifications positive versus negative allostersic modulation, the detailed comparison between binding pockets can also be used to derive new hypotheses on ligand structures and effects. Our preliminary studies indicate that the mGluR5 ligand 3,3`-DFB interacts with rhodopsin probably at the same site as *11-cis* retinal. However, it is not clear how similar or dissimilar the 3,3`-DFB bound structure is compared to rhodopsin *11-cis* bound state. This, along with the studies aimed at investigating the effects of 3,3`-DFB stabilized rhodopsin structure on signaling proteins will lead to understanding of as how different or similar is the TM domain between the

different GPCR class members. Such studies may shed light on the structural conservation of GPCRs, despite their sequence variability and further may lead to the understanding of the evolution of the specificity and diversity of GPCRs to different ligands.

Finally, the studies on the interaction between the chemokine, CXCL11, and rhodopsin and the comparison to the corresponding interaction with CXCR3 suggests that EC loop 2 plays a major role in binding to the chemokine ligand in both cases. Since the recent crystal structures of class A GPCRs showed variability in the structure of EC loop 2 in comparison to rhodopsin, research focusing on deciphering the secondary structure of EC loop 2 in CXCR3 would be beneficial to understand the specificity in binding of CXCL11 to chemokine receptors as compared to rhodopsin.

BIOGRAPHICAL NOTE

Naveena Yanamala was born on October 25th 1979 in Kadapa, India, where she spent all her childhood until begin of her bachelor's degree studies in computer applications at S. V. University, India, where she graduated in 2001. She received the "Rastrapathi Guide Award" from the President of India in New Delhi in 1994. Prior to joining the University of Pittsburgh, she received a Master's Degree in Information Technology with a specialization in Bioinformatics from the International Institute of Information Technology, Hyderabad in India. She was also a research scholar at the School of Computer Science at Carnegie Mellon University with Prof. Raj Reddy. Since May 2006, she has been a graduate student with Prof. Judith Klein-Seetharaman at the University of Pittsburgh, Pittsburgh, USA.

BIBLIOGRAPHY

Acharya S, Karnik SS (1996) Modulation of GDP release from transducin by the conserved Glu134-Arg135 sequence in rhodopsin. *The Journal of biological chemistry* **271:** 25406-25411

Acher FC, Bertrand HO (2005) Amino acid recognition by Venus flytrap domains is encoded in an 8-residue motif. *Biopolymers* **80:** 357-366

Albert AD, Boesze-Battaglia K, Paw Z, Watts A, Epand RM (1996) Effect of cholesterol on rhodopsin stability in disk membranes. *Biochimica et biophysica acta* **1297:** 77-82

Albert AD, Young JE, Yeagle PL (1996) Rhodopsin-cholesterol interactions in bovine rod outer segment disk membranes. *Biochimica et biophysica acta* **1285:** 47-55

Anderson JJ, Rao SP, Rowe B, Giracello DR, Holtz G, Chapman DF, Tehrani L, Bradbury MJ, Cosford ND, Varney MA (2002) [3H]Methoxymethyl-3-[(2-methyl-1,3-thiazol-4-yl)ethynyl]pyridine binding to metabotropic glutamate receptor subtype 5 in rodent brain: in vitro and in vivo characterization. *J Pharmacol Exp Ther* **303:** 1044-1051

Andrews G, Jones C, Wreggett KA (2008) An intracellular allosteric site for a specific class of antagonists of the CC chemokine G protein-coupled receptors CCR4 and CCR5. *Molecular pharmacology* **73:** 855-867

Anzini M, Canullo L, Braile C, Cappelli A, Gallelli A, Vomero S, Menziani MC, De Benedetti PG, Rizzo M, Collina S, Azzolina O, Sbacchi M, Ghelardini C, Galeotti N (2003) Synthesis, biological evaluation, and receptor docking simulations of 2-[(acylamino)ethyl]-1,4-benzodiazepines as kappa-opioid receptor agonists endowed with antinociceptive and antiamnesic activity. *Journal of medicinal chemistry* **46:** 3853-3864

Archer E, Maigret B, Escrieut C, Pradayrol L, Fourmy D (2003) Rhodopsin crystal: new template yielding realistic models of G-protein-coupled receptors? *Trends Pharmacol Sci* **24:** 36-40

Arimoto R, Kisselev OG, Makara GM, Marshall GR (2001) Rhodopsin-transducin interface: studies with conformationally constrained peptides. *Biophysical journal* **81:** 3285-3293

Armstrong N, Gouaux E (2000) Mechanisms for activation and antagonism of an AMPA-sensitive glutamate receptor: crystal structures of the GluR2 ligand binding core. *Neuron* **28:** 165-181

Armstrong N, Sun Y, Chen GQ, Gouaux E (1998) Structure of a glutamate-receptor ligand-binding core in complex with kainate. *Nature* **395:** 913-917

Arnis S, Fahmy K, Hofmann KP, Sakmar TP (1994) A conserved carboxylic acid group mediates light-dependent proton uptake and signaling by rhodopsin. *The Journal of biological chemistry* **269:** 23879-23881

Baehr W, Morita EA, Swanson RJ, Applebury ML (1982) Characterization of bovine rod outer segment G-protein. *The Journal of biological chemistry* **257:** 6452-6460

Baldwin JM, Schertler GF, Unger VM (1997) An alpha-carbon template for the transmembrane helices in the rhodopsin family of G-protein-coupled receptors. *Journal of molecular biology* **272:** 144-164

Ballesteros JA, Jensen AD, Liapakis G, Rasmussen SG, Shi L, Gether U, Javitch JA (2001) Activation of the beta 2-adrenergic receptor involves disruption of an ionic lock between the cytoplasmic ends of transmembrane segments 3 and 6. *The Journal of biological chemistry* **276:** 29171-29177

Becker OM, Shacham S, Marantz Y, Noiman S (2003) Modeling the 3D structure of GPCRs: advances and application to drug discovery. *Curr Opin Drug Discov Devel* **6:** 353-361

Bennett MP, Mitchell DC (2008) Regulation of membrane proteins by dietary lipids: effects of cholesterol and docosahexaenoic acid acyl chain-containing phospholipids on rhodopsin stability and function. *Biophysical journal* **95:** 1206-1216

Berkhout TA, Blaney FE, Bridges AM, Cooper DG, Forbes IT, Gribble AD, Groot PH, Hardy A, Ife RJ, Kaur R, Moores KE, Shillito H, Willetts J, Witherington J (2003) CCR2: characterization of the antagonist binding site from a combined receptor modeling/mutagenesis approach. *Journal of medicinal chemistry* **46:** 4070-4086

Bhave G, Nadin BM, Brasier DJ, Glauner KS, Shah RD, Heinemann SF, Karim F, Gereau RWt (2003) Membrane topology of a metabotropic glutamate receptor. *The Journal of biological chemistry* **278:** 30294-30301

Bhola NE, Grandis JR (2008) Crosstalk between G-protein-coupled receptors and epidermal growth factor receptor in cancer. *Front Biosci* **13:** 1857-1865

Birdsall B, King RW, Wheeler MR, Lewis CA, Jr., Goode SR, Dunlap RB, Roberts GC (1983) Correction for light absorption in fluorescence studies of protein-ligand interactions. *Analytical Biochemistry* **132:** 353-361

Boesze-Battaglia K, Hennessey T, Albert AD (1989) Cholesterol heterogeneity in bovine rod outer segment disk membranes. *The Journal of biological chemistry* **264:** 8151-8155

Booth V, Clark-Lewis I, Sykes BD (2004) NMR structure of CXCR3 binding chemokine CXCL11 (ITAC). *Protein Sci* **13:** 2022-2028

Borhan B, Souto ML, Imai H, Shichida Y, Nakanishi K (2000) Movement of retinal along the visual transduction path. *Science (New York, NY* **288:** 2209-2212

Bouley R, Sun TX, Chenard M, McLaughlin M, McKee M, Lin HY, Brown D, Ausiello DA (2003) Functional role of the NPxxY motif in internalization of the type 2 vasopressin receptor in LLC-PK1 cells. *American journal of physiology* **285:** C750-762

Brouillard R, Dubois J-E (1977) Mechanism of the structural transformations of anthocyanins in acidic media. *J Am Chem Soc* **99:** 1359-1364

Brown MF (1994) Modulation of rhodopsin function by properties of the membrane bilayer. *Chemistry and physics of lipids* **73:** 159-180

Bubis J (1998) Effect of detergents and lipids on transducin photoactivation by rhodopsin. *Biological research* **31:** 59-71

Camacho CJ, Zhang C (2005) FastContact: rapid estimate of contact and binding free energies. *Bioinformatics* **21:** 2534-2536

Campanella GS, Lee EM, Sun J, Luster AD (2003) CXCR3 and heparin binding sites of the chemokine IP-10 (CXCL10). *The Journal of biological chemistry* **278:** 17066-17074

Carr HY, Purcell EM (1954) Effects of diffusion on free precession in uclear magnetic resonance experiments. *Phys Rev* **94:** 630-638

Cartier L, Hartley O, Dubois-Dauphin M, Krause KH (2005) Chemokine receptors in the central nervous system: role in brain inflammation and neurodegenerative diseases. *Brain Res Brain Res Rev* **48:** 16-42

Cascieri MA, Koch GE, Ber E, Sadowski SJ, Louizides D, de Laszlo SE, Hacker C, Hagmann WK, MacCoss M, Chicchi GG, Vicario PP (1999) Characterization of a novel, non-peptidyl antagonist of the human glucagon receptor. *The Journal of biological chemistry* **274:** 8694-8697

Cha K, Reeves PJ, Khorana HG (2000) Structure and function in rhodopsin: destabilization of rhodopsin by the binding of an antibody at the N-terminal segment provides support for involvement of the latter in an intradiscal tertiary structure. *Proceedings of the National Academy of Sciences of the United States of America* **97:** 3016-3021

Chabre M, Bigay J, Bruckert F, Bornancin F, Deterre P, Pfister C, Vuong TM (1988) Visual signal transduction: the cycle of transducin shuttling between rhodopsin and cGMP phosphodiesterase. *Cold Spring Harbor Symposia on Quantitative Biology* **53 Pt 1:** 313-324

Chalmers DT, Behan DP (2002) The use of constitutively active GPCRs in drug discovery and functional genomics. *Nat Rev Drug Discov* **1:** 599-608

Chambers JJ, Nichols DE (2002) A homology-based model of the human 5-HT2A receptor derived from an in silico activated G-protein coupled receptor. *J Comput Aided Mol Des* **16:** 511-520

Cherezov V, Rosenbaum DM, Hanson MA, Rasmussen SG, Thian FS, Kobilka TS, Choi HJ, Kuhn P, Weis WI, Kobilka BK, Stevens RC (2007) High-resolution crystal structure of an engineered human beta2-adrenergic G protein-coupled receptor. *Science (New York, NY* **318:** 1258-1265

Christopher J R Illingworth PDS, Kevin E. B. Parkes, Christopher R. Snell, Matthew P Campbell and Christopher A Reynolds (2008) High-connectivity ligand binding sites. . *(Submitted)*

Christopoulos A, Kenakin T (2002) G protein-coupled receptor allosterism and complexing. *Pharmacological reviews* **54:** 323-374

Christopoulos A, Lanzafame A, Mitchelson F (1998) Allosteric interactions at muscarinic cholinoceptors. *Clinical and experimental pharmacology & physiology* **25:** 185-194

Christopoulos A, May LT, Avlani VA, Sexton PM (2004) G-protein-coupled receptor allosterism: the promise and the problem(s). *Biochemical Society transactions* **32:** 873-877

Colvin RA, Campanella GS, Manice LA, Luster AD (2006) CXCR3 requires tyrosine sulfation for ligand binding and a second extracellular loop arginine residue for ligand-induced chemotaxis. *Molecular and cellular biology* **26:** 5838-5849

Comeau SR, Gatchell DW, Vajda S, Camacho CJ (2004) ClusPro: an automated docking and discrimination method for the prediction of protein complexes. *Bioinformatics* **20:** 45-50

Conn PJ, Christopoulos A, Lindsley CW (2009) Allosteric modulators of GPCRs: a novel approach for the treatment of CNS disorders. *Nat Rev Drug Discov* **8:** 41-54

Conn PJ, Pin J-P. (1997) PHARMACOLOGY AND FUNCTIONS OF METABOTROPIC GLUTAMATE RECEPTORS. Vol. 37, pp. 205-237.

Crane IJ, Liversidge J (2008) Mechanisms of leukocyte migration across the blood-retina barrier. *Seminars in immunopathology* **30:** 165-177

Crane IJ, McKillop-Smith S, Wallace CA, Lamont GR, Forrester JV (2001) Expression of the chemokines MIP-1alpha, MCP-1, and RANTES in experimental autoimmune uveitis. *Investigative ophthalmology & visual science* **42:** 1547-1552

Davidson FF, Loewen PC, Khorana HG (1994) Structure and function in rhodopsin: replacement by alanine of cysteine residues 110 and 187, components of a conserved disulfide bond in rhodopsin, affects the light-activated metarhodopsin II state. *Proceedings of the National Academy of Sciences of the United States of America* **91:** 4029-4033

Davis IW, Murray LW, Richardson JS, Richardson DC (2004) MOLPROBITY: structure validation and all-atom contact analysis for nucleic acids and their complexes. *Nucleic acids research* **32:** W615-619

Davoust J, Bienvenue A, Fellmann P, Devaux PF (1980) Boundary lipids and protein mobility in rhodopsin-phosphatidylcholine vesicles. Effect of lipid phase transitions. *Biochimica et biophysica acta* **596:** 28-42

De Grip WJ (1982) Thermal stability of rhodopsin and opsin in some novel detergents. *Methods Enzymol* **81:** 256-265

Deraet M, Rihakova L, Boucard A, Perodin J, Sauve S, Mathieu AP, Guillemette G, Leduc R, Lavigne P, Escher E (2002) Angiotensin II is bound to both receptors AT1 and AT2, parallel to the transmembrane domains and in an extended form. *Can J Physiol Pharmacol* **80:** 418-425

Dorsam RT, Gutkind JS (2007) G-protein-coupled receptors and cancer. *Nature reviews* **7:** 79-94

Douglas RH, Partridge JC, Dulai KS, Hunt DM, Mullineaux CW, Hynninen PH (1999) Enhanced retinal longwave sensitivity using a chlorophyll-derived photosensitiser in Malacosteus niger, a deep-sea dragon fish with far red bioluminescence. *Vision research* **39:** 2817-2832

Dragic T, Trkola A, Thompson DA, Cormier EG, Kajumo FA, Maxwell E, Lin SW, Ying W, Smith SO, Sakmar TP, Moore JP (2000) A binding pocket for a small molecule inhibitor of HIV-1 entry within the transmembrane helices of CCR5. *Proceedings of the National Academy of Sciences of the United States of America* **97:** 5639-5644

Dryja TP, Berson EL, Rao VR, Oprian DD (1993) Heterozygous missense mutation in the rhodopsin gene as a cause of congenital stationary night blindness. *Nature genetics* **4:** 280-283

Dryja TP, Finn JT, Peng YW, McGee TL, Berson EL, Yau KW (1995) Mutations in the gene encoding the alpha subunit of the rod cGMP-gated channel in autosomal recessive retinitis pigmentosa. *Proceedings of the National Academy of Sciences of the United States of America* **92:** 10177-10181

Dryja TP, McGee TL, Berson EL, Fishman GA, Sandberg MA, Alexander KR, Derlacki DJ, Rajagopalan AS (2005) Night blindness and abnormal cone electroretinogram ON responses in patients with mutations in the GRM6 gene encoding mGluR6. *Proceedings of the National Academy of Sciences of the United States of America* **102:** 4884-4889

Eilers M, Reeves PJ, Ying W, Khorana HG, Smith SO (1999) Magic angle spinning NMR of the protonated retinylidene Schiff base nitrogen in rhodopsin: expression of 15N-lysine- and 13C-glycine-labeled opsin in a stable cell line. *Proceedings of the National Academy of Sciences of the United States of America* **96:** 487-492

Espinoza-Fonseca LM, Trujillo-Ferrara JG (2005) Identification of multiple allosteric sites on the M1 muscarinic acetylcholine receptor. *FEBS letters* **579:** 6726-6732

Fahmy K, Sakmar TP (1993) Regulation of the rhodopsin-transducin interaction by a highly conserved carboxylic acid group. *Biochemistry* **32:** 7229-7236

Farrens DL, Altenbach C, Yang K, Hubbell WL, Khorana HG (1996) Requirement of rigid-body motion of transmembrane helices for light activation of rhodopsin. *Science (New York, NY* **274:** 768-770

Farrens DL, Khorana HG (1995) Structure and function in rhodopsin. Measurement of the rate of metarhodopsin II decay by fluorescence spectroscopy. *The Journal of biological chemistry* **270:** 5073-5076

Fielding L, Rutherford S, Fletcher D (2005) Determination of protein-ligand binding affinity by NMR: observations from serum albumin model systems. *Magnetic Resonance in Chemistry* **43:** 463-470

Filipek S, Krzysko KA, Fotiadis D, Liang Y, Saperstein DA, Engel A, Palczewski K (2004) A concept for G protein activation by G protein-coupled receptor dimers: the transducin/rhodopsin interface. *Photochem Photobiol Sci* **3:** 628-638

Filipek S, Teller DC, Palczewski K, Stenkamp R (2003) The crystallographic model of rhodopsin and its use in studies of other G protein-coupled receptors. *Annual review of biophysics and biomolecular structure* **32:** 375-397

Findlay JB, Pappin DJ (1986) The opsin family of proteins. *The Biochemical journal* **238:** 625-642

Finn RD, Tate J, Mistry J, Coggill PC, Sammut SJ, Hotz HR, Ceric G, Forslund K, Eddy SR, Sonnhammer EL, Bateman A (2008) The Pfam protein families database. *Nucleic acids research* **36:** D281-288

Fiser A, Sali A (2003) Modeller: generation and refinement of homology-based protein structure models. *Methods Enzymol* **374:** 461-491

Floriano WB, Hall S, Vaidehi N, Kim U, Drayna D, Goddard WA, 3rd (2006) Modeling the human PTC bitter-taste receptor interactions with bitter tastants. *J Mol Model* **12:** 931-941

Floriano WB, Vaidehi N, Goddard WA, 3rd (2004) Making sense of olfaction through predictions of the 3-D structure and function of olfactory receptors. *Chem Senses* **29:** 269-290

Freddolino PL, Kalani MY, Vaidehi N, Floriano WB, Hall SE, Trabanino RJ, Kam VW, Goddard WA, 3rd (2004) Predicted 3D structure for the human beta 2 adrenergic receptor and its binding site for agonists and antagonists. *Proceedings of the National Academy of Sciences of the United States of America* **101:** 2736-2741

Fredriksson R, Lagerstrom MC, Lundin LG, Schioth HB (2003) The G-protein-coupled receptors in the human genome form five main families. Phylogenetic analysis, paralogon groups, and fingerprints. *Molecular pharmacology* **63:** 1256-1272

Freeman R, Hill HDW (1971) Fourier Transform Study of NMR Spin-Lattic Relaxation by "Progressive Saturation". *Journal of Chemical Physics* **54:** 3367-3377

Fritze O, Filipek S, Kuksa V, Palczewski K, Hofmann KP, Ernst OP (2003) Role of the conserved NPxxY(x)5,6F motif in the rhodopsin ground state and during activation. *Proceedings of the National Academy of Sciences of the United States of America* **100:** 2290-2295

Fung BK (1983) Characterization of transducin from bovine retinal rod outer segments. I. Separation and reconstitution of the subunits. *The Journal of biological chemistry* **258:** 10495-10502

Fung BK, Nash CR (1983) Characterization of transducin from bovine retinal rod outer segments. II. Evidence for distinct binding sites and conformational changes revealed by limited proteolysis with trypsin. *The Journal of biological chemistry* **258:** 10503-10510

Gao ZG, Chen A, Barak D, Kim SK, Muller CE, Jacobson KA (2002) Identification by site-directed mutagenesis of residues involved in ligand recognition and activation of the human A3 adenosine receptor. *The Journal of biological chemistry* **277:** 19056-19063

Garriga P, Liu X, Khorana HG (1996) Structure and function in rhodopsin: correct folding and misfolding in point mutants at and in proximity to the site of the retinitis pigmentosa mutation Leu-125-->Arg in the transmembrane helix C. *Proceedings of the National Academy of Sciences of the United States of America* **93:** 4560-4564

Gasparini F, Andres H, Flor PJ, Heinrich M, Inderbitzin W, Lingenhohl K, Muller H, Munk VC, Omilusik K, Stierlin C, Stoehr N, Vranesic I, Kuhn R (2002) [(3)H]-M-MPEP, a potent, subtype-selective radioligand for the metabotropic glutamate receptor subtype 5. *Bioorg Med Chem Lett* **12:** 407-409

Gerig JT (1989) Fluorine nuclear magnetic resonance of fluorinated ligands. *Methods Enzymol* **177:** 3-23

Gibson NJ, Brown MF (1991) Membrane lipid influences on the energetics of the metarhodopsin I and metarhodopsin II conformational states of rhodopsin probed by flash photolysis. *Photochemistry and photobiology* **54:** 985-992

Gibson NJ, Brown MF (1991) Role of phosphatidylserine in the MI-MII equilibrium of rhodopsin. *Biochemical and biophysical research communications* **176:** 915-921

Goodsell DS, Morris GM, Olson AJ (1996) Automated docking of flexible ligands: applications of AutoDock. *J Mol Recognit* **9:** 1-5

Goudet C, Gaven F, Kniazeff J, Vol C, Liu J, Cohen-Gonsaud M, Acher F, Prezeau L, Pin JP (2004) Heptahelical domain of metabotropic glutamate receptor 5 behaves like rhodopsin-like receptors. *Proceedings of the National Academy of Sciences of the United States of America* **101:** 378-383

Greasley PJ, Fanelli F, Scheer A, Abuin L, Nenniger-Tosato M, DeBenedetti PG, Cotecchia S (2001) Mutational and computational analysis of the alpha(1b)-adrenergic receptor. Involvement of basic and hydrophobic residues in receptor activation and G protein coupling. *The Journal of biological chemistry* **276:** 46485-46494

Gross AK, Rao VR, Oprian DD (2003) Characterization of rhodopsin congenital night blindness mutant T94I. *Biochemistry* **42:** 2009-2015

Gschwind A, Prenzel N, Ullrich A (2002) Lysophosphatidic acid-induced squamous cell carcinoma cell proliferation and motility involves epidermal growth factor receptor signal transactivation. *Cancer Research* **62:** 6329-6336

Haimovici R, Ciulla TA, Miller JW, Hasan T, Flotte TJ, Kenney AG, Schomacker KT, Gragoudas ES (2002) Localization of rose bengal, aluminum phthalocyanine tetrasulfonate, and chlorin e6 in the rabbit eye. *Retina (Philadelphia, Pa* **22:** 65-74

Hall SE, Floriano WB, Vaidehi N, Goddard WA, 3rd (2004) Predicted 3-D structures for mouse I7 and rat I7 olfactory receptors and comparison of predicted odor recognition profiles with experiment. *Chem Senses* **29:** 595-616

Hamm HE, Deretic D, Hofmann KP, Schleicher A, Kohl B (1987) Mechanism of action of monoclonal antibodies that block the light activation of the guanyl nucleotide-binding protein, transducin. *The Journal of biological chemistry* **262:** 10831-10838

Hampson DR, Huang XP, Pekhletski R, Peltekova V, Hornby G, Thomsen C, Thogersen H (1999) Probing the ligand-binding domain of the mGluR4 subtype of metabotropic glutamate receptor. *The Journal of biological chemistry* **274:** 33488-33495

Harmar AJ (2001) Family-B G-protein-coupled receptors. *Genome biology* **2:** REVIEWS3013

Hoare SR (2005) Mechanisms of peptide and nonpeptide ligand binding to Class B G-protein-coupled receptors. *Drug discovery today* **10:** 417-427

Hoare SR, Sullivan SK, Ling N, Crowe PD, Grigoriadis DE (2003) Mechanism of corticotropin-releasing factor type I receptor regulation by nonpeptide antagonists. *Molecular pharmacology* **63:** 751-765

http://www.cambridgesoft.com/software/ChemDraw/

http://www.pymol.org

Hu J, Mora S, Colussi G, Proverbio MC, Jones KA, Bolzoni L, De Ferrari ME, Civati G, Spiegel AM (2002) Autosomal dominant hypocalcemia caused by a novel mutation in the loop 2 region of the human calcium receptor extracellular domain. *J Bone Miner Res* **17:** 1461-1469

Huang XP, Prilla S, Mohr K, Ellis J (2005) Critical amino acid residues of the common allosteric site on the M2 muscarinic acetylcholine receptor: more similarities than differences between the structurally divergent agents gallamine and bis(ammonio)alkane-type hexamethylene-bis-[dimethyl-(3-phthalimidopropyl)ammonium]dibromide. *Molecular pharmacology* **68:** 769-778

Hulme EC, Lu ZL, Bee MS (2003) Scanning mutagenesis studies of the M1 muscarinic acetylcholine receptor. *Receptors & channels* **9:** 215-228

Hummel P, Vaidehi N, Floriano WB, Hall SE, Goddard WA, 3rd (2005) Test of the Binding Threshold Hypothesis for olfactory receptors: explanation of the differential binding of ketones to the mouse and human orthologs of olfactory receptor 912-93. *Protein Sci* **14:** 703-710

Humphrey W, Dalke A, Schulten K (1996) VMD: visual molecular dynamics. *J Mol Graph* **14:** 33-38, 27-38

Hwa J, Garriga P, Liu X, Khorana HG (1997) Structure and function in rhodopsin: packing of the helices in the transmembrane domain and folding to a tertiary structure in the intradiscal domain are coupled. *Proceedings of the National Academy of Sciences of the United States of America* **94:** 10571-10576

Hwa J, Klein-Seetharaman J, Khorana HG (2001) Structure and function in rhodopsin: Mass spectrometric identification of the abnormal intradiscal disulfide bond in misfolded retinitis pigmentosa mutants. *Proceedings of the National Academy of Sciences of the United States of America* **98:** 4872-4876

Hwa J, Reeves PJ, Klein-Seetharaman J, Davidson F, Khorana HG (1999) Structure and function in rhodopsin: further elucidation of the role of the intradiscal cysteines, Cys-110, -185, and -187, in rhodopsin folding and function. *Proceedings of the National Academy of Sciences of the United States of America* **96:** 1932-1935

Hwang TL, Shaka AJ (1995) Water Suppression That Works. Excitation Sculpting Using Arbitrary Wave-Forms and Pulsed-Field Gradients. *Journal of Magnetic Resonance, Series A* **112:** 275-279

Isayama T, Alexeev D, Makino CL, Washington I, Nakanishi K, Turro NJ (2006) An accessory chromophore in red vision. *Nature* **443:** 649-649

Isin B, Rader AJ, Dhiman HK, Klein-Seetharaman J, Bahar I (2006) Predisposition of the dark state of rhodopsin to functional changes in structure. *Proteins* **65:** 970-983

Jaakola VP, Griffith MT, Hanson MA, Cherezov V, Chien EY, Lane JR, Ijzerman AP, Stevens RC (2008) The 2.6 angstrom crystal structure of a human A2A adenosine receptor bound to an antagonist. *Science (New York, NY* **322:** 1211-1217

Janz JM, Farrens DL (2004) Rhodopsin activation exposes a key hydrophobic binding site for the transducin alpha-subunit C terminus. *Journal of Biological Chemistry* **279:** 29767-29773

Jastrzebska B, Fotiadis D, Jang GF, Stenkamp RE, Engel A, Palczewski K (2006) Functional and structural characterization of rhodopsin oligomers. *The Journal of biological chemistry* **281:** 11917-11922

Jastrzebska B, Maeda T, Zhu L, Fotiadis D, Filipek S, Engel A, Stenkamp RE, Palczewski K (2004) Functional characterization of rhodopsin monomers and dimers in detergents. *The Journal of biological chemistry* **279:** 54663-54675

Jensen AA, Spalding TA (2004) Allosteric modulation of G-protein coupled receptors. *Eur J Pharm Sci* **21:** 407-420

Jobert AS, Zhang P, Couvineau A, Bonaventure J, Roume J, Le Merrer M, Silve C (1998) Absence of functional receptors for parathyroid hormone and parathyroid hormone-related peptide in Blomstrand chondrodysplasia. *The Journal of clinical investigation* **102:** 34-40

Johren K, Holtje HD (2002) A model of the human M2 muscarinic acetylcholine receptor. *J Comput Aided Mol Des* **16:** 795-801

Kalatskaya I, Schussler S, Blaukat A, Muller-Esterl W, Jochum M, Proud D, Faussner A (2004) Mutation of tyrosine in the conserved NPXXY sequence leads to constitutive phosphorylation and internalization, but not signaling, of the human B2 bradykinin receptor. *The Journal of biological chemistry* **279:** 31268-31276

Karnik SS, Khorana HG (1990) Assembly of functional rhodopsin requires a disulfide bond between cysteine residues 110 and 187. *The Journal of biological chemistry* **265:** 17520-17524

Karnik SS, Sakmar TP, Chen HB, Khorana HG (1988) Cysteine residues 110 and 187 are essential for the formation of correct structure in bovine rhodopsin. *Proceedings of the National Academy of Sciences of the United States of America* **85:** 8459-8463

Karperien M, van der Harten HJ, van Schooten R, Farih-Sips H, den Hollander NS, Kneppers SL, Nijweide P, Papapoulos SE, Lowik CW (1999) A frame-shift mutation in the type I parathyroid hormone (PTH)/PTH-related peptide receptor causing Blomstrand lethal osteochondrodysplasia. *The Journal of clinical endocrinology and metabolism* **84:** 3713-3720

Kassack MU, Hogger P, Gschwend DA, Kameyama K, Haga T, Graul RC, Sadee W (2000) Molecular modeling of G-protein coupled receptor kinase 2: docking and biochemical evaluation of inhibitors. *AAPS PharmSci* **2:** E2

Kaushal S, Khorana HG (1994) Structure and function in rhodopsin. 7. Point mutations associated with autosomal dominant retinitis pigmentosa. *Biochemistry* **33:** 6121-6128

Kew JN (2004) Positive and negative allosteric modulation of metabotropic glutamate receptors: emerging therapeutic potential. *Pharmacology & therapeutics* **104:** 233-244

Kim JM, Altenbach C, Thurmond RL, Khorana HG, Hubbell WL (1997) Structure and function in rhodopsin: rhodopsin mutants with a neutral amino acid at E134 have a partially activated conformation in the dark state. *Proceedings of the National Academy of Sciences of the United States of America* **94:** 14273-14278

Kim SK, Gao ZG, Van Rompaey P, Gross AS, Chen A, Van Calenbergh S, Jacobson KA (2003) Modeling the adenosine receptors: comparison of the binding domains of A2A agonists and antagonists. *Journal of medicinal chemistry* **46:** 4847-4859

Kinsella GK, Rozas I, Watson GW (2005) Comparative molecular dynamics simulations of uncomplexed, 'agonist-bound' and 'antagonist-bound' alpha1A adrenoceptor models. *Biochemical and biophysical research communications* **333:** 737-741

Kinsella GK, Rozas I, Watson GW (2006) Computational study of antagonist/alpha1A adrenoceptor complexes--observations of conformational variations on the formation of ligand/receptor complexes. *Journal of medicinal chemistry* **49:** 501-510

Kisselev OG, Meyer CK, Heck M, Ernst OP, Hofmann KP (1999) Signal transfer from rhodopsin to the G-protein: evidence for a two-site sequential fit mechanism. *Proceedings of the National Academy of Sciences of the United States of America* **96:** 4898-4903

Klein-Seetharaman J (2002) Dynamics in rhodopsin. *Chembiochem* **3:** 981-986

Klein-Seetharaman J, Getmanova EV, Loewen MC, Reeves PJ, Khorana HG (1999) NMR spectroscopy in studies of light-induced structural changes in mammalian rhodopsin: applicability of solution (19)F NMR. *Proceedings of the National Academy of Sciences of the United States of America* **96:** 13744-13749

Klein-Seetharaman J, Reeves PJ, Loewen MC, Getmanova EV, Chung J, Schwalbe H, Wright PE, Khorana HG (2002) Solution NMR spectroscopy of [alpha -15N]lysine-labeled rhodopsin: The single peak observed in both conventional and TROSY-type HSQC spectra is ascribed to Lys-339 in the carboxyl-terminal peptide sequence. *Proceedings of the National Academy of Sciences of the United States of America* **99:** 3452-3457

Klein-Seetharaman J, Yanamala NV, Javeed F, Reeves PJ, Getmanova EV, Loewen MC, Schwalbe H, Khorana HG (2004) Differential dynamics in the G protein-coupled receptor rhodopsin revealed by solution NMR. *Proceedings of the National Academy of Sciences of the United States of America* **101:** 3409-3413

Knoflach F, Mutel V, Jolidon S, Kew JN, Malherbe P, Vieira E, Wichmann J, Kemp JA (2001) Positive allosteric modulators of metabotropic glutamate 1 receptor: characterization, mechanism of action, and binding site. *Proceedings of the National Academy of Sciences of the United States of America* **98:** 13402-13407

Knowles A, Priestley A (1978) The preparation of 11-cis-retinal. *Vision research* **18:** 115-116

Koenig BW, Kontaxis G, Mitchell DC, Louis JM, Litman BJ, Bax A (2002) Structure and orientation of a G protein fragment in the receptor bound state from residual dipolar couplings. *Journal of molecular biology* **322:** 441-461

Koeppen BH, Herrmann K (1977) Flavonoid glycosides and hydroxycinnamic acid esters of blackcurrants (Ribes nigrum). Phenolics of fruits 9. *Zeitschrift fur Lebensmittel-Untersuchung und -Forschung* **164:** 263-268

Kohara A, Toya T, Tamura S, Watabiki T, Nagakura Y, Shitaka Y, Hayashibe S, Kawabata S, Okada M (2005) Radioligand binding properties and pharmacological characterization of 6-amino-N-cyclohexyl-N,3-dimethylthiazolo[3,2-a]benzimidazole-2-carboxamid e (YM-298198), a high-affinity, selective, and noncompetitive antagonist of metabotropic glutamate receptor type 1. *J Pharmacol Exp Ther* **315:** 163-169

Kohn J, Wilchek M (1978) A colorimetric method for monitoring activation of Sepharose by cyanogen bromide. *Biochemical and biophysical research communications* **84:** 7-14

Kolakowski LF, Jr. (1994) GCRDb: a G-protein-coupled receptor database. *Receptors & channels* **2:** 1-7

Krejci A, Tucek S (2001) Changes of cooperativity between N-methylscopolamine and allosteric modulators alcuronium and gallamine induced by mutations of external loops of muscarinic M(3) receptors. *Molecular pharmacology* **60:** 761-767

Kucharska AZ, Jan O (2002) Anthocyanins in fruits of prunus padus(bird cherry). **82:** 1483-1486

Kumel G, Daus H, Mauch H (1979) Improved method for the cyanogen bromide activation of agarose beads. *Journal of chromatography* **172:** 221-226

Kunishima N, Shimada Y, Tsuji Y, Sato T, Yamamoto M, Kumasaka T, Nakanishi S, Jingami H, Morikawa K (2000) Structural basis of glutamate recognition by a dimeric metabotropic glutamate receptor. *Nature* **407:** 971-977

Kusnetzow AK, Altenbach C, Hubbell WL (2006) Conformational states and dynamics of rhodopsin in micelles and bilayers. *Biochemistry* **45:** 5538-5550

Langmead CJ, Christopoulos A (2006) Allosteric agonists of 7TM receptors: expanding the pharmacological toolbox. *Trends Pharmacol Sci* **27:** 475-481

Laskowski RA, MacArthur MW, Moss DS, Thornton JM (1993) PROCHECK: a program to check the stereochemical quality of protein structures. *J Appl Cryst* **26:** 283-291

Latypov RF, Liu D, Gunasekaran K, Harvey TS, Razinkov VI, Raibekas AA (2008) Structural and thermodynamic effects of ANS binding to human interleukin-1 receptor antagonist. *Protein Science* **17:** 652-663

Lavreysen H, Janssen C, Bischoff F, Langlois X, Leysen JE, Lesage AS (2003) [3H]R214127: a novel high-affinity radioligand for the mGlu1 receptor reveals a common binding site shared by multiple allosteric antagonists. *Molecular pharmacology* **63:** 1082-1093

Le Y, Cui Y, Ying G, Iribarren P, Wang JM (2003) The role of chemokine receptors in the promotion of viral infections. *Contributions to microbiology* **10:** 210-231

Lee J, Lee HK, Kim CY, Hong YJ, Choe CM, You TW, Seong GJ (2005) Purified high-dose anthocyanoside oligomer administration improves nocturnal vision and clinical symptoms in myopia subjects. *The British journal of nutrition* **93:** 895-899

Lee K, Brown D, Urena P, Ardaillou N, Ardaillou R, Deeds J, Segre GV (1996) Localization of parathyroid hormone/parathyroid hormone-related peptide receptor mRNA in kidney. *The American journal of physiology* **270:** F186-191

Lee K, Deeds JD, Chiba S, Segre GV (1995) Parathyroid hormone induces sequential c-fos expression in bone cells in vivo: a model for intercellular communication in bone. *Mineral and electrolyte metabolism* **21:** 120-122

Lee K, Deeds JD, Chiba S, Un-No M, Bond AT, Segre GV (1994) Parathyroid hormone induces sequential c-fos expression in bone cells in vivo: in situ localization of its receptor and c-fos messenger ribonucleic acids. *Endocrinology* **134:** 441-450

Levi MAB, Scarminio IS, Poppi RJ, Trevisan MG (2004) Three-way chemometric method study and UV-Vis absorbance for the study of simultaneous degradation of anthocyanins in flowers of the Hibiscus rosa-sinensys species. *Talanta* **62:** 299-305

Lewis JW, Kliger DS (2000) Absorption spectroscopy in studies of visual pigments: spectral and kinetic characterization of intermediates. *Methods in Enzymology* **315:** 164-178

Li S, Huang S, Peng SB (2005) Overexpression of G protein-coupled receptors in cancer cells: involvement in tumor progression. *International journal of oncology* **27:** 1329-1339

Liaw CW, Grigoriadis DE, Lorang MT, De Souza EB, Maki RA (1997) Localization of agonist- and antagonist-binding domains of human corticotropin-releasing factor receptors. *Molecular endocrinology (Baltimore, Md* **11:** 2048-2053

Lila MA (2004) Anthocyanins and Human Health: An In Vitro Investigative Approach. *Journal of biomedicine & biotechnology* **2004:** 306-313

Lin SW, Sakmar TP (1996) Specific tryptophan UV-absorbance changes are probes of the transition of rhodopsin to its active state. *Biochemistry* **35:** 11149-11159

Liu X, Garriga P, Khorana HG (1996) Structure and function in rhodopsin: correct folding and misfolding in two point mutants in the intradiscal domain of rhodopsin identified in retinitis pigmentosa. *Proceedings of the National Academy of Sciences of the United States of America* **93:** 4554-4559

Lodowski DT, Angel TE, Palczewski K (2009) Comparative Analysis of GPCR Crystal Structures. *Photochemistry and photobiology* **85:** 425-430

Loewen MC, Klein-Seetharaman J, Getmanova EV, Reeves PJ, Schwalbe H, Khorana HG (2001) Solution 19F nuclear Overhauser effects in structural studies of the cytoplasmic domain of mammalian rhodopsin. *Proceedings of the National Academy of Sciences of the United States of America* **98:** 4888-4892

Lomas-Neira J, Ayala A (2005) Pepducins: an effective means to inhibit GPCR signaling by neutrophils. *Trends in immunology* **26:** 619-621

Lopez-Rodriguez ML, Murcia M, Benhamu B, Olivella M, Campillo M, Pardo L (2001) Computational model of the complex between GR113808 and the 5-HT4 receptor guided by site-directed mutagenesis and the crystal structure of rhodopsin. *J Comput Aided Mol Des* **15:** 1025-1033

Lui VW, Thomas SM, Zhang Q, Wentzel AL, Siegfried JM, Li JY, Grandis JR (2003) Mitogenic effects of gastrin-releasing peptide in head and neck squamous cancer cells are mediated by activation of the epidermal growth factor receptor. *Oncogene* **22:** 6183-6193

Maj M, Bruno V, Dragic Z, Yamamoto R, Battaglia G, Inderbitzin W, Stoehr N, Stein T, Gasparini F, Vranesic I, Kuhn R, Nicoletti F, Flor PJ (2003) (-)-PHCCC, a positive allosteric modulator of mGluR4: characterization, mechanism of action, and neuroprotection. *Neuropharmacology* **45:** 895-906

Malherbe P, Kew JN, Richards JG, Knoflach F, Kratzeisen C, Zenner MT, Faull RL, Kemp JA, Mutel V (2002) Identification and characterization of a novel splice variant of the metabotropic glutamate receptor 5 gene in human hippocampus and cerebellum. *Brain research* **109:** 168-178

Malherbe P, Knoflach F, Broger C, Ohresser S, Kratzeisen C, Adam G, Stadler H, Kemp JA, Mutel V (2001) Identification of essential residues involved in the glutamate binding pocket of the group II metabotropic glutamate receptor. *Molecular pharmacology* **60:** 944-954

Malherbe P, Kratochwil N, Knoflach F, Zenner MT, Kew JN, Kratzeisen C, Maerki HP, Adam G, Mutel V (2003) Mutational analysis and molecular modeling of the allosteric binding site of a novel, selective, noncompetitive antagonist of the metabotropic glutamate 1 receptor. *The Journal of biological chemistry* **278:** 8340-8347

Malherbe P, Kratochwil N, Zenner MT, Piussi J, Diener C, Kratzeisen C, Fischer C, Porter RH (2003) Mutational analysis and molecular modeling of the binding pocket of the metabotropic glutamate 5 receptor negative modulator 2-methyl-6-(phenylethynyl)-pyridine. *Molecular pharmacology* **64:** 823-832

Malien-Aubert C, Dangles O, Amiot MJ (2001) Color stability of commercial anthocyanin-based extracts in relation to the phenolic composition. Protective effects by intra- and intermolecular copigmentation. *Journal of agricultural and food chemistry* **49:** 170-176

Man O, Gilad Y, Lancet D (2004) Prediction of the odorant binding site of olfactory receptor proteins by human-mouse comparisons. *Protein Sci* **13:** 240-254

Manzo A, Caporali R, Montecucco C, Pitzalis C (2003) Role of chemokines and chemokine receptors in regulating specific leukocyte trafficking in the immune/inflammatory response. *Clinical and experimental rheumatology* **21:** 501-508

Margry RJ, Jacobs CW, de Grip WJ, Daemen FJ (1982) Interference of detergents in immunoassays of rhodopsin. *Vision research* **22:** 1447-1449

Marti-Renom MA, Stuart AC, Fiser A, Sanchez R, Melo F, Sali A (2000) Comparative protein structure modeling of genes and genomes. *Annual review of biophysics and biomolecular structure* **29:** 291-325

Matsumoto H, Inaba H, Kishi M, Tominaga S, Hirayama M, Tsuda T (2001) Orally administered delphinidin 3-rutinoside and cyanidin 3-rutinoside are directly absorbed in rats and humans and appear in the blood as the intact forms. *Journal of agricultural and food chemistry* **49:** 1546-1551

Matsumoto H, Nakamura Y, Iida H, Ito K, Ohguro H (2006) Comparative assessment of distribution of blackcurrant anthocyanins in rabbit and rat ocular tissues. *Experimental eye research* **83:** 348-356

Matsumoto H, Nakamura Y, Tachibanaki S, Kawamura S, Hirayama M (2003) Stimulatory effect of cyanidin 3-glycosides on the regeneration of rhodopsin. *Journal of Agricultural & Food Chemistry* **51:** 3560-3563

May LT, Leach K, Sexton PM, Christopoulos A (2007) Allosteric modulation of G protein-coupled receptors. *Annual review of pharmacology and toxicology* **47:** 1-51

Mayer ML (2006) Glutamate receptors at atomic resolution. *Nature* **440:** 456-462

McGhie TK, Rowan DR, Edwards PJ (2006) Structural identification of two major anthocyanin components of boysenberry by NMR spectroscopy. *Journal of Agricultural & Food Chemistry* **54:** 8756-8761

McMenamin PG, Forrester JV, Steptoe RJ, Dua HS (1992) Ultrastructural pathology of experimental autoimmune uveitis. Quantitative evidence of activation and possible high endothelial venule-like changes in retinal vascular endothelium. *Laboratory investigation; a journal of technical methods and pathology* **67:** 42-55

Mehler EL, Periole X, Hassan SA, Weinstein H (2002) Key issues in the computational simulation of GPCR function: representation of loop domains. *J Comput Aided Mol Des* **16:** 841-853

Meiboom S, Gill D (1958) Modified Spin-Echo Method for Measuring Nuclear Relaxation Times. *Rev Sci Instrum* **29:** 688-691

Miedlich SU, Gama L, Seuwen K, Wolf RM, Breitwieser GE (2004) Homology modeling of the transmembrane domain of the human calcium sensing receptor and localization of an allosteric binding site. *The Journal of biological chemistry* **279:** 7254-7263

Mitchell DC, Straume M, Litman BJ (1992) Role of sn-1-saturated,sn-2-polyunsaturated phospholipids in control of membrane receptor conformational equilibrium: effects of cholesterol and acyl chain unsaturation on the metarhodopsin I in equilibrium with metarhodopsin II equilibrium. *Biochemistry* **31:** 662-670

Mitsukawa K, Yamamoto R, Ofner S, Nozulak J, Pescott O, Lukic S, Stoehr N, Mombereau C, Kuhn R, McAllister KH, van der Putten H, Cryan JF, Flor PJ (2005) A selective metabotropic glutamate receptor 7 agonist: activation of receptor signaling via an allosteric site modulates stress parameters in vivo. *Proceedings of the National Academy of Sciences of the United States of America* **102:** 18712-18717

Morin D, Cotte N, Balestre MN, Mouillac B, Manning M, Breton C, Barberis C (1998) The D136A mutation of the V2 vasopressin receptor induces a constitutive activity which permits discrimination between antagonists with partial agonist and inverse agonist activities. *FEBS letters* **441:** 470-475

Morris GA, Goddsell DS, Halliday RS, Huey R, Hart WE, Belew RK, Olson AJ (1998) Automated docking using a lamarckian genetic algorithm and an empirical binding free energy function. *J Comp Chem* **19:** 1639-1662

Motoyama H, Hamanaka T, Kawase N, Boucher F, Kito Y (1985) Effect of phospholipids and detergents on transitions and equilibrium between the bleaching intermediates of rhodopsin. *Canadian journal of biochemistry and cell biology = Revue canadienne de biochimie et biologie cellulaire* **63:** 1152-1159

Muff R, Born W, Kaufmann M, Fischer JA (1994) Parathyroid hormone and parathyroid hormone-related protein receptor update. *Molecular and cellular endocrinology* **100:** 35-38

Muhlemann A, Ward NA, Kratochwil N, Diener C, Fischer C, Stucki A, Jaeschke G, Malherbe P, Porter RH (2006) Determination of key amino acids implicated in the actions of allosteric modulation by 3,3'-difluorobenzaldazine on rat mGlu5 receptors. *Eur J Pharmacol* **529:** 95-104

Murakami M, Kouyama T (2008) Crystal structure of squid rhodopsin. *Nature* **453:** 363-367

Mustafi D, Palczewski K (2009) Topology of class A G protein-coupled receptors: insights gained from crystal structures of rhodopsins, adrenergic and adenosine receptors. *Molecular pharmacology* **75:** 1-12

Muth ER, Laurent JM, Jasper P (2000) The effect of bilberry nutritional supplementation on night visual acuity and contrast sensitivity. *Altern Med Rev* **5:** 164-173

Muto T, Tsuchiya D, Morikawa K, Jingami H (2007) Structures of the extracellular regions of the group II/III metabotropic glutamate receptors. *Proceedings of the National Academy of Sciences of the United States of America* **104:** 3759-3764

Nakaishi H, Matsumoto H, Tominaga S, Hirayama M (2000) Effects of black current anthocyanoside intake on dark adaptation and VDT work-induced transient refractive alteration in healthy humans. *Altern Med Rev* **5:** 553-562

Nikiforovich GV, Marshall GR (2001) 3D model for TM region of the AT-1 receptor in complex with angiotensin II independently validated by site-directed mutagenesis data. *Biochemical and biophysical research communications* **286:** 1204-1211

O'Brien JA, Lemaire W, Chen TB, Chang RS, Jacobson MA, Ha SN, Lindsley CW, Schaffhauser HJ, Sur C, Pettibone DJ, Conn PJ, Williams DL, Jr. (2003) A family of highly selective allosteric modulators of the metabotropic glutamate receptor subtype 5. *Molecular pharmacology* **64:** 731-740

O'Brien JA, Lemaire W, Wittmann M, Jacobson MA, Ha SN, Wisnoski DD, Lindsley CW, Schaffhauser HJ, Rowe B, Sur C, Duggan ME, Pettibone DJ, Conn PJ, Williams DL, Jr. (2004) A novel selective allosteric modulator potentiates the activity of native metabotropic glutamate receptor subtype 5 in rat forebrain. *J Pharmacol Exp Ther* **309:** 568-577

Offermanns S, Iida-Klein A, Segre GV, Simon MI (1996) G alpha q family members couple parathyroid hormone (PTH)/PTH-related peptide and calcitonin receptors to phospholipase C in COS-7 cells. *Molecular endocrinology (Baltimore, Md* **10:** 566-574

Okada T, Fujiyoshi Y, Silow M, Navarro J, Landau EM, Shichida Y (2002) Functional role of internal water molecules in rhodopsin revealed by X-ray crystallography. *Proceedings of the National Academy of Sciences of the United States of America* **99:** 5982-5987

Okuno Y, Tamon A, Yabuuchi H, Niijima S, Minowa Y, Tonomura K, Kunimoto R, Feng C (2008) GLIDA: GPCR--ligand database for chemical genomics drug discovery--database and tools update. *Nucleic acids research* **36:** D907-912

Oldham WM, Hamm HE (2008) Heterotrimeric G protein activation by G-protein-coupled receptors. *Nature Reviews Molecular Cell Biology* **9:** 60-71

Oprian DD, Molday RS, Kaufman RJ, Khorana HG (1987) Expression of a synthetic bovine rhodopsin gene in monkey kidney cells. *Proceedings of the National Academy of Sciences of the United States of America* **84:** 8874-8878

Palczewski K, Kumasaka T, Hori T, Behnke CA, Motoshima H, Fox BA, Le Trong I, Teller DC, Okada T, Stenkamp RE, Yamamoto M, Miyano M (2000) Crystal structure of rhodopsin: A G protein-coupled receptor. *Science (New York, NY* **289:** 739-745

Papermaster DS (1982) Preparation of retinal rod outer segments. *Methods Enzymol* **81:** 48-52

Park H, Lee J, Lee S (2006) Critical assessment of the automated AutoDock as a new docking tool for virtual screening. *Proteins* **65:** 549-554

Park JH, Scheerer P, Hofmann KP, Choe HW, Ernst OP (2008) Crystal structure of the ligand-free G-protein-coupled receptor opsin. *Nature* **454:** 183-187

Parker C, A (1968) *Photoluminescence of solutions.*, New York: Elsevier.

Parmentier ML, Prezeau L, Bockaert J, Pin JP (2002) A model for the functioning of family 3 GPCRs. *Trends Pharmacol Sci* **23:** 268-274

Partridge NC, Bloch SR, Pearman AT (1994) Signal transduction pathways mediating parathyroid hormone regulation of osteoblastic gene expression. *Journal of cellular biochemistry* **55:** 321-327

Peng JY, Vaidehi N, Hall SE, Goddard WA, 3rd (2006) The predicted 3D structures of the human M1 muscarinic acetylcholine receptor with agonist or antagonist bound. *ChemMedChem* **1:** 878-890

Petrel C, Kessler A, Maslah F, Dauban P, Dodd RH, Rognan D, Ruat M (2003) Modeling and mutagenesis of the binding site of Calhex 231, a novel negative allosteric modulator of the extracellular Ca(2+)-sensing receptor. *The Journal of biological chemistry* **278:** 49487-49494

Phillips WJ, Cerione RA (1988) The intrinsic fluorescence of the alpha subunit of transducin. Measurement of receptor-dependent guanine nucleotide exchange. *The Journal of biological chemistry* **263:** 15498-15505

Pinkerton AB, Vernier JM, Schaffhauser H, Rowe BA, Campbell UC, Rodriguez DE, Lorrain DS, Baccei CS, Daggett LP, Bristow LJ (2004) Phenyl-tetrazolyl acetophenones: discovery of positive allosteric potentiatiors for the metabotropic glutamate 2 receptor. *Journal of medicinal chemistry* **47:** 4595-4599

Plante EO, Maude MB, Anderson RE (1977) Regeneration of Rhodopsin: effect of quaternary ammonium detergents. *Experimental eye research* **24:** 377-382

Pontus M, Delmelle M (1975) Effect of detergents on the conformation of spin-labeled rhodopsin. *Experimental eye research* **20:** 599-603

Porter RH, Jaeschke G, Spooren W, Ballard TM, Buttelmann B, Kolczewski S, Peters JU, Prinssen E, Wichmann J, Vieira E, Muhlemann A, Gatti S, Mutel V, Malherbe P (2005) Fenobam: a clinically validated nonbenzodiazepine anxiolytic is a potent, selective, and noncompetitive mGlu5 receptor antagonist with inverse agonist activity. *J Pharmacol Exp Ther* **315:** 711-721

Prado GN, Suetomi K, Shumate D, Maxwell C, Ravindran A, Rajarathnam K, Navarro J (2007) Chemokine signaling specificity: essential role for the N-terminal domain of chemokine receptors. *Biochemistry* **46:** 8961-8968

Prilla S, Schrobang J, Ellis J, Holtje HD, Mohr K (2006) Allosteric interactions with muscarinic acetylcholine receptors: complex role of the conserved tryptophan M2422Trp in a critical cluster of amino acids for baseline affinity, subtype selectivity, and cooperativity. *Molecular pharmacology* **70:** 181-193

Qi Y, Bar-Joseph Z, Klein-Seetharaman J (2006) Evaluation of different biological data and computational classification methods for use in protein interaction prediction. *Proteins* **63:** 490-500

Raddatz R, Schaffhauser H, Marino MJ (2007) Allosteric approaches to the targeting of G-protein-coupled receptors for novel drug discovery: a critical assessment. *Biochemical pharmacology* **74:** 383-391

Rader AJ, Anderson G, Isin B, Khorana HG, Bahar I, Klein-Seetharaman J (2004) Identification of core amino acids stabilizing rhodopsin. *Proceedings of the National Academy of Sciences of the United States of America* **101:** 7246-7251

Rao VR, Cohen GB, Oprian DD (1994) Rhodopsin mutation G90D and a molecular mechanism for congenital night blindness. *Nature* **367:** 639-642

Rasmussen SG, Choi HJ, Rosenbaum DM, Kobilka TS, Thian FS, Edwards PC, Burghammer M, Ratnala VR, Sanishvili R, Fischetti RF, Schertler GF, Weis WI, Kobilka BK (2007) Crystal structure of the human beta2 adrenergic G-protein-coupled receptor. *Nature* **450:** 383-387

Renk GE, Crouch RK, Feix JB (1988) Lack of interaction of rhodopsin chromophore with membrane lipids. An electron-electron double resonance study using 14N:15N pairs. *Biophysical journal* **53:** 361-365

Ridge KD, Lu Z, Liu X, Khorana HG (1995) Structure and function in rhodopsin. Separation and characterization of the correctly folded and misfolded opsins produced on expression of an opsin mutant gene containing only the native intradiscal cysteine codons. *Biochemistry* **34:** 3261-3267

Rodriguez AL, Nong Y, Sekaran NK, Alagille D, Tamagnan GD, Conn PJ (2005) A close structural analog of 2-methyl-6-(phenylethynyl)-pyridine acts as a neutral allosteric site ligand on metabotropic glutamate receptor subtype 5 and blocks the effects of multiple allosteric modulators. *Molecular pharmacology* **68:** 1793-1802

Rottman JB (1999) Key role of chemokines and chemokine receptors in inflammation, immunity, neoplasia, and infectious disease. *Veterinary pathology* **36:** 357-367

Ruan KH, Wu J, So SP, Jenkins LA (2003) Evidence of the residues involved in ligand recognition in the second extracellular loop of the prostacyclin receptor characterized by high resolution 2D NMR techniques. *Arch Biochem Biophys* **418:** 25-33

Sakmar TP (2002) Structure of rhodopsin and the superfamily of seven-helical receptors: the same and not the same. *Curr Opin Cell Biol* **14:** 189-195

Sakmar TP, Menon ST, Marin EP, Awad ES (2002) Rhodopsin: insights from recent structural studies. *Annual Review of Biophysics & Biomolecular Structure* **31:** 443-484

Sali A, Potterton L, Yuan F, van Vlijmen H, Karplus M (1995) Evaluation of comparative protein modeling by MODELLER. *Proteins* **23:** 318-326

Salom D, Lodowski DT, Stenkamp RE, Le Trong I, Golczak M, Jastrzebska B, Harris T, Ballesteros JA, Palczewski K (2006) Crystal structure of a photoactivated deprotonated intermediate of rhodopsin. *Proceedings of the National Academy of Sciences of the United States of America* **103:** 16123-16128

Scheerer P, Park JH, Hildebrand PW, Kim YJ, Krauss N, Choe HW, Hofmann KP, Ernst OP (2008) Crystal structure of opsin in its G-protein-interacting conformation. *Nature* **455:** 497-502

Scheerer P, Park JH, Hildebrand PW, Kim YJ, Krausz N, Choe H-W, Hofmann KP, Ernst OP (2008) Crystal structure of opsin in its G-protein-interacting conformation. *Nature* **455:** 497-502

Schertler GF (2005) Structure of rhodopsin and the metarhodopsin I photointermediate. *Current Opinion in Structural Biology* **15:** 408-415

Schipani E, Kruse K, Juppner H (1995) A constitutively active mutant PTH-PTHrP receptor in Jansen-type metaphyseal chondrodysplasia. *Science (New York, NY* **268:** 98-100

Schulz A, Schoneberg T (2003) The structural evolution of a P2Y-like G-protein-coupled receptor. *The Journal of biological chemistry* **278:** 35531-35541

Scotton CJ, Wilson JL, Milliken D, Stamp G, Balkwill FR (2001) Epithelial cancer cell migration: a role for chemokine receptors? *Cancer Res* **61:** 4961-4965

Sefcik MD, Schaefer J, Stejskal EO, McKay RA, Ellena JF, Dodd SW, Brown MF (1983) Lipid bilayer dynamics and rhodopsin-lipid interactions: new approach using high-resolution solid-state 13C NMR. *Biochemical and biophysical research communications* **114:** 1048-1055

Shim JY, Welsh WJ, Howlett AC (2003) Homology model of the CB1 cannabinoid receptor: sites critical for nonclassical cannabinoid agonist interaction. *Biopolymers* **71:** 169-189

Shortridge MD, Hage DS, Harbison GS, Powers R (2008) Estimating protein-ligand binding affinity using high-throughput screening by NMR. *Journal of combinatorial chemistry* **10:** 948-958

Sokal I, Pulvermuller A, Buczylko J, Hofmann KP, Palczewski K (2002) Rhodopsin and its kinase. *Methods in Enzymology* **343:** 578-600

Soudijn W, Van Wijngaarden I, AP IJ (2004) Allosteric modulation of G protein-coupled receptors: perspectives and recent developments. *Drug discovery today* **9:** 752-758

Spijker P, Vaidehi N, Freddolino PL, Hilbers PA, Goddard WA, 3rd (2006) Dynamic behavior of fully solvated beta2-adrenergic receptor, embedded in the membrane with bound agonist or antagonist. *Proceedings of the National Academy of Sciences of the United States of America* **103:** 4882-4887

Stenkamp RE, Filipek S, Driessen CA, Teller DC, Palczewski K (2002) Crystal structure of rhodopsin: a template for cone visual pigments and other G protein-coupled receptors. *Biochimica et biophysica acta* **1565:** 168-182

Stott K, Stonehouse, Jonathan, Keeler, James, Hwang, Tsang-Lin, and Shaka, A. J. (1995) Excitation Sculpting in High-Resolution Nuclear Magnetic Resonance Spectroscopy: Application to Selective NOE Experiments *J Am Chem Soc* **117:** 4199 - 4200

Stubbs GW, Smith HG, Jr., Litman BJ (1976) Alkyl glucosides as effective solubilizing agents for bovine rhodopsin. A comparison with several commonly used detergents. *Biochimica et biophysica acta* **426:** 46-56

Suresh P, Wanchu A (2006) Chemokines and chemokine receptors in HIV infection: role in pathogenesis and therapeutics. *Journal of postgraduate medicine* **52:** 210-217

Swanson CJ, Bures M, Johnson MP, Linden AM, Monn JA, Schoepp DD (2005) Metabotropic glutamate receptors as novel targets for anxiety and stress disorders. *Nat Rev Drug Discov* **4:** 131-144

Szundi I, Lewis JW, Kliger DS (2005) Effect of digitonin on the rhodopsin meta I-meta II equilibrium. *Photochemistry & Photobiology* **81:** 866-873

Tang CM, Insel PA (2004) GPCR expression in the heart; "new" receptors in myocytes and fibroblasts. *Trends in cardiovascular medicine* **14:** 94-99

Taylor CM, Barda Y, Kisselev OG, Marshall GR (2008) Modulating G-protein coupled receptor/G-protein signal transduction by small molecules suggested by virtual screening. *Journal of medicinal chemistry* **51:** 5297-5303

Tengel T, Fex T, Emtenas H, Almqvist F, Sethson I, Kihlberg J (2004) Use of 19F NMR spectroscopy to screen chemical libraries for ligands that bind to proteins. *Organic & biomolecular chemistry* **2:** 725-731

Thomas SM, Bhola NE, Zhang Q, Contrucci SC, Wentzel AL, Freilino ML, Gooding WE, Siegfried JM, Chan DC, Grandis JR (2006) Cross-talk between G protein-coupled receptor and epidermal growth factor receptor signaling pathways contributes to growth and invasion of head and neck squamous cell carcinoma. *Cancer Research* **66:** 11831-11839

Thompson JD, Higgins DG, Gibson TJ (1994) CLUSTAL W: improving the sensitivity of progressive multiple sequence alignment through sequence weighting, position-specific gap penalties and weight matrix choice. *Nucleic acids research* **22:** 4673-4680

Thompson MA (ArgusLab 4.0.1) ArgusLab 4.0.1. *Planaria Software LLC, Seattle, WA* **http://www.arguslab.com**

Tirupula KC, Balem F, Yanamala N, Klein-Seetharaman J (2009) pH-dependent Interaction of Rhodopsin with Cyanidin-3-glucoside. 2. Functional Aspects. *Photochemistry and photobiology* **85:** 463-470

Tiurin VA, Korol'kov SN, Berman AL, Kagan VE (1987) [Structural stabilization of lipids and visual pigment rhodopsin in the photoreceptor membrane by vitamin E]. *Biulleten' eksperimental'noi biologii i meditsiny* **104:** 391-394

Trabanino RJ, Hall SE, Vaidehi N, Floriano WB, Kam VW, Goddard WA, 3rd (2004) First principles predictions of the structure and function of g-protein-coupled receptors: validation for bovine rhodopsin. *Biophysical journal* **86:** 1904-1921

Trent JO, Wang ZX, Murray JL, Shao W, Tamamura H, Fujii N, Peiper SC (2003) Lipid bilayer simulations of CXCR4 with inverse agonists and weak partial agonists. *The Journal of biological chemistry* **278:** 47136-47144

Tsuchiya D, Kunishima N, Kamiya N, Jingami H, Morikawa K (2002) Structural views of the ligand-binding cores of a metabotropic glutamate receptor complexed with an antagonist and both glutamate and Gd3+. *Proceedings of the National Academy of Sciences of the United States of America* **99:** 2660-2665

Us D (2003) [Chemokine receptors: their role in human immunodeficiency virus (HIV) pathogenicity and resistance to HIV infections]. *Mikrobiyoloji bulteni* **37:** 75-87

Vaidehi N, Floriano WB, Trabanino R, Hall SE, Freddolino P, Choi EJ, Zamanakos G, Goddard WA, 3rd (2002) Prediction of structure and function of G protein-coupled receptors. *Proceedings of the National Academy of Sciences of the United States of America* **99:** 12622-12627

Vaidehi N, Schlyer S, Trabanino RJ, Floriano WB, Abrol R, Sharma S, Kochanny M, Koovakat S, Dunning L, Liang M, Fox JM, de Mendonca FL, Pease JE, Goddard WA, 3rd, Horuk R (2006) Predictions of CCR1 chemokine receptor structure and BX 471 antagonist binding followed by experimental validation. *The Journal of biological chemistry* **281:** 27613-27620

Vassilatis DK, Hohmann JG, Zeng H, Li F, Ranchalis JE, Mortrud MT, Brown A, Rodriguez SS, Weller JR, Wright AC, Bergmann JE, Gaitanaris GA (2003) The G protein-coupled receptor repertoires of human and mouse. *Proceedings of the National Academy of Sciences of the United States of America* **100:** 4903-4908

Veitch NC, Grayer RJ (2008) Flavonoids and their glycosides, including anthocyanins. *Natural product reports* **25:** 555-611

Vriend G (1990) WHAT IF: a molecular modeling and drug design program. *J Mol Graph* **8:** 52-56, 29

Wald G, Brown PK (1953) The molar extinction of rhodopsin. *The Journal of general physiology* **37:** 189-200

Warne T, Serrano-Vega MJ, Baker JG, Moukhametzianov R, Edwards PC, Henderson R, Leslie AG, Tate CG, Schertler GF (2008) Structure of a beta1-adrenergic G-protein-coupled receptor. *Nature* **454:** 486-491

Washington I (2007) Chlorophyll derivatives as visual pigments for super vision in the red. *Photochemical & Photobiological Sciences* **6:** 775-779

Washington I, Brooks C, Turro NJ, Nakanishi K (2004) Porphyrins as photosensitizers to enhance night vision. *Journal of the American Chemical Society* **126:** 9892-9893

Washington I, Zhou J, Jockusch S, Turro NJ, Nakanishi K, Sparrow JR (2007) Chlorophyll derivatives as visual pigments for super vision in the red. *Photochem Photobiol Sci* **6:** 775-779

Werner K, Lehner I, Dhiman HK, Richter C, Glaubitz C, Schwalbe H, Klein-Seetharaman J, Khorana HG (2007) Combined solid state and solution NMR studies of alpha,epsilon-15N labeled bovine rhodopsin. *Journal of Biomolecular NMR* **37:** 303-312

Werner K, Richter C, Klein-Seetharaman J, Schwalbe H (2008) Isotope labeling of mammalian GPCRs in HEK293 cells and characterization of the C-terminus of bovine rhodopsin by high resolution liquid NMR spectroscopy. *Journal of Biomolecular NMR* **40:** 49-53

Wessling-Resnick M, Johnson GL (1987) Transducin interactions with rhodopsin. Evidence for positive cooperative behavior. *Journal of Biological Chemistry* **262:** 12444-12447

Wiedmann TS, Pates RD, Beach JM, Salmon A, Brown MF (1988) Lipid-protein interactions mediate the photochemical function of rhodopsin. *Biochemistry* **27:** 6469-6474

Williams TP, Baker BN, McDowell JH (1974) The influence of lipids on dynamic properties of rhodopsin. *Experimental eye research* **18:** 69-75

Winzell MS, Ahren B (2007) G-protein-coupled receptors and islet function-implications for treatment of type 2 diabetes. *Pharmacology & therapeutics* **116:** 437-448

Yang K, Farrens DL, Altenbach C, Farahbakhsh ZT, Hubbell WL, Khorana HG (1996) Structure and function in rhodopsin. Cysteines 65 and 316 are in proximity in a rhodopsin mutant as indicated by disulfide formation and interactions between attached spin labels. *Biochemistry* **35:** 14040-14046

Yang R, Gerstenfeld LC (1996) Signal transduction pathways mediating parathyroid hormone stimulation of bone sialoprotein gene expression in osteoblasts. *The Journal of biological chemistry* **271:** 29839-29846

Yawadio R, Tanimori S, Morita N (2007) Identification of phenolic compounds isolated from pigmented rices and their aldose reductase inhibitory activities. *Food Chemistry* **101:** 1616-1625

Yeagle PL, Selinsky BS, Albert AD (1984) Perturbations of phospholipid head groups by membrane proteins in biological membranes and recombinants. *Biophysical journal* **45:** 1085-1089

Yeo GS, Siddle K (2003) Attractin' more attention - new pieces in the obesity puzzle? *The Biochemical journal* **376:** e7-8

Yoshie O (2005) [Role of chemokines and chemokine receptors in leukocyte trafficking]. *Nippon rinsho* **63 Suppl 4:** 437-443

Yowell CW, Daaka Y (2002) G protein-coupled receptors provide survival signals in prostate cancer. *Clinical prostate cancer* **1:** 177-181

Zhang Q, Bhola NE, Lui VW, Siwak DR, Thomas SM, Gubish CT, Siegfried JM, Mills GB, Shin D, Grandis JR (2007) Antitumor mechanisms of combined gastrin-releasing peptide receptor and epidermal growth factor receptor targeting in head and neck cancer. *Molecular Cancer Therapeutics* **6:** 1414-1424

Zheng GZ, Bhatia P, Daanen J, Kolasa T, Patel M, Latshaw S, El Kouhen OF, Chang R, Uchic ME, Miller L, Nakane M, Lehto SG, Honore MP, Moreland RB, Brioni JD, Stewart AO (2005) Structure-activity relationship of triazafluorenone derivatives as potent and selective mGluR1 antagonists. *Journal of medicinal chemistry* **48:** 7374-7388